Advanced Multi-Band Modulation Technology for Underwater Communication Systems

by

Hamada Ahmed Hamada Esmaiel

B. Eng. (Hons), M. Sc. Eng

Submitted in fulfilment of the requirements for the Degree of

Doctor of Philosophy

University of Tasmania

January, 2015

Abstract

In recent years, underwater communication (UWC) systems have been attractive in the development of civilian and military applications. However, there are many challenging issues surrounding such communication systems due to severe channel conditions such as ambient noise, frequency selectivity, multi-path with significant tap delays and Doppler shifts. In order to conduct effective ocean exploration, solutions for these problems are desirable to ensure efficient image transmission over an underwater acoustic channel.

This thesis investigates and develops signal processing techniques for UWC systems to communicate effectively in an underwater channel. Techniques such as provision of efficient image transmission over an underwater acoustic channel, achieving a low bit error rate, increasing bandwidth and saving transmitted energy are covered. Based on the time reversal technique, an orthogonal frequency division multiplexing (OFDM) based communication scheme for use in underwater acoustic channels was developed. The OFDM guard interval to improve bandwidth and energy efficiency with the aim to increase the underwater network lifetime was adopted and carefully customized.

Efficient image transmission for an underwater channel can be considered to be the critical task of next generation underwater acoustic communication systems. In this thesis, a novel rate allocation scheme for efficient transmission of image bit streams in an underwater acoustic channel with optimum bit rate is proposed. Optimality is achieved in the sense that the overall peak signal to noise ratio (PSNR) of the image transmission is maximized under channel bit rate and bit error rate constraints. Based on a modified Set Partitioning in Hierarchical Trees (M-SPIHT) image coder, four different groups of bit-streams are generated based on their significance. The significant bits, the sign bits, the set bits and the refinement bits are transmitted in four different groups with different protection levels in order to reduce the total distortion of the reconstructed image. In addition, the Hierarchical Quadrature Amplitude Modulation (HQAM) is used to provide unequal error protection based on the modulation technique.

For efficient underwater communication, the multipath issue must be addressed. To reduce the multipath effect, feedback wave focusing techniques are used, leading to a time reversal process. In such a process, at the very beginning of the communication the transmitter transmits a probe symbol sequence that is recorded by the receiver. The received probe sequence, serving as channel information, is time reversed and transmitted back to the transmitter. In time reversal operations, each multipath signal sequence received convolves with the time-reversed version of its corresponding channel estimate based on this probe signal. Thus, signal focusing can be achieved at the transmitter if the channel does not change significantly.

This thesis considers a passive time reversal system in the multipath UWA fading channels with significant delays. By combining the time reversal technique with single-input multiple-output OFDM (SIMO-OFDM), a novel transmission scheme is proposed to transmit progressive image data with progressive protection in the presence of inter-block interferences. The proposed new unequal error protection scheme can significantly improve the peak signal-to-noise ratio of the reconstructed image. In addition, by using the time reversal technique, multiple time-dispersive fading channels can be made impulse-like. As such, a moderated guard interval length can be used without introducing much inter-block interference, even in a UWA with a long tap delay. Based on this, a

demonstrably robust performance with significant bandwidth efficiency can be achieved. In addition, the guard interval can be designed shorter than the maximum channel tap delay.

In UWA communication, the zero padding OFDM (ZP-OFDM) multicarrier system is preferred for less transmission power consumption in the guard interval because the OFDM system requires a long guard interval to avoid inter-block interference problems. In this thesis, streams of new OFDM schemes for better energy efficiency as well as significant bit error rate improvement are proposed. Based on the preamble signal and a training sequence, a receiver design is proposed for a UWA communication system. The Doppler scaling factor and UWA channel feature are estimated by using the preamble and the training sequence that is used to update the estimated parameter to avoid preamble signal retransmission. Due to underwater channel features such as frequency selective and time varying, the proposed schemes are evaluated via simulated channels as well as real channels measured from sea-going experiments. The results of the study show that the proposed systems outperform conventional OFDM systems in energy and spectrum efficiency as well as the received image quality.

In this thesis, efficient image transmissions over an underwater acoustic channel are studied by optimal designs in both the transmitter and the receiver. Improvements of inter-carrier interference reduction methods for multicarrier systems used in underwater communication systems have also been achieved. Improvements are demonstrated in both the image transmission system over the underwater channel and the multicarrier modulation used in underwater communication with data image transmission. As a consequence of this research, up until now four peer-reviewed journal papers and three conference papers have been published.

Declaration

Some of the research presented in this thesis has resulted in some publications. These publications are listed at the end of Chapter 1.

All work presented in this thesis is original, to the best knowledge of the author. References and acknowledgements to other researchers have been given as appropriate.

Acknowledgements

A great number of people deserve thanks for their valuable guidance and assistance. First in the list are my supervisors Dr. Danchi Jiang and Prof. J.C. Oliver. Without their care and encouragement, all the research stages would not have been completed as scheduled. Second is the School of Engineering team, without which any improvement, modifications and fittings of all required work, would have been possible. The Science Library, Document Delivery and the various administrative staff also deserve the author's sincere appreciation.

Special thanks to Prof. T.C. Yang for his support with the ASCOT01 experimental data. Without such support, I could not apply my new schemes to a real data field. I also thank Dr. Dai Linglong for his help and support with simulation programs.

Very special thanks to my brothers, sisters, all my relatives and friends in Egypt, particularly my mother, who inevitably asked in our weekly phone call '*What are you doing now? And have you finished?*' To which, when I answered in the negative the next question was predictably '*When will you finish?*' The effect was to make me monitor and report my progress compulsively.

Finally, to anyone whom I may have forgotten, I ask forgiveness and offer my sincerest thanks.

Contents

List of Figures

List of Tables

Nomenclature

Acronyms

SNR	Signal–to–Noise Ratio
ISI	Inter-Symbol Interference
SIMO	Single-Input Multiple-Output
OFDM	Orthogonal Frequency Division Multiplexing
UEP	Unequal Error Protection
ICI	Inter-Carrier Interference
IDFT	Inverse Discrete Fourier Transform
IDCT	Inverse Discrete Cosine Transform
BER	Bit Error Rate
KSP	Known Symbol Padding
TR	Time Reversal
UWA	Underwater Acoustic
IBI	Inter-Block Interference
CIR	Channel Impulse Response
SPIHT	Set Partitioning in Hierarchical Trees
MSE	Mean Squared Error
HQAM	Hierarchical Quadrature Amplitude Modulation
ZP	Zero Padding
PSNR	Peak Signal–to–Noise Ratio
CFO	Carrier Frequency Offset
SIR	Signal–to–Interference Ratio
DFT	Discrete Fourier Transform
DCT	Discrete Cosine Transform
ZP-OFDM	Zero Padding OFDM
CP-OFDM	Cyclic Prefix OFDM
ZPN-OFDM	Zero-Pseudorandom Noise OFDM
PN	Pseudorandom Noise
TDS-OFDM	Time-Domain Synchronisation OFDM
TS	Training Sequence
CS	Compressive Sensing
PNZI	Pseudorandom Noise with Zero Insertion
DSF	Doppler Scaling Factor
PZP	Progressive Zero Padding
DPN	Dual-PN Padding
UW	Underwater
PSD	Power Spectral Density

AN	Attenuation-Noise
UWAN	Underwater Acoustic Noise
FEC	Forward Error Correction
GF	Galois Field
R-S	Reed Solomon
R-S BTC	Reed Solomon Block Turbo Codes
LDPC	Low Density Parity Check Code
MCM	Multi-Carrier Modulation
MIMO	Multiple-Input Multiple-Output
PAPR	Peak-to-Average Power Ratio
OSDM	Orthogonal Signal-Division Multiplexing
RLS-DFE	Recursive Least Square Differential Feedback Equalizer
RM	Rate Maximization
MM	Margin Maximization
DF	Decode-and-Forward
CNR	Carrier-to-Noise Ratio
MR	Multiple Resampling
FBMC	Filter Bank Multicarrier
FMT	Filtered Multi-tone Modulation
PSK	Phase Shift Keying
SLIM	Sparse Learning via Iterative Minimization
CG	Conjugate Gradient
OMP	Orthogonal Matching Pursuit
BP	Basis Pursuit
BEM	Basis Expansion Model
WLS	Windowed Least-Squares
UMSNs	Underwater Multimedia Sensor Networks
JPEG	Joint Photographic Experts Group
QAM	Quadrature Amplitude Modulation
DWT	Discrete Wavelet Transform
DPCM	Differential Pulse Code Modulation
VQ	Vector Quantization
PET	Priority Encoding Transmission
JSCC	Joint Source Channel Coding
EEP	Equal Error Protection
M-SPIHT	Modified Set Partitioning in Hierarchical Trees
LIP	Least Insignificant Pixels
LSP	Least Significant Pixels
LIS	Least Insignificant Sets
NCB	Non-Critical Bits

CB	Critical Bits
SEP	Symbol Error Probability
PDF	Probability Density Function
HP	High-Priority
LP	Low-Priority
LSB	Least Significant Bits
MSB	Most Significant Bits
MMSE	Minimum Mean Square Error
LMS	Least Mean Squares
GI	Guard Interval
SOMP	Simultaneous Orthogonal Matching Pursuit
FIR	Finite Impulse Response
UW-OFDM	Unique Word OFDM
DTMB	Digital Terrestrial Multimedia Broadcast
DVB-T2	Digital Video Broadcasting –Second Generation Terrestrial
LFM	Linear Frequency Modulated
SC	Single-Carrier
ZOS	Zadoff-Chu Sequence
ACF	Auto-Correlation Function
OLA	Overlapping and Adding
IFFT	Inverse Fast Fourier Transform
IPS	Iterative Padding Subtraction
SINR	Signal–to–Interference–plus–Noise Ratio
FDPNTS	Frequency Domain Pseudorandom Noise Training Sequence
FDPNPS	Frequency Domain Pseudorandom Noise Preamble Signal
GIL	Guard Interval length -containing overhead information-
TGIL	Total Guard Interval length
AWGN	Additive White Gaussian Noise
SSIR	Signal–to–Signal and Interference Ratio
SIR	Signal–to–Interference Ratio
ZPNZ-OFDM	Double-Side Zero Delimited Pseudorandom Noise OFDM
TFT-OFDM	Time-Frequency Training Sequence OFDM
SISR	Signal–to–Interfered–Signal Ratio
LTV	Linear Time Varying

Chapter 1

Introduction

1.1 Overview

Effective underwater wireless communications are ctitical to many military and civil applications. In addition to submarine communication, underwater communication can also be used in many civil applications such as ocean exploration, undersea rescue, undersea disaster management, offshore oil production, pollution monitoring in environmental systems, collection of scientific data recorded at ocean bottom stations, speech transmission between divers, and mapping of the ocean floor for detection of objects as well as for the discovery of new resources [1]. However, underwater wireless communication systems are not easy to construct. There are real challenges associated with them, such as underwater channel modelling, signal attenuation in oceans, limited bandwidth especially for communication over long distances, high power consumption, low signal–to–noise ratio (SNR), inter-symbol interference (ISI) and multipath channel features with significant tap delays. Due to high absorption and attenuation of electromagnetic waves in underwater channels and rapid absorption and scattering of optical waves in such channels, acoustic channels are the most preferred channels to use in underwater wireless communications. Digital signal processing is indispensible for such underwater wireless communication problems.

For the optimal exploration and use of oceans and seas, researchers have been attracted to the development and deployment of video and image transmission in underwater acoustic communication [2]. High-speed underwater image transmission systems might be the next generation of undersea expeditions. Based on underwater sensor networks and digital image processing methodologies, researchers have worked to transmit images over underwater acoustic channels [3, 4]. However, current acoustic communication technologies cannot effectively support image transmission due to challenging nature of using underwater communication channels [5]. This is the focus of my thesis.

As the data rate increases, the delay spread can increase and extend over tens or hundreds of data symbols, increasing significantly the complexity of the time domain equalizer. Single-input multiple-output (SIMO) orthogonal frequency division multiplexing (OFDM) (SIMO-OFDM) has been proposed to address this problem [6]. In this thesis, in addition to using OFDM for high bandwidth efficiency, unequal error protection (UEP) techniques are proposed to improve the peak signal-to-noise ratio of reconstructed received images. This UEP technique is proposed based on the operation of source coded as well as feature of channel characteristics.

In this thesis, the inter-carrier interference (ICI) problem of OFDM is analysed and solved in detail. Two different implementation methods of orthogonality transformers are employed (based on the inverse discrete Fourier transform (IDFT) and inverse discrete cosine transform (IDCT)) using pulse shaping function techniques. Also, new OFDM schemes have been proposed to improve the energy and spectrum efficiency as well as bit error rate (BER) performance of multi-carrier modulation. These new OFDM schemes use known symbol padding (KSP) as guard intervals to save the pilot symbol sequence and increase bandwidth and energy efficiency. Thanks to the capability of the time reversal (TR) technique to focus and reduce multipath channels, TR is used in combination

with the SIMO system to reduce the expected mutual interference between this KSP training sequence and OFDM data blocks.

1.2 Underwater Acoustic Communication

Despite the fact that the acoustic signal is the most preferred for transmission over the underwater acoustic (UWA) channel, such communication faces two main challenging issues, namely, the multipath propagation feature due to the refraction from the surface and bottom of the ocean, and the Doppler shift effect due to the relevant motion between the transmitter and receiver [7, 8]. Thus, the underwater acoustic channel is considered as a double-selective fading channel [7]. Due to the low propagation speed of acoustic signals, the fast variation of the UWA channel multipath is one of the most challenging problems. In addition, distortion caused by the Doppler shift is different in each path [7]. If multicarrier communication systems can be used to remove such multipath effects, they will be sensitive to the Doppler shift (due to the channel feature or transmitted receiver oscillator mismatch) and need long guard intervals to avoid inter-block interference (IBI). Furthermore the long guard intervals can significantly affect the bandwidth efficiency in communication systems originally with low bandwidth. In such types of channels usually zero padding is used as a guard interval instead of a cyclic prefix to save the transmission power spent on the guard interval [9].

Efficient use of available channel bandwidth is essential in all communication systems and can lead to efficient image and video transmission. Such use becomes critical in the case of limited bandwidth channels such as UWA channels. To this end, SIMO-OFDM has been proposed to solve the UWA channel multipath problem, and furthermore OFDM itself uses bandwidth efficiently. However, the actual bandwidth achieved by SIMO-OFDM is lower due to a large guard interval. This guard interval can be reduced if the time reversal (TR) technique is used to focus the channel impulse response (CIR), which is also proposed in this thesis.

The principle of time reversal is based on the symmetricity of the linear wave equation feature, where the sound signal transmitted can be received at different points. These signals can be reversed and retransmitted, resulting in focused signals at the original source location. The frequency domain equivalent of TR is the active phase conjugation. Based on the TR technique delay spread can be reduced and CIR focusing improves the SNR as well as fading effect. The TR capability to focus increases as the number of receivers increases. Using a combination of OFDM multicarrier systems with the TR technique, multipath time dispersive fading channels associated with the SIMO-OFDM can be converted to a single channel with channel time dispersion reduction in addition to reduced channel fading [10]. By using such a combination a moderated guard interval can be used without significant IBI even if the original channel has a long tap delay. In this way, not only can efficient bandwidth be achieved, but also the OFDM demodulator number is reduced to one.

Due to the small bandwidth of the OFDM sub-carriers, if they are normalized to the Doppler shift, acoustic OFDM is very sensitive to the Doppler shift effect. Normally the Doppler shift is a large wide range in UWA OFDM communication systems. Non-uniform Doppler shift compensation has been proposed to solve such a problem [9]. Another effective way to solve this is the synchronization between the transmitter and receiver using a preamble signal.

1.3 Contributions

This thesis provides solutions for significant UWA communication problems. We can classify UWA communication problems discussed in this thesis into two categories: efficient image transmission issues and OFDM multicarrier schemes.

The next generation of UWA communication will involve high speed image transmission. However, current UWA communication can only provide a limited data rate, where the available bandwidth is limited. This limited bandwidth encourages us to provide an efficient use for this available bandwidth. In addition to the limited channel bandwidth, a strong channel coder is required due to the high rate of long burst error. When image signals are transmitted over such channels, the burst error produced due to the channel feature can lead to the loss of a large part of the image signal. To deal with such a challenge, image transmission over the band limited UWA channels will be discussed in two aspects: (1) efficient data compression and (2) bandwidth efficient modulation. In this thesis, the two aspects are considered where efficient data compression can be achieved by using Set Partitioning in Hierarchical Trees (SPIHT). SPIHT is an efficient wavelet-based progressive image-compression technique designed to minimize the mean-squared error (MSE) between the original and decoded image. Also, the efficient bandwidth can be achieved using unequal error protection (UEP) optimization technique formulated by taking the particular channel feature into account at the transmitter or by using a special modulation technique such as the Hierarchical Quadrature Amplitude Modulation (HQAM). To improve the bit error performance of image transmission over the UWA channel, in this thesis the Reed Solomon coder (R-S) channel coding technique is proposed.

Due to the UWA channel features such as multipath propagation and frequency selective fading, there are many obstacles for reliable and high data rate UWA communication. OFDM is a frequency division multiplexing scheme utilized as a digital multi-carrier modulation method for high speed broadband communication systems that can be used for UWA communication. OFDM performs well against multipath interference and has the ability to combat frequency selective fading and high frequency band efficiency, and as such, is preferred for UWA communication. However, due to the multipath problem in an UWA channel, a long guard interval is usually required. This multipath signal effect can be reduced by using the TR technique combined with the SIMO-OFDM system. Also, by careful calculation of the zero padding (ZP) length required for each transmitted data block to minimize the total inter-block interference (IBI) noise of the received image, a new transmission scheme can be proposed to provide a significant improvement in the peak signal–to–noise ratio (PSNR) of received images.

However, one of the main OFDM disadvantages is its sensitivity to carrier frequency offset (CFO) which distorts the orthogonality between subcarriers due to inter-carrier interference (ICI). Bandwidth limited systems often employ pulse shaping techniques for the reduction of such ICI, and minimize the likelihood of errors at the receiver. The purpose of pulse shaping is to reduce the side lobes as much as possible, since the contribution of the side lobes to the ICI power results in a decrease in the signal to interference ratio (SIR). In this thesis, the ICI and SIR performance under pulse shaping will be studied for an underwater acoustic channel and Performance comparison of OFDM discrete Fourier transform (DFT)-based and discrete cosine transform (DCT)-based will be discussed.

Researchers prefer zero padding OFDM (ZP-OFDM) for UWA communication instead of the cyclic prefix OFDM (CP-OFDM) as the consumption of less transmission power can be achieved [6, 9, 11, 12]. In this thesis, new schemes will be proposed to achieve a significant improvement in the consumption of the transmitted power and an increase in the energy efficiency of OFDM multicarrier systems. These new schemes are called zero-pseudorandom noise OFDM (ZPN-OFDM), where no pilot signals are used for CIR estimation.

Significant improvement in the spectrum and energy efficiency can be achieved by using the pseudorandom noise (PN)-sequence padding time-domain synchronization OFDM (TDS-OFDM) transmission scheme. In this thesis, TDS-OFDM will be used as an appealing alternative to the traditional CP-OFDM and ZP-OFDM technology in UWA communication. In this study, a new correlation based coder for inter-block and inter-symbol interference for the TDS-OFDM problem is proposed, denoted time reversal single-input multiple-output TDS-OFDM. Such a coder is tested for multipath UWA channels with significant tap delays. A Zadoff–Chu sequence with perfect autocorrelation property is adopted as a training sequence (TS) for a TDS-OFDM system for more accurate channel estimation. In the proposed multicarrier scheme a TS with length shorter than the channel order can be used without introducing notable inter-block interference. Based on the compressive sensing (CS) channel estimation method, this TS can be interleaved by zeroes for more energy efficiency and reduction of the mutual interference of training sequence in OFDM data blocks. Furthermore, the TS amplitude can be reduced.

Based on the preamble signal, UWA channel features such as the Doppler shift can be estimated as in the studies by [6, 13]. Unfortunately, this preamble needs to be updated according to the varying UWA channel Doppler shift. Hence, such a communication system needs to resend the preamble signal, which reduces the bandwidth efficiency. In this work, a receiver design is provided based on the TDS-OFDM system to use the TS to update the estimated parameters estimated using the initial preamble. In summary, the following points indicate the contribution of the work:

1. A communication system with unequal error protection is proposed for image transmission over an UWA channel.
2. Progressive protection is proposed for image transmission over an UWA channel in inter-block interference noise present by using a progressive zero padding for the time reversal SIMO-OFDM system.
3. OFDM inter-carrier interference analysis and mitigation are performed by using pulse shaping function.
4. A novel transmission scheme called a zero-pseudorandom noise training sequence OFDM (ZPN-OFDM) is proposed, to be used in UWA communication and provide significant bit error rate improvement as well as energy improvement.
5. Based on a new correlation based coder with a Zadoff-Chu sequence, the inter-block and inter-symbol interference can be removed in the time reversal TDS-OFDM system in an UWA channel.
6. The Doppler scaling factor (DSF) and UWA channel parameter is estimated and updated in the receiver design proposed for TR-TDS-OFDM.
7. Using a compressive sensing channel estimation technique and pseudorandom noise training sequence interleaved by zeroes, a new communication scheme called pseudorandom noise with zero insertion (PNZI-OFDM) is proposed for an UWA communication system to improve energy consumption as well as improve significantly the bit error rate.

8. A novel transmission scheme called a double-side zero delimited pseudorandom noise OFDM (ZPNZ-OFDM) is proposed for the time reversal single-input multiple-output orthogonal frequency division multiplexing system (SIMO-OFDM). The proposed transmission scheme can achieve a significant improvement in the signal–to–interfered–signal ratio of received the OFDM data block as well as the pseudorandom noise training sequence. Moreover, the pseudorandom noise amplitude in the ZPNZ-OFDM can be reduced to achieve a greater improvement in energy efficiency.

1.4 Thesis Outline

This thesis is organized as follows. Chapter 2 describes the background and literature review of multicarrier modulation operation in an UWA channel. It also surveys the research literature for the state of the art in UWA systems. The Main of this chapter has been published in [J4] of the publication list. Chapter 3 presents different unequal error protection methods for image transmission over an UWA channel. It also represents channeling of image transmission over UWA communication systems. Two UEP methods are discussed: (1) UEP based on a modulation technique; (2) UEP based on a rate allocation method. The Main of this chapter has been published in [J3] and [C1-C2] of the publication list. Chapter 4 introduces a transmission scheme called a progressive zero padding (PZP) time reversal orthogonal frequency division multiplexing (TR-OFDM) for the transmission of progressively organized image data blocks for time-dispersive fading channels with a short guard interval. Such image data blocks are usually obtained by Set Partitioning in Hierarchical Tress (SPHIT) coders. The new scheme provides a significant improvement in the peak signal–to–noise ratio (PSNR) of received images by careful calculation of the zero padding length according to the significance of data blocks to minimize the total inter-block interference (IBI) noise of the entire image. The Main of this chapter well be published in [J6] of the publication list. Chapter 5 analyzes and discusses the carrier frequency offset problem in an OFDM multicarrier system and its effect in the inter-carrier interference (ICI) and signal to interference ratio (SIR). Also, the performance of OFDM discrete Fourier transform (DFT)-based pulses and discrete cosine transform (DCT)-based pulses are compared. The Main of this chapter has been published in [C4] of the publication list. In Chapter 6, a novel transmission scheme called a zero-pseudorandom noise training sequence OFDM (ZPN-OFDM) is proposed, where the frame structure of dual-PN padding TDS-OFDM is modified by replacing the first PN sequence with zero sequence. ZPN-OFDM provides a significant bit error rate (BER) improvement as well as an energy efficiency improvement. The Main of this chapter has been published in [J1] of the publication list. Chapter 7 discusses time reversal SIMO-OFDM based on the TDS-OFDM. This chapter includes a correlation based coder to reduce the mutual interference between the training sequence and OFDM data blocks in the time reversal single-input multiple-output TDS-OFDM system. Also, a short guard interval is used to improve the bandwidth efficiency with a Zadoff-Chu sequence to improve linear channel estimation methods of TDS-OFDM systems. The Main of this chapter has been published in [J2] of the publication list. Chapter 8 focuses on receiver design and UWA channel parameters with updating the estimated channel parameter using the TDS-OFDM training sequence. The Main of this chapter has been published in [J7] of the publication list. In chapter 9, a novel training sequence, the pseudorandom noise with zero insertion, for any multicarrier system which uses a known symbol padding as a training sequence is proposed. Zeroes are inserted in the pseudo-noise bit sequence which used in the known symbol padding orthogonal frequency division multiplexing (KSP-OFDM) training sequence to reduce the guard interval energy loss in

significant tap delay channels, without any detrimental effects on other pseudo-noise properties required for synchronization and channel estimation. The Main of this chapter has been published in [J5] of the publication list. In chapter 10 a novel transmission scheme called the zero-pseudorandom noise-zero orthogonal frequency division multiplexing (ZPNZ-OFDM) is proposed for the time reversal single-input multiple-output orthogonal frequency division multiplexing system (SIMO-OFDM). The Main of this chapter has been published in [J8] of the publication list. Finally, conclusions are drawn in chapter 11 and the thesis ends with suggestions for future work.

1.5 Publications Arising from this Research

- Journal Papers

[J1] **H. Esmaiel** and D. Jiang, "Zero-pseudorandom noise training OFDM", *Electronics Letters*, vol. 50, pp. 650-652, 2014.

[J2] **H. Esmaiel** and D. Jiang, "Time reversal time-domain synchronisation orthogonal frequency division multiplexing over multipath fading channels with significant tap delays", *The IET Journal of Engineering*, vol. 1, pp. 1-10, 2014.

[J3] **H. Esmaiel** and D. Jiang, "Optimum bit rate for image transmission over underwater acoustic channel", *Journal of Electrical and Electronic Engineering*, vol. 2, no. 4, pp. 64-74, 2014.

[J4] **H. Esmaiel** and D. Jiang, "Review article: multicarrier communication for underwater acoustic channel", *International Journal of Communications, Network and System Sciences*, vol. 6, pp. 361-376, 2013.

[J5] **H. Esmaiel** and D. Jiang, "Pseudorandom noise with zero insertion technique for OFDM systems in underwater acoustic channel", *IET Communication Journal* (resubmission after major revision).

[J6] **H. Esmaiel** and D. Jiang, "An image transmission technique adaptive to underwater time-dispersive fading channels with progressive zero padding OFDM", *Wireless Personal Communications* (under review).

[J7] **H. Esmaiel** and D. Jiang, "Spectrum and energy efficient OFDM multicarrier modulation for underwater acoustic channel", to be submitted to *EURASIP Journal on Advances in Signal Processing*.

[J8] **H. Esmaiel** and D. Jiang, "Zero-pseudorandom noise-zero OFDM system", to be submitted to *IET Signal Processing Journal*.

- Conference Papers

[C1] **H. Esmaiel** and D. Jiang, "Image transmission over underwater acoustic environment using OFDM technique with HQAM mapper", in *IEEE International Conference on Information Science and Technology (ICIST)*, pp. 1596-1601, 2013.

[C2] **H. Esmaiel** and D. Jiang, "SPIHT coded image transmission over underwater acoustic channel with unequal error protection using HQAM", in *IEEE International Conference on Information Science and Technology (ICIST)*, pp. 1365-1371, 2013.

[C3] **H. Esmaie**l and D. Jiang, "OFDM inter-carrier interference reduction using pulse shaping function for underwater acoustic communications systems," in *IEEE International Conference on Electronics, Communications and Computers (JEC-ECC)*, pp. 104-109, 2013.

Chapter 2

Multicarrier Communication for Underwater Acoustic Channel

2.1 Introduction

This chapter is written largely based on our review paper [170] arising from my PhD study. Underwater acoustic (UWA) channels are considered to be "quite possibly nature's most unforgiving wireless medium" [14]. The complexity of underwater acoustic channels is dominated by the ocean environment characteristics which include significant tap delay, double-side-spreading, Doppler-spreads, frequency-selective fading, and limited bandwidth [15]. However, efficient underwater (UW) communications are critical to many types of scientific and civil missions in the ocean, such as ocean monitoring, ocean exploration, undersea rescue, and undersea disaster response. Human knowledge of the oceans rests on our ability to collect information from remote undersea locations. Together with sensor technology and vehicular technology, wireless underwater acoustic communications are desirable to enable new applications ranging from environmental monitoring to the gathering of oceanographic data, marine archaeology, and search and rescue missions.

New technologies of high-speed communication for image and video transmission are also desirable to facilitate the next generation of efficient undersea expeditions. However, current acoustic communication technologies can only provide limited data rates due to the particular physical features of the channel [5]. The corresponding wireless technology for undersea communications still needs significant further development. Research has been active for over a decade on designing the methods for underwater wireless information transmission. However, electro-magnetic waves only propagate over extremely short distances in underwater channels. In contrast, acoustic waves propagate over much longer distances. Acoustic waves can, in fact, be used in an underwater channel; however, this presents a communication system designer with many difficulties.

Fig. 2.1 [16] illustrates the scenario of shallow water multipath propagation. In such a situation, in addition to the direct path, the signal also propagates via reflections from the surface and bottom of the body of water, resulting in a multipath effect with much larger time dispersion than that of wireless channel propagation in air.

There are many issues that have to be carefully examined when designing an acoustic based transmission system for underwater channels. Some of these are [17]: (1) attenuation to the absorption of acoustic waves in water which limits the distance that sound can travel in this environment. (2) Low propagation speed of sound, roughly around 1,500 m/s. (3) Multipaths due to reflection from the bottom and surface of the sea, causing echoes and interference. (4) The transmitted signal suffers from the heterogeneous characteristics of the underwater channel as well as Doppler's effect caused by the movement of transmitter and receiver. (5) Noise in the ocean. The noise level can mask the portion of the signal and block the corresponding carried data.

The properties of the underwater medium are also extremely varied and change in both space and time. Fluctuations due to environmental characteristics include seasonal changes, geographical variations both in temperature and salinity, seabed relief, currents, tides, internal waves, movement of the acoustic systems and their targets, etc. All this makes the underwater acoustic signal fluctuate randomly. As such, the selection of modulation

and error correction techniques is very challenging. To mitigate the bandwidth limitation, multicarrier modulation is used in an underwater acoustic channel. This is an alternative to overcome the long-time delays in underwater acoustic channels. It increases the symbol interval and thereby decreases the inter-symbol interference (ISI) [18].

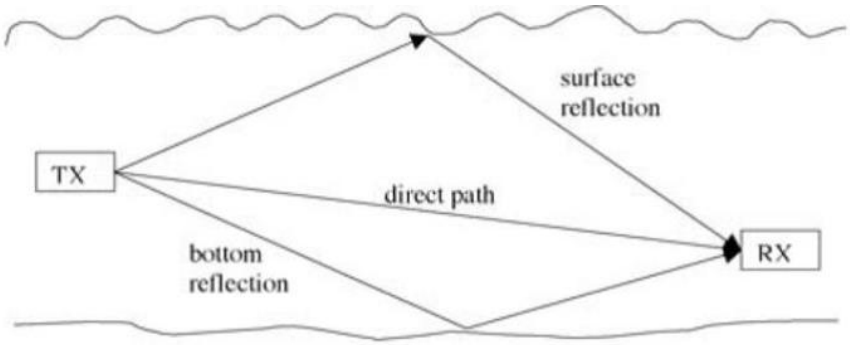

Fig. 2.1. Shallow water multipath propagation: in addition to the direct path, the signal propagates via reflections from the surface and bottom. Taken from Milica Stojanovic [16].

In this chapter, we aim to provide a brief overview of the key developments, both theoretical and applied, in the field. We also hope to provide an insight into some of the open problems and challenges facing researchers in this field in the near future. Rather than attempting to provide an exhaustive survey of all research in the field, we will concentrate on multicarrier modulation for underwater acoustic channel simulation, and challenges, ideas and developments that are likely to be keystones of future digital signal processing for underwater acoustic communication systems.

This chapter summarizes several aspects of underwater acoustic communication. It is organized as follows. First, a brief summary of acoustic propagation properties in seawater is given. Then the channel coding performance for multicarrier modulation in underwater acoustic communication systems is analysed and multicarrier modulations for underwater acoustic communications presented. Finally, the underwater acoustic channel estimation for underwater communication, the Doppler shift estimation for underwater acoustic communications, and image and video transmission over underwater acoustic (UWA) channels with multicarrier modulation are discussed in this chapter.

2.2 Acoustic Wave Propagation Properties in Seawater

A good understanding and reasonably accurate modelling of the underwater acoustic channel is the required basis upon which all other works for underwater networks can be carried out. Several models are already available for calculating and predicting the attenuation [19, 20], which can also help to model other aspects of the underwater acoustic channel. Furthermore, parameters of frequency, distance, depth, acidity to salinity, and temperature of the underwater environment can be used to characterize how the channel acts and how a network can perform. This section summarizes underwater channel models for that purpose.

2.2.1 Propagation Loss

The transmitted acoustic signal in underwater acoustic communication has reduced strength with increasing distance due to many factors such as absorption caused by magnesium sulphate and boric acid, particle motion and geometrical spreading, etc. Propagation loss is composed mainly of three aspects, namely, geometrical spreading,

attenuation and the anomaly of propagation. The latter is nearly impossible to model. However it is known that the signal attenuation, in dB, that occurs over a transmission distance l for a signal frequency f can be approximated as [21]:

$$10 \cdot \log A(1, f) = k \cdot 10 \cdot \log l + l.10.\log \vartheta, \tag{2-1}$$

where ϑ is the absorption coefficient in dB/km, which can be obtained from the particular model characterizing it and k represents the geometrical spreading factor with a value between 1~2.

2.2.2 Absorption Coefficient

Attenuation by absorption occurs due to the conversion of acoustic energy into heat in sea-water. This process is frequency dependent since at higher frequencies more energy is absorbed. The attenuation by absorption models considered for inclusion into the Thorp model [21] eq. (2-2) provides the absorption coefficient in dB/km as a function in carrier frequency f_c :

$$10 \cdot \log \vartheta = \frac{0.1 \cdot f_c^2}{1 + f_c^2} + \frac{40 \cdot f_c^2}{4100 + f_c^2} + 2.75 \cdot 10^{-4} \cdot f_c^2 + 0.003. \tag{2.2}$$

2.2.3 Ambient Noise Model

Ambient noise in the ocean can be described as Gaussian and having a continuous power spectral density (p.s.d.) [21]. The four most prominent sources for ambient noise are turbulence, shipping, wind driven waves and thermal noise. Their p.s.d. in dB re µPa per Hz are given by the formulae eq. (2-3), eq. (2-4), eq. (2-5), and eq. (2-6) shown below [21]:

$$10 \cdot \log N_t(f) = 17 - 30 \cdot \log f, \tag{2-3}$$

$$10 \cdot \log N_s(f) = 40 + 20(s - 0.5) + 26 \cdot \log f - 60 \cdot \log(f + 0.03), \tag{2-4}$$

$$10 \cdot \log N_w(f) = 50 + 7.5\sqrt{\omega} + 20 \cdot \log f - 40 \cdot \log(f + 0.4), \tag{2-5}$$

$$10 \cdot \log N_{th}(f) = -15 + 20 \cdot \log f. \tag{2-6}$$

The ambient noise in the ocean is affected by different factors in specific frequency ranges. In the noise models given in eq. (2-3) to eq. (2-6), the effect of coloured noise denoted by $N_t(f)$ represents the turbulence noise at frequency f, $N_s(f)$ the shipping noise (with S as the shipping factor which lies between 0 and 1), $N_w(f)$ the wind driven wave noise (with ω as the wind speed in m/s), and $N_{th}(f)$ the thermal noise. The composite noise p.s.d. can be obtained in µPa from [21]:

$$N(f) = N_t(f) + N_s(f) + N_w + N_{th}(f). \tag{2-7}$$

2.2.4 Signal–to–Noise Ratio

In an UWA channel, the signal-to-noise ratio can be calculated [22] based on signal attenuation and the noise p.s.d. Specifically, the SNR observed at the receiver can be calculated in µPa per dB per Hz using the following equation:

$$SNR(l,f) = \frac{P}{A(l,f)N(f)\Delta f}, \tag{2-8}$$

where $SNR(l,f)$ is the SNR over a distance l and a transmission center frequency f, P is the signal transmission power and Δf represents the receiver noise bandwidth. Equation (2-8) clearly shows that the underwater acoustic channel SNR is a function of transmission frequency. As such, we can find the optimal frequency for the UWA channel to maximize SNR. The attenuation-noise (AN) factor, given by $A(l, f)$ can be used to reflect the frequency dependent part of the SNR. By close analysis of this relationship, it can also be used to determine the optimal frequency at which the maximal narrow-band SNR is achieved for each transmission distance l.

Since the SNR is inversely proportional to the attenuation-noise factor, the optimal frequency $f_o(l)$ is that for which the value of 1/AN (represented in dB per μPa per Hz) is the highest over the combination of a certain distance. In Fig. 2.2 [22] the frequency-dependent part of the narrowband SNR, $1/A(1,f)N(f)$, is shown. In this plot the attenuation and noise parameters are selected as $k = 1.5$, $S = 0.5$, and $\omega = 0$, to reflect the UWA channel with moderate shipping activity and no wave noise.

It can be seen that there is a frequency for which the narrowband SNR is maximized for a particular distance, for the given attenuation and noise constants. This optimal frequency denoted by $f_o(l)$, can be selected as the carrier frequency f_c for that particular transmission distance [22].

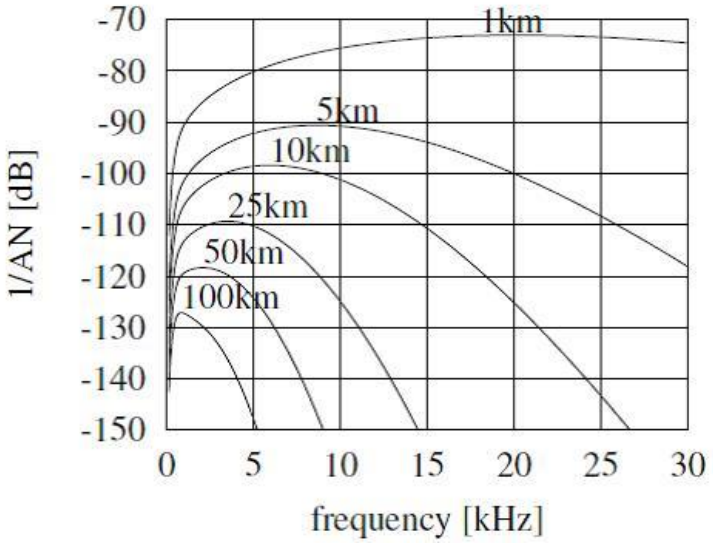

Fig. 2.2. Narrowband SNR, $1/A(1,f)N(f)$; $k = 1.5$; $s = 0$; $\omega = 0$. Taken from Milica Stojanovic [22].

2.2.5 Channel Capacity

As per the Shannon theorem, the channel capacity, i.e. the theoretical upper limit on data that can be communicated through an undistorted channel subject to additive white Gaussian noise is given by the following formula [21]:

$$C = B \cdot \log_2\left(1 + \frac{S}{N}\right), \tag{2-9}$$

where B is the channel bandwidth in Hz and S/N represents the channel SNR. The basic Shannon relationship shown in eq. (2-9) can be extended to be applicable in cases where the noise is dependent on frequency to take the

form as [21]:

$$C = \int_B \log_2\left(1 + \frac{S(f)}{N(f)}\right) df. \tag{2-10}$$

For time-invariant channels of a certain time interval with Gaussian noise we can obtain the total capacity by dividing the total bandwidth into multiple narrow sub-bands and summing their individual capacities collectively. Each sub-band has a small width Δf which is centred on the transmission frequency, i.e. the bandwidth. In the case where the transmission bandwidth, *B(l)*, over a distance l is known along with the transmission power *P(l)*, we can extend eq. (2-10) to obtain the channel capacity over a distance l [21]:

$$C = \int_B \log_2\left(\frac{P(l)}{A(l,f)N(f)B(l)}\right) df. \tag{2-11}$$

The choice of the underlying absorption coefficient model imposes a dependence of the capacity on depth, temperature, salinity and acidity as well.

2.2.6 Doppler Shift and UWA Channel Multipath

In underwater communication, the relative movement between the transmitter and receiver due to the constant motion of nodes results in Doppler shifts, which significantly distort received signals. It is required to estimate the Doppler shift and compensate it for all UWA channel applications. In contrast to terrestrial communication where the Doppler effect is modelled by a frequency shift, due to the slow sound speed in water, the effect of transceiver motion on the duration of the symbol cannot be neglected [23]. Doppler phase φ_d, depends on the relative velocity v and the ratio between the carrier frequency f_c and the symbol rate $R = 1/T$ [24] caused in the received signal as:

$$\varphi_d = -2\pi f_c T \frac{\Delta}{1-\Delta} = -2\pi \frac{f_c}{R} \frac{v}{c-v}. \tag{2-12}$$

From [25, 26] UWA channel multipath representation for multipath arrival p is characterized by its mean magnitude gains ϑ_p and delay t_p. These quantities are dependent on the path length l_p, which in turn is a function of the given range *R*.

The path magnitude gain is given by $\vartheta_p = \Gamma_p / \sqrt{A(l_p, f_c)}$, where $\Gamma_p = (1/\sqrt{2})^{r_p}$ is the amount of loss due to reflection at the bottom and surface, and r_p is the number of reflections for path p. From eq. (2-1) the acoustic propagation loss, represented by (l_p, f_c), results in the following formula:

$$A(l_p, f_c) = l_p^k [\alpha(f_c)]^{l_p}. \tag{2-13}$$

The delay for path p, given by $t_p = l_p / c$ ($c = 1500$ m/s is the speed of sound in water) and l_p is the path length for path p [26]. $r_p = 0,1,3,5,7$ for each path respectively, the path lengths can be calculated using planar geometry.

2.2.7 Underwater Acoustic Noise Model

An empirical model for the noise of the acoustic underwater channel in shallow water from the analysis of field

data measurements has been presented in [27]. In this paper, a probability density function for the noise amplitude distribution is proposed and the associated likelihood functions are derived. As a result, an expression to the probability of symbol error for binary signalling is presented for the channel. In addition, the results of simulations conducted using the field collected noise samples are presented in order to verify the noise effect on the performance of underwater acoustic communication binary signalling systems. The analysis of field data measurements has shown that the noise amplitude distribution presents a good fit with the author's *t* distribution. From [27] the symbol error probability of the binary UWA noise (UWAN) channel can be expressed as:

$$P_e = k\sqrt{2E_b/N_o}\int_0^{\infty}\left[(4E_b/N_o)(x+1)^2+5\right]^{-2.75}dx. \tag{2-14}$$

where x is a vector of M discrete amplitude levels of noise, integer $k = 1,2,\ldots..,M$, and E_b/N_o is the energy per bit to noise power spectral density ratio.

2.2.8 Underwater Acoustic Channel Simulator

The signal transmission in underwater acoustic communications can be modelled as a time-varying channel. In particular, the noise-free signal at the receiver is described as a convolution [7]:

$$y(t) = \int_{-\infty}^{\infty} h(t,\tau)s(t-\tau)d\tau, \qquad t \in [0, Ts], \tag{2-15}$$

between the channel impulse response $h(t,\tau)$ and the source signal $s(t)$, where Ts is the signal duration. This description of linear time-variant systems is quite generic. In underwater acoustic communications, other variants of the description may also be used. For example, for a channel with discrete multipath components, the model [9, 28, 29] used and UWA channel is represented as:

$$c(\tau,t) = \sum_p A_p(t)\delta(\tau - \tau_p(t)). \tag{2-16}$$

Within a data block of interest, each path delay can be associated with one Doppler scale factor as:

$$\tau_p(t) = \tau_p - a_p t, \tag{2-17}$$

and the path amplitudes are assumed constant within one data block $A_p(t) \approx A_p$. Furthermore, we assume that the UWA channel can be well approximated by N_p dominant discrete paths. Hence, the channel model can be simplified to be:

$$c(\tau,t) = \sum_{p=1}^{N_p} A_p\delta(\tau - [\tau_p - a_p t]). \tag{2-18}$$

Due to the adopted channel model, the received pass-band signal over the UWA becomes:

$$\tilde{y}(t) = \sum_p A_p e^{j2\pi f_c(t+a_p t-\tau_p)}\sum_{k=0}^{N-1} a_k p(t + a_p t - \tau_p)e^{j2\pi f_k(t+a_p t-\tau_p)} + \tilde{n}(t), \tag{2-19}$$

where $\tilde{n}(t)$ is the additive white Gaussian noise.

2.3 Channel Coding Performance for Multicarrier Modulation in Underwater Acoustic Communication

It is required that digital communication systems, particularly for underwater use, perform accurately and reliably in the presence of noise and interference. Among many possible ways to achieve this goal, forward error correction coding is the most effective and economical. The fast temporal variations, long multipath delay spreads, and severe frequency-dependent attenuations of underwater acoustic communication channels that impede underwater acoustic data transmission are extremely complex. To alleviate this problem, channel coding is indispensable in UWA communication systems to increase the reliability [30]. Also, for underwater communication, commonly used symbol demodulation schemes do not depend on the noise power, so bit error performance without error correcting coding will not be improved [31]. Here, forward error correction (FEC) is a type of error correction which improves simple error detection schemes by enabling the receiver to correct errors once they are detected. This reduces the need for retransmissions and energy consumption [32].

The power of error correcting codes increases with the channel coding length constraint and approaching the Shannon limit with a large number of length constraints. But in return, the complexity of the decoder also increases with length constraint [33]. For these reasons, it is desirable to construct long codes and minimize the complexity of the decoder. The concatenation of codes is a cheap solution for multicarrier modulation in underwater acoustic communication [34]. The major drawback of the concatenation code is that the decoder is unable to decode correctly in the presence of a burst of erroneous bits. Hence, an interleaver can be designed to introduce a dependency between the bit inputs. In order to minimize the error rate, two evolved coding schemes are employed [32] which are summarized in the following two subsections.

2.3.1 Reed Solomon Coder

Reed Solomon codes (n,k,t) are cyclic codes, built from n symbols with a maximum of $n = q-1$, where q is the number of elements in the Galois Field (GF^q) $(q = 2^n)$ and t is the power correcting code. So the number of control symbols is $2t$.

Joël Trubuil et al. [35] developed a sufficiently robust acoustic link allowing the transmission of different information using the Reed Solomon coder and conventional coding to protect data transmission over the underwater acoustic channel. Where an underwater acoustic link is designed to transmit different kinds of data as text, images and speech signal, a blind spatial-temporal equalizer is used to reduce different underwater acoustic perturbations. To improve the underwater acoustic link performance and obtain a higher code rate, Reed Solomon block turbo codes (R-S BTC) have been introduced and tested in real conditions, with the aim of decreasing the bit error rate (BER). Differential coding has been used to solve the phase ambiguities. A channel block coder algorithm is applied to the transmission of constant data. Where block codes are FEC codes, a limited number of errors can be detected and corrected without retransmission. Block codes have been used to improve the performance of a communications system when other means of improvement (such as increasing transmitter power or using a stronger modulator) are impractical [36].

2.3.2 Low Density Parity Check Code (LDPC)

LDPC codes are a special type of linear block code. The parity-check matrix H of LDPC codes are very sparse, i.e. they can be specified by a matrix containing mostly 0's [37]. It is used to reduce error codes and achieve credible transmission performance of underwater digital signals. It has also been recommended to use turbo codes in

underwater digital speech communication systems but simulation results in underwater digital speech systems discussed in [37] have shown that LDPC has a better performance than a turbo coder.

Modification in the LDPC has been proposed to match better multicarrier underwater communication systems [38] by focusing on matching the coding symbols with the modulation symbols. Experimental results show that with real data, whenever the uncoded BER is below 0.1, normally no decoding errors will occur. For the rate of $1/2$ of non-binary LDPC codes used in [38] it is consistent with the simulation results. The unencoded BER can serve as a quick performance indicator to assess how likely the decoding will succeed. The research results show that the LDPC coder system has a better error correction performance and can achieve a better BER under the relatively lower SNR [30].

Performances of LDPC codes with different parameters over different underwater acoustic communication channels are studied [30], by adjusting the encoding and decoding parameters according to different underwater acoustic channels.

When an LDPC coder is used as the channel coder for zero-padding orthogonal frequency division multiplexing (ZP-OFDM) multicarrier modulation, the spectral efficiency ς and the data rate R are [39, 40]:

$$\varsigma = \frac{T}{T+T_g} \cdot \frac{|S_D|}{K} \cdot r \cdot \log_2 M \qquad bits/s/Hz, \tag{2-20}$$

$$R = \alpha B \qquad kb/s. \tag{2-21}$$

where T is the ZP-OFDM symbol duration, T_g is the guard interval, K is number of all subcarriers, $|S_D|$ is data subcarrier in total, r is the rate of non-binary LDPC code [38], M is the quadrature amplitude modulation symbol, and B is the channel bandwidth. LDPC produces high block error rate (BLER) performance in ZP-OFDM multi-carrier systems.

2.4 Multi-Carrier Modulation for Underwater Acoustic Communications

Multi-carrier modulation systems are well known to be attractive for communications through multi-path communications channels. The traditional approach expects the symbol duration of the transmitted signal to be larger than the channel delay spread. This results in a low rate "sampling" of the channel impulse response (once per symbol in each sub-channel) and a sub-channel bandwidth that is less than the coherence bandwidth of the physical propagation channel [41].

Multi-carrier modulations (MCM) have become popular in UWA channel for two reasons. First, a signal can be processed in a receiver without the increase of noise or interference caused by linear equalization of a single carrier signal; second, the long symbol period used in MCM ensures greater immunity to impulse noise and fast fades [42].

2.4.1 Orthogonal Frequency Division Multiplexing

Multicarrier modulation in the form of orthogonal frequency division multiplexing (OFDM) has been studied and implemented for broadband wired and wireless communications for the past two decades. OFDM is widely

adopted because of a number of its advantages as discussed in [43-45], namely: (1) orthogonality of subcarrier signals that allows: (a) Easy generation of transmit signal through an inverse fast Fourier transform (IFFT) block. (b) Easy separation of the transmitted data symbols at the receiver through a fast block. (c) Easy equalization through a scalar gain per subcarrier. (d) Easy adoption to multiple-input multiple-output (MIMO) channels. (2) Closely spaced orthogonal subcarriers partition the available bandwidth into a maximum collection of narrow sub-bands. (3) Adaptive modulation schemes can be applied to subcarrier bands to maximize bandwidth efficiency/transmission rate. (4) The very special structure of OFDM symbols simplifies the tasks of carrier and symbol synchronizations.

OFDM as an MCM is particularly efficient when noise is spread over a large portion of the available bandwidth. It transmits signals over multiple orthogonal sub-carriers simultaneously and performs robustly in severe multi-path environments achieving high spectral efficiency. OFDM is used in underwater communications as a superiour alternative to single carrier broadband modulation to achieve high data rate transmission [9, 16, 46, 47]. It has been proved to be an effective technique for combating the multipath delay spread without the need for complex time-domain equalizers, due to its robustness against frequency selective fading and narrowband interference. In fact, if the number of subcarriers is large enough, each subcarrier only deals with flat fading rather than with frequency selective fading as a wideband carrier does.

The narrowband interference will affect only one or two of the whole bunch of subcarriers. The major issue in applying OFDM to underwater channels is the motion induced Doppler distortion which creates a non-uniform frequency offset in a wideband acoustic signal [9, 16, 46, 47].

2.4.1.1 ZP-OFDM for Underwater Acoustic Communication

Zero-padded (ZP) [39, 40, 48] OFDM has been extensively investigated for high data rate underwater acoustic communication. Frequency-domain oversampling methods [40] are used to avoid information loss incurred by the overlap-add operation. A larger FFT size is used to improve system performance over underwater acoustic channels with significant Doppler spread. The system is validated using real data collected from field experiments. Zero padding is used instead of the conventional cyclic prefix in order to save transmission power during the long guard interval. ZP-OFDM transmitted and received signals in the time domain during underwater channel paths signals after implemented to make zero padded guard interval accept channel path delay shown in Fig. 2.3 [40].

For ZP-OFDM with symbol duration T, the subcarrier spacing is $\Delta f = 1/T$, and the subcarriers are located at frequencies

$$f_k = f_c + \frac{k}{T}, \qquad k = \frac{-K}{2}, \ldots\ldots, \frac{K}{2-1}, \tag{2-22}$$

where f_c is the center frequency, and K is the total number of subcarriers, leading to the bandwidth $B = K/T$. $s[k]$ denotes the information symbol on the k^{th} subcarrier. The transmitted pass-band signal is [40]:

$$\tilde{x}(t) = 2\,\mathrm{Re}\left(\sum_{k \in S_A} s[k] e^{j2\pi f_k t} g(t) \right), \qquad t \in [0, T'], \tag{2-23}$$

where T' is the ZP-OFDM block duration as shown in Fig. 2.3 [40].

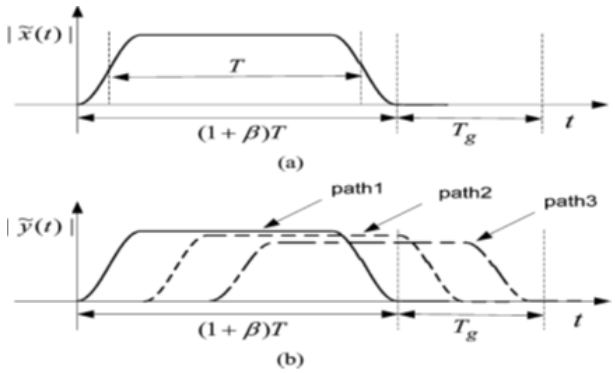

Fig. 2.3. Illustration transmitted and received signals in the time domain. (a) One transmitted ZP-OFDM block. (b) One received ZP-OFDM block. Taken from Zhaohui Wang et al. [40].

The baseband signal $z(t)$ is obtained with the pass-band to baseband downshifting and low-pass filtering, leading to [40]:

$$z(t)=\sum_{p=1}^{N_p}A_p e^{j2\pi f_c(b_p t-\tau_p)}\sum_{k\in S_A}s[k]e^{j2\pi m/k((1+b_p)k-\tau_p)}g((1+b_p)t-\tau_p), \tag{2-24}$$

where b_p represents the residual Doppler rate satisfying:

$$1+b_p=\frac{1+a_p}{1+\hat{a}}. \tag{2-25}$$

ZP-OFDM saves the power transmitted and increases channel capacity. In [49] authors derived bounds to the channel capacity of OFDM systems over the underwater acoustic fading channel as a function of the distance between the transmitter and the receiver.

2.4.1.2 Pilot Signal Design for OFDM Multicarrier Transmission

The challenges in pilot design for multicarrier transmission over underwater acoustic time-varying channels are two-fold [50, 51]: (1) sets of adjacent observations are needed to estimate the inter-carrier interference (ICI) coefficients. (2) Keeping pilot and data symbols orthogonal at the receiver is challenging due to the ICI. Generally there are three types of pilot insertion methods for OFDM systems: comb-type, block-type and hexagonal grid-type [52]. Random selection of pilot subcarriers is motivated by the compressive sensing [53] with the systematic use of pilot blocks in regular intervals as seen in non-sparse channel estimation of time-varying channels [39].

In [50] authors are interested in how to address the ICI between data and pilot subcarriers without guard zeroes. As spectral efficiency decreases, it is debatable whether data symbol carrying subcarriers should be used as observations in channel estimation, which also contain ICI originating from the pilot symbols. The performance under varying amounts of pilot overhead has also been studied. Specifically, the authors in [50] of the study were looking for an optimum trade-off between using more pilots or a more robust modulation scheme to achieve the highest spectral efficiency.

2.4.1.3 OFDM Based on Discrete Cosine Transform for Underwater Acoustic Communication

The orthogonal feature of conventional OFDM can also be achieved by inversing the DCT (IDCT)-DCT structure for underwater communication, which reduces the implementation area and increases computational speed, as only a real calculation is required. This system provides higher peak-to-average power ratio (PAPR) reduction and

achieves better noise immunity and hence a better BER performance than standard OFDM while maintaining a low implementation cost [42, 54].

DCT based OFDM is a better technology for UWA communication because the bandwidth required for DCT is half of that required for DFT when both systems have the same number of subcarriers which will be matched with underwater channel limited bandwidth. It has also been shown that the speed of calculation of orthogonal components is increased three fold while the implementation size reduces to half as compared to a fast FFT based design [54]. Furthermore, it is known that the DCT basis have excellent spectral compaction and energy concentration properties which in turn lead to improved performance with suitable channel estimation [54]. As DCT is widely adopted in image/video coding standards, by using it for modulation/demodulation on frequency selective channels it will result in a better integrated system design and a reduced overall implementation cost [54].

2.4.1.4 Orthogonal Signal-Division Multiplexing for Underwater Acoustic Communication

Orthogonal signal-division multiplexing (OSDM) is proposed as an UWA communication system scheme that measures the multipath profile without an adaptation or interpolation process to achieve stable communication in doubly spread channels [55]. The performance comparison of the OSDM scheme and existing schemes in doubly spread channels has been investigated. The ill-conditioned problem exists for conventional OSDM, which employs a single transducer in the receiver. The introduction of a multichannel receiver has been found to be effective against the ill-conditioned problem. Evaluation of OSDM communication is done by comparing it to existing schemes with single-carrier recursive least square differential feedback equalizer (RLS–DFE) and OFDM [56]. OSDM with a multichannel receiver is attractive in terms of communication quality. It achieves much better BER performance compared to the other schemes in both static and dynamic channels, although its complexity is less than that of RLS–DFE. OSDM can become in the future a viable alternative offering a highly reliable communication environment for UWA communication with multipath and Doppler spread (tested only for shallow water) with practical complexity [55].

2.4.1.5 Time Domain Synchronous Orthogonal Frequency Division Multiplexing

A time domain synchronous orthogonal frequency division multiplexing (TDS-OFDM) scheme with dual pseudorandom noise (PN) sequence [57] is proposed in [58] for UWA communication. A TDS-OFDM system is used for the underwater acoustic channel as shown in Fig. 2.4. [58].

Conventional performance of a ZP-OFDM receiver is severely limited by the ICI due to the fast channel variations within each OFDM symbol. Furthermore, the UWA channel is wideband in nature due to the small ratio of the carrier frequency to the signal bandwidth [40, 59]. In [60], a cyclic shift keying spread spectrum OFDM method is proposed as a UWA communication system.

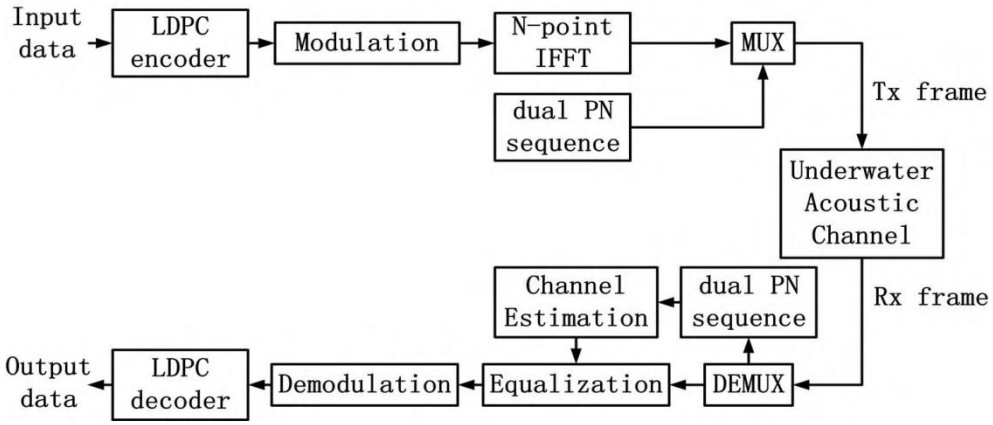

Fig. 2.4. TDS-OFDM system for Underwater Acoustic Channel. Taken from Jinxing Hao et al. [58].

The aim of this work was to solve the problem of low data rates of direct sequence spread spectrum underwater acoustic communication [61] and that of the complexity of the receivers of the M-array spread spectrum. This study also aimed to improve bandwidth efficiency and bit rates. This method results in a high data rate compared to conventional methods and a low bit error rate.

The main problem with TDS-OFDM is the inter-block interference between the training sequence and OFDM data blocks. To solve this problem, extensive efforts have been made. The proposed methods can be divided into two categories [146]. The first one is a classical iterative interference cancellation algorithm [165] and its extension methods without changing the TDS-OFDM system frame structure [166]. However, only slight improvements can be achieved with these methods [146], especially in long tap delay UWA channels. The other categories rely on modification of the TDS-OFDM frame structure for significant interference cancellation [146]. For example, within OFDM data blocks, redundant frequency-domain pilots are scattered in the unique word OFDM (UW-OFDM) [167] to generate the time-domain training sequence (TS) so that a significant interference reduction can be achieved. But it cannot remove the interference reduction of OFDM data blocks to the TS. Another simple and efficient way is the dual PN padding OFDM (DPN-OFDM) scheme [168], where two repeated guard intervals are used in every TDS-OFDM symbol to avoid the interference from the OFDM data block to the second PN sequence. Thanks to DPN-OFDM simplicity and good performance, DPN-OFDM is currently under extensive investigation and hardware implementation for the evaluation standard of digital terrestrial multimedia broadcast (DTMB) [146, 168, 169]. However, the duplicated guard interval length causes a significant decrease in the energy and system spectrum efficiency, especially in the channels with significance tap delay such as an UWA channel.

The TDS-OFDM (also known as known symbol padding KSP-OFDM [171]) is the key of DTMB technology in the Chinese digital television terrestrial broadcasting (DTTB) standard [146]. TDS-OFDM is proposed to avoid the use of a pilot signal for energy and bandwidth efficiency as in CP-OFDM and ZP-OFDM. However, TDS-OFDM energy and spectrum efficiency can cause significant bit error rate performance deterioration due to IBIs between the training sequence and OFDM data blocks [172].

The structure comparison among CP-OFDM, ZP-OFDM and TDS-OFDM signals in the time domain is shown in Fig. 2.5, in which the CP used by CP-OFDM is replaced by a zero padding segment in ZP-OFDM and by a PN training sequence in TDS-OFDM. The i-th TDS-OFDM transmitted signal frame denoted by

$s_i = [s_{i,0}, s_{i,1}, \ldots, s_{i,P-1}]^T$ consists of two independent parts: a known PN sequence $c_i = [c_{i,0}, c_{i,1}, \ldots, c_{i,M-1}]^T$ of M length and OFDM data blocks $x_i = [x_{i,0}, x_{i,1}, \ldots, x_{i,N-1}]^T$ of length N:

$$S_i = \begin{bmatrix} C_i \\ X_i \end{bmatrix}_{P\times 1}, \tag{2-26}$$

where the length of the TDS-OFDM signal frame is $P = M + N$.

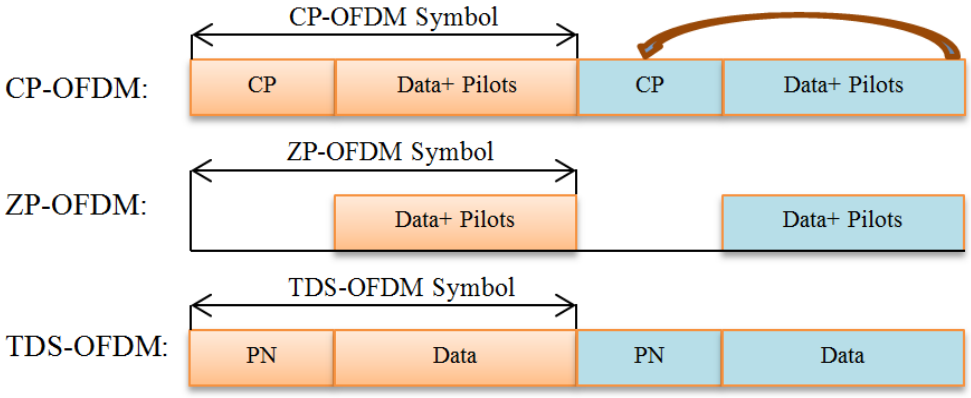

Fig. 2.5. TDS-OFDM, ZP-OFDM and CP-OFDM signal structure comparison in the time domain.

In multipath channels, IBIs between the OFDM data blocks and PN sequences can be illustrated as in Fig. 2.6. With perfect channel estimation, such mutual interference can be completely removed from the TDS-OFDM data block. As such, after PN sequence subtraction, TDS-OFDM is equivalent to ZP-OFDM. The impact of mutual interference between the PN sequence and TDS-OFDM data blocks in the conventional TDS-OFDM is solved by using the DPN-OFDM technique. In a DPN-OFDM frame, the guard interval is duplicated to receive a PN sequence free of IBI, and based on this, perfect channel estimation can be obtained. The difference between the received frames of these TDS-OFDM schemes over multi-path channels is shown in Fig. 2.6.

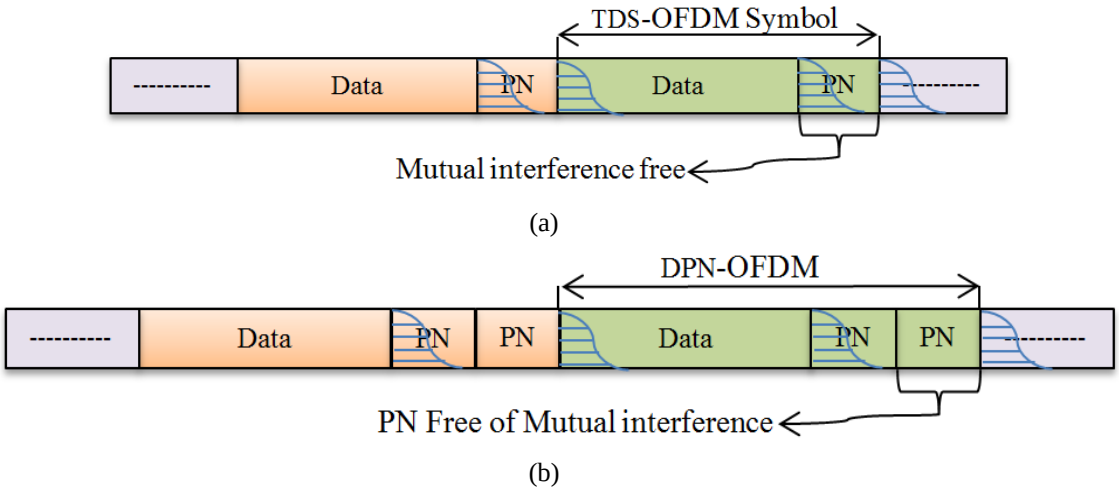

Fig. 2.6. TDS-OFDM received frame. (a) Conventional TDS-OFDM scheme; (b) The dual PN padding OFDM (DPN-OFDM) scheme.

2.4.1.6 Power and Bit Loading for Underwater Acoustic OFDM System

Adaptive bit and power loading is a constraint optimization problem with generally two cases of practical interest, where the objectives are the achievable data rate maximization (RM) and system margin maximization (MM) [62].

In [51, 63, 64] researchers propose a different optimization model for UWA channels, which is achieved by two algorithms: one is the bandwidth-efficient bit-loading algorithm, the other is the Lloyd algorithm based limited feedback procedure. These aim at minimizing the power consumption under constraints of the constant symbol data rate and desired BER. Algorithms are employed to quantize the CSI at the receiver and construct the codebook, which is adopted to achieve the limited feedback process. After selecting an initial bit-loading vector upon the current CSI, the receiver will broadcast its index to the transmitter, then the transmitter will compute the bandwidth-efficient bit-loading algorithm and allocate the corresponding power and bits to each OFDM subcarrier. Algorithms are also used for UWA cooperative communication systems, which involve the Decode-and-Forward (DF) transmission protocol [51, 65].

The ambient noise power $\omega(f_i)$ for each OFDM sub-carrier can be proposed as [51, 65]:

$$\omega(f_i) = \int_{f_{iL}}^{f_{iH}} N(f_i) d(f_i) = \int_{f_{iL}}^{f_{iH}} 10^{\frac{N_0}{10}} \cdot f_i^{-\frac{9}{5}} d(f_i), \tag{2-27}$$

where f_{iL} and f_{iH} are the bound of $i-th$ sub-carrier frequency. The maximum capacity of a UWA SISO-OFDM system with total system transmission power constraint is described as [51, 65]:

$$\begin{aligned} &\max_{\varepsilon_i} \quad C = \sum_{i=1}^{N} \Delta f \cdot \log_2\left(1 + \frac{\varepsilon_i g_i}{\Gamma}\right) \\ &s.t. \quad \sum_{i=1}^{N} \varepsilon_i \le \varepsilon_s, \quad \varepsilon_i \ge 0, \quad i = 1,\ldots,N \end{aligned}, \tag{2-28}$$

N is the number of sub-channels, Δf is the sub-channel transmitted bandwidth, ε_i is the transmitted power in the $i-th$ sub-channel, ε_s the total transmitted power, g_i is the sub-channel power gain in which the power loading will be based on this parameter, and $g_i = |H_i|^2 / \sigma_i^2$, where $|H_i|$ is the fading amplitude of the $i-th$ sub-channel, $|H_i|^2$ is the sub-channel power, σ_i^2 is the ambient noise power and its constant of $i-th$ sub-channel, and $\varepsilon_i g_i$ is the SNR or carrier-to-noise ratio (CNR) per sub-channel. Γ is the "SNR gap" for characterizing the difference between the SNR needed to achieve a certain data rate for a practical system and the theoretical limit.

2.4.1.7 OFDM Receiver Designs for Underwater Acoustic Communication

OFDM receiver designs for underwater acoustic channels with user and path specific Doppler scaling distortions were proposed in [66]. This method was motivated by the cooperative communications framework [67], where distributed transmitter/receiver pairs may experience significantly different Doppler distortions, as well as by the single user scenarios, where distinct Doppler scaling factors may exist among different propagation paths. The conventional approach of front end resampling that corrects common Doppler scaling may not be appropriate in such scenarios, rendering a post FFT signal that is contaminated by user and path-specific inter-carrier interference. To counteract this problem, the authors propose a family of front end receiver structures that utilize multiple resampling (MR) [68] branches, with each one matched to the Doppler scaling factor of a particular user and path. Following resampling, FFT modules transform the Doppler shift compensated signals into the frequency domain for further processing through linear or nonlinear detection schemes. As part of the overall receiver structure, a

gradient descent approach is also proposed to refine the channel estimates obtained by standard sparse channel estimators.

2.4.2 Filter-bank Multicarrier for Underwater Communications

In order to combat the time dispersion of UWA channels, it has been proposed to deploy the OFDM technique with a sufficiently long CP. Moreover, to keep the bandwidth efficiency of the transmission high, long OFDM symbols that are at least four times the length of the CP should be used. Due to small sideband power leakage, filter bank multicarrier techniques are considered as interesting alternatives to traditional OFDMs for spectrum pooling cognitive radio [69]. This leads to an OFDM system in which channel variation over each OFDM symbol may be unacceptably large, thus, resulting in a significant level of ICI [70]. For that filter bank multicarrier (FBMC) systems can be optimized for robust performance in the doubly dispersive UWA channels [70]. OFDM multicarrier has a loss bandwidth efficiency of the transmission due to the allocation of 20% of each OFDM symbol to its CP. This is equivalent of saying the CP length is one quarter of the length of each fast FFT block in the OFDM system. Moreover, since the length of CP should be at least equal to the duration of the channel impulse response, and the latter is usually very long in UWA channels, very long symbols are used in the OFDM systems for UWA communications [70]. On the other hand, to avoid ISI, the prototype filter $p(t)$ is designed as a Nyquist filter [71, 72]. The design method proposed in [73] constructs an isotropic filter according to the equation.

$$p(t) = \sum_{k=0}^{L} a_k h_{4k}(t), \tag{2-29}$$

where $h_k(t)$ are the set of Hermits functions defined as [70]:

$$h_n(t) = \frac{1}{(2\pi)^{n/2}} e^{\pi t^2} \frac{d^n}{dt^n} e^{-2\pi t^2}. \tag{2-30}$$

In [70] it is noted that the presence of the channel will result in a disturbed ambiguity function, $A_p^d(\tau, v)$, in which the null points of $A_p(\tau, v)$ are smeared out. Thus, it is argued that to design a robust prototype filter, the constraints on the nulls of the ambiguity function $A_p(\tau, v)$ may be relaxed. Each null point is replaced by a region in the (τ, v)-plane, which is termed a null region. Thus, to design $p(t)$, one should choose to minimize the cost function:

$$\zeta = \gamma_0 \int_{Ao} \left| A_p(\tau, v) - 1 \right|^2 d\tau\tau d + \sum_{k=1}^{N} \gamma_k \int_{A_k} \left| A_p(\tau, v) \right|^2 d\tau dv. \tag{2-31}$$

where γ_k are sets of positive weighting factors, A_0 is the region around $(\tau, v) = (0,0)$ over which the peak of $A_p(\tau, v)$ remains approximately equal to one, and A_k for $k = 1,2,\ldots\ldots,N$ are sets of null regions.

UWA communication methods using a class of FBMC systems were proposed [70]. This class of FBMC system was designed to be robust against dispersions in time and frequency domain. When the FBMC technique is compared with OFDM, it is clear that there is a wide gap between the performance of FBMC and OFDM in terms of saving bandwidth [70]. For the single-user communications case, OFDM offers lower complexity while FBMC offers higher bandwidth efficiency. For the MIMO communications case, OFDM provides full flexibility while FBMC can be used in certain MIMO setups. Only filtered multi-tone modulation (FMT) can offer the same flexibility as OFDM. However, FMT suffers from the same bandwidth loss as OFDM [74]. FBMC for underwater

communication still has not been the focus of much research and will need to be investigated more in the future.

2.4.3 MIMO for Underwater Acoustic Channel

Multi-input multi-output (MIMO) techniques have been extensively discussed in underwater acoustic communications to overcome the bandwidth limitation of an undersea channel [75]. Combined with OFDM modulation, MIMO techniques provide substantial spectral efficiency and reasonable robustness against frequency fading while keeping simple equalizer structure [76-79]. A long acoustic multipath, however, limits the applicability of MIMO channel estimation methods that require inversion of a matrix whose size is proportional to both the number of transmitted elements and the multipath spread. To overcome this problem, an adaptive algorithm is used [80] that does not require matrix inversion and operates in a decision-directed manner, thus reducing both the computational complexity and the overhead. Reduction in complexity has been sought through selection of significant impulse response coefficients which results in a reduced-size matrix inversion [81-83]. MIMO-OFDM design consists of the following key components: (1) null subcarriers are inserted at the transmitter to facilitate the compensation of Doppler shifts at the receiver; (2) pilot tones are used for MIMO channel estimation, and (3) an iterative receiver structure is adopted that couples MIMO detection with channel decoding [75].

OFDM has a number of desirable features, including low complexity of implementation and mature technologies that keep it as the dominant technology for single-user (point-to-point) underwater communications. Moreover, while OFDM can be easily adopted for MIMO channels, development of MIMO-FBMC systems/networks is still nontrivial and may be very limited. Only FMT, the less bandwidth-efficient member of the class of FBMC systems, can offer a similar level of flexibility as OFDM in MIMO channels. Therefore, the poor frequency spectra of subcarrier signals in OFDM are the main issue that may limit the applicability of OFDM in present and future development of broadband underwater communication systems. FBMC [84], on the other hand, is an elegant method to underwater multicarrier communications.

2.5 Underwater Acoustic channel Estimation

To reduce the computation complexity of signal processing and improve the accuracy of symbol detection, receiver structures that are matched to the physical-feedback equalizer were designed first in [85]. These rely on an adaptive channel estimator for parameters computation. The channel estimation complexity is reduced in size by selecting only the significant components whose delay span is often much shorter than the multipath spread of the channel. This estimation is used to cancel the post-cursor ISI prior to the linear equalizer involved. Optimal coefficient selection is performed by truncation in magnitude. The advantages of this approach are the number reduction in receiver parameters, optimal implementation of sparse feedback, and efficient parallel implementation of adaptive algorithms for the multichannel pre-combiner, fractionally spaced channel estimators and the short feed forward equalizer filters [86].

Coherent modulation schemes such as phase shift keying (PSK), along with adaptive decision feedback equalizers (DFE) for spatial diversity, are used as an effective way of communication in such channels [87, 88]. However, the long delay spread and rapid time variation of the channel often make this approach computationally too complex

for real-time implementations [89]. Although the underwater channel has a long impulse response, the multipath arrivals are often separated. This introduces the possibility of using a sparse equalizer with tap placement based on the actual channel response. This can potentially dramatically reduce the number of required taps and hence leads to a lower complexity, faster channel tracking and an enhanced performance [90].

In [90] the authors have proposed an algorithm to track the channel explicitly and determine the tap placement for the DFE based on this channel estimate. The equalizer and the channel estimator are updated individually throughout the packet. The channel estimator can also update either the whole estimation or a set of selected channel coefficients at one time in batch, depending on computational and channel considerations [91].

The channel estimation algorithms can cope with spatial diversity by multi-channel combining before equalization. Adaptive estimation is performed using minimum mean square error as the overall optimization criterion. The receiver is implemented in a multichannel configuration which provides the array processing gain necessary for many of the underwater acoustic channels. The complexity of the detection algorithm is linear with respect to the number of received elements and dependent on the modulation level of the transmitted signals [92]. DFE structures may suffer from error propagation due to the feedback of possible erroneous decisions in the loop.

Hence, powerful FEC codes are needed to ensure low BER communication. Turbo codes are a class of powerful codes that utilize iterative information exchange between two decoders to correct errors. Inspired by this idea, researchers have developed turbo equalization techniques where iterative interactions between the equalizer and a decoder result in joint estimation, equalization and decoding [93].

A new channel estimation equalization and phase correction scheme has been developed in [85]. The new scheme estimates the acoustic fading channel without separating the phase drift and phase rotation for each symbol and then the SIMO received signals are equalized and combined. Finally, the phase drift/rotation of symbols is corrected per group of symbols using estimated average phase drift/rotation.

Authors in [39] considered sparse channel estimation using subspace methods and compressed sensing on channels subject to moderate Doppler effects and extended the compressed sensing receivers to handle channels with different Doppler scales on different paths. Channel estimation and efficient symbol detection were studied by J. Ling et al. [94], where the design of state-of-the-art training sequences and sparse learning via iterative minimization (SLIM) algorithm was proposed to achieve sparse channel estimation. The authors developed a conjugate gradient (CG) based detector, which exploits the diagonalization properties of the circulate channel matrix to significantly improve the performance of MIMO underwater acoustic communications.

The UWA communication system under consideration employs OFDM and receiver pre-processing to compensate for the Doppler effects before channel estimation. First, the original homotopic algorithm was extended from real-valued signals to the complex valued ones. Then two enhancements to the sparse recovery-based UWA channel estimator were proposed by exploiting the UWA channel temporal correlations, including the use of a first-order Gauss–Markov model and the recursive least-squares algorithm for channel tracking. Moreover the authors propose a scheme to optimize the pilot placement over the OFDM subcarriers based on the discrete stochastic approximation.

Sparse channel estimation for multicarrier underwater acoustic communication were proposed by Christian R. Berger et al. [39]. Based on the path-based channel model, subspace methods are well-known techniques from the

array-processing literature used to address the channel estimation problem. Also, recent compressed sensing techniques were employed to develop some new methods, namely orthogonal matching pursuit (OMP) and basis pursuit (BP) [95, 96], based on the continuous time characterization of the path delays. Also the compressed sensing receivers can be extended to handle channels with different Doppler scales on different paths, supplying ICI pattern estimates that can be used to equalize the ICI [39].

Using extensive numerical simulation and experimental results, researchers found that in comparison to the LS receiver, the subspace methods show significant performance improvements on channels that are sparse but perform worse if most received energy comes from a diffuse multipath. To improve LS estimation, a simple windowing and de-windowing technique has been used to improve the accuracy of an existing basis expansion model (BEM) and develop a windowed least-squares (WLS) estimator for doubly-selective fading channels [97]. The compressed sensing algorithms do not suffer this drawback, and benefit significantly from the increased time resolution using sophisticated dictionaries. When accounting for different Doppler scales on different paths, BP can effectively handle channels with very large Doppler spread.

2.6 Doppler Shift Estimation for Underwater Acoustic Communications

In underwater acoustic transmissions, Doppler effects can be caused by propagation medium movements or by the relative velocity between the transmitter and the receiver [24]. It often causes additional difficulties for the processing of received signals. For instance, for underwater acoustic communications with submarines navigating at speeds up to 25 knots (12.8 m/s) it is challenging, due to the large Doppler range that the receiver must be able to cope with. Doppler effects result in a compression/expansion of the transmitted signal [98]. At the receiver side, it is desirable to remove the effect of these phenomena before any further processing, such as timing and carrier recovery. A receiver which performs optimal phase synchronization and channel equalization jointly has been suggested for underwater communication systems [99].

Based on cross-correlation among training sequences located at the beginning and end of transmitted data frames, an algorithm was developed for Doppler shift estimation by Joël Trubuil [24]. From these training sequences two phase estimates are calculated, a coarse one and a precise one. The precise estimation has a much smaller ambiguity range than the coarse one, but it yields higher precision for the estimated Doppler frequency. The authors showed that a convenient combination of the coarse and precise phases leads to a good Doppler shift estimation within the speed range under consideration in the particular application discussed. Frequency-dependent Doppler shifts were caused by the low carrier frequency of the underwater acoustic channel communication.

Depending on the null subcarrier of the ZP-OFDM, multi-carrier facilitates Doppler compensation, and the pilot subcarriers used in channel estimation, where an application of OFDM is investigated in wideband UWA channels with non-uniform Doppler shifts [5]. To compensate for the non-uniform Doppler distortion, a two-step approach was used by resampling followed by high-resolution uniform compensation of the residual Doppler. Also based on this, a block-by-block receiver is suitable for fast-varying channels. Based on the availability of pilot tones in the OFDM transmission, a method was developed to estimate the offset parameters, and a hybrid channel estimator was then proposed to combine the offset compensated [100].

Compressed sensing (CS) can be developed as a method to solve the channel estimation problems for an UWA

system. Based on the existence of a sparse representation of the treated signal and an over-complete dictionary with a set of non-orthogonal bases, in [101] a new type of channel estimator using the compressed sensing theory is proposed, leading to a sparse channel estimation from the high dependence on Doppler compensation. Instead of using various compensation approaches, the proposed index is designed by modelling Doppler shifts as the atoms shift in an over-complete dictionary. From the results, this method improves the mean square error (MSE) performance with lower complexity and hardware cost. In addition, the method has the additional benefit of being less sensitive to Doppler rate variety.

2.7 Multicarrier Communication for Image and Video Transmission over an Underwater Acoustic Channel

Recently, there has been a growing interest in the development and deployment of image and video transmission techniques for underwater communication networks for scientific, environmental, commercial, and military purposes [2, 102]. High-speed underwater image transmission capabilities can enable the next generation of undersea expeditions. Efficient image transmission over band-limited underwater channels relies on two aspects [103]: (1) efficient data compression, and (2) bandwidth efficient modulation.

The compressed sensing technique [104] generates the minimum amount of information necessary for transmission which makes it useful in underwater communication. The combination of compressed sensing and nonlinear analogy processing has also been employed as joint source and channel coding [5]. Underwater multimedia sensor networks (UMSNs) [105] were proposed and immediately drew attention in the research community. However, the practical implementation of the current design of these applications directly depends on reliability and quality-aware communication capabilities of the deployed UMSNs. Comprehensive performance evaluation of error concealment and error correction algorithms for quality-aware image transmission over UMSNs is reported P. Sarisaray-Boluk [3].

For high-speed image transmission using multicarrier modulation [106, 107] minimum mean square error (MMSE) based equalization with the placement of a pilot symbol of three sub-carrier payload resulted in good performance close to the ideal performance of the equalization. Set Partitioning in Hierarchical Trees (SPIHT) is an efficient wavelet-based progressive image-compression technique, designed to minimize the MSE between the original and decoded image used for the high compression technique [108-111]. Since the underwater acoustic channel suffers from significant bit error rates, some mechanism to protect the encoded image is required.

The real-time wireless video transmission from an underwater vehicle to a surface platform represents one of the last milestones in the development of autonomous systems for ocean exploration and monitoring. The goal of combining video transmission over UWAC approaches is to mitigate the gap between the bit rate needed for video transmission and that supported by the acoustic channel. Konstantinos Pelekanakis [112] developed a video transmission technique for the underwater acoustic channel using the coherent single carrier modulation technique for phase detection. For this, a high rate acoustic link for underwater video transmission was implemented, where image encoding was accomplished using the JPEG DCT, scalar quantization and run-length Huffman encoding. Transmitter processing includes signal constellations.

A system employing variable rate quadrature amplitude modulation (QAM) techniques was designed and applied to the experimental data transmitted over a short vertical channel. Excellent results were obtained at bit rates up to 150 kbps, using modulation methods with bandwidth efficiency as high as 6 bits/sec/Hz. Such rates are sufficient to support real-time transmission of compressed video. The feasibility of real-time video transmission over short horizontal acoustic links was addressed in [113] where the standard MPEG- 4 video compression technique and a wavelet- based method were combined with acoustic transmission based on coded OFDM modulation to study the feasibility of video transmission using an acoustic system for deep-sea oilfield supervisory control and inspection. The wavelet-based encoder algorithm includes techniques that deal with spatial and temporal redundancies in the video sequences. In contrast to MPEG-4 compression, spatial redundancies are exploited by applying the discrete wavelet transform (DWT) to each of the frames composing the video sequence. A motion compensation algorithm [114] to reduce temporal redundancies has been incorporated, which is a core functionality of the MPEG-4 encoder. The codec is based on the popular differential pulse code modulation (DPCM) model, which is widely used in video compression standards. Its main components are the DWT multilevel decomposition of the input frame using the bi-orthogonal wavelet, and quantization of the DWT coefficients using vector quantization (VQ). The images are smoother due to the high quantization ratio for the high sub-bands of the wavelet decomposition and, as expected, no blocking effect is noticed at all [113].

2.8 Conclusion

In this chapter, we surveyed the major aspects of multicarrier communication techniques used for data transmission over the underwater acoustic channel, which can be summarized as: (1) underwater channel model and the challenges involved in multicarrier communication modulation such as OFDM and FBMC; (2) advances and areas emerging in underwater acoustics technology applications; (3) channel characteristics and channel models in reducing noise and channel noise estimates; (4) multicarrier modulation and multi-input multi-output techniques detailed description for underwater communication; (5) Doppler estimation and underwater channel estimation; (6) performance evaluation for different channel coders used for underwater acoustic multicarrier modulation; and (7) techniques used for high speed image and video transmission over UWAC.

Chapter 3
Unequal Error Protection for Image Transmission over Underwater Acoustic Channel

3.1 Introduction

Next generation techniques for underwater (UW) communication are expected to be able to support image transmission over underwater acoustic (UWA) channels with high-speed data transmission. However, only a limited data rate can be provided by the current acoustic communication. The main UW communication problems are the narrow bandwidth available as well as extensive multipath propagation in the UWA channel.

Transmission of progressive Set Partitioning In Hierarchical Trees (SPIHT) over an UWA channel has been discussed and proposed by Laura Toni [115]. Said and Pearlman [108] introduced the SPHIT algorithm to provide the highest peak signal–to–noise ratio (PSNR) value of received decoded image for a given compression ratio. PSNR is one of the most common methods to measure the quality of reconstructed images of lossy compression code. PSNR can be used as a human perception for reconstruction image quality [116]. Consequently, the SPHIT coder based on the wavelet algorithm is probably the most widely used for image compression, as well as being a basic standard of compression for all subsequent algorithms [111, 117].

The robustness of the transmitted image quality in the case of a deteriorating channel can be significantly increased [118] by using the unequal error protection (UEP) as well as providing graceful degradation. UEP was adapted to packet networks by Albanese et al. in the priority encoding transmission (PET) scheme [119].

UEP methods can be classified into three categories; 1) joint source channel coding (JSCC), where given the total transmission rate, both source rate and channel rate are optimized [120]; 2) rate allocation, where at a given total transmission rate both source rate and channel rate are fixed and the distribution of the channel rate over a source packets is optimized [121]; 3) UEP based on amodulation method using a HQAM modulation, where HQAM can be assigned unequal protection levels to the different transmitted bits [111, 117]. In this chapter, UEP based on a rate allocation system or HQAM modulation will be proposed for the UWA channel.

Quadrature amplitude modulation (QAM) provides an equal error protection (EEP) to all modulated bits. Equal error protection is the performance when unequal error protection is not used. HQAM is a modification technique for QAM, where UEP can be achieved. HQAM provides an UEP modulation method, where a step protection with two levels is used so that stronger protection is used for important bits and a low protection level for the less important bits. This method provides an UEP without increasing transmitted data rate and is not affected by channel characteristics [117].

Another UEP method is also proposed in this chapter. A rate allocation scheme for efficient image bit-stream transmission over the UWA channel with optimum bit rate is achieved based on channel characteristics. Optimum conditions are achieved in the sense that the comprehensive PSNR of the image transmission is maximized under channel bit rate and bit error rate constraints.

A modified Set Partitioning in Hierarchical Trees (M-SPIHT) image coder is proposed. Four different blocks of bit-streams based on their significance are generated. Significant bits, sign bits, set bits and refinement bits are achieved. In addition to the careful selection of each component and intuitive justification in the detailed system design, simulation results have also been included to demonstrate that the proposed scheme outperforms the equal error protection for image over underwater channel, indicating that the suggested scheme provides major improvements in the PSNR performance in contrast to well known solid coding schemes.

In this chapter, the SPHIT coder four output bit-stream groups is transmitted in four different flocks with different protection levels over a single carrier communication system, so as to reduce the total distortion of reconstructed images in the rate allocation UEP method. The four data groups obtained based on modified SPHIT are merged to produce two bit streams with two significance levels in the modulation UEP method. In the UEP based on the modulation method, the SPHIT algorithm is used as a source coder for encoded and 16-HQAM is used as a modulation transmission technique for the coded image over the UWA channel as a single carrier modulation system. Furthrmore, 16-HQAM is employed as a mapper technique applied and tested over the zero padded (ZP) orthogonal frequency division multiplexing (OFDM) ZP-OFDM multicarrier system. For different types of images and with different values of modulation parameters the PSNR of reconstructed image analysis is presented and carried out through the simulation and significant improvement is achieved.

This chapter has been organized as follows: a brief introduction about the SPHIT coder is proposed. Then, the Reed Solomon (R-S) coder for an UWA channel is proposed. Also, hierarchical 16-QAM modulation as an unequal error technique is described and analysed. Then, a novel rate allocation method is proposed for an UW communication system scheme and proposed UEP system simulations and results are presented. A summary of the major techniques and contributions of this chapter is included.

3.2 SPIHT Coding Overview

Sophisticated image compression techniques based on wavelet algorithms have been latterly reported for underwater transmission see [109, 110] for example. In these works, the SPIHT coder has been demonstrated as advantageous in many aspects including advanced bit error ratio, continuous-tone with a high compression ratio, lossy and lossless compression, and progressive processing. SPIHT was originally introduced by Said and Pearlman [108]. It gives the elevated PSNR for certain compression ratios for a broad assortment of image compression coders [111, 117]. As such, it has been widely used in image applications, and sets as an essential performance benchmark the evaluation of new image coding techniques. These features make the SPIHT compression technique a reasonable choice for realistic underwater transmissions. In this way, a simple source compression scheme was investigated previously by Chris Murphy [109], where the SPIHT source coding scheme was applied to underwater transmissions. The encoded bit-stream was divided into consecutive chunks before transmitting over underwater links. The expected attenuation of the UWA channel is extremely challenging and many different paradigms have been proposed to measure it.

The SPIHT [108] coder is a compression technique designed for progressive transmission. In particular, information bits are sorted according to the bit information significance. The protection level of transmitted data must take this feature into account and progressive protection is provided to the transmitted bits. This methodology

is used to reduce the distortion in the reconstructed image (reduce the difference between the original and the reconstructed images). In this section, a brief introduction and analysis about the methodology of SPHIT and how it works is introduced.

3.2.1 Coding Overview

Consider X as the original image and $\hat{X}$ as the reconstructed image in the SPIHT decoder. The mean square error (MSE) distortion measured between the original and the reconstructed images will be:

$$D_{MSE}\left(X-\hat{X}\right)=\frac{\left|X-\hat{X}\right|^2}{M_N}=\frac{1}{M_N}\sum_i\sum_j\left(X(i,j)-\hat{X}(i,j)\right)^2, \tag{3-1}$$

where $X(i,j)$ and $\hat{X}(i,j)$ are the original and reconstructed images pixels, respectively, at (i,j) location. The total number of pixels in the image is M_N. Furthermore, based on the Euclidean norm, the unitary transformation is invariant and can be represented as:

$$D_{MSE}\left(X-\hat{X}\right)=D_{MSE}\left(Y-\hat{Y}\right)=\frac{1}{M_N}\sum_i\sum_j\left(Y(i,j)-\hat{Y}(i,j)\right)^2, \tag{3-2}$$

where Y is the wavelet transform image and $\hat{Y}$ the reconstructed version of Y at the decoder based on wavelet decomposition. Based on eq. (3-2) when the decoder is with a correct decoded coefficient, the MSE is decreased by $\left|Y_{i,j}\right|^2/M_N$. In this way, for significant MSE reduction the coefficients with high magnitude should be transmitted first, where content of information is larger. Moreover, the value of each coefficient $(|y(i,j)|)$ can be ranked according to its binary representation, and the most significant bits should be transmitted first. This is actually the idea of bit-plane coding for progressive transmission. The SPIHT incorporates these two concepts. After ordering the coefficients by magnitude it will transmit first the most significant bits.

3.2.2 SPHIT Coded Output Bit Stream Classification

Set Partitioning in Hierarchical Trees (SPIHT) is an algorithm based on the hierarchical partitioning of wavelet coefficients into a spatial orientation tree, where all sub-bands coefficients are included in each branch to identify the particular position in the image [108, 118, 122]. The most insignificant coefficients are sequentially encoded together as an insignificant set symbol. An appropriately defined partitioning rule can be utilized to further split the insignificant set to efficiently extract the significant coefficients iteratively. In this way, based on the quality of the decoded image, the SPHIT coder is considered the best available coder due to progressive rate control and transmission, as well as coding process simplicity, etc. [108]. In particular, after image decomposition with 9/7 tap wavelets by the method reported by Antonini et al. [123], the general SPHIT coding algorithm encodes images by splitting the decomposed image into considerable sections on the basis of the significance classification function as:

$$S_n(\Gamma)=\begin{cases}1, & if \quad \max_{(i,j)\in\Gamma}\left\{\left|Y(i,j)\right|\geq 2^n\right\}\\ 0, & otherwise\end{cases}, \tag{3-3}$$

where $Y(i,j)$ represents the wavelet coefficient at the pixel (i,j) for n bit plane. The algorithm works in two iterative loops, the sorting loop and the refinement loop. To implement the SPHIT coder, the algorithm keeps three related groups [124]: first index of least insignificant pixels (LIP), the index of least significant pixels (LSP), and the index of least insignificant sets (LIS). A quantization process is applied to the sorted wavelet coefficients of these different groups using a certain quantization level. On the basis of a subset split into different groups ordered to their significant and the importance, notification encoded with a bit-stream to realize the best encoding quality than the overall the previous schemes [125]. In the compilation process, initially the algorithm takes in the LIP and evaluates its element's value versus updated threshold value and expresses their relevance by 0 or 1. For the significant coefficient, the sign of the coefficient is coded as well as the corresponding pixel. Then the coded pixel is sent to the LSP group. After checking the LIS, the threshold for significant set coefficients will be updated. The particular tree/set significant bits are classified into children or grandchildren based on the updated significance threshold. The insignificant set is represented as a zero-tree in the encoded bits in the output bit streams. At the end of each iteration, the classification process determines the refinement bits. The output from the SPIHT algorithm at the updated bit significance pixels is moved to the LSP at each threshold update, leading to the refinement of significant pixels with a reduced error rate. The threshold is increased with two steps until the output bit-stream ends.

The sorting pass will be performed on four separate lists rather than three: the first roster for least insignificant sets (LIS), the roster for the least insignificant pixels (LIP), the roster for the least significant pixels (LSP), and finally the roster for refinement path. The LSP and LIP consist of the nodes indicating the single pixels while the descendant nodes are represented by the LIS. The highest coefficients can be represented by the number of bits in the following formula:

$$n_{\max} = \log_2\left(\max_{\{i,j\}}\left\{\left|Y(i,j)\right|\right\}\right), \tag{3-4}$$

which is similar to that in [108]. While screening image pixels, classified LIP of pixels can be obtained based on the significance degree using eq. (3-3). The resultant $S_n(\Gamma)$ is then forwarded to the coded bits. All of those significance pixels will be sent to the LSP group with their sign bits sent to the output stream. Similarly, sets in LIS will be tested and sent forward to LSP if they are significant, or else into LIP. For refinement loops, the n^{th} generality significant bits of the coefficients in the LSP are used. By iteratively going through all n that are decreased by one, the desired rate can be obtained until every LSP node is processed.

A different type of bit with a different degree of vulnerability to errors has been obtained based on the SPHIT sorting algorithm. For significant coded bits a small error is more severe. Error in these significant bits can damage the local image. On the other hand, some other bits have a low sensitivity to errors.

Coded SPHIT algorithms can be classified into two classes: non-critical bits (NCB) and critical bits (CB) [111, 117], based on the bit sensitivity levels to be used in the modulation UEP methods. The most significant bits are the critical bits that can cause the synchronization loss between the decoder and encoder. The reconstructed process can fail if there are errors in these critical bits. On other hand, the non-critical bits cause less error sensitive level and the effect of this error is a single coefficient. These significant bits are generated during the test of the set bits and the refinement bits.

3.3 UWA Channel Reed Solomon Coder

Reed Solomon is a type of forward error correcting code. It is a systematic linear block code [126, 127]. Each code block is organized into m-bit data-word units with a specific length. Its length is usually 3 to 8 bits. For example, with 8-bit code length all probable data-words are suitable for coding. Each systematically generated code-word is composed of the original version of the encoded data-word in addition to the "parity" symbols subjoined to it. Symbol error probability (SEP) of R–S in a communication channel is P_E. For a hard input R-S decoder and assuming the independence of the errors to the channel SEP and P_E is a function in symbol-error correcting capability p_e, the maximum number of correctable errors t can be written as follows [128]:

$$P_E \approx \frac{1}{2^m - 1} \sum_{s=t+1}^{2^m-1} s \binom{2^m - 1}{s} p_e^s (1 - p_e)^{2^m - 1 - s}, \tag{3-5}$$

where m is the number of bits/symbol. The maximum number of correctable errors t for an (N, K) R–S code can be calculated as $t=0.5(n-k)$.

For shallow water communication, UWA noise (UWAN) is neither Gaussian nor white distributed [129-131]. José S. G. Panaro et al. [27] have reported a model of probability density function for the underwater acoustic noise issue based on real measurements at sea. This analytical expression is given for the UWA channel SEP in the case of using BPSK transmission. For binary signaling, the related likelihood functions are obtained and an SEP expression is obtained. The SEP of the binary UWA noise channel can be estimated as a Student's t pdf and it is expressed by eq. (2-14).

3.4 UEP Based on Hierarchical 16-QAM

HQAM is a dc-free modulation scheme and it has more spectral efficiency [111, 117]. Transmission systems based on hierarchical systems combined with the source coder is achieved by classifying information into several layers according to the information significance, transmitting this information with different levels of protection according to their significance, and transmitting each layer with different reliability [111, 117]. Coded images using SPHIT coders in this case classifies the data stream into two types of bits; 1) significant information having "high-priority" (HP); 2) non-significant bit stream for "low-priority" (LP) information.

One of challenges of image transmission in a UWA channel is the large amount of long burst errors. Due to the fading effect of the underwater acoustic channel, significant long burst errors and sporadic failure can occur. For this, image transmission over the underwater channel is far more challenging than in stationary and more predictable wired or wireless environments. With conventional image code protection transmission image signals over UWA channel probably will be loss and sophisticated coding techniques are needed for this reason. Therefore, the encoded bit streams are encoded with the same protection level using R-S channel encoding.

In this case, the HP and LP information are mapped onto non-uniformly spaced constellation points after being de-multiplexed into a single stream and creating different error protection levels [132]. In this way, UEP for the

transmitted data bits can be achieved by HQAM modulation, and HP bits are mapped as the Most Significant Bits (MSB) of the modulation constellation points. The LP coded image data bits are mapped as the Least Significant Bits (LSB) of the modulation constellation points [133]. A step protection level to the transmitted data with regard to its importance can be achieved based on the UEP modulation methods. UEP modulation methods are preferred particularly for image data transmission in case of no-bandwidth change. An improvement in reconstructed image quality at low UWA channel SNR conditions can be achieved by using 16-HQAM. In hierarchical QAM, by using its characteristics, higher protection levels can be provided to the most important data and this protection level can be controlled using modulation parameter value α. α is the ratio of b and c, where b is the distance between quadrants and c is the distance between the points within the a quadrant.

In Fig. 3.1, the modulation parameter $\alpha = b/c$ is shown. The α value should not exceed the square root of the carrier power.

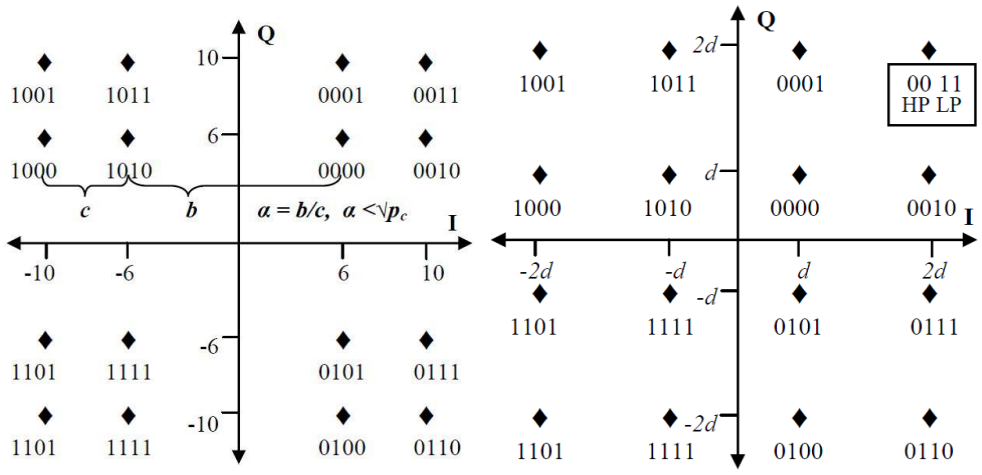

(a) (b)

Fig. 3.1. 16-HQAM constellation diagrams, (a) α = 3, (b) α = 1. Taken from Md. Abdul Kader et al. [111].

3.4.1 Communication Systems and Simulated Results

In this section, the proposed scheme for image transmission in the UWA channel based on modulation UEP will be simulated using a particular channel model implementation, where the distance between transmitter and receiver is separated by around 5 Km in 40 m depth of water and the relative velocity is set to be 8 m/s, where eq. (2-12) is used to detect the Doppler shift effect [24]. Attenuation-Noise (AN) factor [21] produces 8.6 KHz as the optimal frequency for our suggested UWA channel physical parameter. Table 3.1 shows the calculation results for relative channel delays and magnitudes for each path. SPIHT generates the source bit-stream with a bit rate of 0.5 bpp. By dividing the source bit stream into packets of length 2000 bits, each packet is divided into 25 blocks with 80 bits in each block. Each block has 10 symbols at each byte. Packets are divided using the SPIHT coder into 2 groups of packets based on the degree of sensitivity (HP and LP) of each packet. The R-S coder is used as equal forward error correction coder, and 4-symbol for each row is selected to be the protection level of R-S symbols. In this way, the total amount of symbols per packet is 350 and the total transmission rate must be less than the underwater channel capacity.

In our proposed underwater communication system, source image is encoded using the SPHIT technique. The SPHIT encoder generates this bit stream based on sensitivity which is organized into two levels. Higher sensitive data bits such as significance bits and sign bits are classified as being HP bits and lower sensitive data bits such as set bits and refinement bits are classified as being LP bits in 16-HQAM coherent modulation technique constellation points after R-S encoding by unequal forward error correction based on modulation parameters. R-S coder provides equal error protection in this case.

Table 3.1

The UWA Channel Profiles used for Simulations in this Chapter.

Parameter	value				
	1st path	2nd path	3rd path	4th path	5th path
amplitude	0.20628	0.14595	0.073	0.0364	0.0182
delay time (ms)	0	0.7	2.24	4.64	9

3.4.1.1 Single Carrier Communication System

Figure 3.2 shows the single carrier (SC) modulation system for the underwater acoustic channel. The receiver will decode the receiving bit-stream by using an HQAM demodulator with R-S decoder and the SPHIT decoding algorithm. Decision-feedback equalizers (DFEs) have been used in conjunction with a training data sequence to equalize the received data in the UWA channel [11]. The receiver employed an adaptive decision feedback equalizer (DFE). The carrier recovery parameters and equalizer coefficients, according to a MMSE criterion, can be jointly estimated. A least mean squares (LMS) approach can be employed to account for time variation in the channel. After HQAM demodulation, the R-S decoder is used to recover the decoded image stream. The SPIHT decoder then reconstructs the image.

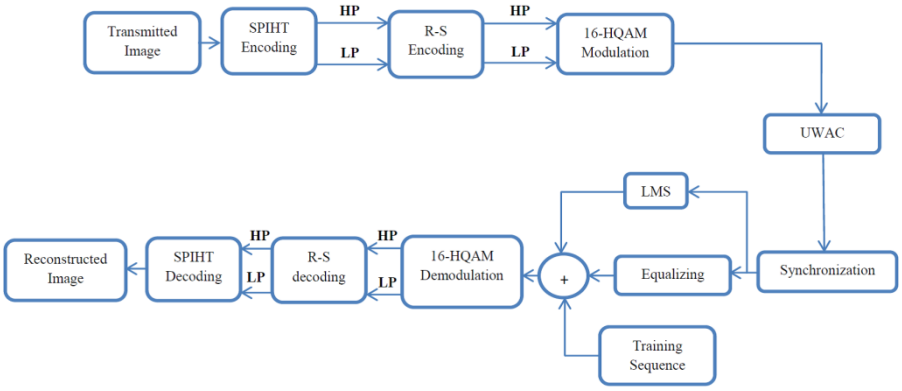

Fig. 3.2, Single carrier modulation system proposed for an UWA channel.

Image transmission in an UWA channel with SC modulation under different physical conditions based on PSNR for both unequal and equal error protection is evaluated. To evaluate the system quality in this simulation, the PSNR of reconstructed images is measured at the receiver side based on the following equation [108]:

$$PSNR = 10\log_{10}\frac{K}{MSE}, \tag{3-6}$$

$$MSE = \frac{1}{M \times N}\sum_{y}\sum_{x}[g(x,y) - g'(x,y)]^2, \tag{3-7}$$

where $g(x,y)$ and $g'(x,y)$ represent the gray values of the pixels in the original and reconstructed image, respectively, N and M represent the height and width of the image, respectively, and the maximal gray value of the image is K. PSNR values of the received image have been measured at different SNR of the UWA channel, as well as different modulation parameters (1 to 5), as is shown in Fig. 3.3.

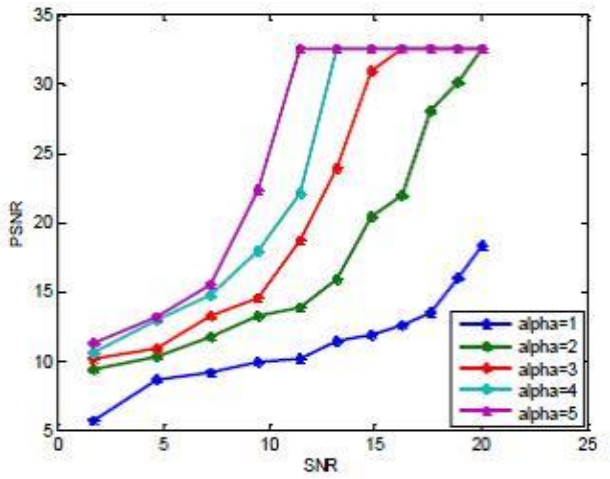

Fig. 3.3. PSNR of reconstructed "Lena" image vs UWA channel SNR.

Fig. 3.3 shows the PSNR of the reconstructed image of "Lena" vs the SNR of the UWA channel. The curves are not fully smooth because of noise in the underwater channel. However, the reconstructed image PSNR increases when the value of α increases for a fixed SNR. Table 3.2 shows different types of images evaluated and tested, including the picture representing the image of Lena, the picture of the dolphin swimming reported in [134] and the picture of the dolphin as an example of a typical underwater image in [135] using EEP and UEP algorithms. Each row represents the reconstructed images for the fixed SNR of the UWA channel and different values of the modulation parameter. It can be seen that for a fixed value of SNR the quality of the reconstructed images increases as well as the value of α. If α increases, the amount of the protection for high priority SPHIT coding bit-stream will increase also.

3.4.1.2 Multi-Carrier Communication System.

In this subsection, we discuss the image transmission over the ZP-OFDM multicarrier modulation system. The UEP is proposed for ZP-OFDM by using 16-HQAM modulation as a mapper. Sensitive data bits such as the significance bit and the sign bit are mapped to the HP bits and less sensitive data bits such as the set bit and the refinement bit are mapped to the LP bits in 16-HQAM modulation constellation points after R-S equal forward error correction encodes each stream separately as shown in Fig. 3.4 [9, 16, 46, 47]. Using a clipping method to reduce the peak–to–average power ratio [136], ZP-OFDM can be used to minimize the transmission power [9].

Simulation results for the calculation of the PSNR value of the reconstructed image transmission over the multi-carrier modulation are shown in Fig. 3.4 for different UWA channel SNR [21] and also for different values of modulation parameter (α= 1 to 5). The transmittion in the multi-carrier modulation system is simulated at fixed SNR=10 dB to show the effect of the UEP method using HQAM. The modulation parameter α=1 represents the traditional quadrature amplitude modulation mapper when unequal error protection is not used. Each experiment is repeated 20 times for more accuracy.

Table 3.2

Reconstructed Images at different SNR and different Value of Modulation Parameters for Image Transmission over an UWA Channel using Single Carrier Communication.

Channel SNR	11.5 dB	10 dB	14 dB
Original Image			
	"Lena Image"	"Dolphin swimming"	"Dolphin"
α=1	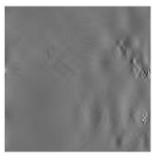		
PSNR	10.1 dB	9.5 dB	22 dB
α=2		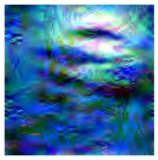	
PSNR	13.8 dB	14.6 dB	30.4 dB
α=3			
PSNR	18.7 dB	20 dB	32.7 dB
α=4			
PSNR	22.3 dB	25.4 dB	32.7 dB
α=5			
PSNR	31.5 dB	31.5 dB	32.7 dB

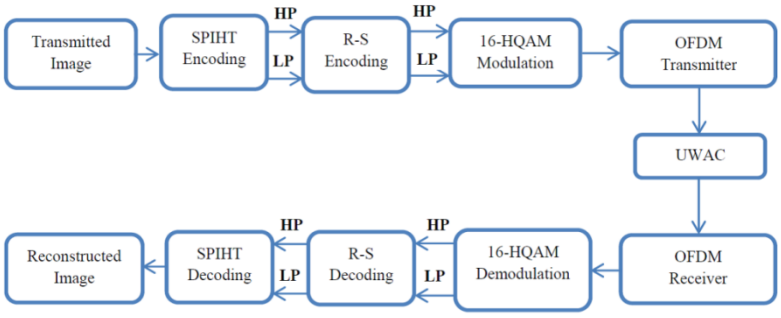

Fig. 3.4. Proposed multi-carrier communication system for image transmission over an UWA channel.

Table 3.3

Reconstructed Images Transmitted using the Proposed MCM System at UWA Channel at SNR= 10 dB and different Value of Modulation Parameters.

Original Image		
α=1		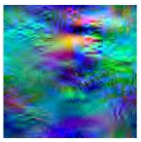
	PSNR=11.5 dB	PSNR=9.33 dB
α=2		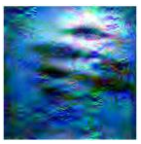
	PSNR=15.1 dB	PSNR=15.77 dB
α=3		
	PSNR=20.5 dB	PSNR=20.96 dB
α=4		
	PSNR=23.4 dB	PSNR=25.29 dB
α=5		
	PSNR=30 dB	PSNR=30.1 dB

3.5 Rate Allocation UEP

Sophisticated channel coding may increase the overhead information given a limited channel bandwidth. To deal with such a challenging channel, effective transmission in UWA channels depends on two factors [103]: (1) effective compression techniques; (2) effective bandwidth use. In this UEP method, we attempt to use both factors to achieve efficient data compression by using an appropriate wavelet-based progressive image-compression technique called SPIHT source coder [108] The aim is to decrease the MSE between encoded and decoded images, with a bandwidth efficiency achieved using unequal error protection optimization technique formulated by taking the particular channel feature into account at the transmitter. In UW communication, commonly modulated symbols should not be affected by the channel noise level. As such, the bit error ratio without channel coding will not be enhanced [137]. Fortunately, the channel coder can increase the transmitted data rate [126].

3.5.1 Coding Operation and Problem Formulation of an Underwater Acoustic Channel

Advanced underwater acoustic encoders with error correction coding haven been proposed for long range underwater acoustic communication [138]. In this chapter, the R-S block channel coder is proposed with adaptive UEP as a rate allocation UEP method. It has been reported by Sara Sandberg and Neele von Deetzen [139] that UEP enhances significantly the quality of the transmission operation as well as minimizing the transmitted rate in highly distorted channels. Albanese et al. [119] succeeded in adapting the UEP to transmit packets over networks in their priority encoding transmission (PET). This technique is based on an optimized rate as addressed in [119, 140]. Here, the UEP technique will be adopted from another perspective. An M-SPIHT source coder is proposed to generate the four types of bit-streams based on coded bit significance in decoded image quality. The M-SPIHT output bit-streams are obtained based on the contribution of each bit-steam in the PSNR of the received image. Then, the protection level of each bit-stream will be adjusted adaptively by using an R-S channel coder.

Here, M-SPIHT is used to classify bits into four different types of groups based on their sensitivity level and their contribution in the reconstructed image PSNR.

Bit error sensitivity (BES) can be analyzed from encoded images using the M-SPIHT coder. For illustrative purposes, assuming the encoded image is corrupted progressively bit-by-bit in order from the beginning until the output bit-stream ends. For oblique bits, the decoded image MSE is calculated. The oblique bit is repaired first, and then the same procedure is applied to the next bit. Our M-SPHIT produces four major types of bit-steams with different levels of sensitivity. The M-SPHIT gives them in order as: (1) the significance bit (2) the sign bits; (3) set bits to determine if setting is significant, (4) refinement bits. In Fig 3.5, it can be observed that the bit groups are ordered by their significance from highest to lowest for a (256*256*8) Lena image and it's order can be given as: significance bits > sign bits > set bits > refinement bits. The four different bit-streams have different significant levels in the received image PSNR. Channel coder overhead information is added for each transmitted packet adaptively by an optimization algorithm. The optimization algorithm is based on the length of the packet, the expected UWA channel SNR and the expected MSE decreases in each packet when a packet is received correctly. Depending on the rate allocation vectors and R-S overhead length, the bit-stream is transmitted.

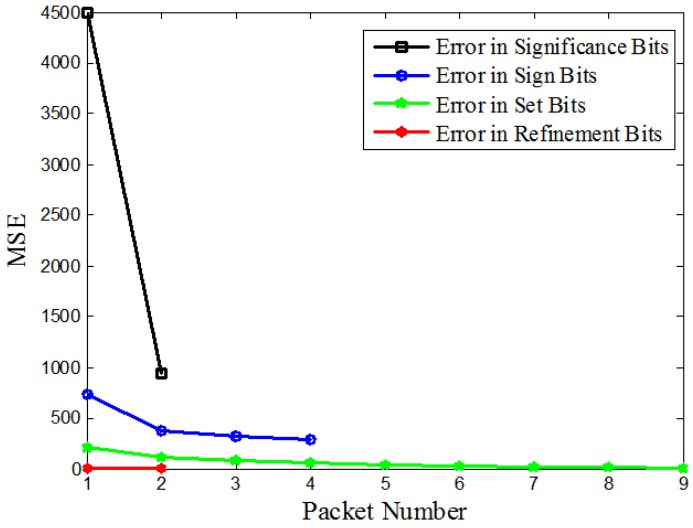

Fig. 3.5. M-SPIHT expected packet sensitivity to error.

The Forward Error Correction (FEC) will use R-S coding for data transmitted over the UWA channel. Assuming the M-SPHIT encode image and its output are split into a series of packets, if $\Delta D_i \geq 0$ is the predict MSE reduction in the decoded i^{th} packet, the total deformation in total received packets can be formulated as:

$$D(l) = D_o - \sum_{i=1}^{l} P_i \Delta D_i, \tag{3-8}$$

here, D_o is the MSE expected for the transmitting packet without any overhead information, P_i is the probability that i^{th} packet is correctly received over the channel, and l is the total transmitted packet number. P_i is the probability of correctly receiving the packet over the UWA channel. It is a function in the transmission data rate and can be written as:

$$P_i = \prod_{j=1}^{i} Q_j(r_j), \tag{3-9}$$

where $Q_j(r_j)$ is the probability of receiving the j^{th} layer correctly at receiver side when it is set at a rate of r_j. Applying eq. (3-9) to eq. (3-8) yields:

$$D(l) = D_o - \sum_{i=1}^{l} \left(\prod_{j=1}^{i} Q_j(r_j) \right) \Delta D_i. \tag{3-10}$$

Optimal rate allocation r_j is the amount of total bits which minimize the received packet distortion based on the eq. (3-10) at a constant transmission rate. The minimal distortion problem can be formulated generally as follows:

$$\min_{r} D(r) \quad Subject \quad to \quad \sum_{j=1}^{l} r_j \leq R, \tag{3-11}$$

where R is the total transmission rate in the equal EEP which must not exceed the channel capacity.

3.5.2 Optimization Technique

The transmitted bit-stream can be split into different coding blocks. Each of these blocks includes k source packets. Each block is encoded by an (N, K) R-S channel coder where (N-K) is the maximum overhead information required to protect each block. These packets are transmitted over the UWA channel. Let P_e be the symbol error probability of the channel. Optimal rate allocation vector r for eq. (3-11) can be obtained by using the Lagrange multipliers equation as:

$$J(r,\lambda) = D(r) + \lambda \sum_{i=1}^{l} r_i. \tag{3-12}$$

The correct receiving conditional probability at transmission rate r_j of the j^{th} source packet is $1 - P_E(r_j)$. Then, eq. (3-9) becomes:

$$P_i = \prod_{j=1}^{i} Q_j(r_j) = \prod_{j=1}^{i} (1 - P_E(r_j)). \tag{3-13}$$

Applying eq. (3-10) and eq. (3-13) into eq. (3-12) one obtains:

$$J(r,\lambda) = D_o + \sum_{i=1}^{l} \left[\left(-\prod_{j=1}^{i} Q_j(r_j) \right) \Delta D_i + \lambda r_i \right]. \tag{3-14}$$

The function in eq. (3-14) can be optimized to determine the appropriate r_j. It is dependent on the condition that the set of distortion difference ΔD_i, as well as the probability of j^{th} layer source packet, are received correctly. There are many solution methods available to solve this optimization problem and in this chapter it is solved based on an alternating variable iterative method [141]. $J = (r_1, \ldots\ldots\ldots, r)$ in eq. (3-14) is the objective optimization function. It is used to minimize one variable each time. The objective optimization function keeps other variables constant until the iterative process reaches convergence. Let $r(0)$ be the initial rate allocation vector, $r(t) = (r_1(t), \ldots\ldots, r_l(t))$ are obtained values at $t = 1, 2, \ldots\ldots$ as follows: $x \in \{r_1, \ldots\ldots\ldots, r_l\}$ is optimized at step t in a round-robin way. In the next step, for $x = r_i$, the following rate optimization is performed:

$$f(r) = r_i^{(t)} = \arg \min_{D_i} J\left(r_1^{(t)}, \ldots\ldots\ldots, r_l^{(t)}\right) = \arg \min_{r_i} \sum_{i=1}^{l} \left[\left(-\prod_{j=1}^{v} Q_j(r_j) \right) \Delta D_i + \lambda r_i \right], \tag{3-15}$$

$$D(r_1, r_2, r_3, \ldots\ldots\ldots, r_l) = D_o - \sum_{i=1}^{l} \left(\prod_{j=1}^{i} Q_j(r_j) \right) \Delta D_i, \tag{3-16}$$

$$R(r_1, r_2, r_3, \ldots\ldots\ldots, r_l) = \sum_{i=1}^{l} r_i, \tag{3-17}$$

where r is the combined transmission rate vector in the UEP system for each transmitted packet with total transmission rate $\sum_{j=1}^{l} r_j \le R$.

R is the maximal total transmission rate in the EEP system. The Lagrange multipliers method can also be used to find the point of minimum overall distortion D, across all transmission rates R_n in the UEP with such maximal rate constraint, leading to:

$$\frac{\partial}{\partial \vec{r}}\left(D+\lambda\left(R_n-R\right)\right)\Big|_{\vec{r}=\vec{r}^*}=0, \tag{3-18}$$

$$\frac{\partial}{\partial \vec{r}}\left\{D_o-\sum_{i=1}^{l}\left(\prod_{j=1}^{i}Q_j\left(r_j\right)\right)\Delta D_i+\lambda\left(\sum_{j=1}^{l}r_j-R\right)\right\}\Big|_{\vec{r}_k=\vec{r}_k^*}=0. \tag{3-19}$$

The gradient-descent type algorithm as a standard non-linear optimization procedure can also be used to minimize optimization problems for a fixed λ [141].

3.5.3 Proposed Rate Allocation UWA Communication System

We propose a communication system scheme based on the UEP rate allocation technique for an UWA channel, as shown in Fig. 3.6. The major components are: (1) the M-SPIHT coder used to generate four types of bit-stream with regard to its significance order; (2) data outputs which are split into a series of stream packets; (3) the predictable decrease in ΔD_i that can be approximately estimated based on the expected change in MSE; (4) the optimization algorithm to generate the optimum bit rate distribution of packets, which is adapted to the optimization algorithm inputs, including packet length, expected decrease in distortion ΔD_i and channel SNR; (5) R-S encoder using the output rate allocation vectors to generate the transmitted bit-stream; (6) the receiving bit-stream to be decoded by using R-S decoder the M-SPIHT decoder.

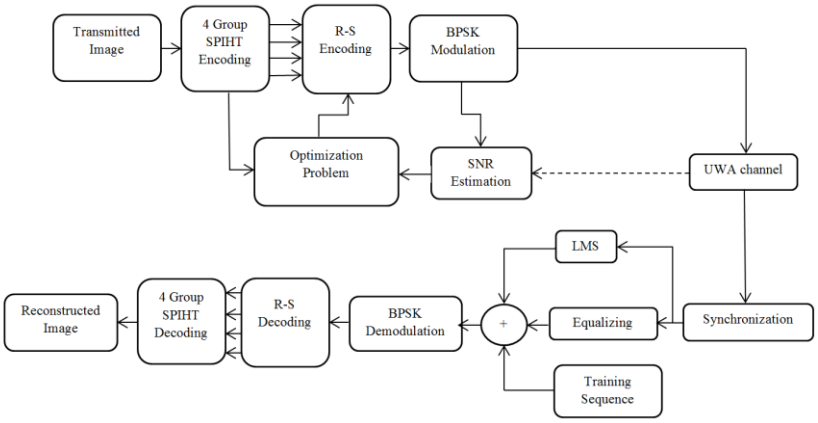

Fig. 3.6. Rate allocation UWA channel configuration.

An SNR estimation block is included in the diagram in Fig. 3.6. In this chapter, SNR is estimated using eq. (2-8) which depends on the distance between the transmitter and receiver, carrier frequency, signal transmission power and receiver noise bandwidth, which are all known at the transmitter. Another important parameter in eq. (2-8) is the ambient noise (considered as feedback signal) which depends on the physical characteristics of the channel. Eq. (2-7) can be used to approximate the ambient noise. This block can also be integrated with other information sources such as the bit-error rate estimation from network management protocols to facilitate direct feedback from the real time communication status to the optimal bit protection level allocation.

At the beginning, modification of the SPIHT coder output bit-stream is introduced. The proposed UWA communication system for image transmission is based on the sensitivity of each block of M-SPIHT output and its contribution in reconstructing image PSNR.

The BES can be evaluated bit-by-bit with corrupted M-SPIHT encoder outputs, starting from the first bit to the last. For each corrupted bit, the MSE of the original and reconstructed images is calculated. For each iteration, the last corrupted bit is corrected first. Then, the next bit is corrected and transmitted.

The resultant BES is depicted in Fig. 3.5. As shown in this figure, the output is ordered to start with the highest significant bits (a first group of bits). The wind generates significant waves, which in turn not only scatter the surface reflection, but also gives these reflections a Doppler shift for which DFEs have been used.

Doppler shift effects are detected based on eq. (2-12). The UWA channel is a time variant channel. The LMS approach can be used to estimate the time delay and equalize such variant channels based on the DFE equalizer. After demodulation, the R-S decoder is used to recover the decoded image stream. Finally, 4 group SPIHT decoders recover the transmitted image.

The M-SPHIT output divides coded packets into four separate groups based on their significance. In particular: (1) two of the encoded packets are for the significant bits and they will have the highest entropy; (2) four packets are used to represent the sign bits in the encoded image; (3) nine of the encoded packets are used to represent the set bits; (4) the last two encoded packets are used to represent the refinement bits in the image. First, the outcomes of the UEP method are compared with the EEP method. For the EEP case, the number of R-S overhead symbols is selected to be six in the encoded packet row which makes the total number of symbols per packet sent to the modulation to be 400.

In the case of UEP, the total numbers of symbols in all encoded packets in eq. (3-15) are selected to be no more than that of EEP with R-S equal to 6 symbols, which should be less than the channel capacity. Each row of the packet and R-S symbols are determined for each encoded packet based on the optimization algorithm to minimize the total distortion. As shown in Fig. 3.7, the sign and significance bit-stream blocks are protected by an eight-symbol, considering the low UWA channel SNR in this case. The set packet groups are protected using four symbols and eight symbols are used to protect the refinement bit-steams.

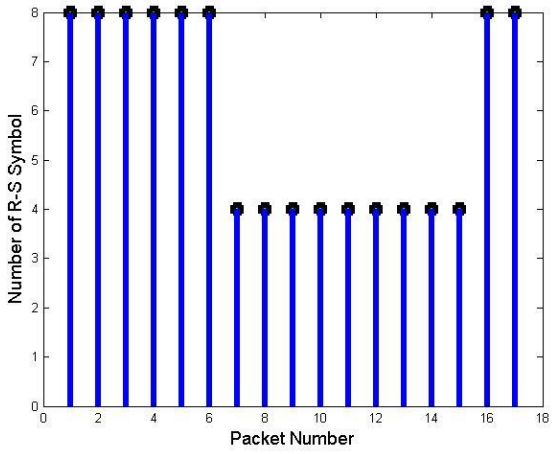

Fig. 3.7. Transmitted “Lena” packets R-S protection levels as determined using the UEP algorithm.

3.5.4 Simulation Results

Image transmission over the underwater channel is simulated under different physical conditions to assess the system performance for both unequal and equal error protection with the R-S channel coder. The parameter of wind speed is selected at different values. Each experiment is run 50 times to collect the average. As shown in Fig. 3.9 and Fig. 3.10, where several variations of the standard "Lena" and "dolphin swimming" images are shown [4, 138] following transmission through the proposed underwater communication system. The reconstructed images are obtained at different wind speed levels using the two protection algorithms, unequal and equal error protection.

In the UEP case, the total number of transmitted symbols (R in eq. (3-11)) in the simulation is 67487. The redundancy symbol number for each encoded group is determined by solving the optimization problem defined in eq. (3-11) (the first two packets are significance packets, followed by four sign packets, nine set packets and finally two refinement packets). R-S symbol redundancy is shown in Fig. 3.8 (b) where the significance packets have eight symbol protection level, the sign and set packets have six symbol protection level, and refinement packets are protected by four symbols. In the simulation of the "dolphin swimming" image, the R-S rate distribution changes under various channel wind conditions, as shown in Fig. 3.9 (b). In particular, at 10 Knot wind speed the packets of significance type are protected by eight symbols, six symbols are used, and the refinement packets are completely unprotected. As a result, the total number of transmitted symbols using UEP is 65999, which is 1488 less than that obtained using the traditional EEP technique.

Figure 3.8 shows the average PSNR of the received Lena image transmitted over the UWA channel by using the proposed scheme, MD-Like allocation shame [110], and equal forward error correction. With the R-S coder all coded images are transmitted at certain total bit budget.

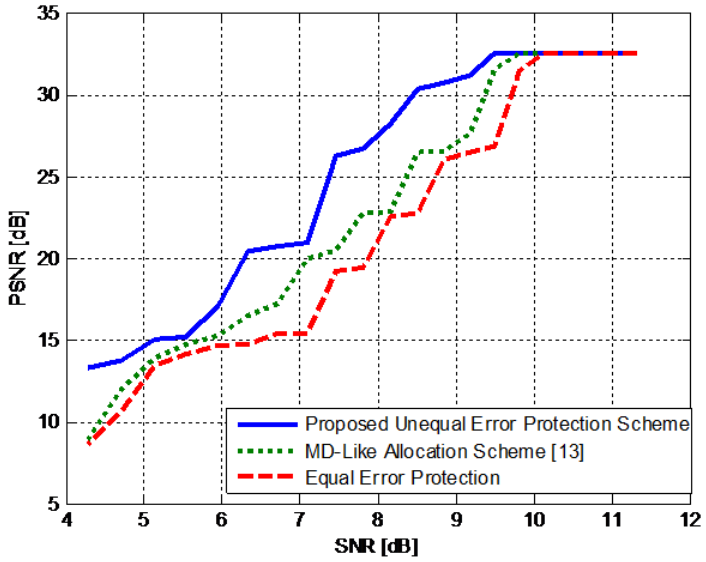

Fig. 3.8. The average PSNR of the received Lena image transmitted over the UWA channel for EEP, MD-Allocation [13] and proposed UEP channel coding, at channel Doppler shift = 29.6 Hz.

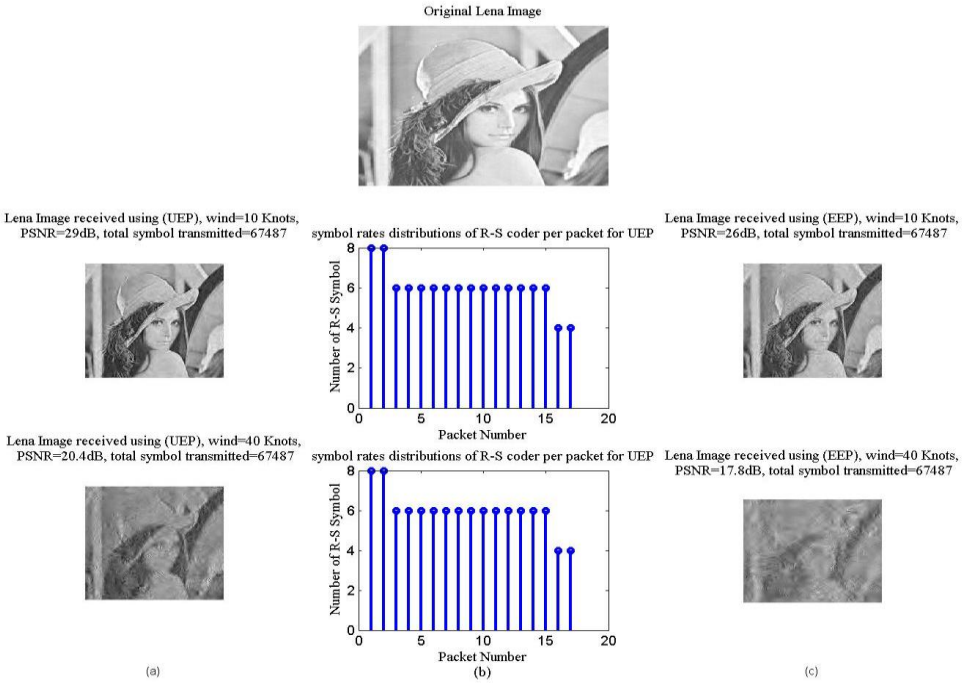

Fig. 3.9. Reconstructed "Lena" image transmitted over the UWA channel with equal and unequal error protection with channel rate distribution of unequal error protection.

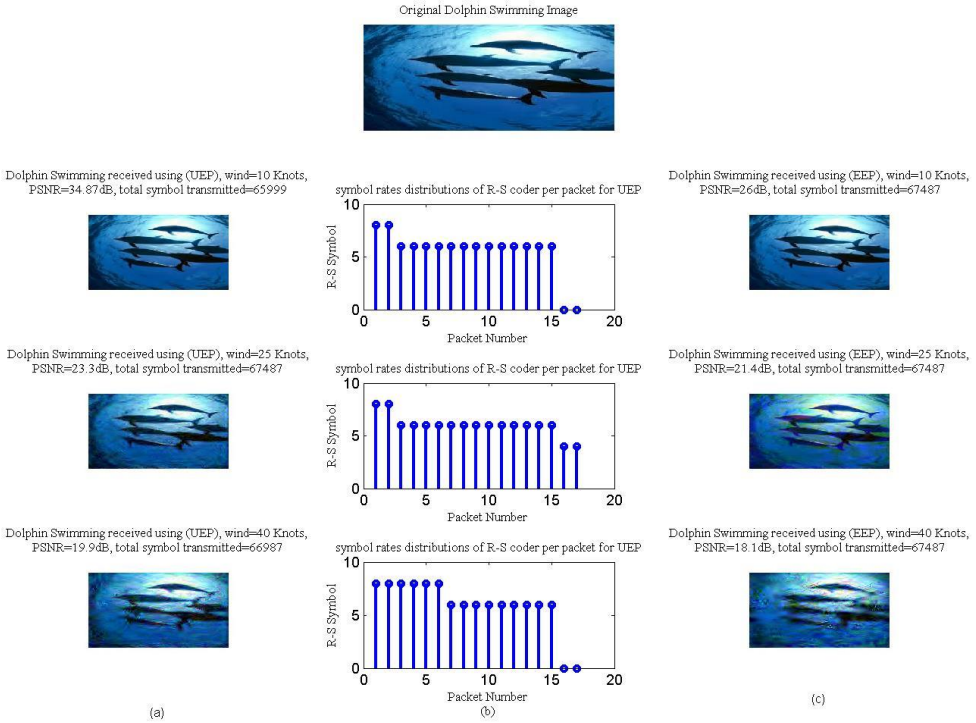

Fig. 3.10. Reconstructed "Dolphin Swimming" image transmitted over the UWA channel with equal and unequal error protection with channel rate distribution of unequal error protection.

Due to significant UWA channel noise, the curves in Fig. 3.8 are not smooth. The unequal error protection rate allocation encoding method improves the PSNR of the received image. From the simulation results, the proposed UEP method outperforms the conventional EEP system by 3.5 dB and the system of MD-like allocation schemes [110] by 2.2 dB in the underwater acoustic channel with a Doppler shift equal 29.6 Hz at fixed total bit budget. The iterative procedure in the proposed system increases the time needed to encode an image, but results in higher PSNR for reconstructing images in a low SNR channel which makes it more suitable for underwater acoustic channels. Also, from the simulation results, the R-S code is shown to be suitable for an underwater acoustic channel. Please note the equal error protection (EEP) represent the performance when unequal error protection is not used.

In our UEP based on 16-HQAM, the proposed unequal error protection is only for a certain communication system HQAM method, but the rate allocation method can be used with any modulation system. Table 3.4 compares our proposed method and other methods developed elsewhere.

Table 3.4

Comparison of UEP based on Rate Allocation Scheme to other UEP Methods.

Items	Proposed scheme	MD-Like allocation scheme [110].	HQAM- approaches
Complexity	Complex	Complex	Simple
CSI (channel state information)	Not required	Required	Not required
Feedback from receiver to transmitter	Not required	Required	Not required
Validity for different communication systems	Valid for any communication system	Valid for any communication system	Specific only for HQAM systems

3.6 Conclusion

In this chapter, an efficient unequal error protection technique is proposed for image transmission in the UWA channel. Based on a modified SPIHT coder scheme, a novel image transmission method has been suggested. A SPIHT coder algorithm has been modified based on the order of significance of the coded bits as well as its contribution in the PSNR of the received image. Two UEP methods are proposed, based on 16-HQAM coherent modulation techniques and using rate allocation image transmission. In particular, four different types of bit-streams are generated by a modified SPIHT coder. These four groups are used directly in the rate allocation case, while both groups merge in UEP using HQAM modulation to produce two vectors of bit-streams representing high and low priority bits. In this chapter, 16-HQAM is tested for high-speed image transmission in single and multi-carrier modulation, where 16-HQAM is used as the modulation system and as a mapper of ZP-OFDM. Simulation results show that 16-HQAM is capable to transmitting high-speed images using the proposed underwater communication systems. The 16-HQAM single carrier modulation system is used based on DFE, while the ZP-

OFDM uses long guard intervals to avoid the inter-block interference problem. Also, an efficient rate allocation image transmission scheme in underwater acoustic systems is discussed. The R-S channel coder is used together with the output of the rate allocation vectors to generate the output bit-stream for transmission. While such techniques can be considered for generic image transmission issues to achieve reasonable efficiency, an optimization problem is carefully formulated by taking the particular channel feature of underwater acoustic communication channels into account, such as Doppler shift and probability bit error distribution. As a result, noticeable reduction of the overall distortion over an underwater acoustic channel using our proposed technique is observed, together with the improvement in PSNR for the reconstructed image. Simulation experiments are included for illustrative purposes with different image types and different physical parameters such as wind speed.

Chapter 4

An Image Transmission Technique Adaptive to Underwater Time-Dispersive Fading Channels with Progressive Zero Padding OFDM

4.1 Introduction

This chapter proposes a novel image transmission technique to adapt to the particular features of underwater time dispersive fading channels. Such a communication channel is known to have a considerably low data rate and every effort to improve efficiency will contribute to better image transmission. Single-input multi-output orthogonal frequency division multiplexing (SIMO-OFDM) has been applied to achieve low bit error rate (BER) in selective fading channels with significant tap delays [10]. Each transmitted SIMO-OFDM block includes a zero padding (ZP) section of codes working as a guard interval (GI) to avoid inter-block interference (IBI). Effective avoidance of the IBI can be ensured by sufficient GI length, which is usually required to be longer than or equal to the maximum channel tap delay. However, for channels with significant tap delays, such GI may lead to significant bandwidth losses.

It is noted that the data transmission technique over time reversal SIMO-OFDM with an insufficient GI recently published by Liu Zhiqiang and T.C. Yang [10] may potentially be a viable scheme to achieve reasonable bandwidth efficiency. On the other hand, unequal error protection (UEP) techniques for image communication have been shown to be capable of reducing the data rate and achieving high peak signals–to–noise ratio (PSNR) based on the error protection level of the channel coder as reported in [139]. Furthermore, PSNR has been shown to be a useful quality metric for the reconstructed image of lossy compression coders and it is a reasonable approximation to human perception of reconstruction image quality [116]. Combining these techniques, in this chapter UEP is further improved to adapt to the channel IBI level in each transmitted block by a progressive zero padding (PZP) by minimizing IBI under the total GI length constraint.

4.2 Progressive SPHIT Image Coder

Our discussion is based on the SPIHT coder already been developed based on the hierarchical partition of wavelet coefficients. By considering the wavelet coefficients as spatially orientated trees, all sub-band coefficients are included in each tree to identify the particular position in the image [108]. It is a progressive image coder and can offer many benefits including the high quality of reconstructed images with high compression ratio [115]. The output of the SPHIT coder consists of data blocks with different levels of significance and priority as shown in Fig. 4.1 [115]. The bits with higher significance are encoded with more redundancy. Each bit block is more significant than the next one. Bit sequence in this SPHIT output can be divided into four different groups ofbits, namely, significance bits, sign bits, set bits and refinement bits, based on their significance [108, 118] and are progressively analysed.

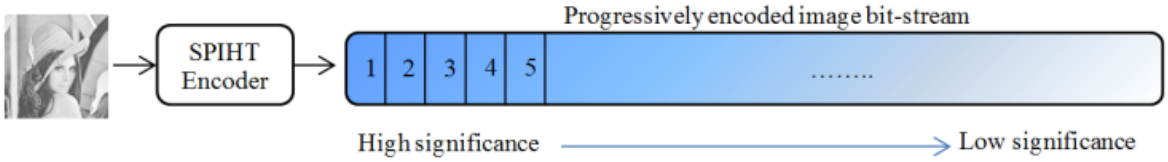

Fig. 4.1. SPHIT progressive source coder.

4.3 Optimal PZP Length

The significance levels of different encoded image blocks are different. The encoded image transmitted in the channel is divided into a series of blocks. In this chapter, we consider different length of guard interval for different blocks in an insufficient GI case. The detailed technique will be developed based on the PZP technique in this section. Such a data sequence will be obtained by using a coder for which different zero padding length is applied to a different data block significance level. Assuming a transmitted image over PZP has N blocks and the i-th block has $L_{ZP(i)}$ zero padding length for generic i, the total zero length in all blocks is $L_{ZP} = \sum_{i=1}^{N} L_{ZP(i)}$, the predicted distortion reduction by using sufficient GI for i-th data blocks is $\Delta D_i \geq 0$ and the highest distortion D_o is the total distortion expected without GI under a maximum IBI. The overall distortion of the all received blocks in one image can be calculated as:

$$D(K) = D_o - \sum_{i=1}^{N} \rho_{in-ZP(i)} \Delta D_i, \tag{4-1}$$

here, $K = \left(L_{ZP(1)}, \ldots, L_{ZP(N)}\right)$ and $\rho_{in-ZP(i)}$ is the signal–to–signal and interference ratio (SSIR) of the TR channel for i-th OFDM transmitted frame, which is also a function of the i-th frame ZP length and $\rho_{in-ZP(i)} = 1$ in sufficient GI case (IBI=0 in this case). Note that for a TR technique, the transmitter transmits a probe bit sequence at the beginning of the communication. The resultant sequence is recorded at the receiver and serves as channel information [10]. From [6] the SSIR can be written as:

$$\rho_{in-ZP(i)} = \frac{\sum_{n=0}^{L_{ZP(i)}} |q[n]|^2}{\sum_{n=-\infty}^{\infty} |q[n]|^2}, \tag{4-2}$$

where $q[n]$ is the TR channel impulse response. By applying (4.2) to the (4.1) it yields:

$$D(K) = D_o - \sum_{i=1}^{N} \frac{\sum_{n=0}^{L_{ZP(i)}} |q[n]|^2}{\sum_{n=-\infty}^{\infty} |q[n]|^2} \Delta D_i. \tag{4-3}$$

The frame ZP length can be optimized by minimizing the distortion of the received blocks based on eq. (4-3) under total ZP overhead length constraint. Such a problem can be formulated as an integer optimization issue given below:

$$\min_{K} \; D(K) \;\; s.t. \;\; \sum_{i=1}^{N} L_{ZP(i)} \le R, \;\; L_{ZP(i)} \ge 0, \text{ and } L_{ZP(i)} \text{ are integers} \tag{4-4}$$

where $R = N \cdot L_{CZP}$ is the total ZP overhead length and L_{CZP} is the ZP length in the case of the conventional time reversal SIMO-OFDM system to keep system bandwidth lower than the conventional system.

The ZP integer programing problem can be solved by existing methods, i.e., Lagrange relaxation method [142], for optimal PZP length for each group of blocks. Consider the unconstrained optimization problem of the following function:

$$J(K,\lambda) = D_o - \sum_{i=1}^{N} \frac{\sum_{n=0}^{L_{ZP(i)}} |q[n]|^2}{\sum_{n=-\infty}^{\infty} |q[n]|^2} \Delta D_i + \lambda L_{ZP(i)}. \tag{4-5}$$

It is dependent on the set of distortion reduction ΔD_i, as well as the SSIR and proportional to the ZP length.

4.4 The Proposed System Model and Simulation Results

Based on the optimal PZP length obtained in the last section, we can design the communication system as shown in Fig. 4.2, where SPHIT output bit-stream can be organized into four types of bit segments ordered by their significance levels as: significance bits > sign bits > set bits > refinement bits. The data blocks can be transmitted by using the time reversal SIMO-OFDM communication system proposed in [10]. In order to evaluate the performance of the proposed progressive zero padding SIMO-OFDM, we consider such a typical implementation where 4- antennas are used at the receiver with 512 subcarriers and QPSK modulation. Where for the number of antenna receiver increases the BER decreases. Recalling that the BER level depends on the residual mutual IBI and the amount of IBI is a function of how TR-channel is impulse-like, as antenna receiver increases the time reversal channel becomes more impulse like.

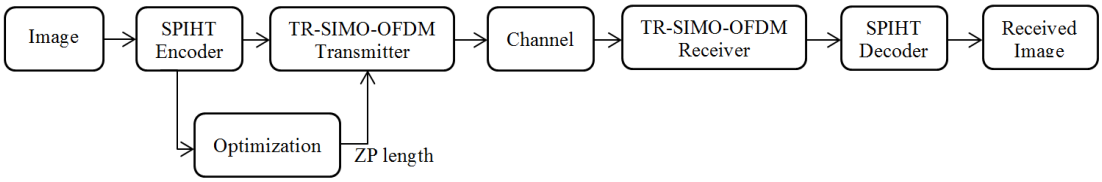

Fig. 4.2. Proposed communication system.

The system is simulated in two types of channels: a simulated channel with impulse response generated based on a multipath fading channel with maximum 32 channel taps delay, and a measured underwater acoustic (UWA) channel adopted from existing experimental data collected in the ASCOT01 experiment conducted off the coast of New England in June 2001[143, 144]. This measured channel is truncated to a 159 channel taps delay. Channel impulse responses (CIR) can be estimated at the receiver using a compressed sensing with simultaneous orthogonal matching pursuit (SOMP) [145, 146] method based on the pilots tones equally spaced in frequency domain.

For illustrative purposes, a 256*256*8 Lena image is adopted as the source image, which is encoded using an SPHIT coder at a 0.5 bpp compression rate. The encoded bits are split into 43 blocks based on the order of their

significance as follows: (1) 4 blocks of significant bits (2) 8 blocks of sign bits (3) 19 blocks of set bits (4) and the final 12 blocks are for the refinement bits group.

For the simulated channel, consider the conventional system with $L_{CZP} = 10$, which is shorter than the maximum number of channel tap delay, 32. As such, the total zero padding length of the transmitted blocks is $L_{CZP} \cdot N = 430$ and the total PZP overhead length to all transmitted blocks must not exceed this. The ZP length distribution for OFDM transmitted data blocks is: (1) 32 for significant bits (2) 19 to sign bits (3) 5 for set bits (4) 4 for refinement bits with 423 PZP overhead which is less than is usually used in the conventional system.

As shown in Fig. 4.3, the proposed PZP scheme significantly improves the PSNR of reconstructed images over the simulated channel, outperforming the conventional system by 4.07 dB.

For the measured UWA channel, consider the case where the ZP length in the conventional time reversal SIMO-OFDM system is $L_{CZP} = 50$. It is shorter than the maximum channel tap delay of 159. In this case a significant IBI may be present. In the proposed PZP-OFDM the restricted PZP overhead will be $L_{CZP} \cdot N = 2150$ and the PZP obtained by the optimization algorithm in this type of channel will be (1) 84 for significant data block group (2) 76 to sign group (3) 48 for a set group (4) 24 in refinement group, respectively, with a 2144 total PZP overhead which is less than what is usually used in the conventional system. As shown in Fig. 4.3, the PZP scheme improves the PSNR of reconstructed images over the UWA channel. It outperforms the conventional time reversal SIMO-OFDM system by 3.44 dB. Table 4.1, shows the OFDM system performance of decoded Lena image at SNR= 25 dB. PZP-OFDM system represent the unequal error protection method and the conventional ZP-OFDM is the equal error protection method or the performance when unequal error protection is not used.

From Fig. 4.3, it can be seen that the proposed method is more efficient even though there is a performance difference between the simulated and measured UWA channel. The reason for the performance difference is because the simulated channel is quite impulse-like even for a small number of receiver antennas because of the accurate channel data and because a UWA channel is a sparse one, a large number of receiver antennas are required to render the TR channel to be impulse-like [10].

Table 4.1

Decoded Lena Image over an UWA Channel and Simulated Channel with Different OFDM Systems.

OFDM system	Simulated channel	UWA channel
ZP-OFDM		
PZP-OFDM		

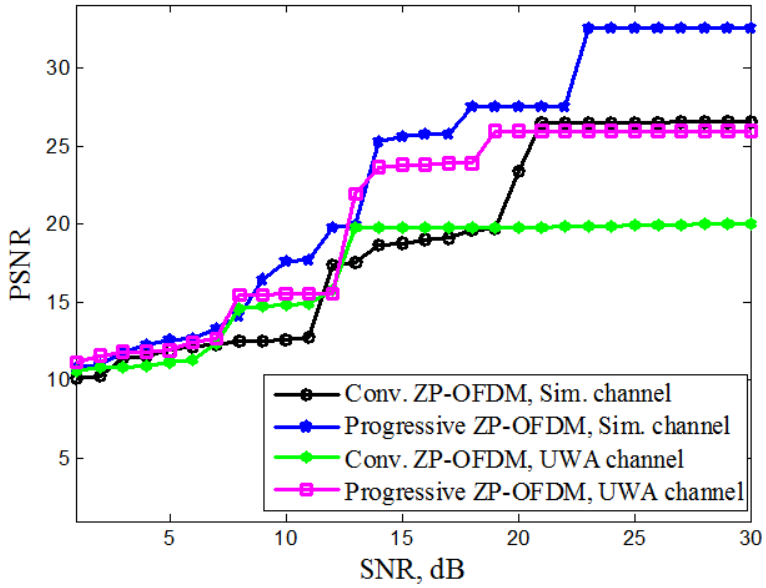

Fig. 4.3. PSNR of the received Lena image over time reversal SIMO-OFDM with conventional ZP and proposed PZP (simulated channel).

4.5 Conclusion

In this chapter, unequal error protection is improved by selecting zero padding length adaptively according to data block significance, resulting in a new transmission scheme called the PZP-OFDM system for image transmission over time reversal SIMO-OFDM without sufficient guard interval length. The new scheme is developed for SPHIT coded images. The length of each PZP block is optimized to minimize the expected distortion and maximize the PSNR of reconstructed images under a total frame length constraint. The proposed design has been evaluated in simulated channels as well as a measured UWA channel in a sea experiment reported elsewhere. The results show that the overall distortion can be effectively reduced in reconstructing images and the PSNR can be improved by more than 4.07 dB and 3.44 dB in simulated and UWA channels, respectively. The proposed PZP-OFDM scheme can also be applied to other scalable image signal sources.

Chapter 5

OFDM Inter-Carrier Interference Reduction using Pulse Shaping Function in Underwater Acoustic communications systems

5.1 Introduction

Nowadays, though wireless communication technology is critical to our modern lifestyle, efficient underwater communication is still not yet achievable. Significant evolution in UW communication will enable new applications ranging from environmental monitoring to gathering of oceanographic data, search and rescue missions and marine archaeology. Because of the limitations of the underwater channel the selection of the type of modulation and error correction techniques has to be carefully considered.

Due to its ability to decompose a frequency selective fading channel into several nearly flat fading channels, multi-carrier modulation (MCM) systems are efficient in communications over multi-path communications channels. However, carrier frequency offset (CFO) is one of the MCM challenging with several associated problems. A simple solution of this problem is choosing modulated symbol duration of the transmitted signal to be larger than or equal to the channel tap delay. In this case, significant bandwidth loses will be incurred, where the low rate "sampling" of the channel impulse response with one per symbol in each sub-channel inefficiently uses coherent channel bandwidth [41], especially for channels having long tap delays such as those in underwater acoustic (UWA) channel. Due to the multicarrier transmits signals in MCM systems, at the receiver it can be processed without increasing the interference noise caused by linear equalization of a single carrier. Also, a much greater immunity to impulse noise and channel can be achieved if MCM modulation systems are used. Multi-carrier modulation has become popular in selective fading channels with significant tap delay such as the UWA channel [42].

Zero-padded (ZP) orthogonal frequency division multiplexing (OFDM) has been extensively investigated for high data rate underwater acoustic communication [39, 48, 147]. In ZP-OFDM cyclic prefix (CP) of conventional CP-OFDM system is replaced by zeroes for more energy efficiency. ZP-OFDM is preferred in long tap delay channels, where it consumes less transmission energy [9].

The sensitivity of OFDM multicarrier systems to CFO causes subcarrier rotation and attenuation and may lead to inter-carrier interference (ICI) between neighboring subcarriers [148]. ICI of OFDM wireless communication systems over wireless selective fading channels can be neglected where the channel time variation will be small compared to OFDM symbol duration. Due to the high speed of electromagnetic waves used in radio communication, the Doppler shift due to transmitter receiver movement can also be neglected. On the contrary, due to the low speed of acoustic waves used in UWA communication, a significant Doppler shift occurs even at low relative speed between transmitter and receiver.

This chapter focuses on the issue of ICI power reduction of OFDM using pulse shaping methods for underwater channels, which is desirable for reliable data detection. Correct reliable data detection is not possible unless the

power of ICI in the OFDM system is minimized. This undesired ICI degrades the performance of the system. Several methods have been reported to reduce ICI, including frequency domain equalization [149, 150], windowing at the receiver [151, 152], ICI self-cancellation scheme [153, 154], and pulse shaping [155-157]. In this chapter, the OFDM inter-carrier interference for both discrete Fourier transform (DFT)-based and discrete cosine transform (DCT)-based is carefully reduced using pulse shaping for an underwater acoustic channel. Technical analysis is included to justify the high performance of IDCT-OFDM due to its super resistance to ICI.

In this chapter the OFDM inter-carrier interference for both discrete Fourier transform (DFT) based and discrete cosine transform (DCT) based is analysed. Then, proposed underwater communication system scheme and simulation results are presented. A summary of the major techniques and contributions of this chapter is included.

5.2 OFDM Inter Carrier Interference Analysis

Orthogonal frequency division multiplexing (OFDM) as a MCM technique is particularly efficient in selective fading channels with noise spread over a large part of available channel bandwidth. Better spectral efficiency with significant performance improvement can be achieved in typical multi-path channels if the signals are transmitted in multiple orthogonal sub-carriers simultaneously. Due to limited channel bandwidth of a UWA channel OFDM has been proposed for use in underwater communications instead of single carrier modulation to achieve higher data rates for transmission [11, 22, 75]. Without sophisticated time-domain equalizers, the OFDM communication system has been proved to be an effective technique for combating the channel multipath tap delays [54]. Due to fast variations of the UWA channel within each OFDM symbol, ZP-OFDM performance is severely limited by the ICI.

ZP-OFDM has good spectral efficiency due to the narrow subcarrier spacing attributed to its orthogonality [115]. Also, according to the transmission conditions on each subcarrier, adaptive modulation schemes can be used on individual subcarriers. In addition, based on DFT and DCT, OFDM multicarrier systems can be implemented in the digital domain. However, OFDM systems suffer from a number of drawbacks. In particular, the sensitivity to CFO causes attenuation and rotation of subcarriers. Significant ICI power occurs hence, the orthogonality between the carriers is lost. Deterioration of performance results in this case, where the CFO attenuates the desired signal and introduces the ICI. Thus, significant decrease in the signal-to-noise ratio (SNR) can be observed and the performance of OFDM degrades in this case [5].

Different methods of ICI reduction have been investigated for OFDM systems in radio frequency, including time domain windowing, ICI self-cancellation, frequency domain equalization and pulse shaping [158]. It is found that the time domain windowing and frequency domain equalization methods are not so efficient because they do not address the major causes of ICI in UWA channels, namely, (a) delay spread of underwater acoustic channel exceeds guard interval; (b) frequency offset at the receiver due to receiver crystal oscillator inaccuracy. But pulse shaping methods and ICI self-cancellation are found to be very efficient in radio frequency. The drawback of the ICI self-cancellation method is the reduction of the spectral efficiency, where the same data is modulated into two or more carriers. The pulse shaping method does not suffer from such efficiency reduction, and are found to be more efficient than all other methods of interest.

The transmitted OFDM subcarrier block with pulse-shaping function can be expressed as [158]:

$$x(t) = e^{j2\pi f_c t} \sum_{k=0}^{N-1} d_k p(t) e^{j2\pi f_k t}. \quad (5\text{-}1)$$

Here, f_k is the subcarrier frequency of the k^{th} subcarrier, f_c is the carrier frequency, $p(t)$ is the pulse shaping function in time domain, and d_k is the data symbol transmitted on $k = 0,1,\ldots\ldots,N-1$ of the subcarrier. Assuming that d_k has normalized average symbol energy and zero mean with uncorrelated data symbols, then [155, 158]:

$$E\left[d_k d_m^*\right] = \begin{cases} 1, & k = m \\ 0, & k \neq m \end{cases}, \quad (5\text{-}2)$$

where d_m^* denotes the complex conjugate of d_m. In addition, it is required that [158]:

$$f_k - f_m = \frac{k-m}{T}. \quad (5\text{-}3)$$

For the subcarrier orthogonality condition,

$$\int_{-\infty}^{\infty} p(t) e^{j2\pi(f_k - f_m)t} dt = \begin{cases} 1, & k = m \\ 0, & k \neq m \end{cases}, \quad (5\text{-}4)$$

where the minimum subcarrier frequency spacing required is $1/T$. Based on eq. (5-4) the Fourier transform of the pulse $p(t)$ must have spectral nulls at the frequencies to ensure subcarrier orthogonality.

5.2.1 Pulse Shape

Due to the fact that the signal bandwidth is not negligible with respect to the centre frequency, the UWA channel is a wideband channel in nature. The corresponding frequency-dependent Doppler drifts render existing ICI reduction with self-cancellation techniques used in radio channels ineffective. We can use pulse shaping for this purpose because it controls the transmitted power for the symbols transmitted and reduces ICI using controlling of pulse side lopes. Using pulse shaping for OFDM systems in narrow band and wideband contexts has been demonstrated in a real UWA time-varying channel proposed by Said Lmai et al. [159]. From the Fourier analysis, those pulses that are well localized in the time domain are widely spread out in the frequency domain, causing significant ICI [148]. The baseband modulated stream is then split into N parallel streams with $1/Ts$ sampling rate. Each stream is transmitted over a given subcarrier and shaped by a pulse shaping waveform. A number of pulse shaping functions are considered for ICI power reduction [158], such as sinc power (SP), raised cosine (RC), better than raised cosine (BTRC), improved sinc power (ISP), and modified raised cosine power (MRCP), pulses were used at the OFDM transmitter for wireless channels. Various pulse shaping functions up-to-date are [148]:

$$P_{REC}(f) = sinc(fT), \quad (5\text{-}5)$$

$$P_{RC}(f) = sinc(fT)\frac{\cos(\pi\wp fT)}{1-(2\wp fT)^2}, \quad (5\text{-}6)$$

$$P_{BTRC}(f) = sinc(fT)\frac{\left[2\beta fT\sin(\pi\wp fT) + 2\cos(\pi\wp fT) - 1\right]}{1+(\Im fT)^2}, \quad (5\text{-}7)$$

$$P_{SP}(f) = sinc^n(fT), \quad (5\text{-}8)$$

$$P_{ISP}(f) = \exp\left(-w(fT)^2\right) sinc^n(fT), \quad (5\text{-}9)$$

$$P_{MRCP}(f)=\left[sinc(fT)\left(\frac{\cos(\pi\lambda fT)}{1-(2\lambda fT)^2}\right)\right]^k, \tag{5-10}$$

where '$\wp$' is the roll-off factor $(0\le\wp\le1)$, 'w' is the design parameter to adjust the amplitude of improved sinc power pulse, 'n' is the degree of the sinc power pulse, '$\Im$' is the constant parameter of the BTRC pulse and 'λ' is the roll-off factor of MRCP pulse. The roll-off factor indicates how much extra bandwidth is utilized in addition to the ideal bandwidth. The parameter 'k' in the modified raised cosine pulse is the power factor to control side lobes. For illustration purposes we only choose the value of 'k' in the range $1\le k\le5$. Spectral comparison of existing pulse shapes are shown in Fig. 5.1 In this figure the pulse shape parameters are chosen to be the following: $\wp=1$, n = 2, w=1, $\lambda=1$, and k = 2. It has been observed that the side lobes are significant for rectangular, raised cosine pulses and less significant for BTRC and ISP pulses. ISP pulse is preferred to other existing pulses due to its lower bandwidth requirements. It also seems that the existing pulse shaping function side lobes power decay slowly, which causes the system to be sensitive to ICI. MRCP pulse shape produces the maximum side lope decay.

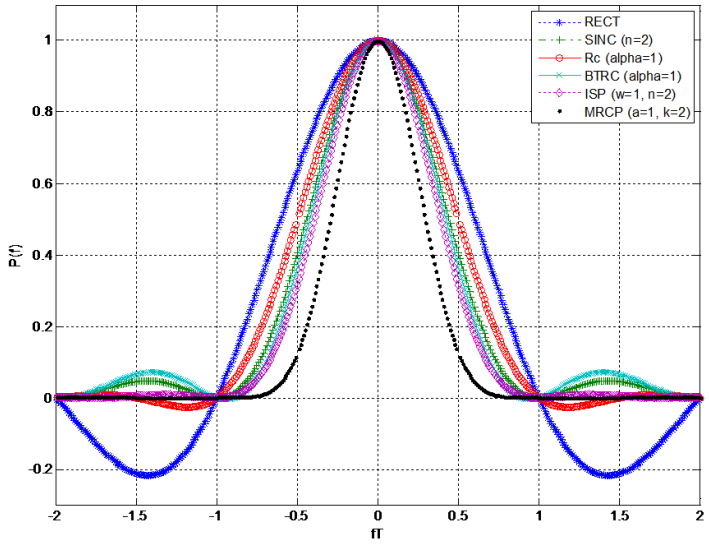

Fig. 5.1. Spectral comparison of pulse shapes.

5.2.2 ICI Analysis for OFDM Based on IFFT for Underwater Channel

This section provides original inter-carrier interference analysis of IFFT-OFDM systems in underwater channel. Frequency offset, Δf , and phase error, θ , are introduced during transmission because of channel distortion or receiver crystal oscillator inaccuracy. The received signal after multiplication by $e^{j[2\pi(-f_c+\Delta f)t+\theta]}$ becomes:

$$\tilde{r}(t)=\sum_p A_p e^{j\left(2\pi\Delta f\left(t+a_p t-\tau_p\right)+\theta\right)}\sum_{k=0}^{N-1}d_k\,p\left(t+a_p t-\tau_p\right)e^{j2\pi f_k\left(t+a_p t-\tau_p\right)}+\tilde{n}(t). \tag{5-11}$$

The m-th sub-channel correlation demodulator, thus, gives the decision variable for transmitted symbol d_m,

$$\hat{d}_m = \int_{-\infty}^{\infty} r(t) e^{-j2\pi f_m t} dt,$$

$$= \sum_p A_p \left[d_m e^{j\theta} \int_{-\infty}^{\infty} p\left(t + a_p t - \tau_p\right) e^{j2\pi\Delta f\left(t + a_p t - \tau_p\right)} dt + e^{j\theta} \sum_{\substack{k \neq m \\ k=0}}^{N-1} d_k \int_{-\infty}^{\infty} p\left(t + a_p t - \tau_p\right) e^{j2\pi\left(f_k - f_m + \Delta f\right)\left(t + a_p t - \tau_p\right)} dt \right], \tag{5-12}$$

where the first term in eq. (5-12) contains the desired signal component, and the second term is the ICI. Combining eq. (5-3) with eq. (5-12) gives:

$$\hat{d}_m = \sum_p A_p \frac{d_m e^{j\left(-2\pi\Delta f \tau_p + \theta\right)}}{\left|1 + a_p\right|} P\left(\frac{-\Delta f}{\left|1 + a_p\right|}\right) + \sum_p A_p \frac{e^{j\left(-2\pi\Delta f \tau_p + \theta\right)}}{\left|1 + a_p\right|} \sum_{\substack{k \neq m \\ k=0}}^{N-1} d_k P\left(\frac{\frac{m-k}{T} - \Delta f}{\left|1 + a_p\right|}\right), \tag{5-13}$$

where $P(f)$ is the Fourier transform of pulse shape $p(t)$. We put $\theta' = -2\pi\Delta f \tau_p + \theta$. Hence, the power of the desired signal becomes:

$$\sigma_m = \sum_p \frac{A_p^2}{\left|1 + a_p\right|^2} \left|d_m\right|^2 \left| P\left(\frac{\Delta f}{\left|1 + a_p\right|}\right) \right|^2 e^{j\theta'} \cdot e^{-j\theta'} = \sum_p \frac{A_p^2}{\left|1 + a_p\right|^2} \left|d_m\right|^2 \left| P\left(\frac{\Delta f}{\left|1 + a_p\right|}\right) \right|^2, \tag{5-14}$$

and the ICI power is:

$$\sigma_{ICI}^m = \sum_p \frac{A_p^2}{\left|1 + a_p\right|^2} \sum_{\substack{k \neq m \\ k=0}}^{N-1} \sum_{\substack{n \neq m \\ n=0}}^{N-1} d_k d_n^* P\left(\frac{\frac{k-m}{T} + \Delta f}{\left|1 + a_p\right|}\right) \cdot P\left(\frac{\frac{n-m}{T} + \Delta f}{\left|1 + a_p\right|}\right) \cdot e^{j\theta'} \cdot e^{-j\theta'},$$

$$= \sum_p \frac{A_p^2}{\left|1 + a_p\right|^2} \sum_{\substack{k \neq m \\ k=0}}^{N-1} \left| P\left(\frac{\frac{k-m}{T} + \Delta f}{\left|1 + a_p\right|}\right) \right|^2. \tag{5-15}$$

One can also consider the comparative performances of the different pulses in terms of the average signal power to average ICI power ratio [160], denoted SIR. By averaging eq. (5-14) over all possible transmitted symbols and combining with eq. (5-15), it yields:

$$SIR = \frac{\sum_p \frac{A_p^2}{\left|1 + a_p\right|^2} \left| P\left(\frac{\Delta f}{\left|1 + a_p\right|}\right) \right|^2}{\sum_p \frac{A_p^2}{\left|1 + a_p\right|^2} \sum_{\substack{k \neq m \\ k=0}}^{N-1} \left| P\left(\frac{\frac{k-m}{T} + \Delta f}{\left|1 + a_p\right|}\right) \right|^2}. \tag{5-16}$$

5.2.3 ICI Analysis for OFDM Based on IDCT for Underwater Channel

Specific signaling format is used to map the inputs bits of the OFDM system based on the DCT to the encoded data. The complex envelope of one IDCT-OFDM subcarrier block with pulse-shaping can be expressed as [161]:

$$x(t) = \sqrt{\frac{2}{N}} \sum_{k=0}^{N-1} d_k \beta_k \cos\left(2\pi f_k t\right), \tag{5-17}$$

$$x(t) = \sqrt{\frac{1}{2N}} \sum_{k=0}^{N-1} d_k \beta_k \left[e^{j2\pi f_k t} + e^{-j2\pi f_k t} \right], \tag{5-18}$$

where $d_0, d_1, \ldots . d_{N-1}$ are the modulated independent data symbols, and

$$\beta_n = \begin{cases} 1/2, & n = 0 \\ 1, & n = 1,2,\ldots\ldots,N-1 \end{cases}. \tag{5-19}$$

Transmitted signal after pulse shape for OFDM system based on IDCT will be,

$$x(t) = \frac{e^{j2\pi f_c t}}{\sqrt{2N}} \sum_{k=0}^{N-1} d_k \beta_k p(t) \left[e^{j2\pi f_k t} + e^{-j2\pi f_k t} \right] \tag{5-20}$$

The decision variable for transmitted symbol d_m, gives the m-th demodulator subchannel. Thus,

$$\begin{aligned} \hat{d}_m &= \sum_p A_p \sqrt{\frac{2}{N}} \sum_{m=0}^{N-1} \beta_m r\left(t + a_p t - \tau_p\right) \cos\left(2\pi f_m \left(t + a_p t - \tau_p\right)\right), \\ &= \sum_p A_p \cdot \begin{bmatrix} e^{j\theta} \beta_k \beta_m \int_{-\infty}^{\infty} d_m p\left(t + a_p t - \tau_p\right) e^{j2\pi\Delta f \left(t + a_p t - \tau_p\right)} dt \\ + e^{j\theta} \sum_{\substack{k \neq m \\ k=0}}^{N-1} d_k \int_{-\infty}^{\infty} p\left(t + a_p t - \tau_p\right) e^{j2\pi\left(f_k - f_m - \Delta f\right)\left(t + a_p t - \tau_p\right)t} dt \\ + \int_{-\infty}^{\infty} p\left(t + a_p t - \tau_p\right) e^{j2\pi\left(f_m - f_k - \Delta f\right)\left(t + a_p t - \tau_p\right)t} dt \end{bmatrix}, \end{aligned} \tag{5-21}$$

$$\hat{d}_m = \sum_p \frac{A_p}{\left|1 + a_p\right|} \begin{bmatrix} d_m \beta_m^2 e^{j\left(-2\pi\Delta f \tau_p + \theta\right)} P\left(\frac{-\Delta f}{\left|1 + a_p\right|}\right) \\ + \frac{e^{j\left(-2\pi\Delta f \tau_p + \theta\right)}}{2} \sum_{\substack{k \neq m \\ k=0}}^{N-1} d_k \beta_k \beta_m P\left(\frac{\frac{m-k}{T} - \Delta f}{\left|1 + a_p\right|}\right) \\ + \frac{e^{j\left(-2\pi\Delta f \tau_p + \theta\right)}}{2} \sum_{\substack{k \neq m \\ k=0}}^{N-1} d_k \beta_k \beta_m P\left(\frac{\frac{k-m}{T} - \Delta f}{\left|1 + a_p\right|}\right) \end{bmatrix}. \tag{5-22}$$

From eq. (5-22) the power of the desired signal will be:

$$\sigma_m = \sum_p \frac{A_p^2}{\left|1 + a_p\right|^2} \left| d_m \beta_m^2 \right|^2 \left| P\left(\frac{\Delta f}{\left|1 + a_p\right|}\right) \right|^2 e^{j\left(-2\pi\Delta f \tau_p + \theta\right)} \cdot e^{j\left(2\pi\Delta f \tau_p + \theta\right)} = \sum_p \frac{A_p^2}{\left|1 + a_p\right|^2} \left| d_m \beta_m^2 \right|^2 \left| P\left(\frac{\Delta f}{\left|1 + a_p\right|}\right) \right|^2. \tag{5-23}$$

Hence, the power of the ICI and SIR can be shown in the following eq. (5-22), and eq. (5-23), respectively:

$$\bar{\sigma}_{ICI}^m = \sum_p \frac{A_p^2}{\left|1 + a_p\right|^2} \left[\sum_{\substack{k \neq m \\ k=0}}^{N-1} \left| \frac{\beta_k \beta_m}{2} \right|^2 \left| P\left(\frac{\frac{k-m}{T} + \Delta f}{\left|1 + a_p\right|}\right) \right|^2 + \sum_{\substack{k \neq m \\ k=0}}^{N-1} \left| \frac{\beta_k \beta_m}{2} \right|^2 \left| P\left(\frac{\frac{m-k}{T} + \Delta f}{\left|1 + a_p\right|}\right) \right|^2 \right], \tag{5-24}$$

$$\bar{\sigma}_{SIR}^m = \frac{\sum_p \frac{A_p^2}{\left|1 + a_p\right|^2} \left| \beta_m^2 \right|^2 \left| P\left(\frac{\Delta f}{\left|1 + a_p\right|}\right) \right|^2}{\sum_p \frac{A_p^2}{\left|1 + a\right|^2} \left[\sum_{\substack{k \neq m \\ k=0}}^{N-1} \left| \frac{\beta_k \beta_m}{2} \right|^2 \left| P\left(\frac{\frac{k-m}{T} + \Delta f}{\left|1 + a_p\right|}\right) \right|^2 + \sum_{\substack{k \neq m \\ k=0}}^{N-1} \left| \frac{\beta_k \beta_m}{2} \right|^2 \left| P\left(\frac{\frac{m-k}{T} + \Delta f}{\left|1 + a_p\right|}\right) \right|^2 \right]}. \tag{5-25}$$

5.3 Simulation Results

The underwater acoustic channel model discussed in chapter 2 is used for simulations in this chapter, with the assumption that the underwater acoustic channel impulse response used is similar to that in [26, 161]. As shown in Fig. 5.2 [26], assuming that the distance between the transmitter and the receiver is 3 km, with 75 m depth, a channel with *5* non-zero taps affected multipath, $f_c = 15kHz$ is used as the optimal carrier frequency. Since the communication distance is much larger than the depth, the exact position of transmitter and receiver can be ignored if they are close to the bottom [26]. If the reflections from the bottom and surface are ideal, as shown in Fig. 5.2, i.e., let $r_p = 0,1,3,5,7$ for each path respectively. Planar geometry is used to calculate the path lengths l_p . Results of relative channel delays and magnitudes are shown in Table 5.1. The 4-QAM modulator is used with symbol duration $T = 4.1ms$.

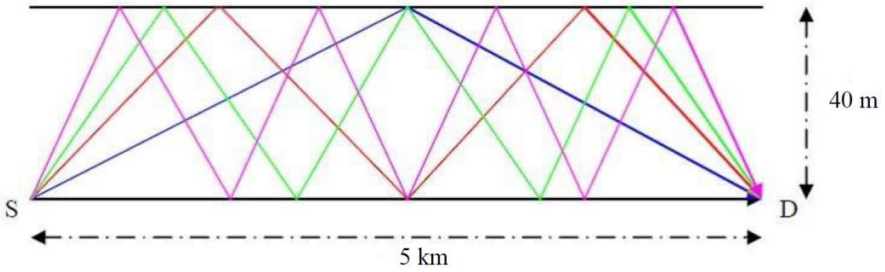

Fig. 5.2. Multipath formation in UWA channels.Taken from Yougan Chen et al. [26].

The ICI power for different sample distances from the transmitter in 256-subcarrier OFDM systems used in the underwater channel is shown in Fig. 5.3 for normalized frequency offset, $\Delta fT = 0.2$. The subfigure on the left shows the OFDM Discrete Fourier Transform (DFT) based case and the one on the right shows OFDM Discrete Cosine Transform (DCT) based case. In this figure the pulse shape parameters are chosen as $\wp = 1$, n = 2, w=1, $\lambda = 1$, and k = 2, respectively. The results show that for sub-carrier location, the minimum ICI power is reached in the case of using the modified raised cosine power pulse (MRCP) shape in comparison to other pulse shapes.

Table 5.1

Parameters of the UWA Channel Simulation.

Parameter	Value				
	1st path	*2nd path*	*3rd path*	*4th path*	*5th path*
Amplitude	0.1873	0.1322	0.0657	0.0325	0.0160
Relative delay time (ms)	0	2.5	10	22.4	39.6
Carrier Frequency (kHz)	15	15	15	15	15
Velocity (kn)	2.916	2.916	2.916	2.916	2.916
Doppler shift in hertz	10	10	10	10	10

The SIR performance with respect to the normalized frequency offset is shown in Fig. 5.4. A 256-subcarrier OFDM system is used in underwater environments where OFDM Discrete Fourier Transform (DFT)-based case is shown on the left and OFDM Discrete Cosine Transform (DCT)-based case is shown on the right. In this figure the pulse shape parameters are selected as $\wp = 1$, n = 2, w=1, $\lambda = 1$, and k = 2, respectively. The result show that the MRCP pulse shape technique outperforms all other pulse shapes in the entire range of normalized frequency offset.

The results also show that for the same pulse shape OFDM based on IDCT has more resistance for ICI and better performance for SIR.

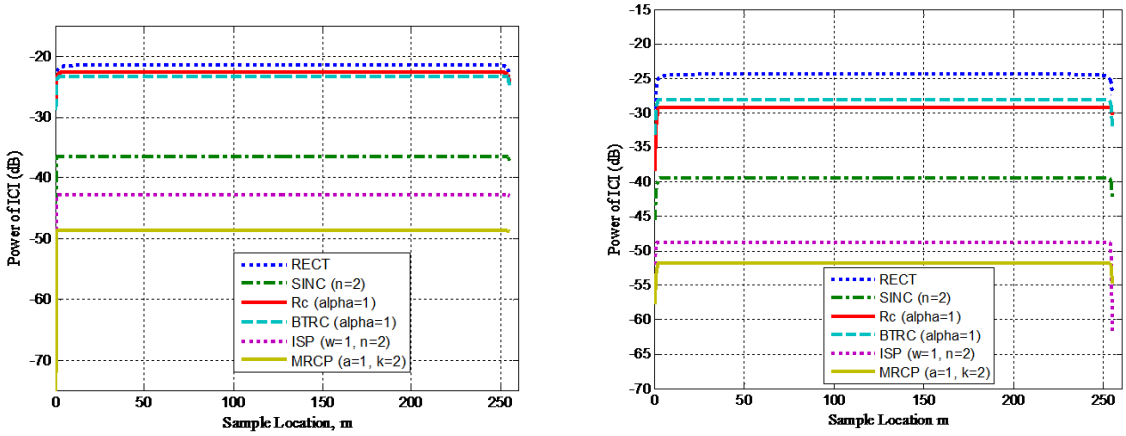

IFFT-OFDM IDCT-OFDM

Fig. 5.3. ICI for difference pulse shaping functions of IFFT-OFDM system over an UWA channel.

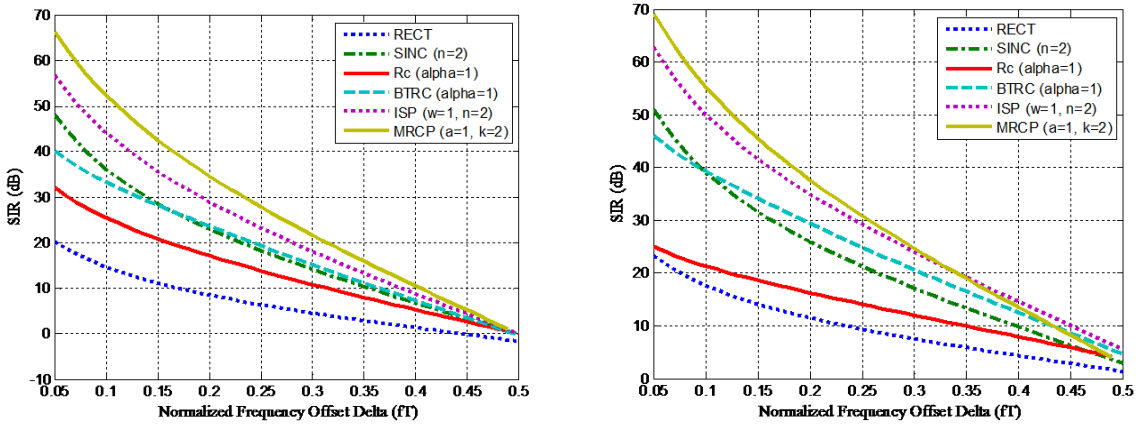

IFFT-OFDM IDCT-OFDM

Fig. 5.4. ICI for difference pulse shaping functions of IDCT-OFDM system over an UWA channel.

Based on the simulation results discussed so far we can propose an underwater communication system in this chapter, which is shown in Fig 5.5. A convolutional coder is used as the channel coder and a 4-QAM modulation as the baseband mapper. The system is tested to compare OFDM systems based on IFFT and IDCT. Since the modification of the raised cosine power pulse shape can achieve the highest performance, it is used as the pulse shape function in our system. The raised cosine power pulse generates the signal with the desirable pulse shaping, where pulse parameters are chosen as the following; w=1, $\lambda = 1$, and k = 2. The OFDM system is implemented by using 256 subcarriers and 64 cyclic prefix lengths. The performance comparison between DFT-OFDM and DCT-OFDM for underwater communication with rectangular pulse shape and MRCP pulse shaping is presented in Fig. 5.6. The result shows that for the same pulse shape OFDM based on IDCT performs better.

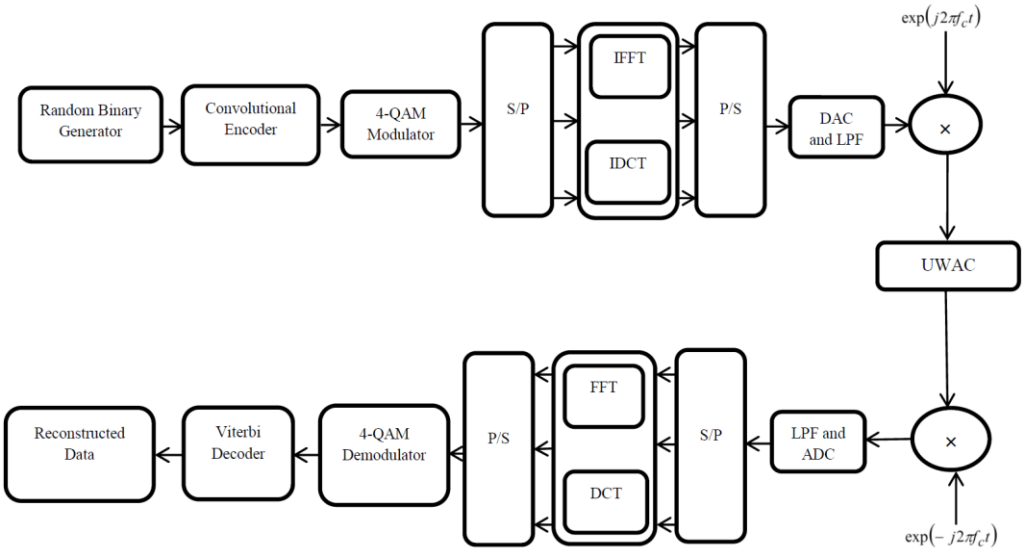

Fig. 5.5. Proposed ZP-OFDM communication system based on pulse shaping function.

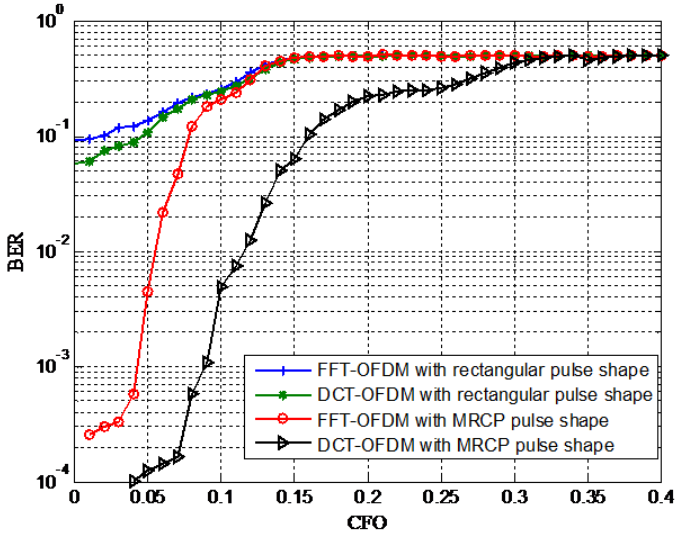

Fig. 5.6. BER performances of OFDM systems at different normalized frequency offset.

The BER performance of OFDM systems in an underwater channel based on the pulse shaping technique is evaluated by using two sets of simulations. First, as shown in Fig. 5.6 the BER performance based on CFO has been investigated using the OFDM model. The results show that the BER increases rapidly with the increase of normalized frequency offset. In these simulations, the underwater acoustic channel specifications are summarized in Table 5.1 with Signal –to– Noise Ratio fixed at 15 dB.

The pulse shape parameters used in the simulation shown in Fig. 5.7 are selected to be $\wp = 1$ and k = 2. A normalized frequency offset of *0.07* is considered for with MRCP pulse shape and also for rectangular pulse shaping. From the simulation results, it is observed that the OFDM system based on pulse shaping function improves BER performance and outperforms conventional OFDM systems.

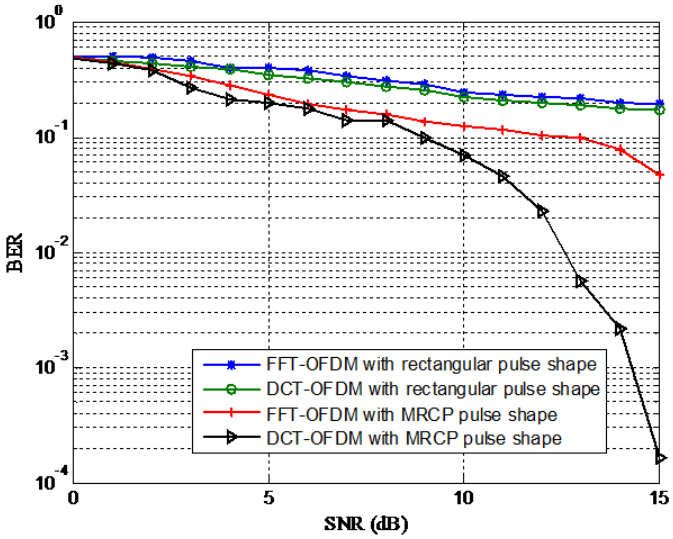

Fig. 5.7. BER performances of OFDM systems with $\Delta fT = 0.07$.

5.4 Conclusion

Inter-carrier Interference (ICI) is a major concern of OFDM systems in underwater acoustic channel communication due to the fact that delay spread in the channel exceeds the guard interval and frequency offset at the receiver. In this chapter, different pulse shaping methods for ICI reduction were investigated for underwater acoustic channels. Systems of interest have been tested for OFDM Discrete Fourier Transform (DFT)-based and Discrete Cosine Transforms (DCT)-based techniques. A number of pulse shaping functions have been considered for ICI power reduction. The system performance with each pulse shaping function has been evaluated and compared with each other using parameters such as the average ICI power and average signal power to average ICI power ratio denoted as SIR. Simulation results show that MRCP pulse shapes achieve the best performance in terms of ICI power reduction and SIR, in comparison to several commonly used conventional pulse shapes including rectangular, sinc pulse shapes etc. Simulation results for the pulse shaping inter-carrier interference reduction technique demonstrate a noticeable improvement in SIR performance. Hence, bit error rate (BER) performance is also improved when tested for an underwater communication system. Technical analysis and simulation results show the effect of pulse shape in the overall BER performance in an underwater acoustic channel. The proposed IDCT-OFDM system shows better performance for underwater acoustic channel communication systems due to higher resistance for ICI than the IFFT-OFDM with the same pulse function. The following chapters provide new OFDM schemes. The performance of each scheme in each case is compared with traditional or relevant benchmark schemes under the same inter-carrier interference reduction conditions without pulse shaping technique.

Chapter 6

Zero-Pseudorandom Noise Training OFDM

6.1 Introduction

The variations of orthogonal frequency division multiplexing (OFDM) technique can be roughly classified into three categories: cyclic prefix OFDM (CP-OFDM), zero padding OFDM (ZP-OFDM), and time domain synchronous OFDM (TDS-OFDM) [144, 146]. The popular CP-OFDM utilizes a CP as a guard interval to alleviate inter-block interference (IBI) in multipath channels [162] and transforms channel responses from linear convolution into circular convolution. As such, a finite impulse response (FIR) channel can be diagonalized by using low-complexity IFFT and FFT for inter-symbol interference (ISI) removing. In ZP-OFDM, the CP is replaced by a ZP to avoid power consumption in the guard interval between OFDM symbols [9, 13, 163]. Unlike CP-OFDM or ZP-OFDM, the TDS-OFDM technique adopts a pseudorandom noise (PN) sequence known to both the transmitter and the receiver as a guard interval as well as a training sequence (TS) for synchronization and channel estimation. The use of PN-sequences as a prefix reduces transmission overhead and improves spectrum efficiency [164].

In multipath channels with significant tap delays, such as in UWA channels, ZP-OFDM is preferred to CP-OFDM because it consumes less transmission energy [9, 170]. In this chapter, a novel transmission scheme called the zero-pseudorandom noise training OFDM (ZPN-OFDM) is proposed and discussed allowing for a significant tap delay multipath channel with good energy efficiency. The energy efficiency of the proposed OFDM scheme is then analysed and the simulation results are presented. Finally, the chapter ends with a summary of the major techniques and contributions of this work.

6.2 Zero-Pseudorandom Noise Training OFDM

Zero-pseudorandom noise training OFDM (ZPN-OFDM) is a novel transmission, where the frame structure of DPN-OFDM is modified by replacing the first PN sequence with a zero sequence. This new scheme is proposed for better energy efficiency than in previous OFDM systems. The decompositions of the transmitted and received signal frame structure of proposed ZPN-OFDM are shown in Fig. 6.1. The proposed frame structure is similar to that in DPN-OFDM but the first PN sequence is replaced by a zero sequence as shown in Fig. 6.1 (a). The decomposition of the received frame is shown in Fig. 6.1 (b), where the PN sequence is in an IBI free region used in channel estimation and the frame synchronization is based on the good autocorrelation property of the PN sequence.

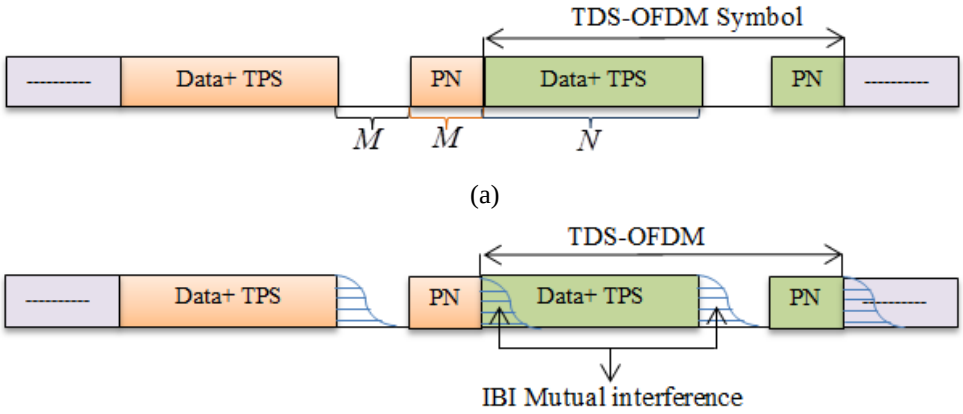

Fig. 6.1. Proposed ZPN-OFDM frame structure; (a) transmitted signal frame; (b) received signal frame.

Let the zero sequence and the PN sequence of the proposed ZPN-OFDM be $\{\mathbf{0}_{1\times M}\}_{k=0}^{M-1}$ and $\{c_{i,k}\}_{k=0}^{M-1}$, respectively. The ZPN-OFDM transmitted symbol, denoted as $a(n)$, can be expressed as:

$$a(n)=\begin{cases}\dfrac{1}{N}\sum_{k=0}^{N-1}S(k)e^{j2\pi kn/N} & n\in[0,N-1]\\ 0 & n\in[N,N+M-1]\\ \{c_{i,k}\}_{k=0}^{M-1} & n\in[N+M,N+2M-1]\end{cases}, \tag{6-1}$$

where $S(k)$ is the OFDM data block in frequency domain, N is the OFDM data block length, and M is half of the guard interval length. This OFDM signal is then passed through a multi-path fading channel. For illustration purposes, the channel can be modelled by a quasi-static L_{ch}-th order finite impulse response (FIR) filter with the channel impulse response (CIR) $\{h_{i,k}\}_{k=0}^{L_{ch}-1}$. It is assumed the length of M is larger than or equal to the maximum channel tap delay, i.e. $M \geq L_{ch}$.

The i-th received OFDM frame $\{r_{i,k}\}_{k=0}^{2M+N-1}$ consists of three parts as in Fig. 1 (b): $\{x_{i,k}\}_{k=0}^{N+L_{ch}-1}$, $i\geq 0$, denoting the convolution output between the information sequence $\{s_{i,k}\}_{k=0}^{N-1}$ and the CIR, $\{\mathbf{0}_{1\times M}\}_{k=0}^{M-1}$ representing the zero sequence and $\{y_{i,k}\}_{k=0}^{M+L_{ch}-1}=0,\ i\geq 0$ representing the linear convolution output between the PN sequence $\{c_{i,k}\}_{k=0}^{M-1}=0,\ i\geq 0$ and the CIR. In particular, the expressions of these three parts are given by:

$$x_{i,k}=s_{i,k}\oplus h_{i,k}=\sum_{l=0}^{L_{ch}-1}s_{i,k-1}\cdot h_{i,l}, \qquad 0\leq k<N+L_{ch}-1 \tag{6-2}$$

$$z_{i,k}=0 \qquad 0\leq k<M \tag{6-3}$$

$$y_{i,k}=c_{i,k}\oplus h_{i,k}=\sum_{l=0}^{L_{ch}-1}c_{i,k-1}\cdot h_{i,l}, \qquad 0\leq k<M+L_{ch}-1 \tag{6-4}$$

where $\oplus$ is the linear convolution. The received signal frame $\{r_{i,k}\}_{k=0}^{N+2M-1}$ can be expressed as:

$$r_{i,k}=u_{i,k}+n_{i,k}, \qquad 0\leq k<N+2M \tag{6-5}$$

where,

$$u_{i,k} = \begin{cases} y_{i-1,k+N} + x_{i,k} & 0 \le k < L_{ch} - 1 \\ x_{i,k} & L_{ch} - 1 \le k < N + L_{ch} - 1 \\ 0 & N + L_{ch} - 1 \le k < N + M \\ y_{i,k} & N + M \le k < N + 2M \end{cases}, \tag{6-6}$$

and $n_{i,k}$ is additive white Gaussian noise (AWGN).

As illustrated in Fig. 6.1 (b), the PN sequence introduces mutual interference to the OFDM data block in multipath channels but the received OFDM data block sequence does not cause any mutual interference of the PN block. In this case, nearly perfect channel estimation can be estimated based on the PN sequence. The basic principle of TDS-OFDM is that, with perfect channel estimation, the contribution of the PN sequence can be completely subtracted from the received OFDM data block and then the received TDS-OFDM symbol is essentially equivalent to a ZP-OFDM symbol which can be converted to a CP-OFDM symbol by the classical overlap and add (OLA) scheme to realize low-complexity channel equalization [173].

Based on received free mutual interference, a PN sequence can be used in linear channel estimation as in [168] or based on compressed sensing as in [58].

6.3 Energy Efficiency

The energy efficiency for proposed OFDM scheme can be calculated as [146]:

$$\eta_0 = \frac{N_{data}}{N_{data} + \beta^2 N_{pilots}} \times \frac{N}{N + \alpha^2 M} \times 100\%, \tag{6-7}$$

where N_{data} and N_{pilots} are the subcarrier number in the OFDM block for the data and pilot subcarriers, respectively. β and α are the amplitude factors imposed on the frequency domain. Both CP-OFDM and ZP-OFDM use pilot amplitude boosting to improve the channel estimation accuracy. In a digital video broadcasting – second generation terrestrial system (DVB-T2), the standard amplitude factor imposed is $\beta = 4/3$ and for reliable channel estimation $\alpha = \sqrt{2}$ is used for the amplitude of PN sequence in the digital terrestrial multimedia broadcast (DTMB) standard [146]. $\alpha = 1$ is proposed for DPN-OFDM and $\alpha = 1/2$ is proposed for ZPN-OFDM. The efficiency of the proposed technique and related OFDM schemes are compared in Table 6.1 based on eq. (6-7). We consider the typical example that the pilot occupation ratio in CP-OFDM is 11.29%, which is specified by the 4-K mode of the DVB-T2 standard [93].

Table 6.1

ZPN-OFDM Energy Efficiency Comparison Related to Conventional OFDM Schemes.

	ZP-OFDM	CP-OFDM	TDS-OFDM	DPN-OFDM	ZPN-OFDM
$M = N/4$	79.75%	65.23%	66.67%	66.67%	94.12%
$M = N/8$	79.75%	72.48%	80.00%	80.00%	96.97%
$M = N/16$	79.75%	76.75%	88.89%	88.89%	98.46%

6.4 Simulation Results

The performance of the proposed ZPN-OFDM transmission scheme was evaluated by simulations. Two different types of channels are used. One is a simulated channel where one channel tap is generated based on a multipath fading channel with maximum tap delay $L_{ch} = 32.$ The other is a measured underwater acoustic channel adopted from an experimental data collection in the ASCOT01 experiment conducted off the coast of New England in June 2001, as reported in [143] and is truncated to have an order $L_{ch} = 128$. In the ASCOT01 experiment, the source is deployed at a depth of 103 meters and four meters above the bottom. Receiving elements with 16 vertical vector sensor arrays is used as a receiver, covering a depth of 30-90 meters. Approximately 10 km was the source-receiver range. Every 120 seconds, the transmitter transmits a probe signal. It is repeated each period of 160 minutes to study the channels. The data bandwidth was 500 Hz with 3550 Hz carrier frequency. A linear frequency modulated (LFM) was used as a probe signal. The received signal is on a large time scale of 120 seconds, and the 16 channels can be acquired with 78 estimates using matched filtering [10]. We investigate the performance of the proposed communication system by testing uncoded and coded bit error rate (BER) performance. In all simulation experiments, the OFDM data sub-carrier number $N_{data} = 1024$ and QPSK modulations are employed. To generate data symbols, random information bits are generated and modulated directly by QPSK modulation in the uncoded case. However, in the coded case the random information bits are first encoded by a rate-1/2 convolutional encoder with generator polynomial [65,57] [174]. Then, the encoded bits are interleaved by a block interleaver of depth 8 prior to QPSK modulation.

Channel characteristic is estimated frame by frame based on compressed sensing as in [58] with $M = 32$ in each frame for simulated channel and $M = 128$ in each frame for the UWA channel case. As shown in Fig. 6.2, the proposed ZPN-OFDM offers significant BER improvement for coded and uncoded systems over the conventional TDS-OFDM systems for both simulated and measured UWA channels.

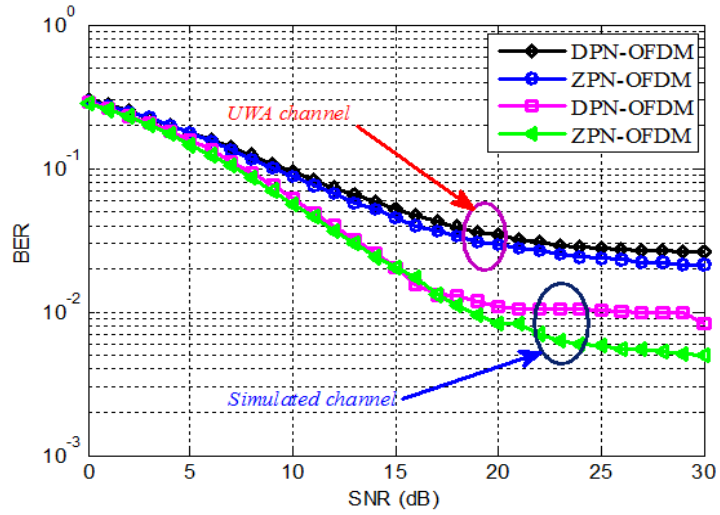

(a)

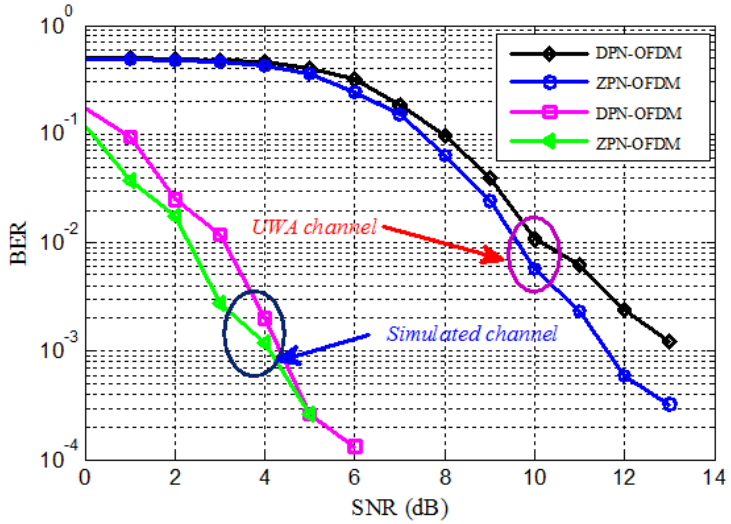

(b)

Fig. 6.2. BER performance for simulated and UWA channels; (a) Uncoded BER performance; (b) Coded BER performance.

6.5 Conclusion

In this chapter a novel OFDM transmission scheme called ZPN-OFDM is proposed, for which an improved frame structure based on a modified DPN format for TDS-OFDM systems is used. The first PN sequence in the DPN-OFDM system is replaced by a zero sequence to reduce the transmission power so as to improve energy efficiency of DPN-OFDM. Energy efficiency becomes very important for channels with significant tap delay like for underwater acoustic systems. Simulation experiments were carefully conducted to test our design by using simulated channels as well as real channels measured from one ocean experiment. Both the simulation and calculation results show that the energy efficiency and BER improvement of the proposed ZPN-OFDM system are greater than for conventional OFDM systems.

Chapter 7

Time Reversal Time-Domain Synchronization Orthogonal Frequency Division Multiplexing over Multipath Fading Channels with Significant Tap Delays

7.1 Introduction

Wireless communication with high-speed data transmission is challenging for channels with significant multipath delays [170]. As the data transmission rate increases, the time dispersion channel significantly increases and becomes more pronounced, leading to a dispersive impulse response. The single-input multiple-output (SIMO) orthogonal frequency division multiplexing (OFDM) technique is a promising approach to achieve low bit error rates (BERs) in such type of channels [136]. SIMO-OFDM relies on diversity combination (e.g. maximum ratio combination) to combat fading, and adopts the multi-carrier (MC) transmissions (in the OFDM form) to avoid cost and complexity of the channel equalization.

In single-carrier (SC) communications the passive time reversal (TR) technique has been widely used due to its spatial and temporal focusing capability. It has been proposed for communication systems for various reasons including data rate improvement, channel multiuser interference reduction and equalizer simplification [175]. TR has also been reported as an anti-dispersion and diversity combination of simulation channel in the SIMO-OFDM [10]. As the result, in SIMO systems, time-reversed OFDM (TR-OFDM) switches multiple time-dispersive fading channels into single channels with reduced channel fading and time dispersion. The TR operation is combined with the time-reversed version of the channel estimate and the multiple received signals to OFDM demodulation. This operation ensures that the short guard interval length can be used without introducing much inter-block-interference (IBI) even for wide dispersion window channels [10]. The receiver complexity can be reduced, where the required number of OFDM demodulators is reduced to be one. Time reversal OFDM has been tested in various real and simulated channels, with noticeable bandwidth efficiency and robust performance demonstrated.

As we descussed in chapter 6, there are three main types of OFDM scheme: cyclic prefix OFDM (CP-OFDM), zero padding OFDM (ZP-OFDM), and time domain synchronous OFDM (TDS-OFDM) [146]. The popular CP-OFDM uses a CP as a guard interval to alleviate IBI in multipath channels [162] and it is also used to transform channel linear convolution into circular convolution, channel using low-complexity inverse fast Fourier transform (IFFT) and fast Fourier transform (FFT) operation can be diagonalized to avoid inter-symbol interference (ISI) to be a finite impulse response (FIR). To tackle the channel transmission zero problem [163] the CP is replaced by a ZP in the ZP-OFDM. Unlike CP-OFDM or ZP-OFDM, TDS-OFDM adopts a known pseudorandom noise (PN) sequence as a training sequence (TS) as well as a guard interval for channel estimation and synchronization. Consequently, it does not require any frequency-domain pilots as usually used in ZP-OFDM and CP-OFDM, leading to a better spectral and energy efficiency [176].

In this chapter, the time reversal technique for the TDS-OFDM SIMO scheme is combined with a Zadoff-Chu sequence (ZOS) [177] as the TS for frame synchronization, channel estimation. Thanks to ZOS perfect autocorrelation properties, as well as the guard interval for long multipath channels.

However, the cost of the spectral efficiency of TDS-OFDM is that the mutual interferences between the TS and the OFDM data block in multipath channels must be removed. In traditional systems the iterative padding subtraction (IPS) algorithm [165] is used whereby IPS is required before the TS-based channel equalization and channel estimation, as in conventional TDS-OFDM demodulation are mutually conditional. To solve this problem, the dual PN-OFDM (DPN-OFDM) scheme has been proposed with two repeated PN sequences [168] and the zero PN-OFDM (ZPN-OFDM) has been proposed with zero and PN sequence, with each sequence having length equal or larger than the maximum channel tap delay. The second PN sequence is not affected by the IBI from the previous OFDM data block and hence can be used for accurate channel estimation. However, the doubled length of the guard interval in DPN-OFDM and ZPN-OFDM obviously compromises the spectral efficiency of TDS-OFDM, especially in long multipath fading channels. In this chapter, a correlation based coder for mutual interference reduction is proposed. Circular convolution is used to convolve an information sequence with a perfect correlated sequence to reduce mutual interference in the TDS-OFDM.

In this chapter, the passive time reversal for multicarrier communication is introduced and the proposed system model analyzed. The mutual interference reduction based on a correlation coder is presented, as well as the correlation based coder capability for system BER performance improvement. The performance is analyzed and further tested. Finally the summary of the major techniques and contributions is included in this chapter.

7.2 Passive Time Reversal for Multicarrier Communication

Time reversal is a feedback wave focusing technique that can be used to transparently compensate for multipath dispersion in digital communications over several types of physical propagation media, such as radio or acoustic channels [178]. The transmitter transmits a probe at the very beginning of the communication, in a time reversal process, which is recorded at the receiver and the received probe is retransmitted and serves as channel information. In the case that the channel does not change significantly, signal focusing can be achieved at the transmitter. This process can be implemented as passive phase conjugation or passive time reversal when a receiving array is available [134]. This chapter considers a passive time reversal system in the multipath fading channels with significant delays such as in shallow water channel, which consists of a single transducer and an M element hydrophone array.

Generally, for a probe source (PS) signal transition $s(t)$, from the i -th element in the received signal of a receiver array is $r_i(t) = s_i(t) \oplus c_i(t)$ without effect of the additive noise where $c_i(t)$ is the channel impulse response (CIR) and $\oplus$ denotes linear convolution. The time reversed version of the received signal $r_i(-t)$ retransmits at the time reversal [179-181]. Matched filtering with $c_i(-t)$ at each receiver element is applied in the passive time reversal and combines them coherently.

To avoid costly channel equalization, SIMO-OFDM adopts multicarrier (MC) transmissions that relies on diversity combining (e.g., maximum ratio combining) and combats fading (in the form of OFDM). Fig. 7.1 [182] shows a

time reversal OFDM system. However, the antenna receives signals and processes them differently between a time reversal OFDM system and an SIMO-OFDM system. In conventional SIMO-OFDM, signal received by vertical line array (VLA) before jointing processed are individually OFDM demodulated while they are jointly processed prior to OFDM demodulation in time reversal OFDM.

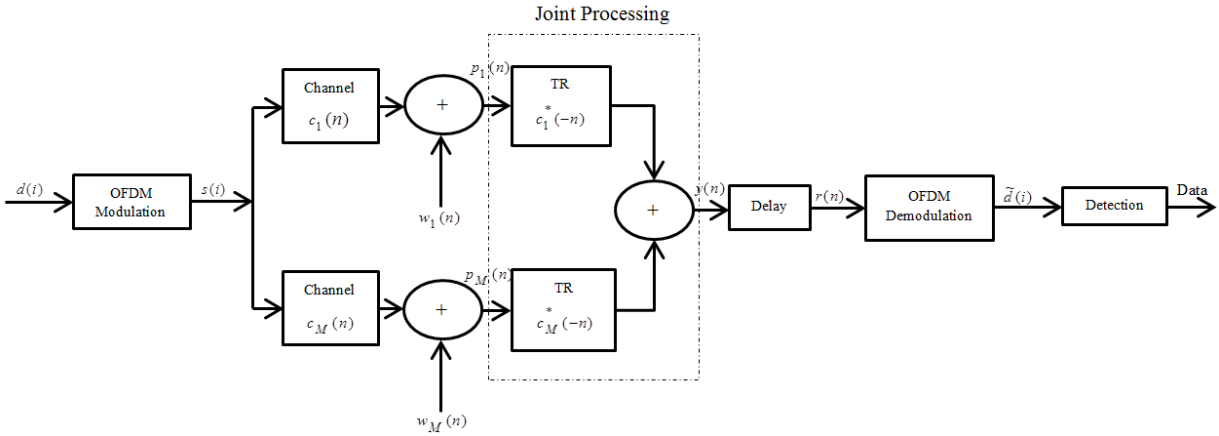

Fig. 7.1. time reversal SIMO-OFDM system model [182].

The time reversal OFDM was tested for CP-OFDM in [10]. In this chapter, time reversal OFDM is tested for TDS-OFDM and solves the IBI mutual interference problem between the TS and OFDM information data block and IBI of OFDM frame on each other when the guard interval is shorter than the maximum channel tap delay. The time reversal time domain synchronization orthogonal frequency division multiplexing (TR-TDS-OFDM) is tested in this chapter in two cases: the first one with a sufficient guard interval (TS length larger than the maximum channel tap delay) and the second one with an insufficient guard interval (TS length shorter than maximum channel tap delay). The guard interval length directly impacts bandwidth efficiency spatially in the long tap delay channels (such as underwater acoustic (UWA) channels), reduces guard interval length, and improves bandwidth efficiency.

7.3 System Model

Assume that the communication channel is a frequency-selective fading, a linear time-invariant (LTI) finite impulse response (FIR) filter [179] with an impulse responses is given by the following formula [10]:

$$c_m(l) = \sum_{p=0}^{L_c} c_{m,p}\,\delta(l-p), \qquad m = 1,\ldots\ldots\ldots,M. \tag{7-1}$$

The performance of time reversal communications is a function in the behaviour of a q -function which combines the number of array elements, the complexity of the channel $c_m(l)$ (i.e., the number of multi-paths), and their spatial distribution [179]. The TR-channel, q assumes as a perfect matched filtering that can be represented as:

$$q(l) := \sum_{m=1}^{M} c_m(l) \oplus c_m^*(-l). \tag{7-2}$$

Time support for TR channel $q(l)$ is $[-L_c, L_c]$ and therefore its maximum order is $L_q = 2L_c$ which doubles that of the $c_m(l)$'s. The received signal $y(n)$ after passive time reversal delayed by τ and $h(l) = q(l-\tau)$ is a delayed version of TR channels with the same order $L_{ch} = L_q = 2L_c$.

In TDS-OFDM, the PN training sequence serves not only as the guard interval of the subsequent OFDM data block, but also as the time-domain TS for channel estimation and synchronization. Since a general PN sequence in conventional TDS-OFDM systems has a non-ideal autocorrelation property, it is not optimal for channel estimation [183]. A Zadoff–Chu sequence [184] is known to have a better impulsive autocorrelation function. As such, it can be adopted as a better TS. Given a ZOS set $\left\{e_i^{(v)}\right\}$ with cardinal size $M, v = 1,2,3,\ldots\ldots M,\ \ i = 0,1,2,3,\ldots\ldots Q-1,$ where each sequence $e_i^{(v)}$ is of length Q, and each sequence element e_i is a complex number, one ZOS with Q length will have the following periodic Auto-Correlation Function (ACF),

$$R_{v,v}(\tau) = \sum_{v=0}^{Q-1} e_i^{(v)} e_{i+\tau}^{*(v)}. \tag{7-3}$$

Here, the subscript addition $i+\tau$ is performed modulo Q, and e_i^* denotes the complex conjugate of sequence element e_i. The sequence set is said to be perfectly auto-correlated if the set has the following characteristic:

$$R_{v,v}(\tau) = \begin{cases} Q, & for \quad \tau = 0 \\ 0, & for \quad \tau \neq 0 \end{cases}. \tag{7-4}$$

The ZOS has perfect autocorrelation. The PN sequence has good autocorrelation, but not perfect [183], which is denoted by $Q\left[1 \quad (1/Q)_{1\times(Q-1)}\right]^T$.

The signal structure comparison between TDS-OFDM and CP-OFDM in the time domain can be shown in Fig. 7.2. The CP used by CP-OFDM can be replaced by the known ZOS. The i-th transmitted TDS-OFDM signal frame denoted by $s_i = \left[s_{i,0}, s_{i,1}, \ldots\ldots s_{i,P-1}\right]^T$ is composed of two independent parts: a known ZOS $e_i = \left[e_{i,0}, e_{i,1}, \ldots\ldots e_{i,L-1}\right]^T$ of length Q, and an OFDM data block $X_i = \left[X_{i,0}, X_{i,1}, \ldots\ldots, X_{i,K-1}\right]^T$ of length K:

$$S_i = \begin{bmatrix} E_i \\ X_i \end{bmatrix}_{N\times 1}, \tag{7-5}$$

where $N = Q + K$ is TDS-OFDM signal frame length.

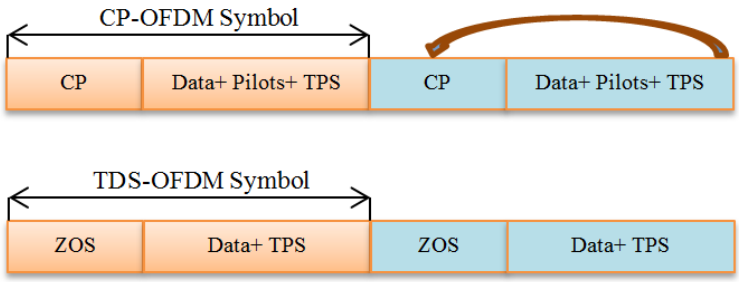

Fig. 7.2. The proposed TDS-OFDM and CP-OFDM signal structure comparison in the time domain.

The system proposed is illustrated in Fig 7.3. The proposed TR-TDS-OFDM transmitter employs standard TDS-OFDM modulation. Let K be the number of subcarriers, Q the guard interval length, I_Q a $Q \times K$ guard interval matrix, $u(i) := \left[u(iK), \ldots\ldots\ldots, u(iK+K-1)\right]^T$ the information block and $s(i) := \left[s(iB), \ldots\ldots, s(iB+B-1)\right]^T$ (with $B = K+Q$) the corresponding transmitted block.

$$s(i) = T_e x(i), \tag{7-6}$$

$$x(i) = u(i) \otimes g(i), \tag{7-7}$$

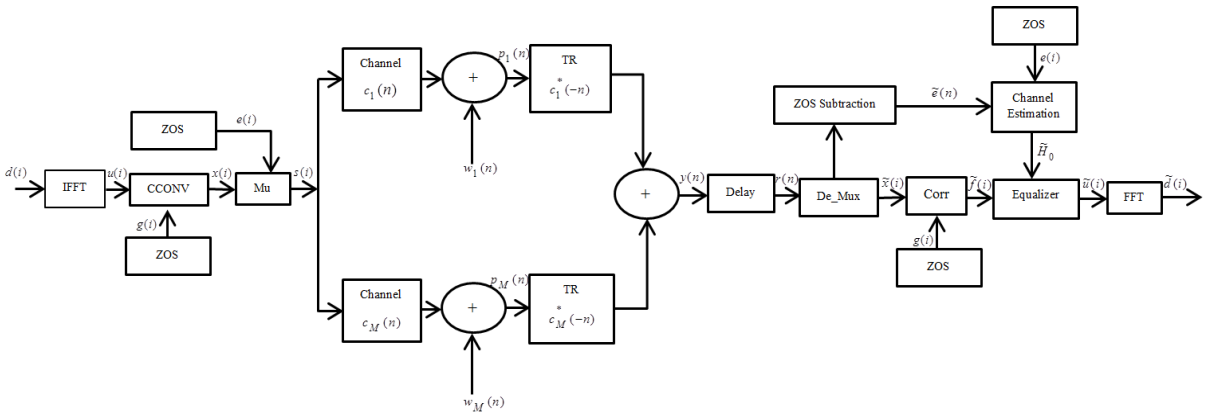

Fig. 7.3. time reversal single-input multiple-output TDS-OFDM proposed communication system.

where $\otimes$ represents the circular convolution, in eq. (7-7), g is K -point ZOS used in correlation based encoder. The $Q \times K$ matrix T_e represents the operation of ZOS TS insertion and $u(i) = F_K^{\mathcal{H}} d(i)$, $d(i)$ is the IFFT input and the $K \times K$ matrix F_K (with $[F_K]_{p,q} = (1/\sqrt{K}) \exp((-j2\pi(p-1)(q-1))/K)$ represents the K-point FFT operation. Let the last L_e be rows I_e of the $K \times K$ identity matrix I_K .

Using passive TR the joint processing of $p_m(n)$ is conducted at the time reversal OFDM receiver. Passive TR is used to focus signals in space and/or time. In the TR-TDS-OFDM context, the TR generates $y(n)$ can be written as $y(n) := \sum_{m=1}^{M} p_m(n) \oplus c_m^*(-n)$ where $\oplus$ is the linear convolution operation. Due to the assumption that channels $c_m(l)$ are LTI, $p_m(n)$ will be $p_m(n) = s(n) \oplus c_m(n) + w_m(n)$. Therefore, $y(n)$ can be related to $s(n)$ in the following way:

$$y(n) = \sum_{l=-L_c}^{L_c} q(l) s(n-l) + z(n). \tag{7-8}$$

According to this, TR-TDS-OFDM transmission works as a single-input single-output (SISO) system when the TDS-OFDM signal is transmitted in a TR channel in eq. (7-2) with additive noise,

$$z(n) := \sum_{m=1}^{M} w_m(n) \oplus c_m^*(-n). \tag{7-9}$$

$y(n)$ is delayed by τ after passive time reversal to yield $r(n) = y(n-\tau)$, which, according to eq. (7-8), is given by:

$$r(n) = \sum_{l=-\frac{L_q}{2}+\tau}^{\frac{L_q}{2}+\tau} h(l) s(n-l) + z(n), \tag{7-10}$$

and $h(l)=q(l-\tau)$ is a version of TR delayed by τ channel with the same order $L_{ch}=L_q=2L_c$ and $z(n):=\sum_{m=1}^{M} w_m(n)\oplus c_m^*(\tau-n)$ (with slightly unorthodox notation without causing confusion).

TR-TDS-OFDM data model can be obtained as:

$$r(i)=H_0 s(i)+H_1 s(i-1)+H_{-1} s(i+1)+\tilde{z}(i). \tag{7-11}$$

Here, for $l=0,\ 1,\ -1$, the $Q\times Q$ matrices H_l are defined to have the $(p,q)-th$ entry $[H_l]_{p,q}=h(lQ+p-q)$. $\tilde{z}(i)$ denotes the additive white Gaussian noise vector. The data model is derived in eq 7.11, without specifying the value of the guard interval relative to the TR channel order L_q. Therefore, eq. (7-11) can be applicable for any guard interval length regardless of whether it is smaller or larger than L_q.

If a sufficient guard interval ($Q=L_{ch}$) is used, by choosing $\tau=Q/2$ such that $h(l)=0$ for $l<0$ or $l>Q$, it can be verified that $H_{-1}=0$, $H_1=0$. Equation (7-11) becomes:

$$r(i)=H_0 s(i)+\tilde{z}(i). \tag{7-12}$$

The decompositions of transmitted and received signal frames are shown in Fig. 7.4 and Fig. 7.5. The i-th received OFDM frame $\{r_{i,k}\}_{k=0}^{Q+K+L_{ch}-2}$ excluding noise consists of two overlapping parts: $\{a_{i,k}\}_{k=0}^{Q+L_{ch}-2}$ representing the output of the linear convolution between the ZOS (TS) $\{e_{i,k}\}_{k=0}^{Q-1}$ and the channel impulse response, and $\{b_{i,k}\}_{k=0}^{K+L_{ch}-2}$ denoting the output of the convolution between the information sequences $\{x_{i,k}\}_{k=0}^{K-1}$ and the channel impulse response. The expressions of received frame are given by:

$$r_{i,k}=y_{i,k}+\tilde{z}_{i,k} \tag{7-13}$$

where $y_{i,k}$, in sufficient guard interval case (i.e. guard interval length longer than maximum channel tap delay), can be written as:

$$y_{i,k}=\begin{cases} b_{i-1,k+N}+a_{i,k} & 0\le k<L_{ch}-1 \\ a_{i,k} & L_{ch}-1\le k<Q-L_{ch}+1 \\ b_{i,k}+a_{i,k} & Q-L_{ch}+1\le k<Q+L_{ch}-1 \\ b_{i,k} & Q+L_{ch}-1\le k<Q+K-L_{ch}+1 \\ b_{i,k}+a_{i+1,k-N} & K+Q-L_{ch}+1\le k<K+Q \end{cases}, \tag{7-14}$$

and in the case of insufficient guard interval (guard interval length shorter than the maximum channel tap delay) it can be written as:

$$y_{i,k}=\begin{cases} b_{i-1,k+N}+b_{i,k}+a_{i,k} & 0\le k<L_{ch}-1 \\ b_{i,k}+a_{i,k} & L_{ch}-1\le k<Q+L_{ch}-1 \\ b_{i,k} & Q+L_{ch}-1\le k<K+Q-L_{ch}+1 \\ b_{i,k}+a_{i+1,k} & Q+K-L_{ch}+1\le k<K+2Q-L_{ch}+1 \\ b_{i,k}+a_{i+1,k-N}+b_{i+1,k-N} & 2Q+K-L_{ch}+1\le k<K+Q \end{cases}, \tag{7-15}$$

In Fig. 7.4, the decompositions of transmitted and received frames for TR-ZP-OFDM are shown. In case of TR-ZP-OFDM, no IBI will be presented in the case that guard interval length is equal or longer than the maximum channel tap delays; it will present only in the case of insufficient guard interval length. In the case of TR-TDS-

OFDM mutual IBI is present in the all cases. For sufficient guard interval length the IBI will be between OFDM data blocks and training sequence as shown in Fig. (7.5, d). In the case of insufficient guard interval length the IBI mutual interference will be between training sequence and OFDM data block and also between the OFDM data blocks themselves as shown in Fig. (7.5, f). The mutual interference will affect channel estimation accuracy and synchronization.

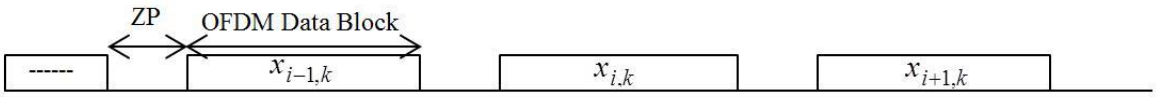

(a) ZP-OFDM Transmitted signal frame

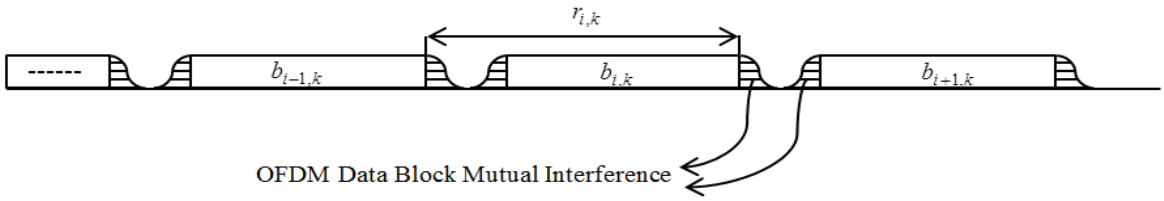

(b) ZP-OFDM Received signal frames

Fig. 7.4. Transmitted and received decomposition signal frames in TR-ZP-OFDM (case: channel tap delay less than guard interval).

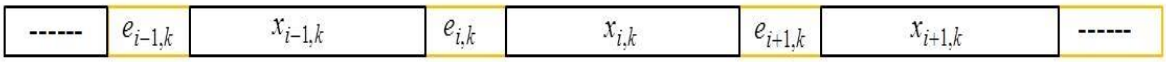

(a) Transmitted signal frame

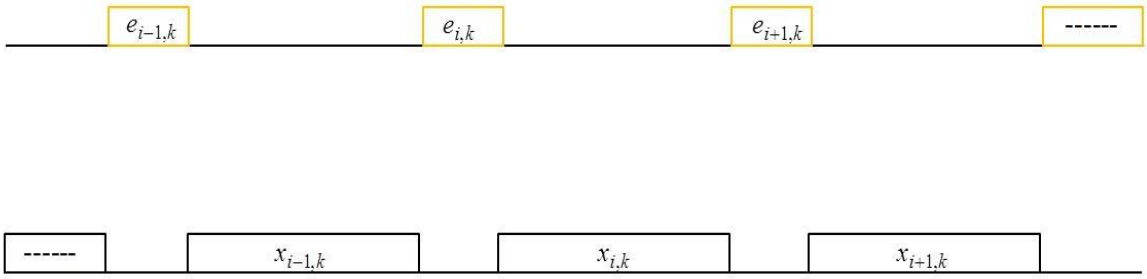

(b) Transmitted signal frame decomposition in time domain.

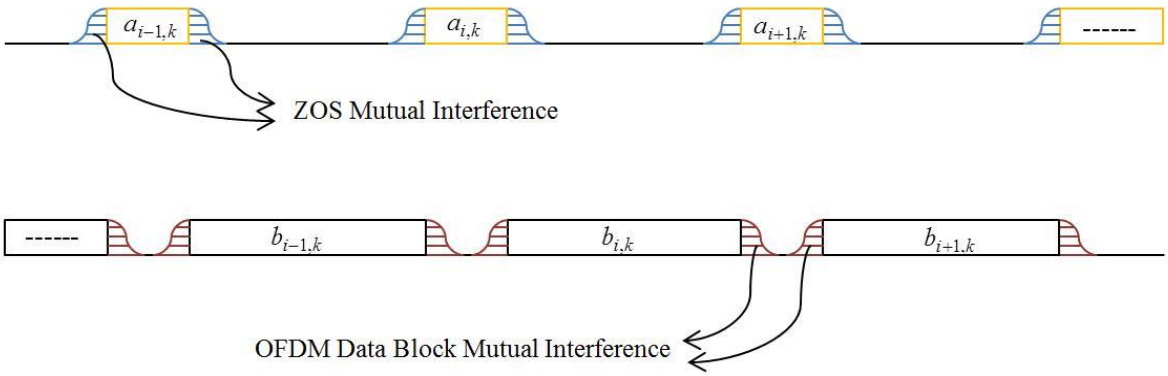

(c) Received signal frame decomposition in time domain (case: channel tap delay less than guard interval)

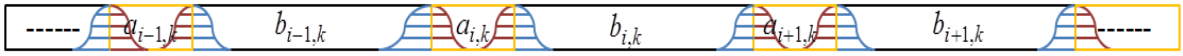

(d) Received signal frames (case: channel tap delay less than guard interval)

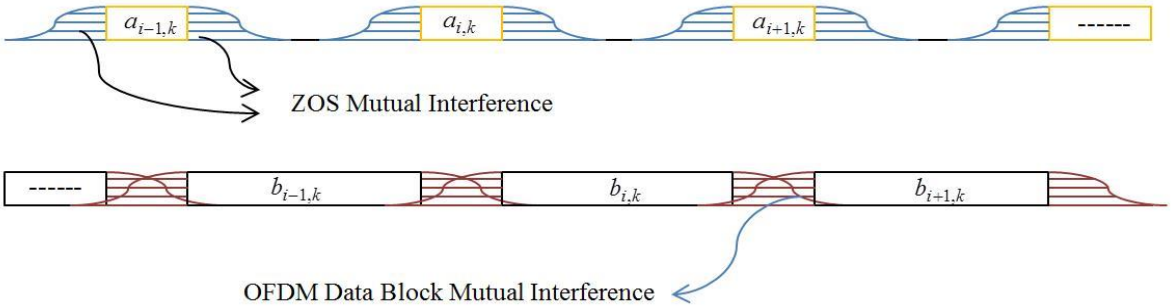

(e) Received signal frame decomposition in time domain (case: channel tap delay greater than guard interval)

(f) Received signal frames (case: channel tap delay greater than guard interval)

Fig. 7.5. Transmitted and received signal frames decomposition in TR-TDS-OFDM.

7.4 Mutual Interference Reduction Based on Correlation Coder

As illustrated in Fig. 7.5, the training sequence and the OFDM data block introduce mutual interference to each other in multipath channels. The basic principle of TDS-OFDM is that with perfect channel information, the contribution of the training sequence can be completely subtracted from the received OFDM data block, and then the received TDS-OFDM symbol is essentially equivalent to a ZP-OFDM symbol, which can be converted into a CP-OFDM symbol by the classical overlapping and adding (OLA) scheme to realize a low-complexity channel equalization [172]. However, perfect channel estimation for some multipath channels is not practically available, particularly for underwater acoustic channels [170].

This chapter proposes a correlation coder for mutual interference reduction. At the transmitter side it is shown in Fig. 7.3. The IFFT output $u(i)$ is convolved with ZOS $g(i)$ with circular convolution data frame with encoder process as in eq. (7-7). At the receiver side as shown in Fig. 7.3, after frame synchronization and TS subtraction, the OFDM data frame will be:

$$\tilde{x}(i)=\begin{cases} b_{i,k}+a_{i,k}+\tilde{z}_{i,k} & Q-L_{ch}+1\le k<Q+L_{ch}-1 \\ b_{i,k}+\tilde{z}_{i,k} & Q+L_{ch}-1\le k<Q+K-L_{ch}+1 \\ b_{i,k}+a_{i+1,k}+\tilde{z}_{i,k} & K+Q-L_{ch}+1\le k<K+Q+L_{ch}-1 \end{cases}, \qquad (7\text{-}16\text{- a})$$

or,

$$\tilde{x}(i)=\begin{cases} b_{i,k}+a_{i,k}+\tilde{z}_{i,k} & L_c-1\le k<Q+L_{ch}-1 \\ b_{i,k}+\tilde{z}_{i,k} & Q+L_{ch}-1\le k<Q+K-L_{ch}+1 \\ b_{i,k}+a_{i+1,k}+\tilde{z}_{i,k} & Q+K-L_{ch}+1\le k<2Q+K-L_{ch} \\ b_{i,k}+a_{i+1,k}+b_{i+1,k-N}+\tilde{z}_{i,k} & 2Q+K-L_{ch}+1\le k<K+Q \end{cases} \quad (7\text{-}16\text{- b})$$

based on TS length eq. (7-16-a) is for sufficient TS length case, and eq. (7-16-b) for insufficient case. Generally, the received OFDM data symbols can be represented as:

$$\tilde{x}(i)=b_{i,k}+v_{i,k}+\tilde{z}_{i,k}, \quad (7\text{-}17)$$

$v_{i,k}$ represents the mutual interference of ZOS TS in an OFDM data frame, where $\tilde{z}_{i,k}$ is the additive white Gaussian noise. The receiver directly uses the known local ZOS $g(i)$ to acquire a rough correlated OFDM data frame. The correlation based decoder operation will be:

$$\tilde{f}(i)=\frac{1}{K}\tilde{x}(i)\otimes g(i)=u(i)+v_i'+z_i', \quad (7\text{-}18)$$

where $v_i'=\frac{1}{K}v_i\otimes g(i)$ denotes the noise term, and $z_i'=\tilde{z}_i\otimes g(i)$. Since the ZOS sequence $g(i)$ is independent of the OFDM data block $u(i)$, v_i' can be regarded as another noise term. The correlated based coder reduces the mutual interference and white noise by K.

7.4.1 Realistic TR Channel

Many benefits can be ensured in the ideal TR channel which depends on how impulse like signals can be realized. To evaluate the "impulse-likeness" of a TR channel, in [10] used two different approaches. For the statistical approach, the TR channel can be expressed as in [10]:

$$q(l)=\begin{cases} \sum_{m=1}^{M}\sum_{p=0}^{L_c}\left|c_{m,p}\right|^2 & l=0 \\ \sum_{m=1}^{M}\sum_{(p,p')\in I(l)}c_{m,p}c_{m,p'}^{*} & l\neq 0 \end{cases}, \quad (7\text{-}19)$$

where $I(l)$ is the set of pairs (p,p') satisfying $p-p'=l$ for $p,p'\in[0,L_c]$. The cardinality of $I(l)$ is $|I(l)|=L_c-|l|+1$. $q(l)$'s is treated as a deterministic signal. In eq. (7-19), the terms in $q(0)$ and $q(l)$, $l\neq 0$, are added coherently as a sum of real numbers and up arbitrarily as a summation of complex numbers respectively. Intuition suggests that $q(l)$, $l\neq 0$ would eventually become negligible relative to $q(0)$ and be suppressed in the case that the number of terms involved in the summations is sufficient, indicating that the $q_{ideal}(l)$ offers a good approximation of $q(l)$ in a multipath-rich channel environment.

7.4.2 BER Performance Improvement Using Correlation Based Coder

After removing mutual interference, the data block between TS and OFDM in TR-TDS-OFDM can be considered as the TR-ZP-OFDM and any equalizer used in ZP can be used in the TDS case. In this section, performance of the proposed system will be discussed and the effect of TS length on the BER performance will be evaluated.

Based on the signal-to-interference plus noise ratio (SINR), the performance of proposed TR-TDS-OFDM detector can be approximately measured:

$$\gamma(q,Q,\tau)=\frac{TrE\left[XsX_s^{\#}\right]}{TrE\left[\left(X_{ISI}+X_{IBI}+X_N\right)\left(X_{ISI}+X_{IBI}+X_N\right)^{\#}\right]} \tag{7-20}$$

where $Tr(\bullet)$ stands for the trace of a matrix and $E(\bullet)$ denotes the statistical expectation. In eq. (7-20), to highlight SINR dependence on the TR channel, γ has been expressed as a function of q,Q and τ $q:=[q(-L_c),\ldots,q(L_c)]^T$. The TS length is Q, the delay is τ, X_{ISI} is the inter-symbol interference, X_{IBI} is the mutual inter-block interference, and X_N are the additive white Gaussian noise.

Cast the channel taps $h(l)'s$ into a vector $h:=[h(-L_{ch}/2+\tau),\ldots,h(-Q/2),\ldots,h(0),\ldots,h(Q/2),\ldots h(L_{ch}/2+\tau)]^T$ and then split it into $h=\bar{h}+\tilde{h}$ where $\bar{h}:=[0,\ldots\ldots0,h(-Q/2),\ldots\ldots,h(0),\ldots\ldots,h(Q/2),0,\ldots\ldots0]^T$ and $\tilde{h}:=[h(-L_{ch}/2),\ldots,h(-Q/2-1),0,\ldots0,\ldots,h(Q/2+1),0,\ldots,h(L_{ch}/2)]^T$ and collect those taps inside and outside the TS window $[-Q/2,Q/2]$, respectively. The inter-symbol interference X_{ISI} will be equal to zero in the case of sufficient TS length, and $X_{ISI}=\tilde{H}_0S(i)$ in the case that the guard interval lengths are shorter than the maximum channel tap delay. X_{IBI} is the mutual inter-block interference. It will be $V_{i,k}$ (the mutual interference between TS and OFDM data block of each frame) in the case of sufficient TS length and will be, $X_{IBI}=V_{i,k}+\tilde{H}_{-1}S(i+1)+\tilde{H}_1S(i-1)$ in the case of insufficient TS length.

After that the correlation based coder SINR will be:

$$\gamma(q,Q,\tau)=\frac{TrE\left[FsF_s^{\#}\right]}{TrE\left[\left(F_{ISI}+F_{IBI}+F_N\right)\left(F_{ISI}+F_{IBI}+F_N\right)^{\#}\right]} \tag{7-21}$$

F_{ISI}, F_{IBI} and F_N is the X_{ISI}, X_{IBI} and X_N, respectively, after reduced by *K* factor. The correlation based coder improves the receiver SINR by the *K* factor without any spectrum efficiency loss.

7.5 Simulation

In this section, the proposed communication system performance will be investigated by testing the coded and uncoded TR-TDS-OFDM BER performance via Monte-Carlo simulations. In the experiments, the sub-carrier number is $K=1024$ with a QPSK modulation. Random information bits are generated and directly modulated by QPSK modulation in the uncoded case to generate data symbols $d(i)$, but for the coded case, convolution coder with [65,57] generator polynomial [174] and 0.5 rate encodes the information bits then interleaves with a 8 depth prior block interleaver. The proposed system is tested for two types of channels. First, a simulated channel where channel taps $c_m(l)$'s are generated based on multipath fading channel as complex Gaussian random variables with equal variance and independent zero-mean. The other is the measured channel discussed in chapter 6 which has been truncated so that $L_{ch}=159.$ The simulation results are averaged over 78 runs for the real measured channels, or over 500 runs for simulated channels.

Channel characteristics are estimated frame by frame, with the periodically transmitted ZOS TS associated with the data signal frame [165]. Channel is estimated as:

$$h_{0,k} = IFFT\left\{\frac{FFT\left(a_{i,k}\right)}{FFT\left(e_{i,k}\right)}\right\}, \tag{7-22}$$

To recover OFDM time domain data information $u(i)$ at low complexity a multi-tap equalizer is used by using a symbol-by-symbol detector.

$$\tilde{u}(i) = \det\left(\tilde{f}(i)/\tilde{h}_0(i)\right) \tag{7-23}$$

Experiment 1 *(The effects of the Guard interval length).* This experiment will simulate the coded and uncoded BER performances of TR-TDS-OFDM with different training sequence lengths. A simulated channel of order $L_{ch} = 32$ is generated and the data is transmitted over M number of receiver antenna. Here we consider a typical implementation at $M = 4$.

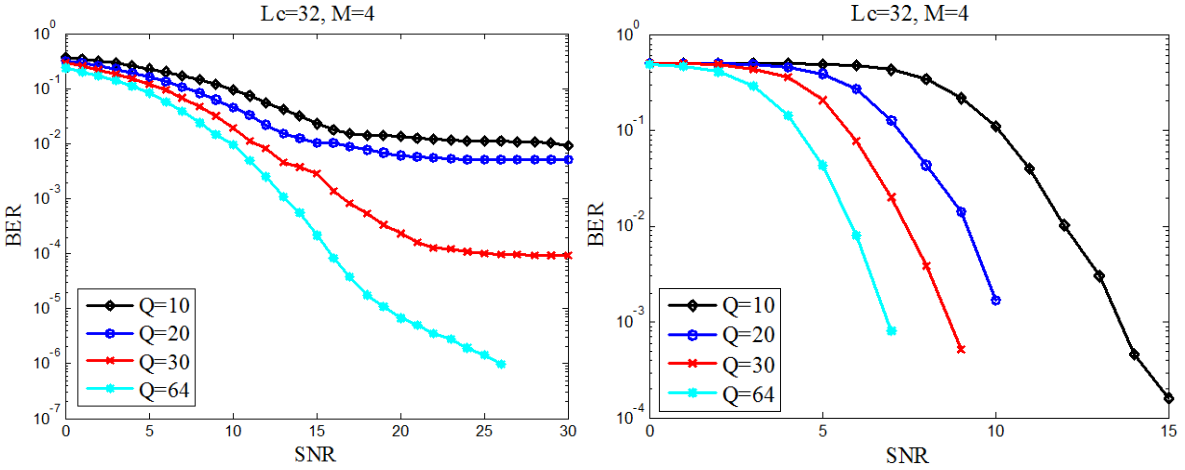

(a) Uncoded BER Performance (b) Coded BER Performance

Fig. 7.6. The BER performance of TR-TDS-OFDM with different guard interval lengths (simulated channels).

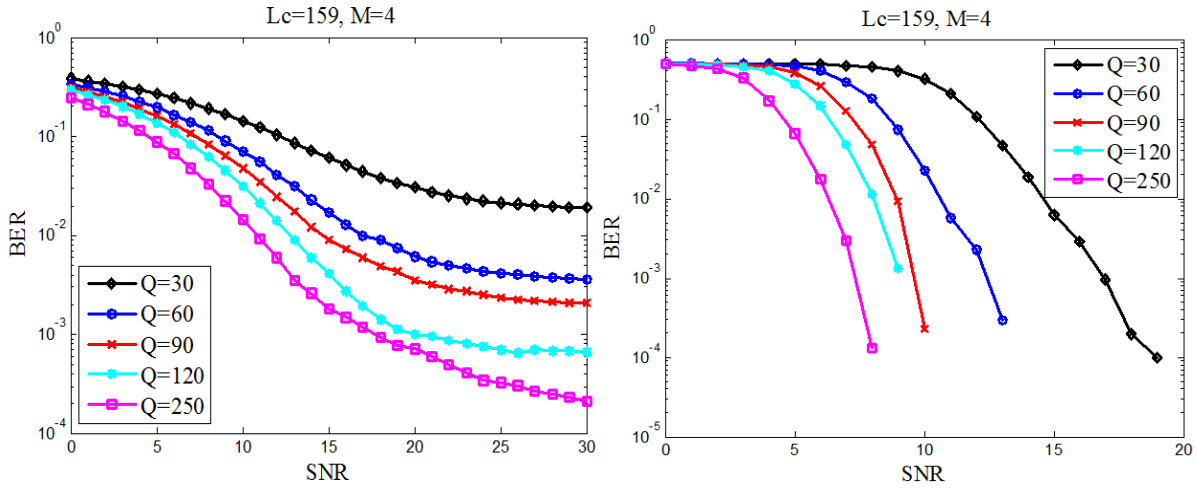

(a) Uncoded BER Performance (b) Coded BER Performance

Fig. 7.7. The BER performance of TR-TDS-OFDM with different guard interval lengths (measured UWA channels).

The channel is estimated based on eq. (7-22). As shown in Fig. 7.6. (a) the uncoded BER performance is saturated at high SNRs in the insufficient guard interval length case (i.e., Q = 10, 20, 30), due to the residual IBI. As a result, as the guard interval length increases a level of performance "floor" decreases. Such error floor does not appear when the TS length is sufficient (i.e., Q= 64). In practice, channel coding is used to remove such error floors as shown in Fig. 7.6, (b). For a measured channel, the same simulation is repeated with guard interval length (i.e., Q=30, 60, 90, 120, 250) and the results are plotted in Figs. 7.7. (a) and 7.7. (b) with the same observations.

Experiment 2 (*Receiver antennas number effect*). In this experiment, different numbers of receiver antennas will be simulated and discussed to evaluate the coded and uncoded BER performance of TR-TDS-OFDM. In this simulation, the simulated channels of order $L_{ch} = 32$ are used. $Q = 16$ is used as the guard interval length. Fig. 7.8 shows the BER performance of proposed TR-TDS-OFDM, where for the number of receiver antennas M increases the error floor decreases. Recalling that the error floor level depends on the residual mutual IBI and the amount of IBI is a function of how TR-channel is impulse-like, these results show that, as M increases the TR channel becomes more impulse like.

Generally, even with a small number of M, the TR channel is quite impulse-like when the channels are rich in multipath; when the channels are sparse to make the TR channel impulse-like a large number of receiver antennas (i.e. large M) are required. These results are quite consistent with observations in the previous subsection. Note that the same conclusion has been drawn for UWA channels based on waveguide physics with CP-OFDM and ZP-OFDM systems [185].

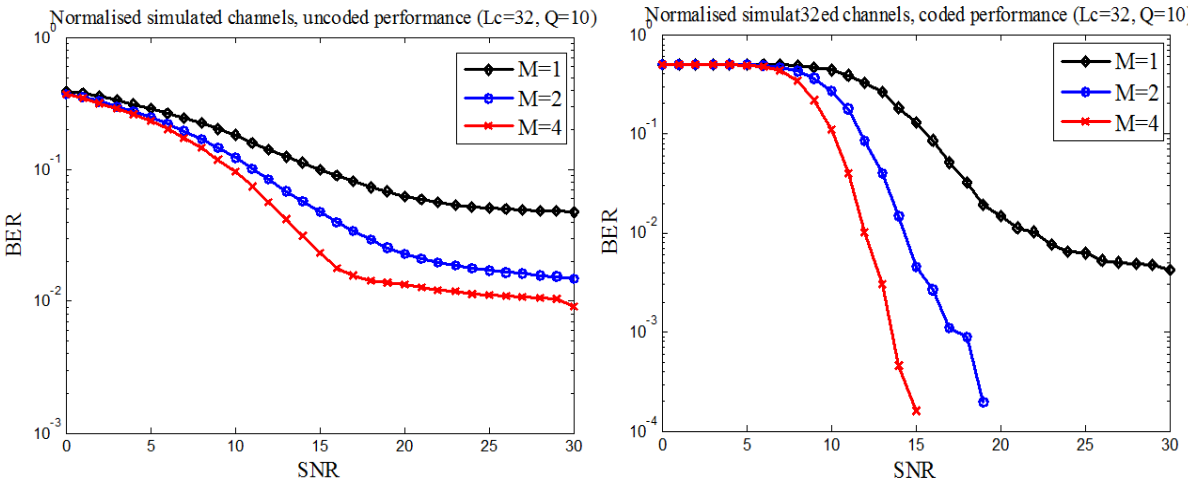

(a) Uncoded BER Performance (b) Coded BER Performance

Fig. 7.8. Uncoded BER performance with different number of receiver antennas M (simulated channels).

Experiment 3 *(performance comparison between proposed and IPS [165]).* In this experiment, the uncoded BER performance of TR-TDS-OFDM will be evaluated. Measured UWA and simulated channels with order $L_c = 32$ are used. The guard interval length is fixed at $Q = 60$ for the measured UWA channel and $Q = 20$ for the simulated channel. The performance floor becomes lower when the proposed correlation based coder are used as shown in Fig. 7.9 and it results in better performance than conventional IPS [165] for different types of channels.

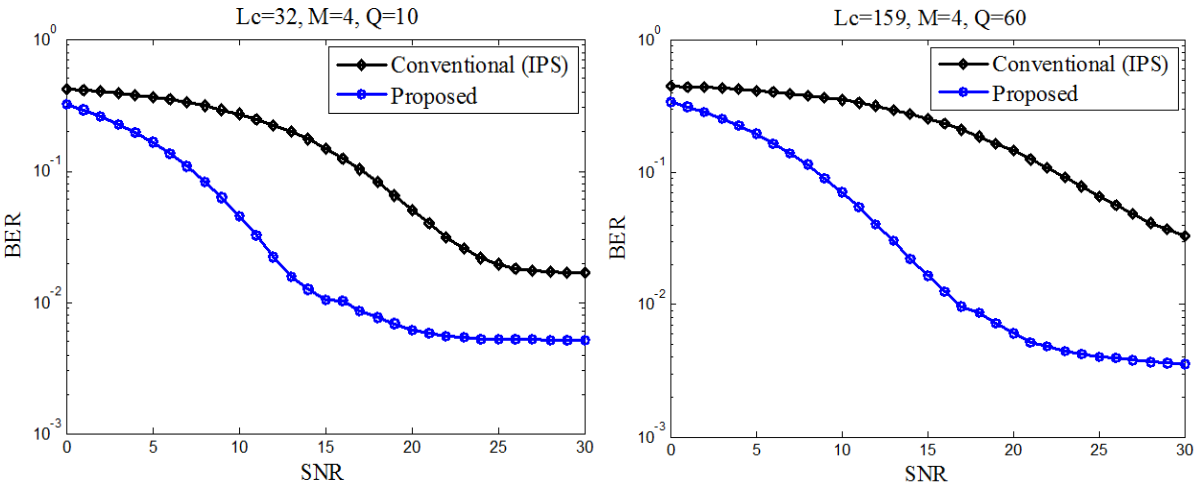

(a) Uncoded BER Performance (simulated channels). (b) Uncoded BER Performance (UWA channels).

Fig. 7.9. Uncoded BER performance with different mutual TR-TDS-OFDM inter-block interference reduction methods.

Experiment 4 (*BER comparison of TR-TDS-OFDM and TR-ZP-OFDM*). In this experiment, the coded and uncoded BER performance of TR-TDS-OFDM and TR-ZP-OFDM will be compared. Measured UWA channel and simulated channel with order $L_{ch} = 32$ are used. Correlation based coder increases the receiver SINR by *K* without spectrum efficiency loss. The performance results displayed in Fig. 7.10 compare the BER performance of time reversal OFDM system for TDS and ZP guard interval. The TR-TDS-OFDM based on correlation coder results in better performance than conventional TR-ZP-OFDM because the correlation based coder not only reduces inter-block interference and inter-symbol interference, but also reduces the Gaussian channel noise by factor *K*.

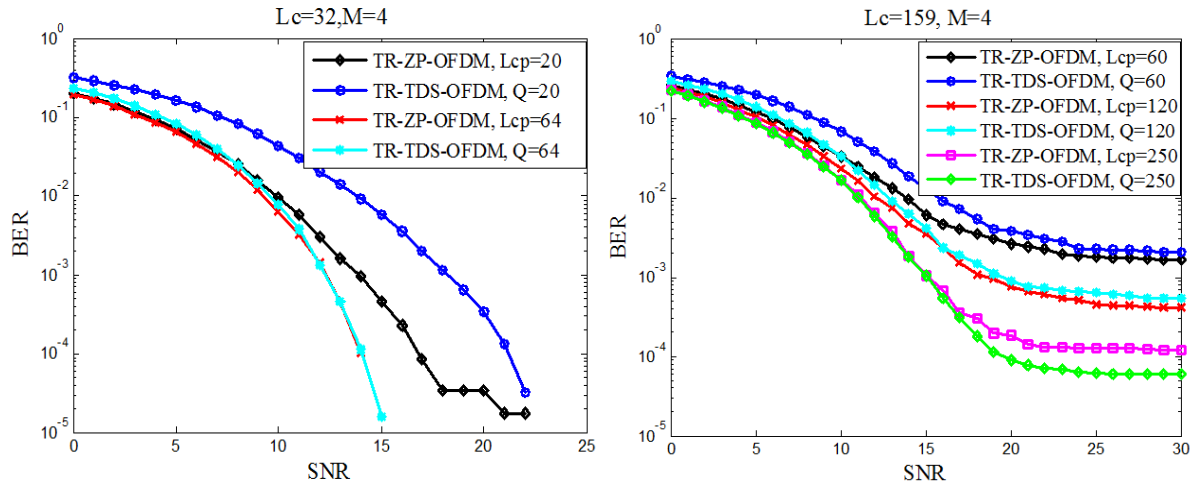

(a) Uncoded BER Performance (simulated channels). (b) Uncoded BER Performance (UWA channels).

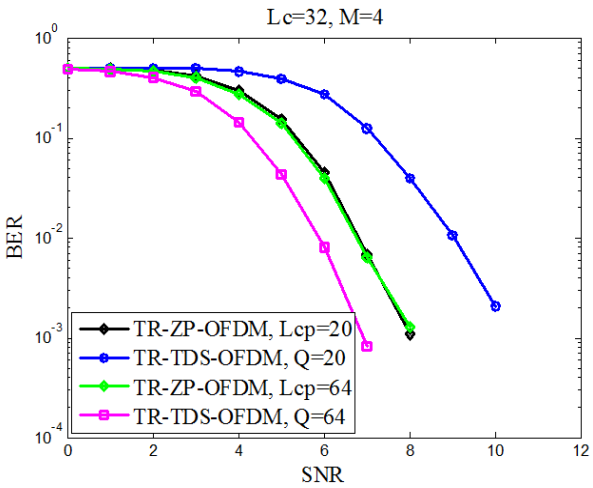

(c) Coded BER Performance (simulated channels).

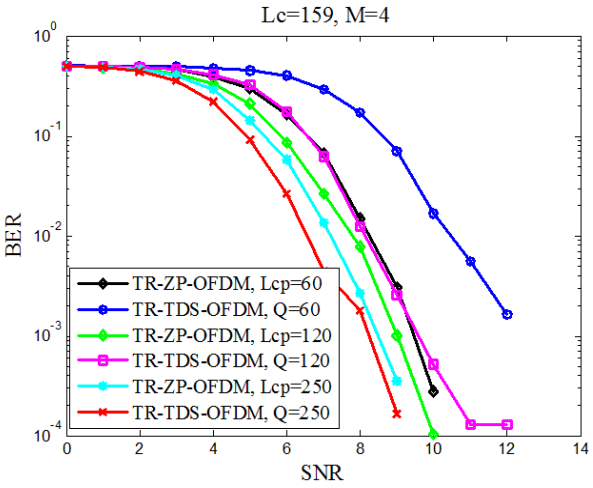

(d) Coded BER Performance (UWA channels).

Fig. 7.10. BER performance comparison between TR-ZP-OFDM and TR-TDS-OFDM.

Experiment 5 (*spectral efficiency comparison of TR-TDS-OFDM and TR-ZP-OFDM*). In this experiment, the effect of using TDS in spectrum efficiency is studied. If N_{data} is the useful sub-carrier information of time reversal OFDM, the bandwidth efficiency will be [146]:

$$\gamma_o = \frac{K}{K + N_{pilots}} \times \frac{N}{N + Q} \tag{7-24}$$

where N is the total sub-carrier, N_{pilots} denotes the number of pilot subcarriers and Q is the guard interval length. Notice that eq. (7-24) only accounts the bandwidth efficiency loss due to the use of guard interval and pilot symbols and its value is generally much higher than the actual bandwidth efficiency because it ignores other possible bandwidth efficiency losses (e.g. the use of training and channel coding, etc.) In TR-ZP-OFDM, 64 pilot tones are used equally spaced in frequency domains to estimate the channels. Table 7.1 shows the comparison of the spectrum efficiency between the proposed TR-TDS-OFDM scheme and conventional TR-ZP-OFDM. It is clear that the proposed scheme shows a significant spectral efficiency improvement.

Table 7.1

TR-ZP and TR-TDS OFDM Spectral Efficiency Comparison.

GI (length)	TR-ZP-OFDM [10]	TR-TDS-OFDM
20 $(L_{ch} = 32)$	91.95%	98.08%
64 $(L_{ch} = 32)$	88.24%	94.12%
60 $(L_{ch} = 159)$	88.56%	94.46%
120 $(L_{ch} = 159)$	83.92%	89.51%
250 $(L_{ch} = 159)$	75.35%	80.38%

7.6 Conclusion

This chapter proposes a more efficient spectrum alternative to the time reversal ZP-OFDM scheme. It uses a correlation based coder to enable TDS-OFDM systems to support time reversal schemes over long multipath

fading channels such as underwater acoustic channels. A proper design of correlation based coder is crucial to the success of TR-TDS-OFDM mutual interference reduction between training sequences and information blocks. A Zadoff-Chu sequence with perfect autocorrelation property is adopted for a correlation based coder to TDS-OFDM system. In this way, not only can a clear BER improvement be achieved, TDS-OFDM can also be effectively used in channels with large delay spread even if guard interval length is shorter than the maximum channel tap delay. The correlation based coder outperforms the detector signal-to-interference plus noise ratio by a factor of K (OFDM sub-carrier number) without any spectrum efficiency loss. It is shown that the proposed scheme outperforms time reversal ZP-OFDM in spectrum by more than 5.7% and with significant BER improvement. Simulation experiments are carefully conducted to test the proposed design by using simulated channels as well as channels measured from an ocean based experiment. The experimental results also support the significant spectral and BER improvements by using the proposed scheme.

Chapter 8

Spectrum and Energy Efficient OFDM Multicarrier Modulation for Underwater Acoustic Channel

8.1 Introduction

The variations of orthogonal frequency division multiplexing (OFDM) techniques can be roughly classified into three categories: cyclic prefix OFDM (CP-OFDM), zero padding OFDM (ZP-OFDM), and time domain synchronization OFDM (TDS-OFDM) [144, 146]. The popular CP-OFDM utilizes a CP as a guard interval to alleviate inter-block-interference (IBI) in multipath channels [162] and the resultant channel responses can be calculated by using a circular convolution operation. As such, a finite impulse response (FIR) channel can be diagonalized by using low-complexity IFFT and FFT for inter-symbol interference (ISI) removing. In ZP-OFDM the CP is replaced by a ZP to avoid power consumption in the guard interval between OFDM symbols [9, 13, 163]. Unlike CP-OFDM or ZP-OFDM, the TDS-OFDM technique adopts a pseudorandom noise (PN) sequence known to both the transmitter and the receiver as a guard interval as well as a training sequence (TS) for synchronization and channel estimation. The use of PN-sequences as a prefix reduces transmission overhead and improves spectrum efficiency [164].

To this end, an increasingly popular approach is to use ZP-OFDM or TDS-OFDM in a single-input multi-output (SIMO) setting. Such an approach combines multi-channels to combat channel fading, and relies on multicarrier modulation to achieve low complexity in a frequency-domain channel [6, 10]. However, because the long guard interval and pilots signal in underwater acoustic (UWA) channel, its use could lead to significant bandwidth and energy efficiency loss [6]. Bandwidth and energy efficiency can be improved using a large data blocks size which, unfortunately, is constrained by channel coherent time and system computation complexity [6]. Another way is to make a multipath channel to be an impulse-like channel using time reversal SIMO-OFDM. In this chapter, TDS-OFDM is proposed rather than the ZP-OFDM to save bandwidth. Moreover, the training sequence amplitude in TDS-OFDM can be reduced to improve the bit error rate and energy efficiency performance.

In this chapter, a preamble based receiver [6] is proposed for the time reversal time reversal single-input multiple-output TDS-OFDM together with progressive estimation of the Doppler scaling factor (DSF). Due to the time variant characteristics of the UWA channel the estimated DSFs tend to vary with time and the estimated DSF error can significantly increase with time that make it necessary for preamble updating. A frequency domain pseudorandom noise training sequence (FDPNTS) is introduced for the time reversal single-input multiple-output TDS-OFDM, as training sequence as well as a guard interval for multipath channel. The FDPNTS of two consequent frames can be used in progressively updated DSF estimation, while the initial DSF estimation obtained based on the preamble signal may cause an increase in error. Amazingly, by the proposed technique the high dimensional original signal can be reconstructed from the low-dimensional observations if the signal is (approximately) sparse based on the ground-breaking compressed sensing (CS) theory [186, 187]. Compressed

sensing is applied for channel estimation in the case of insufficiently long FDPNTS where it is shorter than the maximum channel tap delay to improve the accuracy of channel estimation.

In particular, in order to improve the spectral and energy efficiency of the OFDM system for an UWA channel based on TDS-OFDM, we will focuse on the following four aspects in this chapter for the detailed design of the receiver:

1) Matched preamble-based parameter estimation scheme to time reversal single-input multiple-output TDS-OFDM for better spectraland energy efficiency to take advantage of the overhead reduction in TDS-OFDM with insufficient FDPNTS.
2) TDS-OFDM training sequence used to update the estimation of DSF which may be change due to time varying feature of the channel.
3) The detailed application of compressed sensing technique to channel estimation for underwater time reversal single-input multiple-output TDS-OFDM .
4) The frequency domain signal amplitude of guard interval in TDS-OFDM is reduced to significantly improve energy efficiency as well as system signal–to–interfered–signal ratio (SISR).

The proposed system design will be carefully developed with efficiency improvement demonstrated by both theoretical analysis and simulation experiments on a measured UWA channel.

The rest of this chapter is organized as follows. First the proposed system model is analyzed and the preamble-based parameter estimation is presented. The received data signal processing is discussed and the performance is first analyzed and then further demonstrated using the practical data. Finally, a summary of the major techniques and contributions of this chapter is included.

8.2 The Proposed System Model

In this section, the details of transmitted data frame and the channel model will be presented. First, the semantics of the transmitted data frame are discussed in detail. Then, the detailed time domain signal waveforms of each data segment are calculated. Based on that, the received signal waveform is formulated for a multipath channel.

8.2.1 The Transmitted Data Frame Semantics

In this subsection, we will compare TR-SIMO-ZP-OFDM [6] and time reversal single-input multiple-output TDS-OFDM in preamble receiver design. Consider SIMO-TDS-OFDM for an UWA channel with a single transmission antenna and N_r receiver antenna. The total channel bandwidth is assumed to be B Hertz. As depicted in Fig. 8.1, the transmitted compound data frame of interest is the concatenation of a preamble segment and a data segment delimited by a zero guard time interval of duration T_g seconds. The preamble segment consists of two frequency domain pseudorandom noise preamble signal (FDPNPS) blocks preceded by a cyclic prefix (CP) of duration T_{cp} seconds. The length of each FDPNPS block is chosen to be larger than or equal to the maximum channel tap delay $\tau_{\max}$. Notice that the preamble segment has the same structure as those in the study of [6], Fig. 1 and [13] Fig. 1.

The same number, K, of symbols in a subcarrier data block is used to generate the i-th OFDM data block used in each FDPNPS training segment. Therefore, each OFDM data block lasts for $T_0 = KT_b$ seconds with subcarrier spacing $\Delta F = B/K$, where $T_b = 1/B$.

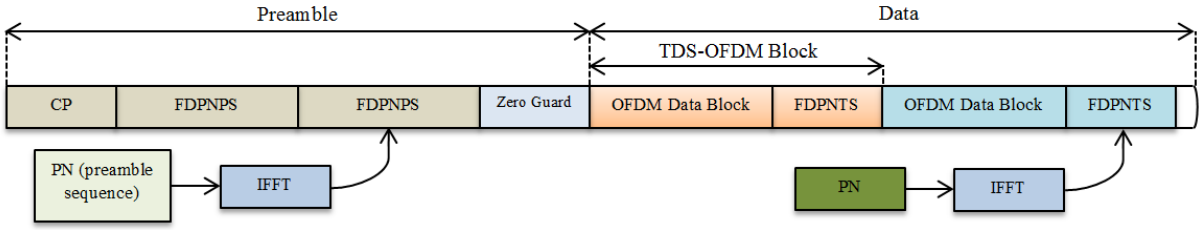

Fig. 8.1. Composite structure of the proposed TDS-OFDM transmitted signal frame.

The lengths of the CP and zero guard intervals are generally larger than the maximum channel tap delay $\tau_{\max}$. Let $a = \left[a[-K/2], \ldots\ldots, a[K/2-1]\right]^T$ be the collection of the K FDPNPS training segment used to generate the preamble symbol, $c[i] := \left[c[i;-Q/2], \ldots\ldots, c[i;Q/2-1]\right]^T$ the collection of the Q FDPNTS's used to generate the i-th TDS-OFDM frame training block, and $b[i] := \left[b[i;-K/2], \ldots\ldots, b[i;K/2-1]\right]^T$ the K data symbols used to generate the i-th data block of the TDS-OFDM symbol frame, where $i = 1, 2, \ldots\ldots$The baseband preamble symbols and data block can be written as:

$$u^{(P)}(t) = \sum_{k=-K/2}^{K/2-1} a[k] e^{j2\pi k\Delta F t}, \qquad -T_{cp} < t < 2T_0, \tag{8-1}$$

and

$$u^{(d)}(t) = \sum_{i=1}^{N_d} u^{(d)}(i; t-(i-1)T_d), \tag{8-2}$$

respectively, where

$$u^{(d)}(i;t) = \begin{cases} u^{(f)} = \sum_{k=-K/2}^{K/2-1} b[i;k] e^{j2\pi k\Delta F t}, & 0 < t < T_0 \\ u^{(c)} = \sum_{k=-Q/2}^{Q/2-1} c[i;k] e^{j2\pi k\Delta F t}, & T_0 < t < T_d \end{cases}, \tag{8-3}$$

and $u^{(f)}$ represents the OFDM data block in the TDS-OFDM data block and $u^{(c)}$ is the FDPNTS. For the i-th TDS-OFDM data block, signal is of duration $T_d := L_d T_b$ with $L_d = K + Q$. Let $D_0 = \left[-T_{cp}, 2T_0\right]$ and $D_i = \left[2T_0 + T_g + (i-1)T_d,\ 2T_0 + T_g + iT_d\right]$ be the time intervals occupied by the preamble signal and the i-th TDS-OFDM block signal, respectively. Note that D_0 is approximately twice D_i for $i \geq 1$.

8.2.2 Channel Model

Assuming that the multipath channel between the transmitter and receiver side is linear time-varying (LTV), its impulse responses can be represented as [6, 13, 39]:

$$c_m(t;\tau) = \sum_{\mu} A_{m,\mu}(t)\delta\left(\tau - \tau_{m,\mu}(t)\right), \tag{8-4}$$

where $A_{m,\mu}(t)$ and $\tau_{m,\mu}(t)$ denote time-varying path amplitudes and delays, respectively. Based on this model, each channel is composed of multiple significant paths, with each path parameterized by time-varying amplitude and a time-varying delay. For the simplicity of receiver processing algorithms development without loss of generality, assume the following:

A1) All path delays experience similar Doppler scaling within the interval D_i, $i = 0,.....,N_d$,

$$\tau_{m,\mu}(t) = \tau_{m,\mu}[i] - \alpha_m[i]t, \qquad t \in D_i,$$

where $\alpha_m[i]$ is the DSF.

A2) The path amplitudes $A_{m,\mu}(t)$ remain constant within the interval D_i, $i = 0,.....,N_d$, such that

$$A_{m,\mu}(t) = A_{m,u}[i], \qquad t \in D_i.$$

The channel parameters $A_{m,\mu}[i]$, $\tau_{m,\mu}[i]$, and $\alpha_m[i]$ are assumed to vary slowly during the entire transmission process.

Readers are referred to [39] and [6, 13] for a brief justification of these assumptions in underwater environments.

Under assumptions A1) and A2), the received preamble and data signals in the baseband are, respectively, written as:

$$r_m^{(P)} = x_m^{(P)}(t) + w_m^{(P)}(t), \tag{8-5}$$

$$r_m^{(d)}(t) = \sum_{i=1}^{N_d} x_m^{(d)}(i; t-(i-1)T_d) + w_m^{(d)}(t), \tag{8-6}$$

where

$$x_m^{(P)}(t) = e^{j2\pi\alpha_m[0]F_c t} \sum_k H_m[0;k]a[k] \times e^{j2\pi k\Delta F(1+\alpha_m[0])t}, \tag{8-7}$$

$$x_m^{(d)}(i;t) = \begin{cases} f_m^{(d)}(i;t) = e^{j2\pi\alpha_m[i]F_c t} \sum_{k=-K/2}^{K/2-1} H_m[i;k]b[i;k] \times e^{j2\pi k\Delta F(1+\alpha_m[i])t}, & 0 < t < T_0 \\ c_m^{(d)}(i;t) = e^{j2\pi\alpha_m[i]F_c t} \sum_{k=-Q/2}^{Q/2-1} H_m[i;k]c[i;k] \times e^{j2\pi k\Delta F(1+\alpha_m[i])t}, & T_0 < t < T_d \end{cases}, \tag{8-8}$$

represent the noise-free received signal parts corresponding to $u^{(P)}(t)$ and $u^{(d)}(i;t)$, respectively; F_c is the carrier frequency; and

$$H_m[i;k] = \sum_\mu A_{m,\mu}[i] e^{-j2\pi(F_c + k\Delta F)\tau_{m,\mu}[i]}, \tag{8-9}$$

denotes the sub-channel gain at the k-th subcarrier within the interval D_i; and both $w_m^{(d)}(t)$ and $w_m^{(P)}(t)$ stand for the additive noise.

8.3 Preamble-Based Parameter Estimation

In this section, the receiver side signal processing is discussed. To simplify such processing, $T_{cp} = T_g \geq \tau_{\max}$ is chosen such that the received preamble signal does not overlap in time with the received data signal and, therefore, can be processed independently. The preamble signal processing is intended to acquire initial estimates of the

channel parameters. Here, the preamble serves for three purposes: time synchronization, coarse DSF estimation, and Doppler shift estimation, as illustrated in Fig. 8.2 [6]. The three tasks are discussed in the following subsection in details. For simplicity without loss of generality, the additive noise in eq. (8-5) is ignored in the remainder of this section, following the approach reported in [6].

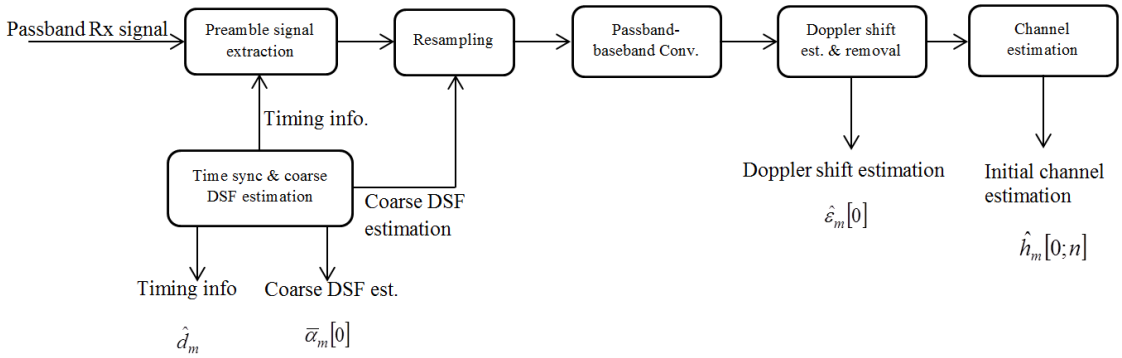

Fig. 8.2 [6]. Preamble-based parameter estimation at the m-th received antenna.

8.3.1 Time Synchronization and Coarse DSF Estimation

A repetitive pattern embedded in $x_m^{(P)}(t)$, exploited in a joint time synchronization and coarse DSF estimation scheme that has been reported in [6, 13] can be adopted in our proposed design. The corresponding N-tap window correlation can be formulated as:

$$\left(\hat{N}_m, \hat{d}_m\right) = \arg\max_{N,d} \frac{\sum_{n=d}^{d+N-1} r_m^*[n] r_m[n+N]}{\sqrt{\sum_{n=d}^{d+N-1} |r_m[n]|^2 \sum_{n=d}^{d+N-1} |r_m[n+N]|^2}}, \tag{8-10}$$

where $r_m[n]$ is the baseband equivalence of the received pass-band signal sampled at a rate λB with an integer parameter λ. In eq. (8-10), the integer $\hat{d}_m$ denotes the starting time of the received preamble signal. The integer $\hat{N}_m$ yields a coarse estimate of initial tap delay $\alpha_m[0]$ as discussed in [6]:

$$\bar{\alpha}_m[0] = \frac{\lambda K - \hat{N}_m}{\hat{N}_m}. \tag{8-11}$$

The estimator in eq. (8-11) can only offer time synchronization and DSF estimation with a precision limited by λ. In OFDM, a small timing error amounts to a phase offset after the passband–to–baseband conversion. This phase offset will be estimated and compensated through the use of FDPNTS in this chapter. Since a small DSF error estimation could lead to significant inter-carrier interference (ICI), it is crucial to refine DSF estimation as well.

8.3.2 Doppler Shift Estimation

The effects of the DSF can be largely mitigated by re-sampling the received preamble signal in pass-band at a re-sampling rate [6] $(\bar{\alpha}_m[0]+1)B$. The resulting signal, after being converted to the baseband, is given by:

$$\bar{z}_m^{(P)}[n] = e^{j2\pi\varepsilon_m[0]n} \sum_k H_m[0;k] a[k] e^{j\frac{2\pi kn}{K}}, \tag{8-12}$$

where the Doppler shift can be calculated as:

$$\varepsilon_m[0] := \frac{\alpha_m[0] - \bar{\alpha}_m[0]}{1 + \bar{\alpha}_m[0]} \times \frac{F_c}{B}. \tag{8-13}$$

It is assumed that $(1+\alpha_m[0])/(1+\bar{\alpha}_m[0]) \approx 1$ to account for possible errors in coarse DSF estimation and the approximation. Since $\bar{z}_m^{(P)}[n+K] = \bar{z}_m^{(P)}[n]\exp(j2\pi\varepsilon_m[0]K)$ for $0 < n \le K-1$, an estimator of $\varepsilon_m[0]$ can be written as:

$$\hat{\varepsilon}_m[0] = \frac{\sum_{n=0}^{K-1} \angle\left(\bar{z}_m^{(P)}[n+K]\bar{z}_m^{(P)^*}[n]\right)}{2\pi K^2}. \tag{8-14}$$

It is worth pointing out that the proposed Doppler shift estimation method only depends on the special structure already embedded in the preamble and does not require additional overheads such as null subcarriers in [9]. Given estimates $\bar{\alpha}_m[0]$ and $\hat{\varepsilon}_m[0]$, an estimate of the overall DSF $\alpha_m[0]$ can be obtained as:

$$\hat{\alpha}_m[0] = \bar{\alpha}_m[0] + \frac{B}{F_c}(1+\bar{\alpha}_m[0])\hat{\varepsilon}_m[0]. \tag{8-15}$$

8.4 Received Data Processing

Before the symbol detection is carrier out, the effects of DSF are proposed to be compensated from the received data $r_m^{(d)}$. Similar to that reported in [6], by using the initial estimation $\bar{\alpha}_m[0]$ and $\hat{\varepsilon}_m[0]$ acquired in preamble-based parameter estimation as shown in Fig. 8.3, the resulting compensated data signal can be written as:

$$z_m^{(d)}[n] = \sum_{i=1}^{N_d} y_m^{(d)}[i; n-(i-1)L_d] + w_m^{(d)}[n], \tag{8-16}$$

where,

$$y_m^{(d)}[i;n] = e^{-j2\pi\left(\frac{\bar{\alpha}_m[0]}{1+\bar{\alpha}_m[0]}\frac{F_c}{B} + \hat{\varepsilon}_m[0]\right)n} \times x_m^{(d)}(i;t)\Big|_{t=\frac{nT_b}{1+\bar{\alpha}_m[0]}}, \tag{8-17}$$

is the compensated signal part corresponding to $x_m^{(d)}(i;t)$, and $w_m^{(d)}[n]$ stands for the effective noise after compensation.

Since $u^{(d)}(i;t)$ is band-limited, it can be represented as

$$u^{(d)}(i;t) = \sum_n u^{(d)}[i;n]\phi(t-nT_b), \tag{8-18}$$

and as the following form in terms of baud-rate samples

$$u^{(d)}[i;n] := u^{(d)}(i;t)\Big|_{t=nT_b} = \begin{cases} \sum_{k=-K/2}^{K/2-1} b[i;k]\exp(2\pi kn/K) \\ \sum_{k=-Q/2}^{Q/2-1} c[i;k]\exp(2\pi kn/Q) \end{cases}. \tag{8-19}$$

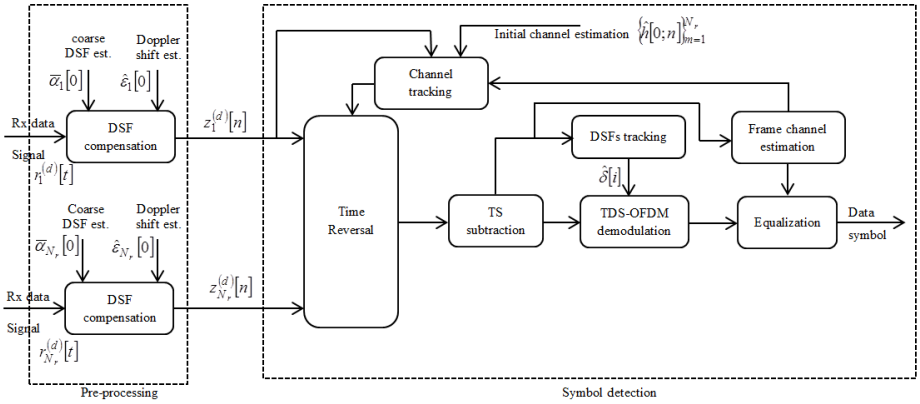

Fig. 8.3. Proposed received data processing.

The sinc function is defined by $\phi(t)=\sin(\pi Bt)/(\pi Bt)$. By using this representation, under assumption A3), (8-17) can be well approximated by:

$$y_m^{(d)}[i;n]\approx e^{j\theta_m[i]}u^{(d)}[i;n]\oplus h_m[i;n], \tag{8-20}$$

where $\oplus$ denotes linear convolution, and

$$h_m[i;n]=\sum_{\mu}A_{m,\mu}[i]e^{-2\pi F_c\tau_{m,\mu}[i]}\phi\left(nT_b-\tau_{m,\mu}[i]\right), \tag{8-21}$$

can be thought of as the baseband equivalent channel impulse response after DSF compensation. The block-dependent phase offset,

$$\theta_m[i]=\frac{2\pi F_c L_d}{B}\frac{\alpha_m[i]-\hat{\alpha}_m[0]}{1+\overline{\alpha}_m[0]}i+\theta_m[0], \tag{8-22}$$

can capture the effect of DSF estimation errors $\delta_m[i]:=\alpha_m[i]-\hat{\alpha}_m[0]$ and constant phase offset $\theta_m[0]$ caused by timing errors. The channel model can be obtained from the channel estimation based on the received FDPNTS of TDS-OFDM frame using CS, such as that in the subsection 8.4.2 included later in this chapter, and initial channel estimation. Note that in eq. (8-22), DSF estimation error $\delta_m[i]$ is assumed to be small enough such that the resultant phase variations across subcarriers can be limited within a TDS-OFDM block. For this, the proposed method can estimate the DSF error $\delta_m[i]$ by using the cross-correlation between FDPNTS of i-th frame and its previous FDPNTS (i-1)-th frame as discussed in the next subsection. $\theta_m[i]$ can be estimated as the average phase offset on the Q frame FDPNTS.

8.4.1 DSFs Progressive Estimation Updating

After receiving the first frame, it is proposed to use the FDPNTS of TDS-OFDM frame for DSFs estimation updating and synchronization to avoid preamble resending. As shown in Fig. 8.1, considering the FDPNTS of i-th frame and previous FDPNTS of (i-1) frame as preamble, the FDPNTS of i-th frame after synchronization and DSFs compensation can be written as:

$$\bar{z}_m^{(c)}[i;n]=e^{j2\pi\delta_m[i](i;n)}\sum_{k=-Q/2}^{Q/2-1}H_m[i;n]c[k]e^{j\frac{2\pi k(i;n)}{Q}}, \tag{8-23}$$

and FDPNTS of its previous (i-1) frame becomes,

$$\bar{z}_m^{(c)}[i-1;n] = e^{j2\pi\delta_m[i-1](i-1;n)} \sum_{k=-Q/2}^{Q/2-1} H_m[i-1;n]c[k]e^{j\frac{2\pi k(i-1;n)}{Q}}. \quad (8\text{-}24)$$

If the changes in the channel impulse responses between the current frame and its previous frame can be ignored, such as in the case of slow varying channels, DSF estimation errors can be considered unchanged between these two consecutive frames. Note that in eq. (8-23) and eq. (8-24) IBI between the training sequence and OFDM data block can be ignored. By exploiting that:

$$\bar{z}_m^{(c)}[i;n] = \bar{z}_m^{(c)}[i-1;n]e^{j2\pi\delta_m[i]Q}, \quad (8\text{-}25)$$

for $0 < n \le Q-1$, an estimator of $\delta_m[i]$ can be formulated as:

$$\hat{\delta}_m[i] = \frac{\sum_{n=0}^{Q-1} \angle\left(\bar{z}_m^{(c)}[i;n]\bar{z}_m^{(c)*}[i-1;n]\right)}{2\pi Q^2}. \quad (8\text{-}26)$$

8.4.2 TR Channel Estimation

In Fig. 8.3, to detect one data block, $b[j]$ TR technique is applied to combine the N_r compensated signals to obtain:

$$z^{(j)}[n] = \sum_{m=1}^{N_r} z_m^{(d)}[n] \oplus \hat{h}_m^*\left[j; \frac{Q}{2} - n\right], \quad (j-1)L_d \le n \le (j-1)L_d + L_d - 1, \quad (8\text{-}27)$$

where $\hat{h}_m[j;n]$ is the estimation of the channel response $h_m[j;n]$. After the TR operation, OFDM demodulated block can be written as $z[j] := \left[z^{(j)}[(j-1)L_d], \ldots\ldots, z^{(j)}[(j-1)L_d + L_d - 1]\right]^T$. An ideal TR channel can offer many benefits. In this chapter, our interests are twofold: i) in the case where the channels involve densely distributed multipaths, the TR channel is quite impulse-like even for a small N_r; ii) in the case where channel multipaths are sparsely distributed, a large number of receiver antennas (i.e., large N_r) are required to render the TR channel impulse-like [10]. Note that for UWA channels, the similar conclusion has been drawn based on waveguide physics [185].

The basic principle of TDS-OFDM is that with perfect channel information, the contribution of the training sequence can be completely subtracted from the received OFDM data block, and then the received TDS-OFDM symbol is essentially equivalent to a ZP-OFDM symbol, which can be converted into a CP-OFDM symbol by the classical overlapping and adding (OLA) scheme to realize a low-complexity channel equalization [173]. For data block $b[j]$, the neat data block after removing the effect of the training sequence can be calculated as:

$$d[j] = F_k R_{ola} z[j], \quad (8\text{-}28)$$

where the $K \times K$ matrix F_K denotes the K-point FFT, and the $K \times L_d$ matrix R_{ola} represents the overlap-add (OLA) operation. Appling eq. (8-16) and eq. (8-20), eq. (8-27) can be expressed as:

$$z^{(j)}[n] = \sum_{i=1}^{N_d} \tilde{y}^{(j)}[i;n-(i-1)L_d] + \tilde{w}^{(j)}[n], \quad (8\text{-}29)$$

where $\tilde{y}^{(j)}[i;n] = u^{(d)}[i;n] \oplus q^{(j)}[i;n]$, with

$$q^{(j)}[i;n]=\sum_{m=1}^{N_r} h_m[i;n]\oplus \hat{h}_m^*\left[j;\frac{Q}{2}-n\right], \tag{8-30}$$

and $\tilde{w}^{(j)}[n]$ is the equivalent noise after the TR operation. It can be readily shown that $\tilde{w}^{(j)}[n]$ is generally coloured while $\tilde{w}_m^{(d)}[n]$'s are white noise.

8.4.3 Channel Estimation using Compressed Sensing

The time reversal single-input multiple-output TDS-OFDM channel can be estimated based on the structured compressive sensing (SCS) techniques as discussed in [146, 186, 187]. The received FDPNTS over UWA multipath channel $c^{(d)}[i;n]=\left[c^{(d)}[i;0],c^{(d)}[i;1],....c^{(d)}[i;Q]\right]^T$ can be denoted by:

$$c^{(d)}[i;n]=\psi[i;n]q[i;n]+w[i;n], \tag{8-31}$$

where,

$$\psi[i;n]=\begin{bmatrix} u^{(c)}[i;0] & u^{(f)}[i-1;N-1] & u^{(f)}[i-1;N-2] & \dots & u^{(f)}[i-1;N-L_{ch}+1] \\ u^{(c)}[i;1] & u^{(c)}[i;0] & u^{(f)}[i-1;N-1] & \dots & u^{(f)}[i-1;N-L_{ch}+2] \\ u^{(c)}[i;2] & u^{(c)}[i;1] & u^{(c)}[i;0] & \dots & u^{(f)}[i-1;N-L_{ch}+3] \\ \vdots & \vdots & \vdots & \ddots & \vdots \\ u^{(c)}[i;Q-3] & u^{(c)}[i;Q-2] & u^{(c)}[i;Q-1] & \dots & u^{(f)}[i+1;N+Q-L_{ch}-1] \\ u^{(c)}[i;Q-2] & u^{(c)}[i;Q-1] & u^{(f)}[i+1;N+Q-1] & \dots & u^{(f)}[i+1;N+Q-L_{ch}] \\ u^{(c)}[i;Q-1] & u^{(f)}[i+1;N+Q-1] & u^{(f)}[i+1;N+Q-2] & \dots & u^{(f)}[i+1;N+Q-L_{ch}+1] \end{bmatrix}.$$

As illustrated in the received training sequence in eq. (8-31), $c^{(d)}[i;n]$ is contaminated by the portion $\left[u^{(f)}_{i-1,N-L_{ch}+1},u^{(f)}_{i-1,N-L_{ch}+2},\dots,u^{(f)}_{i-1,N-1}\right]^T$ of the previous OFDM data block $u^{(f)}_{i-1}$, and $\left[u^{(f)}_{i+1,N+Q-L_{ch}+1},u^{(f)}_{i+1,N+Q-L_{ch}},.....u^{(f)}_{i+1,N+Q-1}\right]^T$ of the next OFDM data block.

The channel impulse response can be estimated based on SCS, by solving the following nonlinear optimization problem as in [146, 186, 187]:

$$\hat{Q}=\arg\min_{Q\in C^{L\times R}} \left\|U^{(c)}\right\|_{p,q}, \quad subject \quad to \quad \left\|C^{(d)}-\psi Q\right\|_{p,q}\le\zeta^2, \tag{8-32}$$

where ζ^2 is the impact of noise.

8.4.4 Receiver Performance

The decomposition of received frame of time reversal single-input multiple-output TDS-OFDM can be shown in Fig. 8.4. From the received frame at high input signal-to-noise ratios (SNRs), the major part of noise originates from the IBI interference. Specifically, for short-to-medium range UWA channel, performance of time reversal single-input multiple-output TDS-OFDM detection can be evaluated by the signal-to-interference ratio (SIR) $\rho_{SIR}^{(j)}$ of $d[j]$.

Following the same steps until arriving to [10], eq. (16), the time reversal single-input multiple-output TDS-OFDM, SIR will be as:

$$\rho_{SIR-TDS}(q,Q,\tau)=\frac{\sum_{n=0}^{Q}\left|q^{(j)}[j;n]\right|^2}{\sum_{n>Q}\left|q^{(j)}[j+1;n]\right|^2+\sum_{n<-Q}\left|q^{(j)}[j-1;n]\right|^2+\alpha\sum_{n\geq 1}\left|q^{(j)}[j;n]\right|^2+\alpha\sum_{n\leq 1}\left|q^{(j)}[j;n]\right|^2}. \quad (8\text{-}33)$$

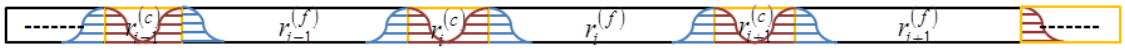

(a) Received signal frames (sufficient PN length)

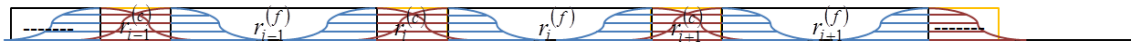

(a) Received signal frames (insufficient PN length)

Fig. 8.4. Decomposition of received signal frames in time reversal single-input multiple-output TDS-OFDM.

The value is clearly dependent on the FDPNTS length, the number of receiver antenna, as well as the amplitude factor imposed on the training sequence frequency-domain α. The number increase of antenna used in the receiver will reduce the multipath power and convert the multipath channel into an impulse channel centred at tab delay equal to zero.

TR channels $q^{(j)}[j+1;n]$, $q^{(j)}[j-1;n]$ and $q^{(j)}[j;n]$ are expected to be nearly the same and therefore the signal–to–interfered–signal ratio (SISR) in the time reversal single-input multiple-output TDS-OFDM will be:

$$\rho_{SISR-TDS}^{(j)}=\frac{\sum_{n=0}^{Q}\left|q^{(j)}[j;n]\right|^2}{\sum_{-\infty}^{\infty}\left|q^{(j)}[j;n]\right|^2+\alpha\sum_{n\geq 1}\left|q^{(j)}[j;n]\right|^2+\alpha\sum_{n\leq 1}\left|q^{(j)}[j;n]\right|^2}. \quad (8\text{-}34)$$

SISR ratio of the proposed time reversal single-input multiple-output TDS-OFDM under different amplitude factor imposed on the training sequence frequency-domain at ($Nr=1$ and $Nr=4$) is shown in Table 8.1.

Table 8.1

SISR of time reversal single-input multiple-output TDS-OFDM at different Level of the Amplitude Factor imposed on the Frequency-Domain Training Sequence α.

		SISR, $\alpha=2$	SISR, $\alpha=1$	SISR, $\alpha=1/2$
$N_r=1$	$Q=K/4$	0.7626	0.8196	0.8653
	$Q=K/8$	0.7536	0.8099	0.8551
	$Q=K/16$	0.6976	0.7497	0.7915
$N_r=4$	$Q=K/4$	0.9316	0.9506	0.9646
	$Q=K/8$	0.9280	0.9470	0.9609
	$Q=K/16$	0.9158	0.9345	0.9482

8.5 Simulation Results

In this section, the performance of the proposed communication system will be investigated by evaluating uncoded and coded BER performance of TDS-OFDM via Monte-Carlo simulations. In all simulation experiments, data symbols are initially generated from a random information bits which are first encoded by a rate 1/2 convolutional coder with the generator polynomial given in [65,57] [174], then the coded bits are interleaved by a block interleaver of depth 8 prior to QPSK modulation in the coded case. The measured channels discussed in chapter 6 are used to evaluate the system performance. They are truncated to length $\tau_{\max} = 128$. A multi-tap equalizer is used for the recovery of OFDM data information $u^{(f)}(i)$ at low complexity by using a symbol-by-symbol detector.

The signaling parameters used are: $T_{cp} = T_g = 60\ ms$, $B = 500Hz$, $F_c = 3550\ Hz$, $K = 512$, and $F_s = 20000\ Hz$. The system performances are carefully evaluated in both sufficient and insufficient guard interval cases. For the first case, the FDPNTS length of *i*-th frame is larger than or equal the maximum channel tap delay $Q = K/4$, and for the second case the FDPNTS length of *i*-th frame is shorter than the maximum channel tap delay. In the second case, two levels of IBI can be evaluated: medium level of IBI level in $Q = K/8$, and high IBI level for $Q = K/16$.

Experiment 1: (*DSFs MSE estimation*). Using preamble $\bar{\alpha}_m[0]$ and Doppler shift $\hat{\varepsilon}_m$, a coarse DSF is estimated as discussed in section 8.3. DSF error $\hat{\delta}_m[i]$ is estimated using a FDPNTS and used for DSF tracking for the current frame then the corresponding estimates of overall DSF in each frame. Fig. 8.5. shows the mean square error (MSE) of the coarse DSF estimation. It can be clearly seen that the MSE of DSF estimation is small and its effect can be ignored in OFDM systems.

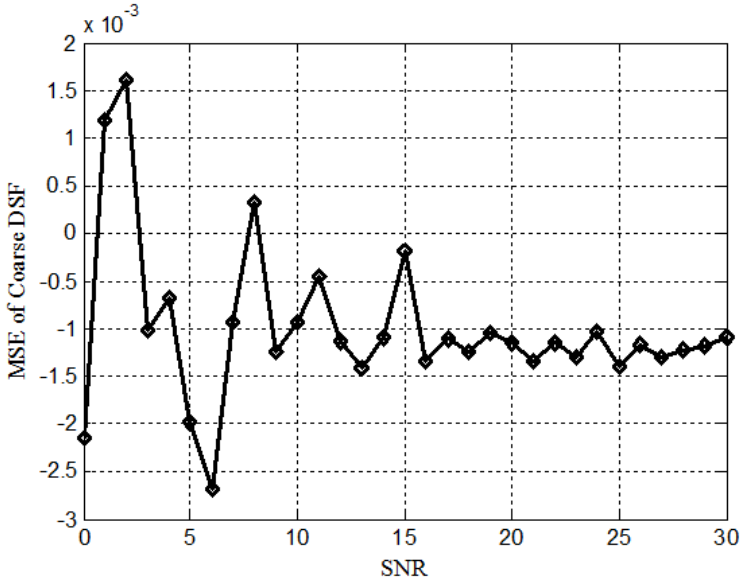

Fig. 8.5. Coarse DSFs MSE.

Experimental 2: *(CS channel estimation performance).* In this experiment, the compressed sensing channel estimation performance in the time reversal single-input multiple-output TDS-OFDM system at ($N_r = 1$ and $N_r = 4$) is evaluated. The proposed system is evaluated based on the CS and time reversal single-input multiple-output TDS-OFDM with linear channel estimation [168, 188, 189]. Simulation experiments are carried out in the two cases (sufficient and insufficient guard time interval). The resultant uncoded and coded BER performance is

shown in Fig. 8.6. The CS method yields significant improvement rather than the TR-TDS-OFDM based on linear channel estimation.

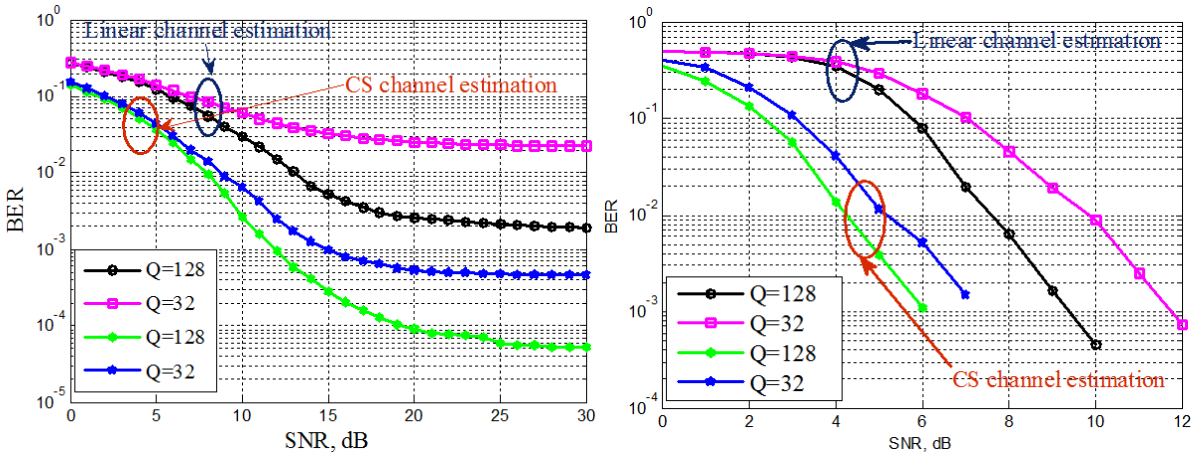

(a) Uncoded BER Performance (b) Coded BER Performance

Fig. 8.6. Channel estimation performance comparison in UWA channel.

Experimental 3: *(training sequence frequency-domain α comparison).* In this experiment, the amplitude factor imposed on frequency domain guard interval effect on the system bit error rate (BER). The time reversal single-input multiple-output TDS-OFDM system is evaluated at $(N_r = 1$ and $N_r = 4)$. The resultant uncoded BER performance is shown in Fig. 8.7. The proposed system represents a significant improvement rather than the conventional system especially in the receiver antenna.

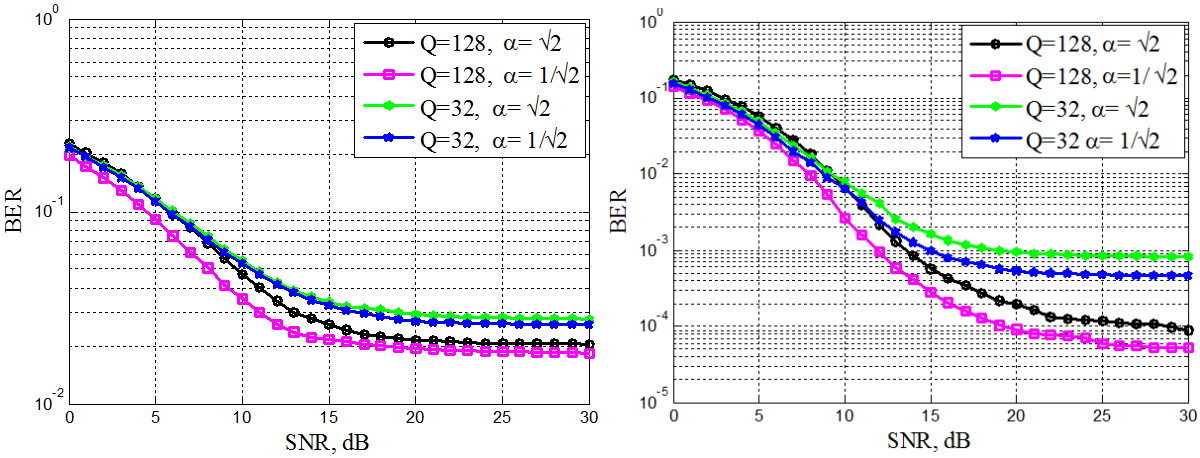

(b) One antenna receiver. (a) Four antenna receiver.

Fig. 8.7. Amplitude factor imposed on the training sequence frequency-domain α comparison.

Experimental 4: (*BER comparison of TDS-OFDM and ZP-OFDM*). In this experiment, coded and uncoded BER performance of proposed time reversal single-input multiple-output TDS-OFDM and TR-SIMO-ZP-OFDM proposed in [10] is compared. Fig. 8.8 shows the comparison of the BER performance for time reversl SIMO-OFDM system of TDS and ZP at the same guard interval values and based on the same channel estimation method. The ZP-OFDM outperforms the proposed scheme slightly due to the residual IBI between the training sequence and OFDM data blocks for receivers with low antenna number. However, the proposed scheme outperforms the conventional ZP-OFDM in the case that the channels are sparse; a large number of

receiver antennas (i.e., large N_r) are available to render the TR channel impulse-like and the residual IBI between the OFDM data blocks and training sequence is reduced.

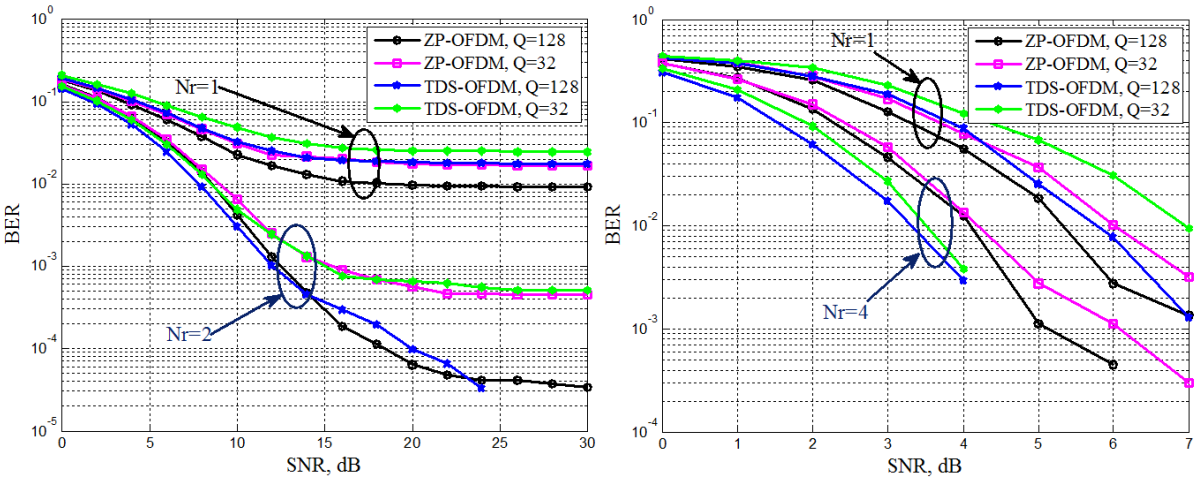

(c) Uncoded BER Performance. (b) Coded BER Performance.

Fig. 8.8. BER performance comparison between ZP-OFDM and TDS-OFDM.

Experimental 5 *(spectral efficiency comparison).* In this experiment, the effect of using proposed time reversal single-input multiple-output TDS-OFDM in bandwidth efficiency improvement is evaluated. The normalized spectrum efficiency ζ_0 of the considered OFDM schemes, compared with the ideal OFDM without any overhead (i.e., no time-domain guard interval and no frequency-domain pilots), is calculated using [146]:

$$\zeta_0 = \frac{K_{data}}{K_{data}+K_{pilot}} \times \frac{K}{K+Q} \times 100\%, \tag{8-35}$$

where K_{data} and K_{pilot} denote the numbers of data subcarriers and pilot subcarriers, respectively. Notice that bandwidth efficiency here only accounts the bandwidth efficiency loss due to the use of guard interval and pilot symbols, and bandwidth efficiency value is general much larger than the actual one because it ignores other possible bandwidth efficiency losses relevant to other factors such as channel coding and the use of training preamble, etc. In Table 8.2 the spectrum efficiency of the proposed scheme is compared with the OFDM system used in underwater communication in [10]. $K_{pilot}=64$ is used for ZP-OFDM as in [10]. It can be clearly seen that the proposed scheme has achieved the best spectrum efficiency, even better than the conventional OFDM underwater communication systems in [10].

Table 8.2

Proposed Scheme Spectral Efficiency Comparison related to Conventional OFDM Schemes.

GI (length)	ZP-OFDM	Conv. TDS-OFDM [189]	Proposed Scheme
$Q=K/4$	82.35%,	94.12%,	94.12%,
$Q=K/8$	77.78%,	88.89%,	88.89%,
$Q=K/16$	70%,	80%,	80%,

Experimental 6: *(energy efficiency comparison).* The energy efficiency η_0 of the considered OFDM schemes can be calculated as [144, 146]:

$$\eta_0 = \frac{K_{data}}{K_{data} + \beta^2 K_{pilot}} \times \frac{K}{K + \alpha^2 Q} \times 100\% \tag{8-36}$$

where β denotes the amplitude factor imposed on the frequency-domain pilots. Pilot amplitude boosting is usually adopted in CP-OFDM and ZP-OFDM data blocks to enhance the receiver channel estimation performance, e.g. $\beta = 4/3$ has been specified by the DVB-T2 standard [146]. $\alpha = \sqrt{2}$ has been specified in the DTMB standard [146]. In this chapter, the training sequence amplitude is selected to be $\alpha = 1/\sqrt{2}$ to improve the energy efficiency and BER improvement whereas with increased number of receiver antennas, TR can convert multipath channel to be impulse channel. The efficiency of the proposed technique and related underwater OFDM schemes are compared in the Table 8.2, based on eq. (8-36). Table 8.3 summarizes the energy efficiency comparison for different OFDM schemes. It is clear that TDS-OFDM has higher energy efficiency than that of ZP-OFDM.

Based on eq. (8-36), if the guard interval length satisfies the following equality, TDS-OFDM outperforms the ZP-OFDM scheme in energy efficiency:

$$M < \frac{N_{pilots}\beta^2 N}{\alpha^2\left(N - N_{pilots}\right)}. \tag{8-37}$$

As shown in Fig. 8.9 conventional TDS-OFDM outperforms the ZP-OFDM only in the short guard interval case. The proposed system outperforms the conventional TDS-OFDM as well as the ZP-OFDM for long guard interval length.

Table 8.3

Proposed Scheme Energy Efficiency Comparison related to Conventionl OFDM Schemes.

GI (length)	ZP-OFDM [10]	Conv. TDS-OFDM	Proposed Scheme
$Q = K/4$	79.75%,	66.67%	88.89%
$Q = K/8$	79.75%,	80%	94.12%
$Q = K/16$	79.75%,	88.89%	96.97%

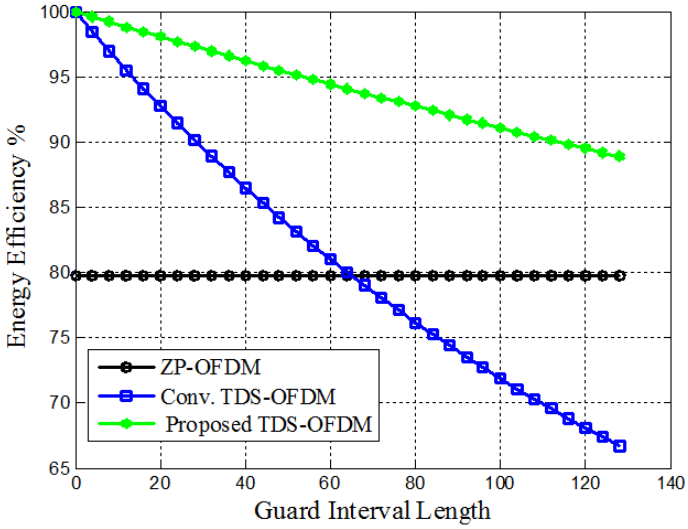

Fig. 8.9. Energy efficiency comparison between ZP-OFDM, Conv. TDS-OFDM and proposed TDS-OFDM.

8.6 Conclusion

In this chapter, a novel improvement to the standard OFDM scheme has been proposed for underwater communication to achieve better spectrum and energy efficiency. The time reversal and theory of CS is combined in the proposed method to develop a TDS-OFDM technique in SIMO underwater communication system with a guard interval shorter than the maximum channel tap delay. A preamble block is proposed for frame synchronization with DSF estimation. DSF updating is analyzed based on TDS-OFDM FDPNTS. Taking advantage of the compression sensing technique, accurate channel estimation can be achieved using much shorter FDPNTS than what is usually required. Since the proposed scheme requires no modification to the basic signal structure of TDS-OFDM, better spectrum efficiency is inherited. The efficiency is further improved by using a guard time interval shorter than the channel tap delay. Furthermore, the guard interval amplitude can also be reduced for better energy efficiency and better signal–to–interfered–signal rate. Each key aspect of the proposed method have been supported by careful analysis. In addition, extensive simulation experiments have also been carefully conducted to validate the proposed design for real channels measured from one marine field experiment. The experimental results show that the proposed system using TDS-OFDM over UWA communication system outperforms ZP-OFDM in spectral and energy efficiency by more than 10.96% and 13.57%, respectively, and outperform conventional TDS-OFDM by 44.42% in energy efficiency. Nevertheless, they also show that the proposed scheme outperforms conventional TDS-OFDM in BER performance.

Chapter 9

Pseudorandom Noise with Zero Insertion Technique for OFDM Systems in Underwater Acoustic Channel

9.1 Introduction

Underwater acoustic communication systems are critical to many types of civil and scientific missions in the ocean, such as ocean exploration, ocean monitoring, undersea disaster management, and undersea rescue [190]. However, communication systems currently available for underwater communication can only achieve very limited data rates due to the physical characteristics of the channel [137]. Orthogonal frequency division multiplexing (OFDM) multicarrier modulation is by far the most preferred modulation technique for multi-path underwater acoustic (UWA) channels due to its capability to convert a frequency selective fading channel into a combination of several nearly flat fading channels [9].

However, implementation details of OFDM can still perform significantly well due to tight throughput, wide propagation dispersion, and the associated inter-block interference (IBIs) in underwater acoustic channels. There are three major types of technique to mitigate inter-block interference (IBI) of OFDM multicarrier systems: cyclic prefix OFDM (CP-OFDM), zero padding OFDM (ZP-OFDM) and known symbol padding OFDM (KSP-OFDM) [191, 192]. For CP-OFDM the CP is used as a guard interval to avoid IBIs in multipath channels. Such CP is replaced in ZP-OFDM by a ZP to solve the channel transmission zero problem and guarantee symbol recovery for any case of the channel zero locations [163, 193], and also to reduce the consumption of the guard interval power [6, 9, 11, 12]. For these reasons, ZP-OFDM is usually preferred in the UWA channel. However, a long guard interval is required to avoid OFDM IBIs [6, 9, 11, 12, 144, 170]. For spectral efficiency, recently time reversal OFDM has proved to be a promising spectral efficient scheme for a single-input multi-output communications (SIMO) system over time dispersive fading channels. In particular, it can convert sparse and multi-path channels into an “impulse-like” channel [6, 10]. Since for ZP-OFDM and CP-OFDM techniques the detailed content of the guard interval is not relevant, the guard interval is not fully utilized for channel estimation and sometimes insufficient for synchronization purposes [191, 194]. To obtain the advantage of the guard interval, a training sequence known to both the transmitter and the receiver is used in the KSP-OFDM to fill the guard interval for channel estimation and synchronization [146, 191]. In this chapter, we attempt to improve the performance further by a new modification of KSP, termed ZP-OFDM, to avoid the spectral and energy waste in the unused frequency pilot signals in the KSP-OFDM.

Let us take a closer look of the major types of KSP-OFDM multicarrier systems including time domain synchronization OFDM (TDS-OFDM) [165], dual pseudorandom noise OFDM (DPN-OFDM) [168] and zero-pseudorandom noise OFDM (ZPN-OFDM) [144]. As a common feature, all these KSP-OFDM multicarrier techniques include a PN sequence as a guard interval for synchronization and channel estimation. However, there are delicate differences among them, resulting in differences in performance. For TDS-OFDM, the received PN

sequence is subject to mutual interference between the PN training sequence and OFDM data block. To address this issue, DPN-OFDM can be proposed to include two periodical PN sequences, with the second PN sequence mutual interference free and can be used for accurate channel estimation [168]. To improve energy efficiency, the first PN sequence in DPN-OFDM can be replaced by a zero sequence. Along this line, in this chapter a modification of PN sequences by the insertion of zeroes appropriately, termed the pseudorandom noise zero insertion (PNZI) technique, will be proposed for the KSP-OFDM multicarrier schemes to improve the energy efficiency bit error rate (BER) in time reversl SIMO-OFDM systems, combining the advantages of both KSP-OFDM and ZP-OFDM schemes. In addition, interleaving PN sequences with zeros does not affect the peak-to-average power ratio (PAPR), where these zeroes can be considered as null-subcarriers.

The rest of this chapter is organized as follows. First, different KSP-OFDM system behaviour and operation are briefly introduced and discussed to lay a foundation for our discussion. After that, the details of PNZI sequence are proposed, and the resultant energy efficiency performance of KSP-OFDM schemes based on the new PNZI sequence is discussed. A detailed time reversal single-input multi-output system incorporated with a generic KSP-OFDM scheme in the underwater acoustic channel is then discussed, and based on this, the system performance is evaluated. Following this, the performance of the different KSP-OFDM schemes incorporated with the proposed PNZI sequence is analyzed and evaluated by simulations and emulated experimental results. Finally, the conclusions of this chapter are presented.

9.2 KSP-OFDM Systems

In this section, the basic properties of KSP-OFDM are reviewed for our discussion. KSP-OFDM [171, 191, 192] is the key technology in digital terrestrial multimedia/broadcasting (DTMB) in Chinese digital television terrestrial broadcasting (DTTB) standard [173]. KSP-OFDM was proposed to avoid pilot signal use as in both CP-OFDM and ZP-OFDM for energy and bandwidth efficiency. However, KSP-OFDM energy and spectrum efficiency can cause significant bit error rate performance deterioration due to IBIs between training sequence and OFDM data blocks [172]. In [189], the authors have discussed how this can be potentially avoided based on the time reversal operation.

The detailed comparison of frame structures among CP-OFDM, ZP-OFDM and KSP-OFDM signals in time domains are shown in Fig. 9.1, where the CP used by CP-OFDM is replaced by zero padding in ZP-OFDM and by a PN training sequence (TS) in KSP-OFDM. Among the three sub-types of KSP-OFDM, the i-th TDS-OFDM transmitted signal frame denoted by $s_i = \left[s_{i,0}, s_{i,1}, \ldots, s_{i,P-1}\right]^T$ consists of two independent parts, a known PN sequence $c_i = \left[c_{i,0}, c_{i,1}, \ldots, c_{i,M-1}\right]^T$ of M length and OFDM data blocks $x_i = \left[x_{i,0}, x_{i,1}, \ldots, x_{i,N-1}\right]^T$ of length N:

$$S_i = \begin{bmatrix} C_i \\ X_i \end{bmatrix}_{P\times 1}, \tag{9-1}$$

where the length of the TDS-OFDM signal frame is $P = M + N$. The i-th DPN-OFDM transmitted signal frame will be:

$$S_i = \begin{bmatrix} C_i \\ C_i \\ X_i \end{bmatrix}_{P\times 1}, \tag{9-2}$$

and in the case of ZPN-OFDM the transmitted signal frame will be:

$$S_i = \begin{bmatrix} \mathbf{0}_{M\times 1} \\ C_i \\ X_i \end{bmatrix}_{P\times 1}, \tag{9-3}$$

where the length of the DPN-OFDM and ZPN-OFDM signal frame is $P = 2M + N$.

In multipath channels, IBIs between the OFDM data blocks and PN sequence in the different KSP-OFDM multicarrier systems can be illustrated as in Fig. 9.2. The basic principle of KSP-OFDM is that, with perfect channel estimation, such mutual interference can be completely removed from the KSP-OFDM data block [173]. As shown in Fig. 9.2. (a), if the received PN sequence is corrupted by the mutual interference, perfect channel estimation will not be available. The dual PN padding OFDM (DPN-OFDM) [168] and zero-pseudorandom noise training OFDM (ZPN-OFDM) [144] can be combined to solve TDS-OFDM IBI problems.

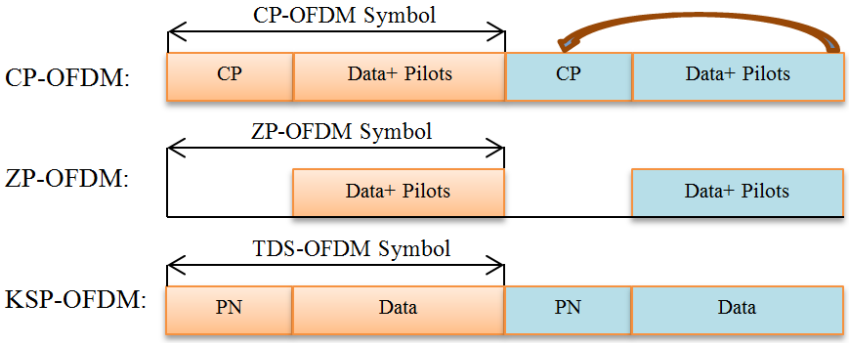

Fig. 9.1. KSP-OFDM, ZP-OFDM and CP-OFDM signal structure comparison in the time domain.

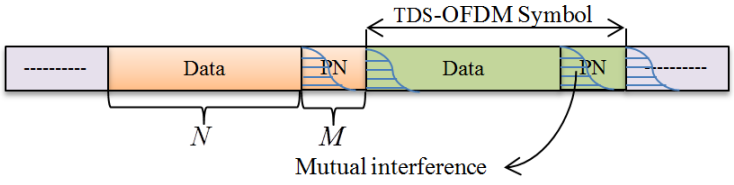

(a)

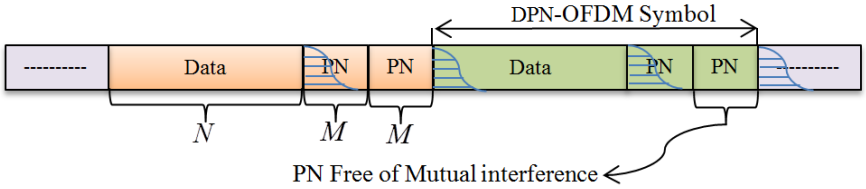

(b)

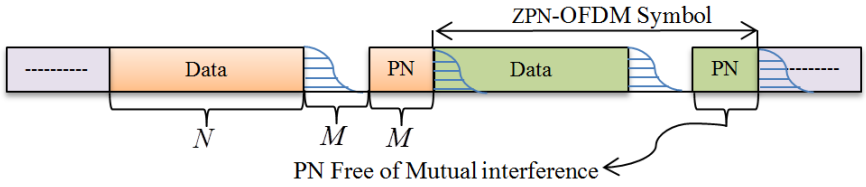

(c)

Fig. 9.2. KSP-OFDM received frames. (a) TDS-OFDM scheme. (b) dual PN padding OFDM (DPN-OFDM) scheme. (c) Zero-pseudorandom noise training OFDM (ZPN-OFDM) scheme.

A received PN sequence is mutual interference free in DPN-OFDM and ZPN-OFDM as shown in Fig. 9.2. (b) and Fig. 9.2. (c), respectively. In this case, nearly perfect channel estimation can be estimated based on the received PN sequence mutual interference free. As such, after PN sequence subtraction, KSP-OFDM can be equivalent to the ZP-OFDM. The impact of mutual interference between the PN sequence and KSP-OFDM data blocks can be reduced by using the time reversl SIMO-OFDM technique, by which an UWA channel can be converted into an "impulse-like" one [189].

9.3 Pseudorandom Noise with Zero Insertion for OFDM (PNZI-OFDM)

It is known that KSP-OFDM systems outperform CP-OFDM in terms of energy and spectral efficiency [144, 173, 188]. But that may not be true for ZP-OFDM depending on the number of subcarriers used as pilots in the ZP-OFDM and the guard interval length, which will be discussed in more detail in this section. In channels with significant tap delay such as a UWA channel, a long guard interval is required to avoid IBI which causes the energy inefficiency in KSP-OFDM schemes. It would be quite natural to expect that the KSP-OFDM schemes with a PNZI training sequence can offer better energy efficiency, which will be carefully discussed in the rest of this chapter.

In KSP-OFDM, a PN sequence with good autocorrelation properties serves as a guard interval as well as for synchronization and channel estimation. In this section, we will show that the introduction of a PNZI training sequence to KSP-OFDM can improve energy efficiency, without being detrimental to its capability of synchronization and channel estimation.

9.3.1 The Proposed PNZI and Its Autocorrelation Property

Given two binary sequences, $a=\lfloor a(0),\ a(1),.....a(M-1)\rfloor$ and $b=\lfloor b(0),\ b(1),.....b(M-1)\rfloor$, of period M, the periodic correlation between a and b is defined by [195]:

$$R_{a,b}(\tau)=\sum_{t=0}^{M-1}(-1)^{a(t)+b(t+\tau)},\qquad 0\le\tau<M, \tag{9-4}$$

the addition operation in $(t+\tau)$ is performed in modul M. $R_a(\tau)$ is the autocorrelation function (ACF) of a when $a=b$, and denoted by $R(\tau)$.

The normalized ACF of a period M PN sequence is given by [196]:

$$R_{PN}(\tau)=\begin{cases}1, & \tau=0\\ -1/M, & \tau\neq 0\end{cases}. \tag{9-5}$$

Consider the PN sequence with zeroes inserted at every other bit $a=\lfloor a(0),\ 0,\ a(1),\ 0,\ a(2).....a(M/2-1),\ 0\rfloor$. The normalized ACF will be:

$$R_{PN-ZI}(\tau)=\begin{cases}1/2, & \tau=0\\ 0, & \tau\neq 0,\quad \tau\ odd\\ -1/2M & \tau\neq 0,\quad \tau\ even\end{cases}, \tag{9-6}$$

In particular, the normalized ACF of sequence

$$a=\begin{bmatrix} 1 & -1 & -1 & -1 & -1 & -1 & 1 & -1 & -1 & -1 & -1 & 1 & 1 & -1 & -1 & -1 & 1\\ -1 & 1 & -1 & -1 & 1 & 1 & 1 & 1 & -1 & 1 & -1 & -1 & -1 & 1 & 1 & 1 & -1\\ -1 & 1 & -1 & -1 & 1 & -1 & 1 & 1 & -1 & 1 & 1 & 1 & -1 & 1 & 1 & -1 & -1\\ 1 & 1 & -1 & 1 & -1 & 1 & -1 & 1 & 1 & 1 & 1 & 1 & 1 & & & & \end{bmatrix}, \tag{9-7}$$

can be shown in Fig. 9.4 (a). For the corresponding PN sequence with zero insertion, a_{ZI} , given by:

$$a_{ZI}=\begin{bmatrix} 1 & 0 & -1 & 0 & -1 & 0 & -1 & 0 & -1 & 0 & -1 & 0 & 1 & 0 & -1 & 0 & -1\\ 0 & -1 & 0 & -1 & 0 & 1 & 0 & 1 & 0 & -1 & 0 & -1 & 0 & -1 & 0 & 1 & 0\\ -1 & 0 & 1 & 0 & -1 & 0 & -1 & 0 & 1 & 0 & 1 & 0 & 1 & 0 & 1 & 0 & -1\\ 0 & 1 & 0 & -1 & 0 & -1 & 0 & -1 & 0 & 1 & 0 & 1 & 0 & 1 & 0 & -1 & 0\\ -1 & 0 & 1 & 0 & -1 & 0 & -1 & 0 & 1 & 0 & -1 & 0 & 1 & 0 & 1 & 0 & -1\\ 0 & 1 & 0 & 1 & 0 & 1 & 0 & -1 & 0 & 1 & 0 & 1 & 0 & -1 & 0 & -1 & 0\\ 1 & 0 & 1 & 0 & -1 & 0 & 1 & 0 & -1 & 0 & 1 & 0 & -1 & 0 & 1 & 0 & 1\\ 0 & 1 & 0 & 1 & 0 & 1 & 0 & 1 & 0 & & & & & & & & \end{bmatrix}, \tag{9-8}$$

the normalized ACF will be shown in Fig. 9.4 (b). After zeroes are inserted into the PN sequence, its autocorrelation has the same pattern but the value is scaled by two. Consequently, the KSP-OFDM scheme synchronization methods will still be valid.

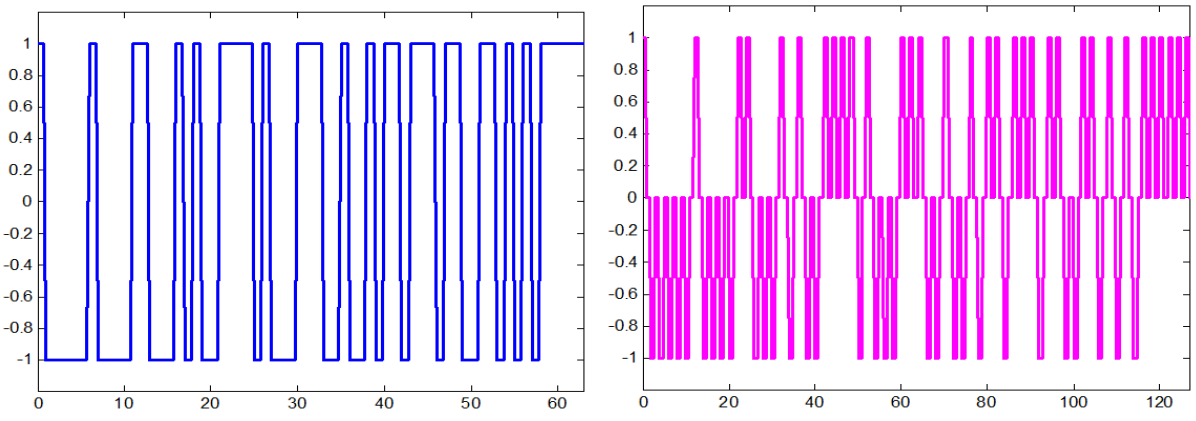

(a) (b)

Fig. 9.3. Training sequences. (a) PN sequence. (b) PNZI sequence.

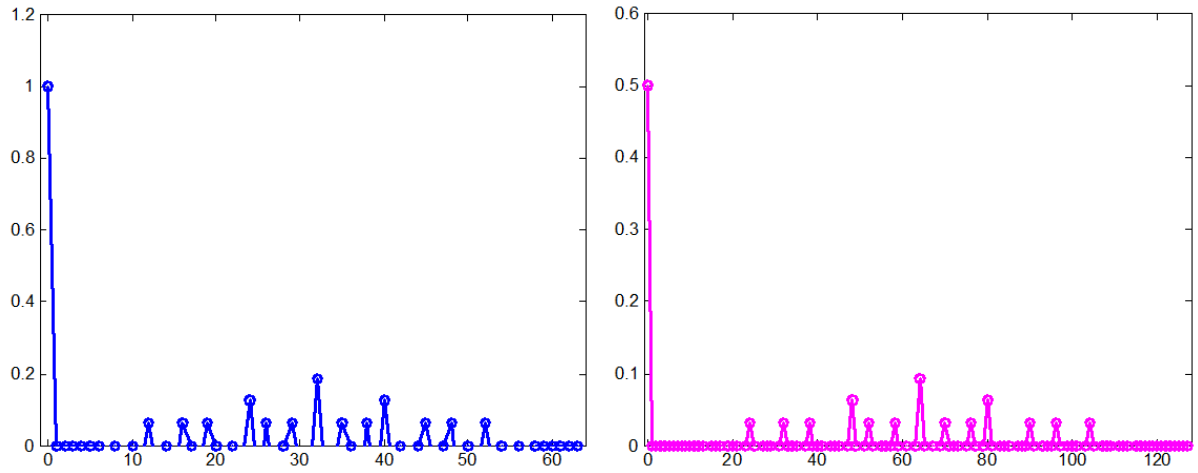

(a) (b)

Fig. 9.4. The normalized autocorrelation function. (a) PN sequence. (b) PNZI sequence.

9.3.2 Channel Estimation

The KSP-OFDM channel can be estimated based on the structured compressive sensing (SCS) techniques as discussed in [146, 186, 187], where an efficiently acquired and reconstructed signal is obtained using the SCS by finding solutions to underdetermined linear systems [186]. This subsection will focus on the TDS-OFDM system channel estimation for generic KSP-OFDM multicarrier systems. The results should also be applicable to DPN-OFDM and ZPN-OFDM systems. The time-domain receiving the PN sequence over the UWA multipath channel $d_i = [d_{i,0}, d_{i,1}, \ldots . d_{i,M-1}]^T$ can be denoted by:

$$d_i = \boldsymbol{\psi}_i h_i + w_i, \tag{9-9}$$

where w_i represent the noise terms, and

$$\boldsymbol{\psi}_i = \begin{bmatrix} c_{i,0} & x_{i-1,N-1} & x_{i-1,N-2} & \cdots & x_{i-1,N-L+1} \\ c_{i,1} & c_{i,0} & x_{i-1,N-1} & \cdots & x_{i-1,N-L+2} \\ c_{i,2} & c_{i,1} & c_{i,0} & \cdots & x_{i-1,N-L+3} \\ \vdots & \vdots & \vdots & \ddots & \vdots \\ c_{i,L-1} & c_{i,L-2} & c_{i,L-3} & \cdots & c_{i,0} \\ c_{i,L} & c_{i,L-1} & c_{i,L-2} & \cdots & c_{i,1} \\ \vdots & \vdots & \vdots & \ddots & \vdots \\ c_{i,M-1} & c_{i,M-2} & c_{i,M-3} & \cdots & c_{i,M-L} \end{bmatrix}. \tag{9-10}$$

As shown in Fig. 9.2 (a), the received training sequence d_i in multipath channel is contaminated by the portion $[x_{i-1,N-L+1}, x_{i-1,N-L+2}, \ldots, x_{i-1,N-1}]^T$ of the previous OFDM data block x_{i-1}. An iterative channel estimation can be used to remove the IBI from the PN sequence and then the SCS method can be used to estimate the channel impulse response. The channel estimation based on the PNZI before the iterative estimation can be obtained in the same way and $\boldsymbol{\psi}_i$ becomes:

$$\boldsymbol{\psi}_i = \begin{bmatrix} c_{i,0} & x_{i-1,N-1} & x_{i-1,N-2} & \cdots & x_{i-1,N-L+1} \\ 0 & c_{i,0} & x_{i-1,N-1} & \cdots & x_{i-1,N-L+2} \\ c_{i,1} & 0 & c_{i,0} & \cdots & x_{i-1,N-L+3} \\ \vdots & \vdots & \vdots & \ddots & \vdots \\ 0 & c_{i,L-2} & 0 & \cdots & c_{i,0} \\ c_{i,L} & 0 & c_{i,L-2} & \cdots & 0 \\ \vdots & \vdots & \vdots & \ddots & \vdots \\ 0 & c_{i,\frac{M}{2}-1} & 0 & \cdots & c_{i,\frac{M}{2}-L} \end{bmatrix}. \tag{9-11}$$

However, the PNZI reduces the active observation data amount in the training sequence by 50%. Consequently, the size of the active observations in the training sequence in the guard interval of the PNZI can be half of the active training sequence of conventional TDS-OFDM schemes. It will be hard to estimate the channel impulse response (CIR) accurately if the number of observed guard intervals is smaller than the dimension of unknown CIR. To this end, the existing compressed sensing (CS) theory can be applied to ensure that the high-dimensional original signal can be reconstructed from the low-dimensional observations if the signal is (approximately) sparse, i.e., the number of nonzero entries of the signal is much smaller than its dimension [146, 187]. As such, the CS method will be applied in the TDS-OFDM schemes based on the PNZI sequence.

9.3.3 Spectral and Energy Efficiency

The energy efficiency for OFDM systems can be calculated as [146, 173]:

$$\eta_0 = \frac{N_{data}}{N_{data} + \beta^2 N_{pilots}} \times \frac{N}{N + \alpha^2 \cdot GIL} \times 100\%, \tag{9-12}$$

where N_{data} and N_{pilots} are the subcarrier number in the OFDM block for the data and pilots subcarriers, respectively. GIL is the length of the guard interval containing overhead information. β is the amplitude factor of the pilot signal imposed in ZP-OFDM and CP-OFDM in the frequency domain normalized to the amplitude of the OFDM data subcarrier in the frequency domain. α is the amplitude factor of the PN training sequence in KSP-OFDM multicarrier systems imposed on the time domain normalized to the amplitude of the OFDM data subcarrier in the time domain. Both CP-OFDM and ZP-OFDM incorporate pilot amplitude boosting to improve the channel estimation accuracy. In digital video broadcasting-second generation terrestrial (DVB-T2)-the standard amplitude factor imposed is $\beta = 4/3$ and for reliable channel estimation $\alpha = \sqrt{2}$ is used for the amplitude of the PN sequence in the digital terrestrial multimedia broadcast (DTMB) standard [146, 173]. $\alpha = 1$ is proposed for DPN-OFDM [168] and $\alpha = 1/2$ is proposed for ZPN-OFDM [144].

If the GIL of any KSP-OFDM scheme satisfies the following inequality, the KSP-OFDM system outperforms the ZP-OFDM scheme in energy efficiency:

$$GIL < \frac{N_{pilots}\beta^2 N}{\alpha^2\left(N - N_{pilots}\right)}. \tag{9-13}$$

Since the modification in the training sequence in any KSP-OFDM scheme reduces the energy loss in the guard interval by 50%, the energy efficiency of the OFDM system based on the new training sequence will be:

$$\eta_0 = \frac{N_{data}}{N_{data} + \beta^2 N_{pilots}} \times \frac{N}{N + \alpha^2 \cdot GIL/2} \times 100\%. \tag{9-14}$$

Using the proposed PNZI sequence will improve any KSP-OFDM system in energy efficiency by:

$$\eta_{imp} = \frac{\alpha^2 N \cdot GIL}{2N^2 + 3\alpha^2 N \cdot GIL + \alpha^4 \cdot GIL^2} \times 100\%. \tag{9-15}$$

The corresponding KSP-OFDM can outperform ZP-OFDM in energy efficiency if the GIL length satisfies:

$$GIL < \frac{2N_{pilots}\beta^2 N}{\alpha^2 \left(N - N_{pilots}\right)}. \tag{9-16}$$

The normalized spectral efficiency γ_0 of any OFDM scheme without any overhead can be obtained as [146]:

$$\gamma_0 = \frac{N_{data}}{N_{data} + N_{pilots}} \times \frac{N}{N + TGIL} \times 100\%, \tag{9-17}$$

where $TGIL$ is the total guard interval length.

The normalized spectral efficiency seems worse than the actual spectral efficiency because many kinds of overhead information have not been included in the channel coder overhead. The normalized bandwidth efficiency will not change in the case of the PNZI sequence.

The detailed parameters used for calculating the energy and spectral efficiency in different OFDM schemes are listed in Table 9.1.

Table 9.1

OFDM Systems Parameters.

	CP-OFDM	ZP-OFDM	TDS-OFDM	DPN-OFDM	ZPN-OFDM
GIL	M	0	M	$2M$	M
$TGIL$	M	M	M	$2M$	$2M$
α	1	0	$\sqrt{2}$	1	0.5
β	$4/3$	$4/3$	0	0	0

9.4 Time Reversal Single-Input Multiple-Output KSP-OFDM

Thanks to its capability for multipath focusing and multipath reduction, time reversal SIMO-OFDM is widely used in UWA communication [6, 10]. Applying the time reversal technique, a probe signal is transmitted at the beginning of the communication, then recorded at the receiver, and based on that the channel information is collected [10]. We can implement time reversal SIMO-OFDM based on either TDS-OFDM, DPN-OFDM or ZPN-OFDM to reduce the effect of mutual interference between the training sequence and OFDM data blocks in multipath channels. For illustrative purposes, the resultant system will be analyzed in detail for TDS-OFDM only, which is included in this section. Similar analysis can be carried out for those based on DPN-OFDM or ZPN-OFDM. The bit error rate performance will be analyzed in detail for the three KSP-OFDM schemes based on the PNZI training sequence.

9.4.1 Time Reversal Single-Input Multiple-Output TDS-OFDM

To analyze the performance of TDS-OFDM with the time reversal technique, consider a TDS-OFDM frame as a sequence with N data blocks. L_d is the data block length. Each block is followed by a training sequence with a length $T_{TS} = L_{TS} T_b$. Here, L_{TS} is the training sequence length, $T_b = 1/B$, and B is the channel bandwidth in Hertz. The TDS-OFDM frame as the i-th signal block can be written as:

$$s(i;t) = \begin{cases} \sum_{k=-N/2}^{N/2-1} x[i;k] e^{j2\pi N \Delta F t} & 0 < t < T_0 \\ c[i;q]_{q=0:M-1} & T_0 < t < T_d \end{cases}, \tag{9-18}$$

where $T_d = T_0 + T_{TS}$. For a linear time-varying (LTV) multipath channel between the transmitter (TxE) and r-th antenna receiver (RxE), the channel impulse response can be represented as [6, 9, 13, 39]:

$$h_r(t;\tau) = \sum_{\mu} A_{r,\mu}(t) \delta(\tau - \tau_{r,\mu}(t)), \tag{9-19}$$

where $A_{r,\mu}(t)$ and $\tau_{r,\mu}(t)$ are the time-varying path amplitudes and delays, respectively. Channel dispersion width $\tau_{\max}$ is the difference between the maximum and minimum channel path delay. To avoid OFDM IBIs the guard interval length is chosen to be longer than or equal to the channel dispersion width.

Normally, for receiver signal processing in UWA communication, the following two assumptions can be made for analysis purposes: i) for one OFDM block the amplitude does not change $A_{r,\mu}(t) \approx A_{r,s}[i]$, and ii) path delay approximately can be as:

$$\tau_{r,\mu}(t) = \tau_{r,\mu}[i] - \alpha_r[i]t, \tag{9-20}$$

where $\alpha_r[i]$ are called Doppler scaling factors (DSFs).

For a brief justification of these assumptions in UWA channels, readers may refer to [6, 9, 13, 40].

In this chapter, we will not be focusing on the DSF estimation or frame synchronization as that can be estimated based on preamble signals as in [6, 13].

For band limited TDS-OFDM systems, the received frame can be represented as:

$$y(i;t) = \sum_{n} y[i;n] \phi(t - nT_b). \tag{9-21}$$

In terms of baud-rate samples where $\phi(t) = \sin(\pi B t)/(\pi B t)$ is conventional OFDM sinc pulse shaping and

$$y[i;n] = s[i;n] \otimes h_r[i;n] = \begin{cases} \sum_{k=-N/2}^{k=N/2-1} x[i;k] \exp(j2\pi k n/N) \otimes h_r[i;n] & 0 \le n < N \\ c[i;q]_{q=0:M-1} \otimes h_r[i;n] & N \le n < N+M \end{cases}, \tag{9-22}$$

where $\otimes$ is the linear convolution operation, and

$$h_r[i;n] = \sum_{\mu} A_{r,\mu}[i] e^{-j2\pi F_c \tau_{r,\mu}[i]} \phi(nT_b - \tau_{r,\mu}[i]),$$

is the channel impulse response after DSF compensation.

In the time reversal SIMO-OFDM, after the time reversal process the received signal can be represented as:

$$\tilde{z}[i;n] = y[i;n] \otimes q[i;n], \tag{9-23}$$

where,

$$q[i;n]=\sum_{r=1}^{R}h_r[i;n]\otimes\hat{h}_r^{*}\left[i;\frac{L_{Ts}}{2}-n\right], \tag{9-24}$$

and $\hat{h}_r[i;n]$ is the estimate of the $h_r[i;n]$. In this chapter, $h_r[i;n]$ can be estimated based on the training sequence and SCS by the simultaneous orthogonal matching pursuit (SOMP) method [6, 22].

After the training sequence is removed, the TDS-OFDM i-th data block can be represented as:

$$u[n]=\sum_{i=1}^{N}\tilde{z}[i;n-(i-1)L_d]+\tilde{v}[n]+\tilde{g}[n]+\tilde{w}[n], \tag{9-25}$$

where $\tilde{v}[n]$ is the IBI effect between the training sequence and OFDM data blocks, $\tilde{g}[n]$ is the IBI effect between the OFDM data blocks themselves in insufficient guard interval cases (when the guard interval length is shorter than the channel delay spread) and $\tilde{w}[n]$ is added white Gaussian noise (AWGN). $\tilde{g}[n]=0$ for sufficient guard interval length (meaning the guard interval length is longer than or equal the channel delay spread). The PN sequence c_i is independent of the OFDM data block x_i and the OFDM data blocks are self-independent on each other. Both $\tilde{g}[n]$ and $\tilde{v}[n]$ are considered as AWGN, the eq. (9-25) can be written as:

$$u[n]=\sum_{i=1}^{N}\tilde{z}[i;n-(i-1)L_d]+\tilde{o}[n], \tag{9-26}$$

where $\tilde{o}[n]$ is the equivalent noise after PN subtraction and time reversal operation. The OFDM symbol detection will be:

$$f[i]=F_k J_{ola} u[i], \tag{9-27}$$

where F_k denotes the K-point FFT matrix, and J_{ola} is overlap-add (OLA) operation $K\times L_d$ matrix used to convert the TDS-OFDM frame to CP-OFDM. After removing the training sequences at the received TDS-OFDM frame, TDS-OFDM is equivalent to the ZP-OFDM [193, 197].

For TR-TDS-OFDM, channel estimation can be carried out based on the received time domain PN sequence $d_i=[d_{i,0},d_{i,1},....d_{i,M-1}]^T$ denoted by:

$$d[i;n]=\phi[i;n]q[i;n]+w[i;n], \tag{9-28}$$

where $\phi[i;n]$ is

$$\phi[i;n]=\begin{bmatrix} c[i;0] & x[i-1;N-1] & x[i-1;N-2] & \dots & x[i-1;N-L_{ch}+1] \\ c[i;1] & c[i;0] & x[i-1;N-1] & \dots & x[i-1;N-L_{ch}+2] \\ c[i;2] & c[i;1] & c[i;0] & \dots & x[i-1;N-L_{ch}+3] \\ \vdots & \vdots & \vdots & \ddots & \vdots \\ c[i;M-3] & c[i;M-2] & c[i;M-1] & \dots & x[i+1;N+M-L_{ch}-1] \\ c[i;M-2] & c[i;M-1] & x[i+1;N+M-1] & \dots & x[i+1;N+M-L_{ch}] \\ c[i;M-1] & x[i+1;N+M-1] & x[i+1;N+M-2] & \dots & x[i+1;N+M-L_{ch}+1] \end{bmatrix}.$$

As illustrated in Fig. 9.5 (c), the received training sequence $d[i;n]$ is contaminated by the portion $[x_{i-1,N-L_{ch}+1},x_{i-1,N-L_{ch}+2},\dots,x_{i-1,N-1}]^T$ of the previous OFDM data block x_{i-1}, and $[x_{i+1,N+M-L_{ch}+1},x_{i+1,N+M-L_{ch}},\dots,x_{i+1,N+M-1}]^T$ of the next OFDM data block.

If a PNZI sequence is used the $\phi[i;n]$ will be:

$$\phi[i;n]=\begin{bmatrix} c[i;0] & x[i-1;N-1] & x[i-1;N-2] & \dots & x[i-1;N-L_{ch}+1] \\ 0 & c[i;0] & x[i-1;N-1] & \dots & x[i-1;N-L_{ch}+2] \\ c[i;1] & 0 & c[i;0] & \dots & x[i-1;N-L_{ch}+3] \\ \vdots & \vdots & \vdots & \ddots & \vdots \\ 0 & c\left[i;\frac{M}{2}-1\right] & 0 & \dots & x[i+1;N+M-L_{ch}-1] \\ c\left[i;\frac{M}{2}-1\right] & 0 & x[i+1;N+M-1] & \dots & x[i+1;N+M-L_{ch}] \\ 0 & x[i+1;N+M-1] & x[i+1;N+M-2] & \dots & x[i+1;N+M-L_{ch}+1] \end{bmatrix}.$$

The received PN sequence, after subtraction and time reversal operation with the equivalent noise in the frequency domain, will be:

$$Y=\varphi Q+\tilde{O}. \tag{9-29}$$

The channel impulse response can be estimated and obtained by SCS, by solving the following nonlinear optimization problem, as in [146, 186, 187]:

$$\hat{Q}=\arg\min_{Q\in C^{L\times R}} \|Q\|_{p,q}, \quad subject \quad to \quad \|Y-\phi Q\|_{p,q}\le\zeta^2, \tag{9-30}$$

where ζ^2 is the impact of noise.

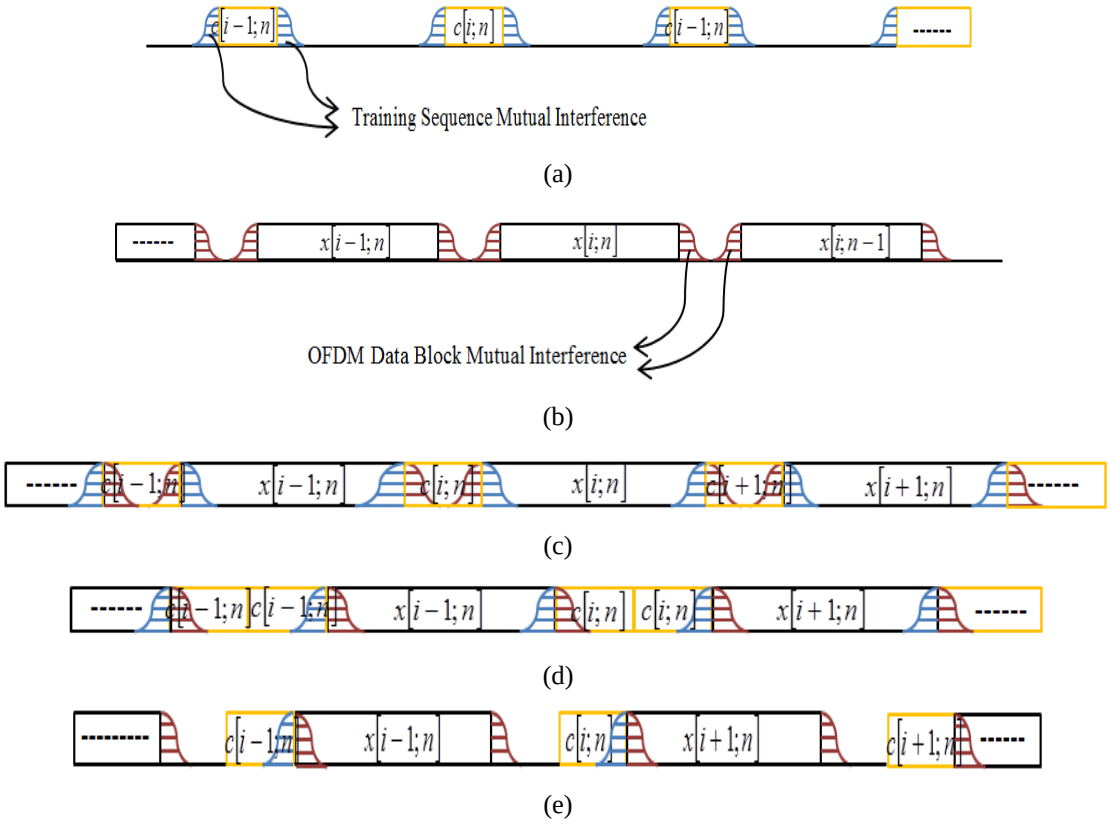

Fig. 9.5. KSP-OFDM received signal frames over time reversal SIMO-OFDM scheme. (a) Received training sequence decomposition in time domain. (b) Received OFDM data block decomposition in time domain. (c) TDS-OFDM received signal frame. (d) DPN-OFDM received signal frame. (e) ZPN-OFDM received signal frame.

If a PNZI sequence is used the $\phi[i;n]$ will be:

$$\phi[i;n]=\begin{bmatrix} c[i;0] & x[i-1;N-1] & x[i-1;N-2] & \cdots & x[i-1;N-L_{ch}+1] \\ 0 & c[i;0] & x[i-1;N-1] & \cdots & x[i-1;N-L_{ch}+2] \\ c[i;1] & 0 & c[i;0] & \cdots & x[i-1;N-L_{ch}+3] \\ \vdots & \vdots & \vdots & \ddots & \vdots \\ 0 & c\left[i;\frac{M}{2}-1\right] & 0 & \cdots & x[i+1;N+M-L_{ch}-1] \\ c\left[i;\frac{M}{2}-1\right] & 0 & x[i+1;N+M-1] & \cdots & x[i+1;N+M-L_{ch}] \\ 0 & x[i+1;N+M-1] & x[i+1;N+M-2] & \cdots & x[i+1;N+M-L_{ch}+1] \end{bmatrix}.$$

9.4.2 Signal-to-Interference Ratio of Time Reversal KSP-OFDM Based on PNZI Sequence

As shown in Fig. 9.5, from the received frame at high signal–to–noise ratios (SNRs), the major part of noise originates from the IBI interference. Specifically, for short–to–medium range UWA channels, performance of time reversal SIMO-OFDM detection over different schemes can be evaluated by using the signal–to–interference ratio (SIR) ρ_{SIR} of receiver data blocks.

The signal–to–interference ratio (SIR) of the time reversal SIMO-OFDM based on ZP-OFDM is eq. (16) in [10]:

$$\rho_{SIR-ZP}(q,M,\tau)=\frac{\sum_{n=0}^{M}|q[i;n]|^2}{\sum_{n>M}|q[i+1;n]|^2+\sum_{n<-M}|q[i-1;n]|^2}. \tag{9-31}$$

In the case of KSP-OFDM, inter-block interference will not only be due to the insufficient guard interval, also it will be present between training sequences and OFDM data block. The SIR for time reversal SIMO-OFDM based on TDS-OFDM can be estimated as:

$$\rho_{SIR-TDS}(q,M,\tau)=\frac{\sum_{n=0}^{M}|q[i;n]|^2}{\sum_{n>M}|q[i+1;n]|^2+\sum_{n<-M}|q[i-1;n]|^2+\alpha\sum_{n\geq 1}|q[i+1;n]|^2+\alpha\sum_{n\leq 1}|q[i;n]|^2}. \tag{9-32}$$

The IBI will increase by interference due to the training sequence in the OFDM data block. The value is clearly dependent on the guard interval length and the number of receiver antenna that will affect the shape of the time reversal channel, as well as the normalized amplitude factor imposed on the training sequence in time-domain to amplitude factor of the OFDM data subcarrier α. When the number of antenna in the receiver increases, the multipath power will reduce and convert the multipath channel into an impulsive channel centered at zero tab delay.

In this chapter, the case where M length is larger than or equal to the maximum channel tap delay is considered. In this case, IBI will not be caused by insufficient guard interval. The usual IBI will be caused in the OFDM data block because of the training sequence interference in the OFDM data block. Then, eq. (9-32) will be:

$$\rho_{SIR-TDS}(q,M,\tau)=\frac{\sum_{n=0}^{M}|q[i;n]|^2}{\alpha\sum_{n\geq 1}|q[i+1;n]|^2+\alpha\sum_{n\leq 1}|q[i;n]|^2}. \tag{9-33}$$

TR channels $q[i+1;n]$, $q[i-1;n]$ and $q[j;n]$ are expected to be nearly the same for slow varying channels. Therefore the SIR of time reversal single-input multiple-output TDS-OFDM based on the PNZI training sequence will be:

$$\rho_{SIR-TDS-ZI} = \frac{\sum_{n=0}^{M} |q[i;n]|^2}{0.5 \cdot \alpha \sum_{n \geq 1} |q[i;n]|^2 + 0.5 \cdot \alpha \sum_{n \leq 1} |q[i;n]|^2}. \quad (9\text{-}34)$$

Here, in the PNZI training sequence the zero interleaved into the PN sequence will reduce the training sequence mutual interference by 50%.

In the same way, the TR-SIMO-DPN-OFDM scheme SIR can be estimated as:

$$\rho_{SIR-DPN} = \frac{\sum_{n=0}^{2M} |q[i;n]|^2}{\alpha \sum_{n \geq 1} |q[i;n]|^2 + \alpha \sum_{n \leq 1} |q[i;n]|^2}. \quad (9\text{-}35)$$

SIR ratio of the TR-SIMO-DPN-OFDM when the PNZI training sequence is used will be:

$$\rho_{SIR-DPN-ZI} = \frac{\sum_{n=0}^{2M} |q[i;n]|^2}{0.5 \cdot \alpha \sum_{n \geq 1} |q[i;n]|^2 + 0.5 \cdot \alpha \sum_{n \leq 1} |q[i;n]|^2}. \quad (9\text{-}36)$$

SIR ratio for TR-SIMO-ZPN-OFDM will be:

$$\rho_{SIR-ZPN} = \frac{\sum_{n=0}^{2M} |q[i;n]|^2}{\alpha \sum_{n \leq 1} |q[i;n]|^2}, \quad (9\text{-}37)$$

and when the PNZI will be used, TR-SIMO-ZPN-OFDM SIR can be calculated as:

$$\rho_{SIR-ZPN} = \frac{\sum_{n=0}^{2M} |q[i;n]|^2}{0.5 \cdot \alpha \sum_{n \leq 1} |q[i;n]|^2}. \quad (9\text{-}38)$$

As in time reversal SIMO-OFDM based on TDS-OFDM, the zero interleave of the PNZI training sequence in time reversal SIMO-OFDM based on the DPN-OFDM and ZPN-OFDM can reduce the mutual interference due to training sequence in OFDM data block by 50 %.

From eq. (9-32, 9-38), there are two aspects to improve SIR of any scheme of KSP-OFDM if guard intervals are sufficient. First, the multipath channel can be converted to impulse-like as much as possible. Second, the mutual interference effect of the training sequence in the OFDM data blocks can be reduced. In this chapter, we attempt both by combining TR and SIMO technologies to convert the UWA multipath channel to an impulse-like channel. The mutual interference of the training sequence in OFDM data symbols is reduced by 50% by using the PNZI sequence.

9.5 Simulation Results

In this section, the KSP-OFDM system based on the PNZI sequence performance will be evaluated using randomly generated information bits. System performance will be evaluated for encoded and unencoded bit error rate (BER) performance. In the unencoded case, random information bits are generated and modulated to generate the data

symbols, but in the encoded case the information bits are encoded using an conventional coder [65,57] with generator polynomials [174] before interleaved by a block interleaver of depth 8 prior to modulation.

System BER performance is evaluated for an UWA channel model adopted from experimental data collected in the ASCOT01 experiment conducted off the coast of New England in June 2001, as reported in[143, 144]. With a maximum 128 channel tap delay as used in [144], the channel characteristics can be estimated frame by frame based on SCS with the SOMP [145, 146] method. A multi-tap equalizer is used to recover the OFDM time domain data information. In all simulations, the OFDM data subcarrier number $N = 512$ and each sub-channel is modulated by QPSK. The system is simulated based on a single and multi-receiver antenna.

KSP-OFDM schemes are evaluated for both a conventional system and a system with the PNZI training sequence.

9.5.1 Signal–to–Interference Ratio Improvement Based on PNZI Training Sequence

In this experiment the SIR improvement is estimated based on the mathematical approach in 9.4.2. The SIR is evaluated for the different Time reversal KSP-OFDM systems based on TDS, DPN or ZPN, respectively, to show the SIR improvement in each case is based on the PNZI training sequence. SIR is evaluated in two cases that the number of antenna receivers is $R = 1$ or $R = 4$ and each KSP-OFDM scheme is compared in each case between a conventional PN training sequence and a PNZI training sequence. Table 9.2 shows the SIRs of different time reversal SIMO-OFDM systems. As shown in Table 9.3, a significant improvement can be observed after using proposed PNZI as the training sequence in all of the Time reversal KSP-OFDM systems. It appears that PNZI versions of all the existing systems can outperform the conventional methods in all cases.

Table 9.2

Time reversal KSP-OFDM Signal-to-Interference Ratio.

	SIR, TDS-OFDM		SIR, DPN-OFDM		SIR, ZPN-OFDM	
	Conv. PN.	PNZI	Conv. PN.	PNZI	Conv. PN.	PNZI
$R = 1$	0.7909	0.8832	0.8425	0.9145	0.9380	0.9680
$R = 4$	0.9335	0.9656	0.9520	0.9754	0.9825	0.9912

9.5.2 TDS-OFDM

In this experiment the TDS-OFDM system based on a conventional PN sequence and that based on the proposed PNZI sequence are simulated to show that BER is improved by using PNZI as the TDS-OFDM training sequence. To avoid inter-block interference between OFDM data blocks, the guard interval is chosen to be equal to the maximum channel tap delay, i.e., $M = 128$. As shown in Fig. 9.6, by using the PNZI sequence a significant BER improvement can be observed in comparison to that with a PN sequence in single and multi-antenna receivers of the time reversal SIMO-OFDM system.

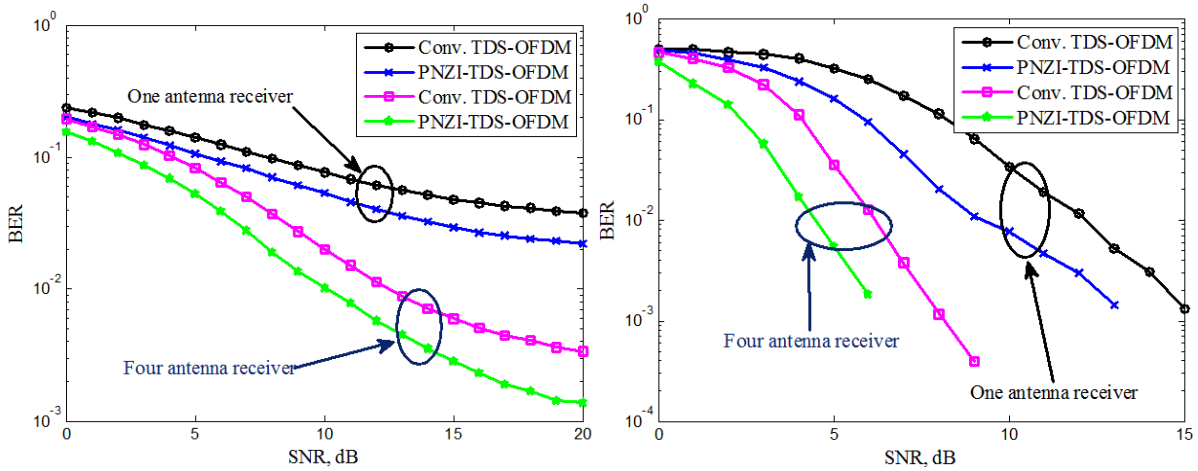

(a) (b)

Fig. 9.6. BER performance of time reversal single-input multiple-output TDS-OFDM based on conventional PN training sequence and proposed PNZI training sequence. (a) Unencoded BER performance. (b) Encoded BER performance.

9.5.3 DPN-OFDM

The BER improvement that can be achieved by using the proposed PNZI sequence in comparison to the conventional PN sequence in TR-SIMO-DPN-OFDM is evaluated using simulation experiments in this subsection. In DPN-OFDM, two PN sequences are used with a minimal length equal to the maximal channel tap delay to avoid IBIs. Each PN is of a sequence length $M = 128$. Fig 9.7 shows the BER performance comparison between the conventional DPN-OFDM with a PN sequence and DPN-OFDM with a PNZI training sequence. As shown in Fig. 9.7, significant BER performance improvements can be observed for both encoded and unencoded DPN-OFDM cases, by using the proposed PNZI sequence.

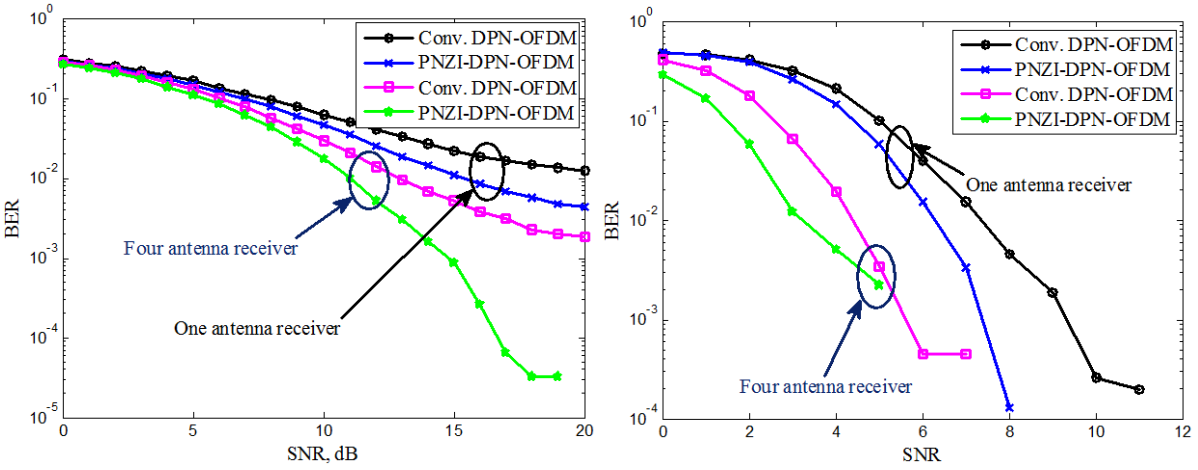

(a) (b)

Fig. 9.7. BER performance of TR-SIMO-DPN-OFDM based on conventional PN training sequence and proposed PNZI training sequence. (a) Unencoded BER performance. (b) Encoded BER performance.

9.5.4 ZPN-OFDM

ZPN-OFDM is proposed to improve the DPN-OFDM energy efficiency by replacing the first PN sequence in the DPN-OFDM with a zero padding sequence. Each zero padding and the PN sequence is of a length equal or longer than the maximum channel tap delay. In this experiment, both zero padding and the PN sequence length are 128 taps. TR-SIMO-ZPN-OFDM with a conventional PN sequence is simulated and compared to the TR-SIMO-ZPN-OFDM with a PNZI sequence to show that the BER can be improved. As shown in Fig. 9.8, the PNZI can improve the BER performance of encoded and unencoded TR-SIMO-ZPN-OFDM. All KSP-OFDM schemes based on the new training sequence outperform the conventional PN training sequence case with regard to BER performance. This improvement is achieved because of the reduction of mutual interference between the training sequence and OFDM data blocks by using the PNZI sequence and SIR improvement as shown and discussed in subsections 9.4.2 and 9.5.2.

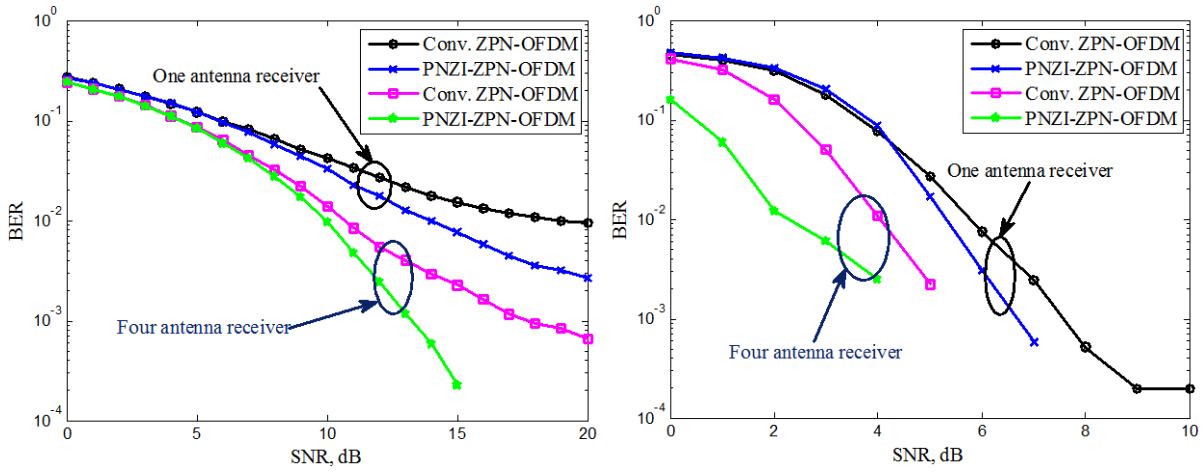

Fig. 9.8. BER performance of TR-SIMO-ZPN-OFDM based on conventional PN training sequence and proposed PNZI training sequence. (a) Unencoded BER performance. (b) Encoded BER performance.

9.5.5 Spectrum and Energy Efficiency Comparisons

This subsection shows that the spectrum and energy efficiency improvement can be achieved by using the new training sequence. In Table 9.3, the spectral efficiency is compared based on eq. (9-17) among the related OFDM schemes. For spectral efficiency, the KSP-OFDM schemes are not affected by the proposed PNZI. As shown in Table 9.3, KSP-OFDM schemes can improve the OFDM spectral efficiency especially in the short guard intervals. The ZP-OFDM scheme is assumed to be with 64 pilots.

The energy efficiency of KSP-OFDM schemes based on a PNZI sequence and the conventional PN sequence are compared using eq. 9.12, as shown in 9.3. The proposed PNZI can significantly improve the energy efficiency of KSP-OFDM systems, even for those with long guard intervals.

Table 9.3

Spectral Efficiency Comparisons.

	ZP-OFDM	TDS-OFDM	DPN-OFDM	ZPN-OFDM
$M = N/4$	70%	80%	66.67%	66.67%
$M = N/8$	77.78%	88.89%	80%	80%
$M = N/16$	82.35%	94.12%	88.89%	88.89%

Table 9.4

Energy Efficiency Comparisons.

	ZP-OFDM	TDS-OFDM		DPN-OFDM		ZPN-OFDM	
		Conv. PN	PNZI	Conv. PN	PNZI	Conv. PN	PNZI
$M = N/4$	79.8%	66.7%	80%	66.7%	80%	94.1%	96.9%
$M = N/8$	79.8%	80%	88.9%	80%	88.9%	96.9%	98.5%
$M = N/16$	79.8%	88.9%	94.1%	88.9%	94.1%	98.5%	99.2%

The energy efficiency improvement achieved by using the proposed PNZI as a training sequence for KSP-OFDM schemes is shown in Fig. 9.9. Significant improvement is achieved in the TDS-OFDM and DPN-OFDM scheme, where low amplitude factors of PN sequence imposed on the time domain used by ZPN-OFDM originally achieve high energy efficiency.

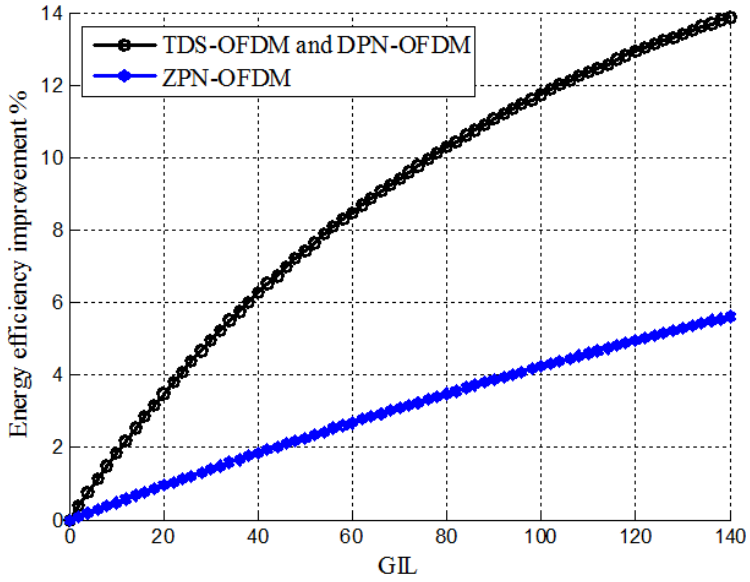

Fig. 9.9. Energy efficiency improvement can be achieved based on the proposed PNZI training sequence in the TDS-OFDM, DPN-OFDM and PNZ-OFDM schemes.

9.6 Conclusion

In channels with significant tap delays such as the UWA channel, the energy and spectral efficiency become critical. A ZP-OFDM multicarrier system is preferred to save energy in transmission, where a long guard interval is required to avoid inter-block interference. In this chapter, a pseudorandom noise with the zero insertion technique is proposed to modify the training sequence of KSP-OFDM schemes for better energy efficiency. The proposed sequence is a pseudorandom noise with zeroes inserted into every other bit. The resultant PNZI training sequence achieves the same level of spectral efficiency of conventional KSP-OFDM schemes with significant energy efficiency improvement. The PNZI sequence has similar autocorrelation function to the conventional sequence for synchronization purposes. A significant bit error rate improvement can be achieved, where training sequence mutual interfere in the OFDM data block can reduced. The proposed technique has been illustrated using simulation experiments for a simulated channel as well as a real UWA channel measured from one sea experiment.

Chapter 10

Double-Side Zero Delimited Pseudorandom Noise OFDM System for Underwater Acoustic Channel

10.1 Introduction

Communication channels with significant signal dispersion such as underwater acoustic (UWA) channels are arguably the most challenging for communication [6]. In such types of channel the complexity of the time domain channel equalizer at the receiver increases with the increase in data rate [6, 99]. Time reversal (TR) single-input multiple-output (SIMO) orthogonal frequency division multiplexing (OFDM) technique has been proposed to address this issue to offer a low-complexity frequency-domain channel equalizer [6, 10].

In fact, OFDM has already been extensively adopted to UWA communication [190]. There are a lot of efforts paid to improve its energy and spectral efficiency to mitigate the complexity and bandwidth limitation of UWA. One natural way to increase the OFDM system spectrum and energy efficiency is to reduce the guard interval length. This can be achieved by channel focusing to reduce the effective channel impulse responses spread. In [10, 189] the focusing of multiple channels has been studied individually and independent of the diversity combining technique.

Generally, there are many variations of OFDM, which can be roughly classified into three groups: cyclic prefix OFDM (CP-OFDM), zero padded OFDM (ZP-OFDM), and time domain synchronous OFDM (TDS-OFDM) [146]. CP is utilized in CP-OFDM as a guard interval to alleviate the inter-block-interference (IBI) in multipath channels. To save the transmission power spent on the guard interval, CP is replaced by ZP in ZP-OFDM. ZP-OFDM is preferred in UWA communication due to the possible transmission power reduction [6, 9, 11, 12]. Unlike the CP-OFDM and ZP-OFDM, TDS-OFDM adopts a pseudorandom noise (PN) sequence as a training sequence (TS) as well as a guard interval for channel estimation and synchronization, known to both sender and receiver. Consequently, TDS-OFDM does not require any frequency-domain pilots as are usually used in CP-OFDM and ZP-OFDM, leading to possible spectrum and energy efficiency improvement without being detrimental to its bit error rate (BER) performance [144, 146].

In this chapter, we will see that TDS-OFDM can only outperform the ZP-OFDM in terms of bandwidth efficiency. Energy efficiency improvement cannot be guaranteed. The major TDS-OFDM issue is the IBI between the training sequence and OFDM data blocks. To address this issue extensive efforts have been made. The related methods can be grouped into two categories [146, 198]. The first one is a classical iterative interference cancellation algorithm [165] and its extensions without changing the TDS-OFDM system and frame structure [166]. However, only slight improvements can be achieved with these methods [146], especially for UWA channels with long tap delays [189]. The other category relies on the modification of the TDS-OFDM frame structure for interference cancellation [146, 198]. For example, within OFDM data blocks, redundant frequency-domain pilots can be designed to be scattered in the unique word OFDM (UW-OFDM) [167] to generate the time-domain TS so that a significant interference reduction can be achieved. However, this technique cannot reduce the interference of OFDM data blocks onto the

TS block. One simple and efficient way to deal with such an issue is the dual PN padding OFDM (DPN-OFDM) scheme [168] and the zero PN OFDM (ZPN-OFDM) [144], whereby two repeated guard intervals are used in every TDS-OFDM symbol to avoid interference from the OFDM data block to the second PN sequence. Unfortunately, the duplicated guard interval causes a significant decrease in system spectrum efficiency especially in the channels with significant tap delay such as an UWA channel. To this end, the time-frequency training sequence OFDM (TFT-OFDM) has been proposed to avoid the conventional iterative interference cancellation by adding a small amount of frequency domain in TDS-OFDM. While working for most wireless communication channels, its performance can be significantly degraded in multipath channels with large tap delay [146, 198]. Recently, a TDS-OFDM interference reduction technique has been proposed in long tap delay channels such as the UWA channel, based on time reversal SIMO-OFDM with correlation based coder [189]. The time reversal is a technique used to focus the multipath channel to be like an impulse channel [10]. However, a significant energy increase of the OFDM data blocks can be observed by using such a correlation based coder.

In this chapter, a new OFDM system called "double-side zero delimited pseudorandom noise" or ZPNZ is proposed to solve the IBI problem of the TDS-OFDM in the time reversal channel based on the structured compressive sensing (SCS) technique. It is expected that the proposed ZPNZ-OFDM scheme can yield a significant BER and energy efficiency improvement. Based on a classical sparse signal reconstruction algorithm called simultaneous orthogonal matching pursuit (SOMP) [187], high-dimensional channel impulse responses (CIR) can be estimated by using a low-dimensional observation signal if the CIR is (approximately) sparse so that the TDS-OFDM synchronization property can be maintained. The proposed ZPNZ-OFDM technique will incorporate the SOMP to improve the signal–to–interfered–signal ratio (SISR) of decoded OFDM data blocks as well as the training sequence. Furthermore, the PN training sequence amplitude can be reduced for more significant BER as well as improving the system energy efficiency.

The rest of the chapter is organized as follows: first, the time reversal SIMO-TDS-OFDM is discussed to lay the foundation of the communication system in this chapter. Then, a detailed explanation of the frame structure of the proposed system will be included. Also, motivation of the proposed system is discussed and the performance of the new scheme is analyzed, discussed, and evaluated. Then, the simulation results are presented to demonstrate the performance of the proposed ZPNZ-OFDM scheme. Finally, the conclusion of this chapter is presented.

10.2 Time Reversal SIMO-OFDM System Model

Time reversal is a feedback wave focusing technique used to compensate the multipath dispersion in digital communications for many types of physical propagation media, such as radio or acoustic channels [178]. The transmitter transmits a probe signal at the beginning of the communication, and the corresponding signal is recorded at the receiver. The received probe serves as channel information and is retransmitted at the receiver. This process can be implemented as passive TR or passive phase conjugation when a receiving array is available [134]. Here we consider a passive TR system in the multipath underwater fading channels. The most attractive feature of passive TR is its computational simplicity [10]. A brief survey of TR can be obtained in [199].

Assuming that TDS-OFDM has N data blocks followed by an M bit training sequence. The i-th TDS-OFDM frame can be written as:

$$a(n)=\begin{cases} x(n)=\dfrac{1}{N}\sum_{k=0}^{N-1}s[n]e^{j2\pi kn/N} & n\in[0,N-1] \\ [c_{i,n}]_{n=0}^{M-1} & n\in[N,N+M-1] \end{cases}. \tag{10-1}$$

Here, M is both the guard interval and training sequence length. For a linear time varying (LTV) multipath channel between the transmitter (TxE) and each r-th antenna receiver (RxE), the channel impulse response can be as [6, 9, 13, 39]:

$$h_r(t;\tau)=\sum_{\mu}A_{r,\mu}(t)\delta(\tau-\tau_{r,\mu}(t)), \tag{10-2}$$

where $A_{r,\mu}(t)'s$ and $\tau_{r,\mu}(t)'s$ are the time-varying path amplitudes and delays, respectively. The channel delay spread $\tau_{\max}$ is the difference between the maximum and minimum channel path delay. To avoid OFDM IBI, the guard interval length is chosen to be longer than or equal to the channel delay spread.

Usually, for received signal processing in UWA communication, the following assumptions can be made:

i) during one OFDM block the signal amplitude does not change $A_{r,\mu}(t)\approx A_{r,s}[i]$,

ii) path delay can be written approximately as:

$$\tau_{r,\mu}(t)=\tau_{r,\mu}[i]-\alpha_r[i]t, \tag{10-3}$$

where $\alpha_r[i]'s$ are Doppler scaling factors (DSFs). For a brief justification of these assumptions in the UWA channel readers may refer to work in [6, 9, 13, 40, 147].

In this chapter, we will not focus on the estimation of DSFs or frame synchronization, as that can be estimated based on a preamble signal as in [6, 13].

For time reversal SIMO-OFDM, after the time reversal process the received signal can be represented as:

$$y(n)=a(n)\otimes q(n), \tag{10-4}$$

where

$$q[n]=\sum_{r=1}^{R}h_r[n]\otimes\hat{h}_r\left[\frac{M}{2}-n\right], \tag{10-5}$$

and $\hat{h}_r[n]$ is an estimation of $h_r[n]$. In this chapter, $h_r[n]$ can be estimated based on the training sequence by using the SCS with the simultaneous orthogonal matching pursuit (SOMP) [40, 146] method.

After removing the training sequence by subtracting, the i-th TDS-OFDM data block can be represented as:

$$u[n]=\sum_{i=1}^{N}\tilde{z}[i;n-(i-1)L_d]+\tilde{v}[n]+\tilde{g}[n]+\tilde{w}[n], \tag{10-6}$$

where $\tilde{v}[n]$ is the IBI effect between the training sequence and OFDM data blocks, $\tilde{g}[n]$ is the IBI effect between the OFDM data blocks themselves in an insufficient guard interval case (when the guard interval length is shorter than the channel delay spread) and $\tilde{w}[n]$ is the additive white Gaussian noise (AWGN). $\tilde{g}[n]=0$ for sufficient guard interval length (meaning the guard interval length is longer than or equal to the channel delay spread). The PN sequence c_i is independent of the OFDM data block s_i and the OFDM data blocks are

independent of each other. Both $\tilde{g}[n]$ and $\tilde{v}[n]$ are considered as AWGN, the eq. (10-6) can be written as:

$$u[n]=\sum_{i=1}^{N}\tilde{z}[n]+\tilde{o}[n], \tag{10-7}$$

where $\tilde{o}[n]$ is equivalent to AWGN and IBI interference between data blocks and training sequence noise after PN subtraction and time reversal operation. The OFDM data detected will be:

$$f[i]=P_k J_{old} u[i], \tag{10-8}$$

where P_k denotes the K-point FFT matrix, and J_{ola} is the overlap-add (OLA) operation $K\times L_d$ matrix used to convert a TDS-OFDM frame to a CP-OFDM one. After removing the training sequences at the receiver, the TDS-OFDM technique is equivalent to the zero-padded OFDM (ZP-OFDM) technique [193, 197]. Fig. 10.1 shows the received TDS-OFDM signal frame decomposition in a time reversal SIMO-OFDM scheme.

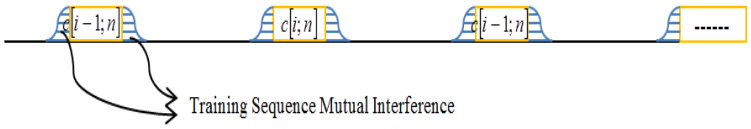

(a)

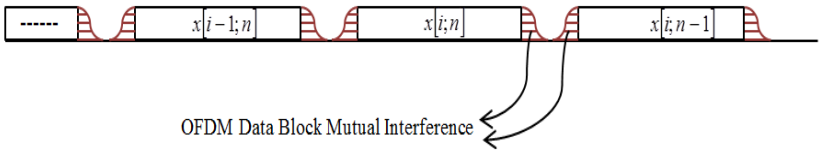

(b)

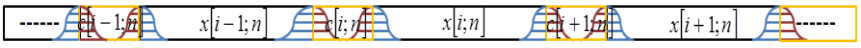

(c)

Fig. 10.1, Received time reversal single-input multiple-output TDS-OFDM signal frame: (a) received training sequence decomposition in time domain; (b) received OFDM data block decomposition in time domain; (c) received time reversal single-input multiple-output TDS-OFDM signal frame.

10.3 Time Reversal Single-Input Multiple-Output ZPNZ-OFDM Frame Structure

In this section, a new OFDM frame structure is proposed to reduce the mutual interference between the training sequence and OFDM data blocks. The transmitted and received time reversal of proposed time reversal single-input multiple-output ZPNZ-OFDM can be decomposed in the form shown in Fig. 10.1. It can be seen that in the received frame the PN sequence is free of IBI in the case that $(M/2+L/2-1)$ is longer than or equal to the channel tap delay, where L represents the inserted PN sequence length, and this PN sequence can be used in channel estimation and synchronization based on the good autocorrelation property of PN sequence.

Let the PN sequence of the proposed ZPNZ-OFDM be $\{c_{i,n}\}_{n=0}^{L-1}$, the ZPNZ-OFDM transmitted symbol denoted as $a(n)$, can be expressed as:

$$a(n)=\begin{cases}\dfrac{1}{N}\sum_{k=0}^{N-1}S(k)e^{j2\pi kn/N} & n\in[0,N-1]\\ 0 & n\in[N,N+M/2-L/2-1]\\ \{c_{i,k}\}_{k=0}^{L-1} & n\in[N+M/2-L/2-1,N+M/2+L/2-1]\\ 0 & n\in[N+M/2-L/2-1,N+M-1]\end{cases}. \tag{10-9}$$

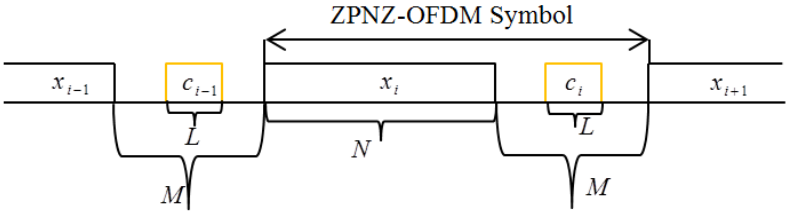

(a)

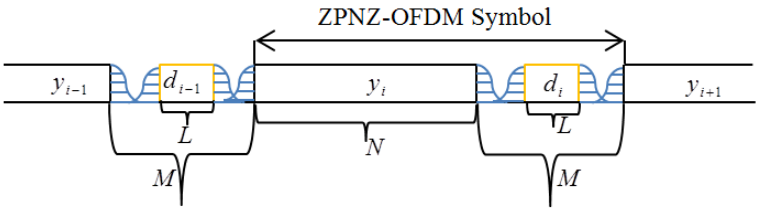

(b)

Fig. 10.2. Proposed time reversal single-input multiple-output ZPNZ-OFDM system frame structure: (a) transmitted signal frame; (b) received signal frame.

After the OFDM signal frame passes through the time reversal channel with maximum channel tap delay L_{ch}, the transmitted and received signal frames of the proposed time reversal single-input multiple-output ZPNZ-OFDM can be decomposed in Fig. 10.2. The i-th received $\{b_{i,n}\}_{n=0}^{N+M+L_{ch}-2}$ does not include the following two overlapping parts: first $\{d_{i,n}\}_{n=0}^{N+L+L_{ch}-2}$ represents the linear convolution output between the PN sequence $\{c_{i,n}\}_{n=0}^{L-1}$ and the linear time variant channel in (5), and second, $\{y_{i,n}\}_{n=0}^{N+L_{ch}-2}$ denotes the convolution output between the OFDM data blocks $\{x_{i,n}\}_{n=0}^{N-1}$ and channel impulse response in eq. (10-5).

The $b_{i,n}$ can be studied in two cases (first, sufficient guard interval -both OFDM data block and training sequence are mutually interference free- $(M/2+L/2-1)\geq L_{ch}$).

$$b_{i,k}=\begin{cases}y_{i,n} & 0\leq n<N+M/2-L/2-L_{ch}\\ y_{i,n}+d_{i,n} & N+M/2-L/2-L_{ch}\leq n<N+M-L_{ch}+1\\ y_{i,n}+d_{i,n}+y_{i+1,n} & N+M-L_{ch}+1\leq n<N+L_{ch}-1\\ y_{i+1,n}+d_{i,n} & N+M/2+L/2+L_{ch}-2\leq n<N+M-L_{ch}+1\end{cases}. \tag{10-10}$$

Secondly, (first, insufficient guard interval -both OFDM data block and training sequence are corrupted by mutual interference- $(M/2+L/2-1)<L_{ch}$),

$$b_{i,k}=\begin{cases} y_{i,n} & 0\le n<N+M/2+L/2-L_{ch} \\ y_{i,n}+d_{i,n} & N+M/2+L/2-L_{ch}\le n<N+M-L_{ch}+1. \\ y_{i,n}+d_{i,n}+y_{i+1,n} & N+M-L_{ch}+1\le n<N+M-L_{ch}+1 \end{cases} \tag{10-11}$$

The communication channel can be estimated based on the SCS techniques as discussed in [39, 146, 167]. The time-domain received PN sequence over UWA multipath channel $d_{i,n}=\left[d_{i,\frac{M}{2}-\frac{L}{2}-1},d_{i,\frac{M}{2}-\frac{L}{2}+1},....d_{i,\frac{M}{2}+\frac{L}{2}-1}\right]^T$ can be denoted by:

$$d_{i,n}=\psi_{i,n}q_{i,n}+w_{i,n}, \tag{10-12}$$

where $w_{i,n}$ represents the noise terms, and

$$\psi_{i,n}=\begin{bmatrix} c_{i,0} & x_{i,N+\frac{M}{2}-\frac{L}{2}-1} & x_{i,N+\frac{M}{2}-\frac{L}{2}} & \cdots & x_{i,N+\frac{M}{2}+\frac{L}{2}-1} \\ c_{i,1} & c_{i,0} & x_{i,N+\frac{M}{2}-\frac{L}{2}-1} & \cdots & x_{i,N+\frac{M}{2}+\frac{L}{2}-2} \\ c_{i,2} & c_{i,1} & c_{i,0} & \cdots & x_{i,N+\frac{M}{2}+\frac{L}{2}-3} \\ \cdots & \cdots & \cdots & \ddots & \cdots \\ c_{i,L-3} & c_{i,L-2} & c_{i,L-1} & \cdots & x_{i,-\frac{M}{2}-\frac{L}{2}-1} \\ c_{i,L-2} & c_{i,L-1} & x_{i,-\frac{M}{2}+\frac{L}{2}-1} & \cdots & x_{i,-\frac{M}{2}-\frac{L}{2}} \\ c_{i,L-1} & x_{i,-\frac{M}{2}+\frac{L}{2}-1} & x_{i,-\frac{M}{2}+\frac{L}{2}-2} & \cdots & x_{i,-\frac{M}{2}-\frac{L}{2}-1} \end{bmatrix}.$$

The received training sequence $d[i;n]$ is contaminated by the portion $\left[x_{i,N+\frac{M}{2}-\frac{L}{2}-1},x_{i,N+\frac{M}{2}-\frac{L}{2}},\ldots,x_{i,N+\frac{M}{2}+\frac{L}{2}-1}\right]^T$ of the x_i, OFDM data block and $\left[x_{i,-\frac{M}{2}+\frac{L}{2}-1},x_{i,-\frac{M}{2}+\frac{L}{2}-2},\ldots,x_{i,-\frac{M}{2}-\frac{L}{2}-1}\right]^T$ of the next OFDM data block.

The received PN sequence, after subtraction and time reversal operation with the equivalent noise in the frequency domain, can be written as:

$$D=\psi Q+W. \tag{10-13}$$

The channel impulse response can be estimated with an SCS technique by solving the following nonlinear optimization problem as in [146, 186, 187]:

$$\hat{Q}=\arg\min_{Q\in C^{L\times R}}\ \|Q\|_{p,q},\quad subject\quad to\quad \|D-\psi Q\|_{p,q}\le\zeta^2, \tag{10-14}$$

where ζ^2 is the impact of noise.

10.4 Performance Analysis of the Proposed System

As illustrated in Fig. 10.2 (a), the PN sequence introduces mutual interference to the OFDM data blocks. Based on the effective compressive sensing technique, channel estimation can be reasonably estimated. The basic principle of TDS-OFDM is that with perfect channel estimation the mutual interference between the PN sequence and OFDM data blocks can be completely removed. Once that is done, TDS-OFDM can be considered as the ZP-

OFDM and any equalizer that works for ZP-OFDM can be used in TDS-OFDM also. In this section, signal–to–interfered–signal ratio (SISR) performance of the proposed system will be discussed, and the energy and spectral efficiency of the proposed system will also be evaluated.

10.4.1 Channel Estimation Computational Complexity:

The computational complexity of the proposed Simultaneous Orthogonal Matching Pursuit channel estimation method proposed in chapters (6-10) required number of complex multiplications includes the following two parts [146]:

1) At the pegging the correlation based partial channel impulse response priori acquisition based on eq. (10-15), the complexity $O(M)$ is required for any TDS-OFDM scheme.

$$\bar{h}_i = \frac{1}{M} c_i \otimes d_i = h_i + u_i, \tag{10-15}$$

2) In the second step of SOMP based joint sparsity pattern recovery (see [146]), the inner product between the residual R and the observation matrix ϕ for each iteration has the complexity $O(RLL_{ch})$. Thus, the total complexity of the SOMP algorithm with S iterations is $O\left(SRL\left(L_{ch}+S^2\right)\right)$. To sum up, the total complexity is $O\left(RM+SRL\left(L_{ch}+S^2\right)\right)$.

Please note: all Proposed OFDM schemes in this thesis has the same complexity, where all of it use the same channel estimation method with different frame structure.

10.4.2 Signal–to–Interfered–Signal Ratio Performance

For received frames with high signal–to–noise ratios (SNRs), the major noise components originate from the IBI interference as shown in Fig. 1 and Fig. 2. Signal–to–interfered–signal ratio (SISR) can be used to evaluate the new ZPNZ-OFDM scheme. Signal–to–interference ratio (SIR) performance ρ_{SIR} of the decoded OFDM data blocks $\hat{S}[i]$ of i-th TR-SIMO-ZP-OFDM data block can be formulated as eq. (28) in [6]:

$$\rho_{SIR-ZP} = \frac{\sum_{n=0}^{M} |q[i;n]|^2}{\sum_{n\geq M+1} |q[i+1;n]|^2 + \sum_{n<0} |q[i-1;n]|^2}. \tag{10-16}$$

In the conventional time reversal single-input multiple-output TDS-OFDM, to measure the SIR in addition to the IBI among OFDM data blocks the mutual interference due to the training sequence needs to be included. The SIR of OFDM data blocks in the case of conventional time reversal single-input multiple-output TDS-OFDM will be:

$$\rho_{SIR-TDS} = \frac{\sum_{n=0}^{M} |q[i;n]|^2}{\sum_{n\geq M+1} |q[i+1;n]|^2 + \sum_{n<0} |q[i-1;n]|^2 + \sum_{n\geq 0} |q[i-1;n]|^2 + \sum_{n\leq 0} |q[i;n]|^2}. \tag{10-17}$$

Following the same procedure, the SIR of the proposed time reversal single-input multiple-output ZPNZ-OFDM will be:

$$\rho_{SIR-ZPNZ} = \frac{\sum_{n=0}^{M}|q[i;n]|^2}{\sum_{n\geq M}|q[i+1;n]|^2 + \sum_{n<-M}|q[i-1;n]|^2 + \alpha\sum_{n\geq(M/2-L/2+2)}|q[i-1;n]|^2 + \alpha\sum_{n\leq(M/2-L/2+2)}|q[i;n]|^2}. \quad (10\text{-}18)$$

The time reversal channels $q[i+1;n]$, $q[i;n]$ and $q[i-1;n]$ are expected to be approximately the same, therefore the signal–to–interfered–signal ratio (SISR) ρ_{SISR} of TR-SIMO-ZP-OFDM systems will be eq. (29) in [6]:

$$\rho_{SISR\_ZP} = \frac{\sum_{n=0}^{M}|q[i;n]|^2}{\sum_{n=-\infty}^{\infty}|q[i;n]|^2}. \quad (10\text{-}19)$$

In the case of time reversal single-input multiple-output TDS-OFDM schemes, the interference will increase where the TS mutual inference is added. Then the SISR of time reversal single-input multiple-output TDS-OFDM will be:

$$\rho_{SISR\_TDS} = \frac{\sum_{n=0}^{M}|q[i;n]|^2}{\sum_{n=-\infty}^{\infty}|q[i;n]|^2 + \alpha\sum_{n\geq 0}|q[i;n]|^2 + \alpha\sum_{n\leq 0}|q[i;n]|^2}, \quad (10\text{-}20)$$

and in case of the time reversal single-input multiple-output ZPNZ-OFDM scheme will be:

$$\rho_{SISR\_ZPNZ} = \frac{\sum_{n=0}^{M}|q[i;n]|^2}{\sum_{n=-\infty}^{\infty}|q[i;n]|^2 + \alpha\sum_{n\geq(M/2-L/2+2)}|q[i;n]|^2 + \alpha\sum_{n\leq(M/2-L/2+2)}|q[i;n]|^2}. \quad (10\text{-}21)$$

10.4.3 Signal–to–Interfered–Signal Ratio of Received PN Sequence

The received PN sequence can be used for channel estimation based on compressive sensing. To evaluate the proposed communication system performance the signal–to–interfered–signal ratio of the received PN sequence for the conventional time reversal single-input multiple-output TDS-OFDM and the proposed time reversal single-input multiple-output ZPNZ-OFDM is estimated.

SISR performance $\rho_{SISR\_PN\_TDS}$ of received PN sequence $d[i]$ in the conventional time reversal single-input multiple-output TDS-OFDM system can be estimated with the same methodology as the OFDM data blocks under the condition of the OFDM data blocks being longer than the maximum channel tap delay:

$$\rho_{SISR\_PN\_TDS} = \frac{\sum_{n=-\infty}^{\infty}|q[i;n]|^2}{\sum_{n=-\infty}^{\infty}|q[i;n]|^2 + \frac{1}{\alpha}\sum_{n=1}^{M}|q[i;n]|^2 + \frac{1}{\alpha}\sum_{n=-M}^{-1}|q[i+1;n]|^2}. \quad (10\text{-}22)$$

SISR of received PN sequence $d[i]$ for the proposed time reversal single-input multiple-output ZPNZ-OFDM $\rho_{SISR\_ZPNZ\_TDS}$ will be:

$$\rho_{SISR\_PN\_ZPNZ} = \frac{\sum_{n=-\infty}^{\infty} |q[i;n]|^2}{\sum_{n=-\infty}^{\infty} |q[i;n]|^2 + \frac{1}{\alpha} \sum_{n=\left(\frac{M}{2}-\frac{L}{2}-1\right)}^{\left(\frac{M}{2}-\frac{L}{2}+L-1\right)} |q[i;n]|^2 + \frac{1}{\alpha} \sum_{n=-\left(\frac{M}{2}+\frac{L}{2}-1\right)}^{-\left(\frac{M}{2}+\frac{L}{2}+L-1\right)} |q[i+1;n]|^2}, \quad (10\text{-}23)$$

$q[i+1;n]$ and $q[i;n]$ are time reversal channel probing signals recorded which are expected to be approximately the same, then, $\rho_{SISR\_PN\_TDS}$ and $\rho_{SISR\_PN\_ZPNZ}$ will be:

$$\rho_{SISR\_PN\_TDS} = \frac{\sum_{n=-\infty}^{\infty} |q[i;n]|^2}{\sum_{n=-\infty}^{\infty} |q[i;n]|^2 + \frac{1}{\alpha} \sum_{n=1}^{M} |q[i;n]|^2 + \frac{1}{\alpha} \sum_{n=-M}^{-1} |q[i;n]|^2}, \quad (10\text{-}24)$$

and,

$$\rho_{SISR\_PN\_ZPNZ} = \frac{\sum_{n=-\infty}^{\infty} |q[i;n]|^2}{\sum_{n=-\infty}^{\infty} |q[i;n]|^2 + \frac{1}{\alpha} \sum_{n=\left(\frac{M}{2}-\frac{L}{2}-1\right)}^{\left(\frac{M}{2}-\frac{L}{2}+L-1\right)} |q[i;n]|^2 + \frac{1}{\alpha} \sum_{n=-\left(\frac{M}{2}+\frac{L}{2}-1\right)}^{-\left(\frac{M}{2}+\frac{L}{2}+L-1\right)} |q[i+1;n]|^2}. \quad (10\text{-}25)$$

10.4.4 Bandwidth and Energy Efficiency

An energy efficiency metric of the OFDM systems can be:

$$\eta_0 = \frac{N_{data}}{N_{data} + \beta^2 N_{pilots}} \times \frac{N}{N + \alpha^2 M} \times 100\%, \quad (10\text{-}26)$$

where N_{data} and N_{pilots} are the subcarrier number in the OFDM data block for the data and pilot subcarriers, respectively. β is the pilot signal amplitude factor imposed on the frequency domain normalized to the OFDM data blocks. α is the training sequence amplitude factor imposed on the time domain normalized to the OFDM data blocks. Both CP-OFDM and ZP-OFDM uses pilot amplitude boosting to improve the channel estimation accuracy. In the conventional digital video broadcasting – second generation terrestrial (DVB-T2), standard amplitude factor is $\beta = 4/3$ and for reliable channel estimation $\alpha = \sqrt{2}$ is used for the amplitude of the PN sequence in the digital terrestrial multimedia broadcast (DTMB) standard [146]. The training sequence amplitude $\alpha = 1/\sqrt{2}$ is proposed to be used in our proposed system. The β and α values in each OFDM scheme is shown in Table 10.1.

Based on eq. (10-25) the TDS-OFDM outperforms the ZP-OFDM scheme in energy efficiency if it has a guard interval length M satisfying:

$$M < \frac{N_{pilots} B^2 N}{\alpha^2 \left(N - N_{pilots}\right)}. \quad (10\text{-}27)$$

The energy efficiency of the proposed OFDM system will be:

$$\eta_0 = \frac{N_{data}}{N_{data} + \beta^2 N_{pilots}} \times \frac{N}{N + \alpha^2 L} \times 100\%. \tag{10-28}$$

This means the ZPNZ-OFDM scheme will outperform the conventional TDS-OFDM energy efficiency by the factor:

$$\eta_{imp\_TDS} = \frac{N\left(\alpha_{TDS}^2 M - \alpha_{ZPNZ}^2 L\right)}{N^2 + \alpha_{TDS}^2 NM + \alpha_{ZPNZ}^2 NL + \alpha_{ZPNZ}^2 \alpha_{TDS}^2 LM} \times 100\%, \tag{10-29}$$

$\alpha_{TDS} = \sqrt{2}$ and $\alpha_{ZPNZ} = 1/\sqrt{2}$ is the amplitude of PN sequence in the conventional TDS-OFDM and ZPNZ-OFDM schemes respectively. Then,

$$\eta_{imp\_TDS} = \frac{N(2M - L)}{N^2 + N(2M + L) + 2LM} \times 100\%. \tag{10-30}$$

Compared to the conventional ZP-OFDM system, ZPNZ-OFDM can outperform in energy efficiency by:

$$\eta_{imp\_ZP} = \frac{\beta^2 NN_{pilots} - \alpha_{ZPNZ}^2 LN_{data}}{NN_{data} + \beta^2 NN_{pilots} + \alpha_{ZPNZ}^2 LN_{data} + \beta^2 \alpha_{ZPNZ}^2 LN_{pilots}} \times 100\%. \tag{10-31}$$

The normalized bandwidth efficiency γ_0 of the considered OFDM schemes without any overhead can be obtained as [146]:

$$\gamma = \frac{N_{data}}{N_{data} + N_{pilots}} \times \frac{N}{N + M} \times 100\%. \tag{10-32}$$

It is worth pointing out that the normalized bandwidth efficiency seems poorer than the actual bandwidth efficiency because many types of the overhead information are not calculated such as the channel coder overhead.

The proposed ZPNZ-OFDM will have TDS-OFDM under the same guard interval, but it will outperform the ZP-OFDM bandwidth with:

$$\gamma_{imp} = \frac{N}{N + M} \times \left(1 - \frac{N_{data}}{N_{data} + N_{pilots}}\right) \times 100\%. \tag{10-33}$$

Table 10.1

Summary the β and α Values in each OFDM Scheme.

	α	β
ZP-OFDM	0	$\beta = 4/3$
Conv. TDS-OFDM	$\sqrt{2}$	0
Proposed ZPNZ-OFDM	$1/\sqrt{2}$	0

10.5 Simulation Results

The proposed time reversal single-input multiple-output ZPNZ-OFDM transmission scheme will be tested by simulation over a measured TR UWA channel with $L_{ch} = 128$ as a maximum channel tap delay in this section.

The TR UWA channel is adopted from data collected in the ASCOT01 experiment conducted off the coast of New England in June 2001, as reported in [10, 143, 144]. System performance was evaluated in coded and uncoded cases with the OFDM system using a 512 data sub-carrier and QPSK modulation. Data symbols were generated using a random information bits modulation by QPSK modulation in the uncoded case. In the coded case, the random information bits are first encoded by a rate 1/2 convolution encoder with a generator polynomial [65,57] [174], then the encoded bits are interleaved by a block interleaver of depth 8 prior to QPSK modulation. Based on SCS channel characteristics, estimated frame-by-frame is based on eq. (10.14). In all analysis and simulation, the PN sequence length of the ZPNZ-OFDM is $L = 26$. $L = 26$ is the observation matrix size based on simulation computation used to estimate the channel impulse response which will be carefully discussed in the rest of this section.

10.5.1 Signal–to–Interfered–Signal Ratio

In this experiment, the SISR improvement is estimated based on the mathematical formulas in section 9.4. The SISR is evaluated for the OFDM data blocks and training sequence in both one antenna receiver and four antenna receivers cases. SISR comparisons of the different time reversal SIMO-OFDM systems are shown in Table 10.2 and Table 10.3. The ZP-OFDM scheme demonstrates the highest performance and the new ZPNZ-OFDM scheme clearly outperforms the conventional systems. SISR of the PN sequence in conventional time reversal single-input multiple-output TDS-OFDM and proposed time reversal single-input multiple-output ZPNZ-OFDM is compared in Table 10.4 and Table 10.5. As the proposed ZPNZ-OFDM scheme outperforms the conventional time reversal single-input multiple-output TDS-OFDM in SISR of the OFDM data blocks, it also improves the SISR of the training sequence.

Table 10.2

Proposed ZPNZ-OFDM Scheme and related OFDM Schemes receiving OFDM data Block SISR: Comparisons of the SIMO-OFDM Systems at $N_r = 1$.

	Conv. TDS-OFDM	ZP-OFDM	ZPNZ-OFDM
$N/4$	0.7909	1	0.9981
$N/8$	0.7778	0.9834	0.9686
$N/16$	0.7349	0.9292	0.878

Table 10.3

Proposed ZPNZ-OFDM Scheme and related OFDM Schemes receiving OFDM data Block SISR: Comparisons of the SIMO-OFDM Systems at $N_r = 4$.

	Conv. TDS-OFDM	ZP-OFDM	ZPNZ-OFDM
$N/4$	0.9335	1	0.9991
$N/8$	0.9280	0.9941	0.9909
$N/16$	0.9149	0.9801	0.9736

Table 10.4

Proposed ZPNZ-OFDM Scheme and Conventional TDS-OFDM Schemes receiving PN Sequence SISR: Comparisons of the SIMO-OFDM Systems at $N_r = 1$.

	Conv. TDS-OFDM	ZPNZ-OFDM
$N/4$	0.8832	0.9687
$N/8$	0.8777	0.8994
$N/16$	0.8587	0.8905

Table 10.5

Proposed ZPNZ-OFDM Scheme and Conventional TDS-OFDM Schemes receiving PN Sequence SISR: Comparisons of the SIMO-OFDM Systems at $N_r = 4$.

	Conv. TDS-OFDM	ZPNZ-OFDM
$N/4$	0.9656	0.9923
$N/8$	0.9638	0.9748
$N/16$	0.9594	0.9696

10.5.2 Energy and Spectral Efficiency

This subsection shows that the spectrum and energy efficiency improvement can be achieved by using the proposed ZPNZ-OFDM scheme. Energy efficiency comparison between the proposed ZPNZ-OFDM scheme and related OFDM schemes is shown in Table 10.6, and Table 10.7. Fig. 10.3 shows the energy efficiencies of different OFDM schemes as a function of the training sequence length used. As shown in the figure, the conventional TDS-OFDM loses its energy efficiency property for long training sequences. The new scheme outperforms the conventional TDS-OFDM as well as ZP-OFDM. The energy efficiency improvement by using the new scheme is shown in Fig. 4 (b). It can be seen that the new scheme outperforms the conventional TDS-OFDM in terms of energy efficiency, while the spectral efficiency remains almost the same. However, the proposed ZPNZ-OFDM scheme outperforms the ZP-OFDM in both energy and bandwidth efficiency. Its spectral performance depends on the length of the pilot signal used in the ZP-OFDM as shown in Fig. 10.4 (a).

Table 10.6

Proposed ZPNZ-OFDM Scheme and related OFDM Schemes Energy Efficiency Comparison.

	Conv. TDS-OFDM	ZP-OFDM	ZPN-OFDM	PNZI-ZPN-OFDM	ZPNZ-OFDM
$N/4$	66.67%	79.75%	94.12%	96.9%	97.52%
$N/8$	80%	79.75%	96.97%	98.5%	97.52%
$N/16$	88.89%	79.75%	98.46	99.2%	97.52%

Table 10.7

Proposed ZPNZ-OFDM Scheme and related OFDM Schemes Spectral Efficiency Comparison.

	Conv. TDS-OFDM	ZP-OFDM	ZPN-OFDM	PNZI-ZPN-OFDM	ZPNZ-OFDM
$N/4$	80%	70%	66.67%	66.67%	80%
$N/8$	88.89%	77.78%	80%	80%	88.89%
$N/16$	94.12%	82.35%	88.89%	88.89%	94.12%

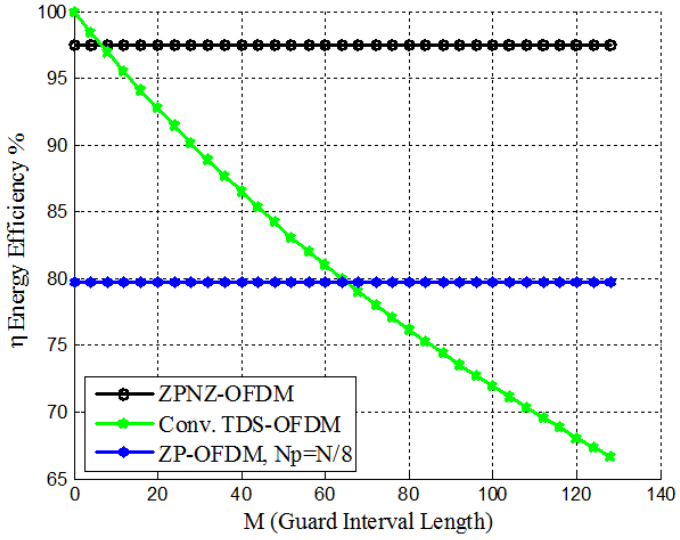

Fig. 10.3. The energy efficiency of OFDM schemes.

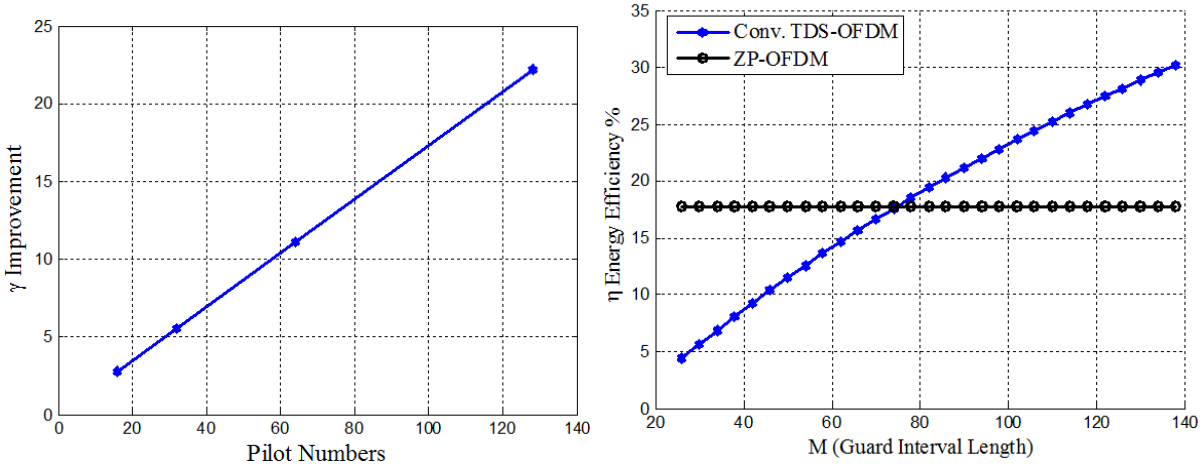

(a) (b)

Fig. 10.4, Performance improvement based on the proposed ZPNZ-OFDM scheme over the conventional OFDM schemes (a) bandwidth efficiency improvement (b) energy efficiency improvement.

10.5.3 Training Sequence Length

To evaluate the performance of the proposed ZPNZ-OFDM scheme in terms of required number of measurement pseudorandom noise length L for reliable CIR signal reconstruction. Fig. 10.5 presents the correct signal recovery probability when different observation number samples are used under the fixed SNR of 20 dB. The estimation of

MSE below 10^{-2} is considered as a correct recovery as in [200]. Only 21 samples are sufficient for the proposed ZPNZ-OFDM scheme, which means the training sequence condition is $L > 21$ for sufficient channel estimation; in this chapter $L = 26$ is chosen.

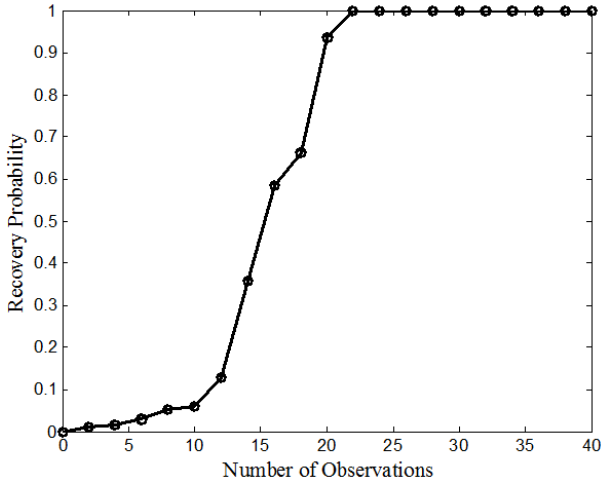

Fig. 10.5. Observation number adopted for the probability of correct signal recovery.

10.5.4 Data Image Transmission over an Underwater Channel

In this experiment, the peak signal-to-noise ratio (PSNR) of the received image transmitted over the proposed ZPNZ-OFDM scheme is compared with the related OFDM schemes. For simulation, the Set Partitioning in Hierarchical Trees (SPIHT) algorithm for image compression generates the source bit-stream with a bit rate of 0.5 bpp. By dividing the source bit stream into packets of 2000 bits, each packet is divided into 25 blocks, with 80 bits in each block. Each block has 10 symbols in each byte. These bits send over the different OFDM schemes with coded and uncoded channels. Insufficient guard intervals with a medium IBI between OFDM data blocks are used and $M = 100$. Tables 10.8 and 10.9 show the average PSNR of the received Lena image transmitted over the coded and uncoded UWA channels by using the proposed schemes. Simulated data show that the ZPNZ-OFDM system provides the best image quality. As a result, a noticeable reduction of the overall distortion over the underwater acoustic channel using our proposed ZPNZ-OFDM technique is observed, together with the improvement in PSNR for the reconstructed image. Simulation experiments are included for illustrative purposes with different image types and different SNR levels. It is shown that the proposed ZPNZ-OFDM system, in addition to saving energy and bandwidth efficiency, can also effectively reduce the overall distortion in the reconstructed image and improve PSNR.

Table 10.8

Proposed ZPNZ-OFDM scheme and related OFDM schemes received image quality comparison (uncoded channel).

SNR	Conv. TDS-OFDM	ZP-OFDM	ZPN-OFDM	PNZI-ZPN-OFDM	ZPNZ-OFDM
10dB	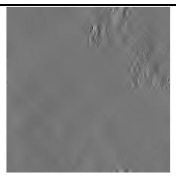	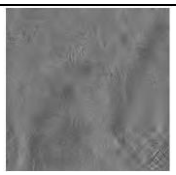		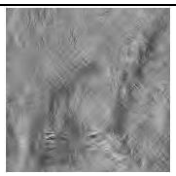	
PSNR	9 dB	15.67 dB	15.3 dB	16.2 dB	20.1 dB
20dB					
PSNR	20.17 dB	23.9 dB	22 dB	24.1dB	27.13 dB

Table 10.9

Proposed ZPNZ-OFDM scheme and related OFDM schemes received image quality comparison (coded channel).

SNR	Conv. TDS-OFDM	ZP-OFDM	ZPN-OFDM	PNZI-ZPN-OFDM	ZPNZ-OFDM
5dB	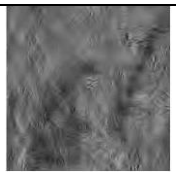				
PSNR	16 dB	20 dB	21.35 dB	23 dB	32.5 dB
8dB					
PSNR	27.25 dB	32.54 dB	32.5 dB	32.5 dB	32.5 dB

10.5.5 BER Performance

In this experiment, the BER performance of the proposed scheme in comparison to ZP-OFDM and conventional TDS-OFDM are evaluated using simulations. This evaluation is conducted in three cases i) sufficient guard interval without any IBI between OFDM data blocks with maximum tap number $M = 128$; ii) insufficient guard interval with a medium IBI between OFDM data blocks and $M = 64$; iii) insufficient guard interval with a significant IBI between OFDM data blocks and $M = 32$. As shown in Figures 10.6, 10.7, 10.8, the BER performance tends to be saturated at high SNRs. These performance floor levels decrease as the guard interval increases. Such error floor is caused by IBI between OFDM data blocks in insufficient guard interval and it is reduced in case i). In practice, the error floor removed by using channel coding.

As shown in Figs. 10.6, 10.7, 10.8, the proposed ZPNZ-OFDM outperforms the conventional TDS-OFDM. For ZP-OFDM in the single antenna receiver case, it outperforms the proposed system, but for the rich antenna receiver $N_r = 4$ ZPNZ-OFDM outperforms the conventional ZP-OFDM. UWA is a sparse channel and a large number of antenna receivers render the TR-channel to be impulse-like which reduces the mutual interference [10].

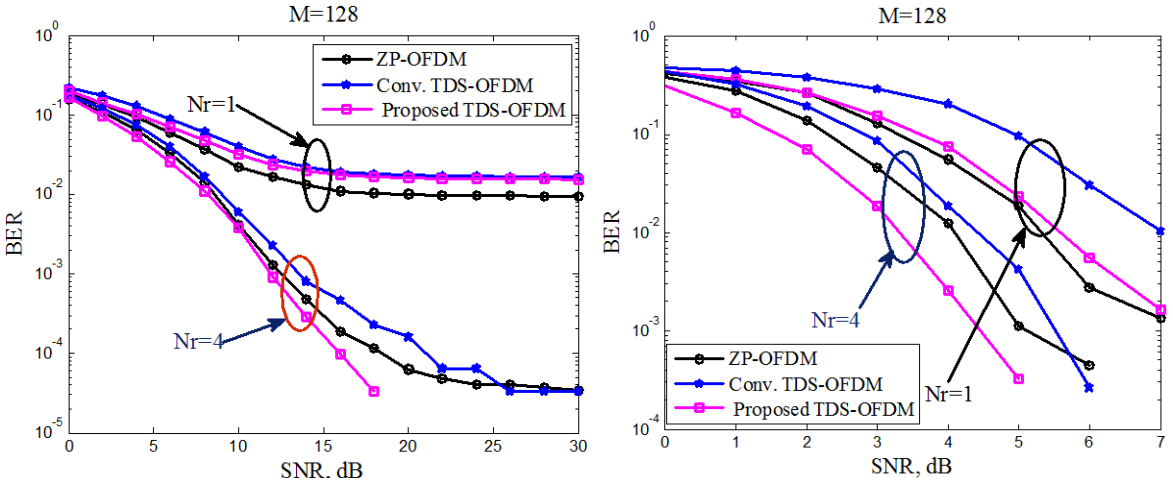

(a) Uncoded BER (b) Coded BER

Fig. 10.6. BER performance of OFDM systems with sufficient guard interval, $M = 128$.

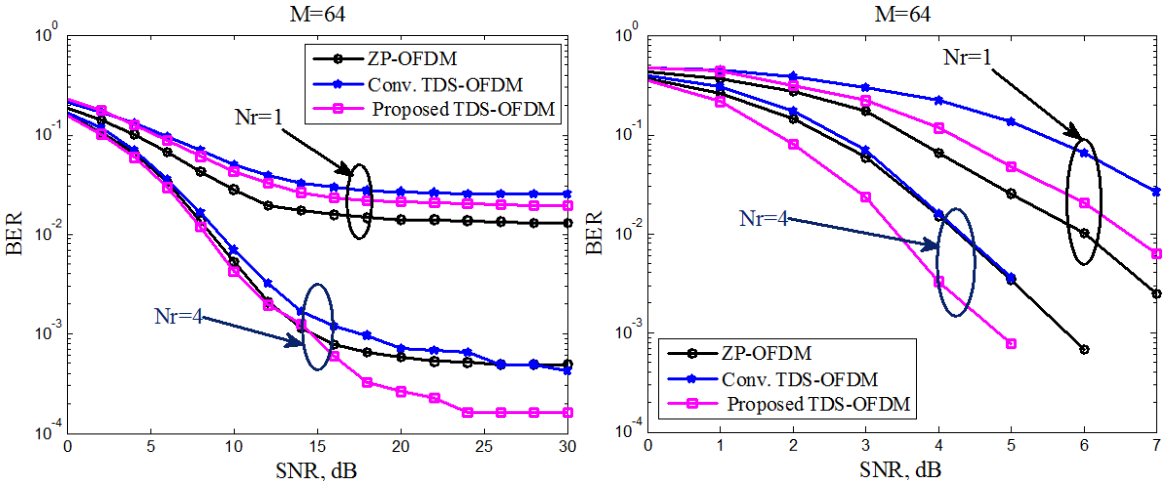

(a) Uncoded BER (b) Coded BER

Fig. 10.7. BER performance of OFDM systems with insufficient guard interval with medium IBI level, $M = 64$.

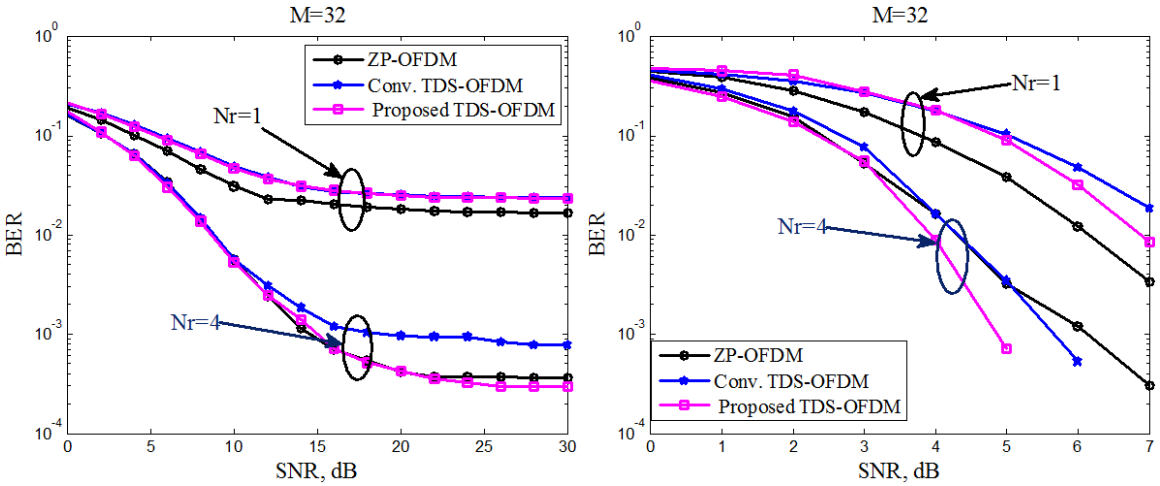

(a) Uncoded BER (b) Coded BER

Fig. 10.8. BER performance of OFDM systems with insufficient guard interval with significant level of IBI, $M = 32$.

10.6 Conclusion

A novel transmission scheme called a "double-side zero delimited pseudorandom noise OFDM (ZPNZ-OFDM)" has been proposed. In such a scheme a new design of training sequence inserted into the guard interval has been introduced to save energy, especially for long tap delay UWA channels. In the proposed new scheme, the PN sequence amplitude can be reduced to achieve a significant reduction of inter-block interference problems between OFDM data blocks and the training sequence. The new OFDM frame structure provides a significant signal–to–interfered–signal ratio. The proposed system design has been evaluated by using real channels measured from one sea-going experiment as well as a theoretical model. In both situations the merits of the proposed system have been confirmed. In particular, the ZPNZ-OFDM scheme outperforms the ZP-OFDM in terms of energy and spectrum, as well as BER performance. Also, ZPNZ-OFDM significantly outperforms the other TDS-OFDM proposed in this thesis in terms of energy and recived image quality.

Chapter 11

Conclusion and Future Work

11.1 Conclusion

In this thesis, several signal processing techniques for underwater acoustic communication networks have been developed and investigated.

An efficient image transmission over the underwater acoustic channel has been proposed. One of the main challenges for underwater communication is the limited channel bandwidth. In this thesis, unequal error protection techniques have been proposed to achieve efficient data protection satisfying a high protection level with limited overhead information. These unequal error protection techniques are based on the classification of the image coded bits. This thesis proposed three types of unequal error protection techniques: (1) based on the modulation using HQAM; (2) based on the rate allocation to achieve an efficient distribution of the channel coder overhead information; (3) based on the guard interval length of the ZP-OFDM multicarrier modulation.

Based on the SPIHT coder, encoded image bits can be classified based on their effects on the quality of the reconstructed image at the receiver. The communication system proposed for underwater channel takes advantage of these features. In the unequal error protection using HQAM modulation method, these encoded bits are classified into two groups corresponding to high priority and low priority bits. HQAM controls the protection level in each group using the modulation parameter. In the unequal error protection using rate allocation method and different length guard intervals, encoded bits are classified into four groups: (1) significant bits; (2) sign bits; (3) set bits; and (4) refinement bits. In the rate allocation method these four groups are protected with different levels of protection using a Reed Solomon channel coder. In the unequal error protection based on the guard interval length, each of these four groups are transmitted over a ZP-OFDM multicarrier system with different zero padding length. Using these unequal error protection techniques, bandwidth can be saved and the PSNR of images reconstructed at the receiver can be improved.

However, multicarrier systems are very sensitive to the carrier frequency offset produced due to the transmitter-receiver mismatched oscillator or transmitter-receiver relative velocity. In this case, the multicarrier system sub-carrier orthogonality can be loose. This thesis included in depth analysis and discussion of the carrier frequency offset problem and proposed a pulse shaping function to mitigate the inter-carrier interference problem.

Energy and spectrum efficiency are very important for communication systems. In underwater communication these factors become even more critical, where channel bandwidth and transmission power are more restrictive than that in wireless communication. To achieve a high multicarrier system, an efficient energy multicarrier system has been proposed in this thesis. By replacing the first pseudorandom noise (PN) of the dual PN OFDM (DPN-OFDM) system with zero padding and using the second PN sequence only for synchronization and channel estimation, ZPN-OFDM yields significant improvement in energy efficiency and bit error rate performance. Compressive sensing is proposed for efficient channel estimation and removes the mutual interference of the

training sequence in the OFDM data blocks. Furthermore the amplitude of the training sequence is reduced for more energy saving.

However, the extra guard interval used in the ZPN-OFDM decreases the spectrum efficiency. Also, as the data rate transmitted over the underwater channel increases, the channel delay spread increases and the efficient guard interval required to the OFDM multicarrier also increases. This will significantly decrease the spectral efficiency of the communication system. To address this problem, OFDM together with single-input multi-output (SIMO) system is proposed in this thesis for an underwater communication system to combat channel fading. While the OFDM itself provides a high spectral efficiency, the actual spectrum efficiency achieved using SIMO-OFDM in underwater communication is often much lower due to long guard intervals.

The proposed time reversal technique combined with SIMO-OFDM can convert the underwater multipath channel into an impulse like channel. In this case, a guard interval length shorter than the maximum channel tap delay can be used. Also, as the benefits of the time reversal SIMO-OFDM, the mutual interference between training sequence and OFDM data blocks in TDS-OFDM can be reduced and a short guard interval can be used. Furthermore, structural compressive sensing has been proposed to achieve accurate channel estimation and reduce the training sequence amplitude to reduce its mutual interference.

Another novel method for energy efficiency improvement has been proposed in this thesis. A novel training sequence, pseudorandom noise with zero insertion, for any of the known symbol padding orthogonal frequency division multiplexing (KSP-OFDM) systems is proposed, where zeroes are inserted into pseudo-noise bit sequence used in the KSP-OFDM training sequence to reduce the guard interval energy use in underwater acoustic channel with significant tap delay, without being detrimental to other pseudo-noise properties required for synchronization and channel estimation. This method is inspired by the observation that long guard intervals in OFDM systems caused by long delays in underwater acoustic channels can cause significant energy waste if KSP-OFDM is used. Zero insertion can be used to avoid this. Also, by using the new ZPNZ-OFDM scheme, high spectral and energy efficiency has been achieved, as well as a high BER performance.

In this thesis, another underwater acoustic (UWA) channel problem has been solved using the TDS-OFDM training sequence. Specifically, most of the UWA communication systems use the preamble signal to estimate the Doppler scaling factor. The problem is over time variant channel is need to resend this preamble. In this thesis, the TDS-OFDM training sequence was used to update the estimation of the Doppler scaling factor due to the time varying feature of the channel.

In this thesis, the TDS-OFDM technique provided for the underwater communication systems where, it adopts a pseudorandom noise (PN) sequence known to both the transmitter and the receiver as a guard interval as well as a training sequence (TS) for synchronization and channel estimation. In the ZPN-OFDM based on the good autocorrelation property of the PN sequences, the received PN sequence is in an IBI free region used in channel estimation and the frame timing and carrier synchronization. For the time reversal TDS-ODM system the Zadoff-Chu sequence (ZOS) is used as training sequence for frame time and carrier frame synchronization and channel estimation. Thanks to ZOS perfect autocorrelation properties. A preamble block is proposed for frame synchronization with Doppler scaling factor (DSF) estimation. Also, DSF updating is analyzed based on TDS-OFDM frequency domain pseudorandom noise training sequence. All proposed techniques have been illustrated

using simulation experiments for a simulated channel as well as a real UWA channel measured from one sea experiment.

11.2 Future Work

The research work presented in this thesis produced promising results. However, these works can be further improved. Future research may include the following:

1) Unequal error protection techniques discussed in chapters 3 and 4 can be used for video transmission over the underwater acoustic channel with a high quality compression technique such as compressive sensing.
2) The OFDM multicarrier system has been discussed in this thesis with an insufficient guard interval for efficient bandwidth to be achieved. However filter bank multicarrier modulation (FBMC) can save bandwidth, where no guard interval is required. Unequal error protection can be used in combination with FBMC for image and video communication over the underwater acoustic channel.
3) The difficulty of using multiuser uplink scenarios over the UWA channel is the elimination of implicit mixed interferences between different PN sequences and inverse discrete Fourier transforms. This problem can be solved using the ZPN-OFDM proposed in chapter 6.
4) The long tap delay in the underwater channel increases the challenge of synchronization. A PN sequence of the ZPN-OFDM proposed in chapter 6 can be used in synchronization of the OFDM multiuser.
5) This thesis discussed point-to-point communication. However, an underwater cognitive acoustic can be used in an underwater acoustic sensor network based on time reversal single-input multi-output OFDM to solve the synchronization problem, avoid inter-simple interference, and inter-block interference with short guard interval.
6) Channel estimation using compressive sensing in underwater acoustic point-to-point communication using KSP-OFDM schemes was proposed in this thesis chapter 9. However, it can be used in cognitive acoustic for an underwater acoustic sensor network.

References

[1] M. Stojanovic, "Acoustic (underwater) communications", *Encyclopedia of Telecommunications,* 2003.

[2] I. F. Akyildiz, D. Pompili, and T. Melodia, "Challenges for efficient communication in underwater acoustic sensor networks", *ACM Sigbed Review,* vol. 1, pp. 3-8, 2004.

[3] P. Sarisaray-Boluk, V. Gungor, S. Baydere, and A. Harmanci, "Quality aware image transmission over underwater multimedia sensor networks", *Ad Hoc Networks,* vol. 9, pp. 1287-1301, 2011.

[4] L. Toni, L. Rossi, N. Agoulmine, and J. Fontaine, "Virtual unequal error protection in underwater image transmission", in *OCEANS*, pp. 1-6, 2010.

[5] I. Iglesias, S. Aijun, J. Garcia-Frias, M. Badiey, and G. R. Arce, "Image transmission over the underwater acoustic channel via compressive sensing", in *45th Annual Conference on Information Sciences and Systems*, pp. 1-6, 2011.

[6] Z. Liu and T. C. Yang, "On overhead reduction in time-reversed OFDM underwater acoustic communications", *IEEE Journal of Oceanic Engineering,* vol. PP, pp. 1-13, 2013.

[7] L. Chunshan, Y. V. Zakharov, and C. Teyan, "Doubly selective underwater acoustic channel model for a moving transmitter/receiver", *IEEE Transactions on Vehicular Technology,* vol. 61, pp. 938-950, 2012.

[8] A. E. Abdelkareem, "Doppler compensation algorithms for DSP-based implementation of OFDM underwater acoustic communication systems", Doctor of Philosophy, Newcastle University, 2012.

[9] L. Baosheng, Z. Shengli, M. Stojanovic, L. Freitag, and P. Willett, "Multicarrier communication over underwater acoustic channels with nonuniform Doppler shifts", *IEEE Journal of Oceanic Engineering,* vol. 33, pp. 198-209, 2008.

[10] L. Zhiqiang and T. C. Yang, "On the design of cyclic prefix length for time-reversed OFDM", *IEEE Transactions on Wireless Communications,* vol. 11, pp. 3723-3733, 2012.

[11] M. Stojanovic, "Low complexity OFDM detector for underwater acoustic channels", in *OCEANS*, 2006, pp. 1-6.

[12] B. Li, S. Zhou, M. Stojanovic, and L. Freitag, "Pilot-tone based ZP-OFDM demodulation for an underwater acoustic channel", in *OCEANS*, 2006, pp. 1-5.

[13] S. F. Mason, C. R. Berger, Z. Shengli, and P. Willett, "Detection, synchronization, and Doppler scale estimation with multicarrier waveforms in underwater acoustic communication", *IEEE Journal on Selected Areas in Communications,* vol. 26, pp. 1638-1649, 2008.

[14] D. Brady and J. C. Preisig, "Underwater acoustic communications", *Wireless Communications: Signal Processing Perspectives,* vol. 8, pp. 330-379, 1998.

[15] A. C. Singer, J. K. Nelson, and S. S. Kozat, "Signal processing for underwater acoustic communications", *IEEE Communications Magazine,* vol. 47, pp. 90-96, 2009.

[16] M. Stojanovic, "Underwater wireless communications: Current achievements and research challenges", *IEEE Oceanic Engineering Society Newsletter,* vol. 41, pp. 10-13, 2006.

[17] Y. Labrador, M. Karimi, D. Pan, and J. Miller, "Modulation and error correction in the underwater acoustic communication channel", *International Journal of Computer Science and Network Security,* vol. 9, pp. 123-130, 2009.

[18] S.-J. Hwang and P. Schniter, "Efficient communication over highly spread underwater acoustic channels", in *International Conference on Mobile Computing and Networking*, 2007, pp. 11-18.

[19] F. De Rango, F. Veltri, and P. Fazio, "A multipath fading channel model for underwater shallow acoustic communications", in *IEEE International Conference on Communications*, pp. 3811-3815, 2012.

[20] L. M. Wolff, E. Szczepanski, and S. Badri-Hoeher, "Acoustic underwater channel and network simulator", in *OCEANS*, pp. 1-6, 2012.

[21] A. Sehgal, I. Tumar, and J. Schönwälder, "AquaTools: An underwater acoustic networking simulation toolkit", in *Oceans*, 2010.

[22] M. Stojanovic, "On the relationship between capacity and distance in an underwater acoustic communication channel", *ACM SIGMOBILE Mobile Computing and Communications Review*, vol. 11, pp. 34-43, 2007.

[23] A. Fish, S. Gurevich, R. Hadani, A. Sayeed, and O. Schwartz, "Delay-Doppler channel estimation with almost linear complexity", *IEEE Transactions on Information Theory*, vol. 59, pp. 7632-7644, 2012.

[24] J. Trubuil and T. Chonavel, "Accurate Doppler estimation for underwater acoustic communications", in *OCEANS*, 2012, pp. 1-5.

[25] M. Vajapeyam, S. Vedantam, U. Mitra, J. C. Preisig, and M. Stojanovic, "Time cooperative schemes for underwater acoustic communications", *IEEE Journal of Oceanic Engineering*, vol. 33, pp. 489-501, 2008.

[26] Y. Chen, X. Xu, L. Zhang, and Z. Zou, "Design and application of dynamic coding in shallow water acoustic communications", in *OCEANS*, pp. 1-6, 2012.

[27] J. S. Panaro, F. R. Lopes, L. M. Barreira, and F. E. Souza, "Underwater acoustic noise model for shallow water communications", presented at the Brazilian Telecommunication Symposium, 2012.

[28] S. Yerramalli and U. Mitra, "On optimal resampling for OFDM signaling in doubly-selective underwater acoustic channels", in *OCEANS*, pp. 1-6, 2008.

[29] G. L. Stüber, *Principles of mobile communication*: Springer, 2011.

[30] X. Xiaomei, C. Yougan, Z. Lan, and F. Wei, "Comparison of the performance of LDPC codes over different underwater acoustic channels", in *12th IEEE International Conference on Communication Technology*, pp. 155-158, 2010.

[31] C. R. Berger, W. Chen, S. Zhou, and J. Huang, "A simple and effective noise whitening method for underwater acoustic orthogonal frequency division multiplexing", *The Journal of the Acoustical Society of America*, vol. 127, p. 2358, 2010.

[32] N. Nasri, L. Andrieux, A. Kachouri, and M. Samet, "Efficient encoding and decoding schemes for wireless underwater communication systems", in *7th International Multi-Conference on Systems Signals and Devices*, pp. 1-6 2010.

[33] M. D. Haque, S. E. Ullah, and M. R. Ahmed, "Performance evaluation of a wireless Orthogonal Frequency Division Multiplexing system under various concatenated FEC channel-coding schemes", in *11th International Conference on Computer and Information Technology*, pp. 94-97, 2008.

[34] M. Chitre, S. Shahabudeen, L. Freitag, and M. Stojanovic, "Recent advances in underwater acoustic communications & networking", in *OCEANS*, pp. 1-10, 2008.

[35] J. Trubuil, A. Goalic, and N. Beuzelin, "Synchronization and channel coding in shallow water acoustic communication", in *OCEANS*, pp. 1-5, 2008.

[36] J. Trubuil, A. Goalic, and N. Beuzelin, "An overview of channel coding for underwater acoustic communications", in *Military Communications Conference*, pp. 1-7,2012.

[37] W. Han, J. Huang, and M. Jiang, "Performance analysis of underwater digital speech communication system based on LDPC codes", in *4th IEEE Conference on Industrial Electronics and Applications*, pp. 567-570, 2009.

[38] J. Huang, S. Zhou, and P. Willett, "Nonbinary LDPC coding for multicarrier underwater acoustic communication", *IEEE Journal on Selected Areas in Communications*, vol. 26, pp. 1684-1696, 2008.

[39] C. R. Berger, S. Zhou, J. C. Preisig, and P. Willett, "Sparse channel estimation for multicarrier underwater acoustic communication: From subspace methods to compressed sensing", *IEEE Transactions on Signal Processing*, vol. 58, pp. 1708-1721, 2010.

[40] Z. Wang, S. Zhou, G. B. Giannakis, C. R. Berger, and J. Huang, "Frequency-domain oversampling for zero-padded OFDM in underwater acoustic communications", *IEEE Journal of Oceanic Engineering*, vol. 37, pp. 14-24, 2012.

[41] A. K. Morozov and J. C. Preisig, "Underwater acoustic communications with multi-carrier modulation", in *OCEANS*, pp. 1-6, 2006.

[42] P. Kumar and P. Kumar, "Performance evaluation of DFT-spread OFDM and DCT-spread OFDM for underwater acoustic communication", in *IEEE Vehicular Technology Conference*, pp. 1-5, 2012.

[43] B. Farhang-Boroujeny, "OFDM versus filter bank multicarrier", *IEEE Signal Processing Magazine*, vol. 28, pp. 92-112, 2011.

[44] R. v. Nee and R. Prasad, *OFDM for wireless multimedia communications*: Artech House, Inc., 2000.

[45] Y. G. Li, *Orthogonal frequency division multiplexing for wireless communications*: Springer-Verlag, 2009.

[46] B. Li, S. Zhou, M. Stojanovic, L. Freitag, J. Huang, and P. Willett, "MIMO-OFDM over an underwater acoustic channel", in *OCEANS*, pp. 1-6, 2007.

[47] A. Thottappilly, "OFDM for Underwater Acoustic Communication", Master of Science, Electrical and Computer Engineering, Virginia Polytechnic Institute and State University, 2011.

[48] B. Li, S. Zhou, M. Stojanovic, L. Freitag, and P. Willet, "Multicarrier underwater acoustic communications over fast-varying channels", *IEEE Journal of Oceanic Engineering*, vol. 33, pp. 198-209, 2008.

[49] C. Polprasert, J. A. Ritcey, and M. Stojanovic, "Capacity of OFDM systems over fading underwater acoustic channels", *IEEE Journal of Oceanic Engineering*, vol. 36, pp. 514-524, 2011.

[50] C. R. Berger, J. Gomes, and J. M. Moura, "Study of pilot designs for cyclic-prefix OFDM on time-varying and sparse underwater acoustic channels", in *OCEANS*, pp. 1-8, 2011.

[51] X. Huang, "Capacity criterion-based power loading for underwater acoustic OFDM system with limited feedback", in *2010 IEEE International Conference on Wireless Communications, Networking and Information Security*, pp. 54-58, 2010.

[52] T. Pedersen and A. Bloomberg, "OFDM pilot-aided underwater acoustic channel estimation", *International Journal of Electrical, Electronics and Computer Systems*, vol. 9, pp. 1-3, 2012.

[53] R. G. Baraniuk, "Compressive sensing", *IEEE Signal Processing Magazine*, vol. 24, pp. 118-121, 2007.

[54] P. Kumar, "DCT based OFDM for underwater acoustic communication", in *1st International Conference on Recent Advances in Information Technology*, pp. 170-176, 2012.

[55] T. Ebihara and K. Mizutani, "Underwater acoustic communication with an orthogonal signal division multiplexing scheme in doubly spread channels", *IEEE Journal of Oceanic Engineering*, pp. 1-12, 2013.

[56] M. Stojanovic, "Recent advances in high-speed underwater acoustic communications", *IEEE Journal of Oceanic Engineering*, vol. 21, pp. 125-136, 1996.

[57] R. Mutagi, "Pseudo noise sequences for engineers", *Electronics and Communication Engineering Journal*, vol. 8, pp. 79-87, 1996.

[58] H. Jinxing, Y. R. Zheng, W. Jintao, and S. Jian, "Dual PN padding TDS-OFDM for underwater acoustic communication", in *Oceans*, pp. 1-4, 2012.

[59] Z. Wang, S. Zhou, J. Catipovic, and P. Willett, "Asynchronous multiuser reception for OFDM in underwater acoustic communications", *IEEE Transactions on Wireless Communications*, vol. PP, pp. 1-12, 2013.

[60] J. Lianyou and H. Jianguo, "Cyclic shift keying spread spectrum OFDM method over underwater acoustic channel", in *IEEE International Conference on Signal Processing, Communication and Computing*, pp. 798-801, 2012.

[61] E. Sozer, J. Proakis, R. Stojanovic, J. Rice, A. Benson, and M. Hatch, "Direct sequence spread spectrum based modem for under water acoustic communication and channel measurements", in *OCEANS*, pp. 228-233, 1999.

[62] N. Papandreou and T. Antonakopoulos, "Bit and power allocation in constrained multicarrier systems: the single-user case", *EURASIP Journal on Advances in Signal Processing*, p. 11, 2008.

[63] X. Huang and V. B. Lawrence, "Bandwidth-efficient bit and power loading for underwater acoustic OFDM communication system with limited feedback", in *IEEE 73rd Vehicular Technology Conference*, pp. 1-5, 2011.

[64] L. Yang, L. Zhou, and M. Yu, "Adaptive bit loading algorithm for OFDM underwater acoustic communication system", in *International Conference on Electronics and Optoelectronics*, pp. V4-350-V4-352, 2011.

[65] H. Xiaopeng and L. Yong, "Capacity criterion-based power allocation for OFDM cooperative underwater acoustic communications with limited feedback", in *Oceans*, pp. 1-4, 2012.

[66] K. Tu, T. M. Duman, M. Stojanovic, and J. G. Proakis, "Multiple-resampling receiver design for OFDM over Doppler-distorted underwater acoustic channels", *IEEE Journal of Oceanic Engineering*, vol. 38, pp. 333-346, 2013.

[67] M. Uysal, *Cooperative communications for improved wireless network transmission: Framework for virtual antenna array applications*: Information Science Reference, 2010.

[68] K. Tu, "Multi-carrier communications over underwater acoustic channels", Doctor of Philosophy, Arizona State University, 2011.

[69] Q. Zhang, A. B. Kokkeler, and G. J. Smit, "An oversampled filter bank multicarrier system for Cognitive Radio", in *19th International Symposium on Personal, Indoor and Mobile Radio Communications*, pp. 1-5, 2008.

[70] P. Amini, C. Rong-Rong, and B. Farhang-Boroujeny, "Filterbank multicarrier for underwater communications", in *49th Annual Allerton Conference on Communication, Control, and Computing*, pp. 639-646, 2011.

[71] B. Le Floch, M. Alard, and C. Berrou, "Coded orthogonal frequency division multiplex", *Proceedings of the IEEE,* vol. 83, pp. 982-996, 1995.

[72] M. ALARD, "Construction of a multicarrier signal", ed: CA Patent CA2,220,107, 1996.

[73] P. Amini, C. H. Yuen, R.-R. Chen, and B. Farhang-Boroujeny, "Isotropic filter design for MIMO filter bank multicarrier communications", in *IEEE Sensor Array and Multichannel Signal Processing Workshop*, pp. 89-92, 2010.

[74] L. Toni, L. Rossi, N. Agoulmine, and J.-G. Fontaine, "Virtual UEP for progressive image transmission in underwater communication", in *wuwnet*, pp. 1-6, 2009.

[75] L. Baosheng, H. Jie, Z. Shengli, K. Ball, M. Stojanovic, L. Freitag, *et al.*, "MIMO-OFDM for high-rate underwater acoustic communications", *IEEE Journal of Oceanic Engineering,* vol. 34, pp. 634-644, 2009.

[76] D. B. Kilfoyle, J. C. Preisig, and A. B. Baggeroer, "Spatial modulation experiments in the underwater acoustic channel", *IEEE Journal of Oceanic Engineering*, vol. 30, pp. 406-415, 2005.

[77] S. Roy, T. M. Duman, V. McDonald, and J. G. Proakis, "High-rate communication for underwater acoustic channels using multiple transmitters and space; time coding: receiver structures and experimental results", *IEEE Journal of Oceanic Engineering*, vol. 32, pp. 663-688, 2007.

[78] R. F. Ormondroyd, "A robust underwater acoustic communication system using OFDM-MIMO", in *OCEANS*, pp. 1-6, 2007.

[79] P. Bouvet and A. Loussert, "An analysis of MIMO-OFDM for shallow water acoustic communications", in *OCEANS*, pp. 1-5, 2011.

[80] M. Stojanovic, "MIMO OFDM over underwater acoustic channels", in *IEEE Forty-Third Asilomar Conference on Signals, Systems and Computers*, pp. 605-609, 2009.

[81] Y. Li, N. Seshadri, and S. Ariyavisitakul, "Channel estimation for OFDM systems with transmitter diversity in mobile wireless channels", *IEEE Journal on Selected Areas in Communications,* vol. 17, pp. 461-471, 1999.

[82] H. Minn and V. K. Bhargava, "An investigation into time-domain approach for OFDM channel estimation", *IEEE Transactions on Broadcasting*, vol. 46, pp. 240-248, 2000.

[83] M. Stojanovic, "OFDM for underwater acoustic communications: Adaptive synchronization and sparse channel estimation", in *IEEE International Conference on Acoustics, Speech and Signal Processing*, pp. 5288-5291, 2008.

[84] B. Saltzberg, "Performance of an efficient parallel data transmission system", *IEEE Transactions on Communication Technology*, vol. 15, pp. 805-811, 1967.

[85] C. A. Belfiore and J. H. Park Jr, "Decision feedback equalization", *Proceedings of the IEEE,* vol. 67, pp. 1143-1156, 1979.

[86] M. Stojanovic, L. Freitag, and M. Johnson, "Channel-estimation-based adaptive equalization of underwater acoustic signals", in *IEEE OCEANS*, pp. 590-595, 1999.

[87] R. Coates, "Underwater acoustic communications", in *OCEANS*, vol. 3, pp. 420-425, 1993.

[88] M. Stojanovic, "Underwater acoustic communication", *Wiley Encyclopedia of Electrical and Electronics Engineering*, 1999.

[89] M. Chitre, S. Shahabudeen, and M. Stojanovic, "Underwater acoustic communications and networking: Recent advances and future challenges", *Marine Technology Society Journal*, vol. 42, pp. 103-116, 2008.

[90] P. Shukla and L. Turner, "Channel-estimation-based adaptive DFE for fading multipath radio channels", in *IEE Proceedings Communications, Speech and Vision*, pp. 525-543, 1991.

[91] P. Zarrinkhat, M. Ardakani, and R. Yazdani, "Channel Estimation Considerations for Iterative Decoding in Wireless Communications", in *IEEE International Conference on Communications*, pp. 1006-1011, 2007.

[92] E. Calvo and M. Stojanovic, "Efficient channel-estimation-based multiuser detection for underwater CDMA systems", *IEEE Journal of Oceanic Engineering*, vol. 33, pp. 502-512, 2008.

[93] J. G. Proakis, E. M. Sozer, J. A. Rice, and M. Stojanovic, "Shallow water acoustic networks", *IEEE Communications Magazine*, vol. 39, pp. 114-119, 2001.

[94] J. Ling, X. Tan, T. Yardibi, J. Li, H. He, and M. L. Nordenvaad, "Enhanced channel estimation and efficient symbol detection in MIMO underwater acoustic communications", in *Forty-Third Asilomar Conference on Signals, Systems and Computers*, pp. 600-604, 2009.

[95] K. Taehyuk and R. A. Iltis, "Matching pursuits channel estimation for an underwater acoustic OFDM modem", in *IEEE International Conference on Acoustics, Speech and Signal Processing*, pp. 5296-5299, 2008,

[96] J. Huang, C. R. Berger, S. Zhou, and J. Huang, "Comparison of basis pursuit algorithms for sparse channel estimation in underwater acoustic OFDM", in *OCEANS*, pp. 1-6, 2010.

[97] Q. Fengzhong and Y. Liuqing, "On the estimation of doubly-selective fading channels", *IEEE Transactions on Wireless Communications*, vol. 9, pp. 1261-1265, 2010.

[98] B. S. Sharif, J. Neasham, O. R. Hinton, and A. E. Adams, "A computationally efficient Doppler compensation system for underwater acoustic communications", *IEEE Journal of Oceanic Engineering*, vol. 25, pp. 52-61, 2000.

[99] M. Stojanovic, J. A. Catipovic, and J. G. Proakis, "Phase-coherent digital communications for underwater acoustic channels", *IEEE Journal of Oceanic Engineering*, vol. 19, pp. 100-111, 1994.

[100] W. Zhaohui, Z. Shengli, J. C. Preisig, K. R. Pattipati, and P. Willett, "Clustered Adaptation for Estimation of Time-Varying Underwater Acoustic Channels", *IEEE Transaction on Signal Processing*, vol. 60, pp. 3079-3091, 2012.

[101] H. Yu and J. Guo, "Compressed sensing: underwater acoustic channel estimation with Doppler shifts", in *8th International Conference on Wireless Communications, Networking and Mobile Computing*, pp. 1-4, 2012.

[102] E. M. Sozer, M. Stojanovic, and J. G. Proakis, "Underwater acoustic networks", *IEEE Journal of Oceanic Engineering*, vol. 25, pp. 72-83, 2000.

[103] C. Pelekanakis, M. Stojanovic, and L. Freitag, "High rate acoustic link for underwater video transmission," in *OCEANS*, pp. 1091-1097, 2003.

[104] I. Iglesias, B. Lu, J. Garcia-Frias, and G. Arce, "Non-linear mappings for transmission of compressed sensing images", in *48th Annual Allerton Conference on Communication, Control, and Computing*, pp. 726-732, 2010.

[105] S. A. Alkharabsheh and M. I. Younis, "Dynamics of MEMS arches of flexible supports", *Journal of Microelectromechanical Systems*, vol. 22, pp. 216-224, 2013.

[106] J.-w. Han, S.-y. Kim, K.-m. Kim, S.-y. Chun, and K. Son, "Design of OFDM System for High Speed Underwater Communication", in *International Conference on Computational Science and Engineering*, pp. 988-992, 2009.

[107] T. B. Santoso and G. Hendrantoro, "Image transmission with OFDM technique in underwater acoustic environment", in *7th International Conference on Telecommunication Systems, Services, and Applications*, pp. 37-41, 2012.

[108] A. Said and W. A. Pearlman, "A new, fast, and efficient image codec based on set partitioning in hierarchical trees", *IEEE Transactions on Circuits and Systems for Video Technology*, vol. 6, pp. 243-250, 1996.

[109] C. Murphy and H. Singh, "Wavelet compression with set partitioning for low bandwidth telemetry from AUVs", in *Proceedings of the Fifth ACM International Workshop on UnderWater Networks*, p. 1, 2010.

[110] B. Tomasi, L. Toni, P. Casari, J. Preisig, and M. Zorzi, "A study on the SPIHT image coding technique for underwater acoustic communications", in *Proceedings of the Sixth ACM International Workshop on Underwater Networks*, pp. 1-9, 2011.

[111] M. A. Kader, F. Ghani, and R. B. Ahmed, "Unequal error protection for SPIHT coded image transmission over erroneous wireless channels", *Asian Transactions on Fundamentals of Electronics, Communication and Multimedia*, vol. 1, pp. 1-6, 2011.

[112] K. Pelekanakis, "Design and analysis of a high-rate acoustic link for underwater video transmission", Master of Science, Massachusetts Institute of Technology, 2004.

[113] J. Ribas, D. Sura, and M. Stojanovic, "Underwater wireless video transmission for supervisory control and inspection using acoustic OFDM", in *OCEANS*, pp. 1-9, 2010.

[114] D. F. Hoag, V. K. Ingle, and R. J. Gaudette, "Low-bit-rate coding of underwater video using wavelet-based compression algorithms", *IEEE Journal of Oceanic Engineering*, vol. 22, pp. 393-400, 1997.

[115] L. Toni, L. Rossi, N. Agoulmine, and J. G. Fontaine, "Virtual unequal error protection in underwater image transmission", in *OCEANS*, pp. 1-6, 2010.

[116] Q. Huynh-Thu and M. Ghanbari, "Scope of validity of PSNR in image/video quality assessment", *Electronics Letters*, vol. 44, pp. 800-801, 2008.

[117] M. A. Kader, F. Ghani, and R. Badlishah, "Development and performance evaluation of hierarchical quadrature amplitude modulation (HQAM) for image transmission over wireless channels", in *Third International Conference on Computational Intelligence, Modelling and Simulation (CIMSiM)*, pp. 227-232, 2011.

[118] U. S. Mohammed and H. Hamada, "Image transmission over OFDM channel with rate allocation scheme and minimum peak-toaverage power ratio", *Journal of Telecommunications*, vol. 2, pp. 70-78, 2010.

[119] A. Albanese, J. Blomer, J. Edmonds, M. Luby, and M. Sudan, "Priority encoding transmission", *IEEE Transactions on Information Theory*, vol. 42, pp. 1737-1744, 1996.

[120] Q. Xu, V. Stankovic, and Z. Xiong, "Distributed joint source-channel coding of video using raptor codes", *IEEE Journal on Selected Areas in Communications,* vol. 25, pp. 851-861, 2007.

[121] C.-Y. Hsu, A. Ortega, and A. R. Reibman, "Joint selection of source and channel rate for VBR video transmission under ATM policing constraints", *IEEE Journal on Selected Areas in Communications,* vol. 15, pp. 1016-1028, 1997.

[122] U. S. Mohammed and H. Hamada, "An efficient rate allocation scheme with selective weighted function for optimum peak-to-average power ratio for transmission of image streams over OFDM channels", *International Journal of Video and Image Processing and Network Security,* vol. 9, 2009.

[123] Y. Sun, R.-m. Li, and X.-l. Cao, "Image compression method of terrain based on Antonini wavelet transform", in *IEEE International Geoscience and Remote Sensing Symposium*, pp. 692-695, 2005.

[124] E. Christophe and W. A. Pearlman, "Three-dimensional SPIHT coding of volume images with random access and resolution scalability", *Journal on Image and Video Processing,* vol. 2008, pp. 1-13, 2008.

[125] Z. Lu, D. Y. Kim, and W. A. Pearlman, "Wavelet compression of ECG signals by the set partitioning in hierarchical trees algorithm", *IEEE Transactions on Biomedical Engineering,* vol. 47, pp. 849-856, 2000.

[126] W. C. Cox, J. A. Simpson, C. P. Domizioli, J. F. Muth, and B. L. Hughes, "An underwater optical communication system implementing Reed-Solomon channel coding", in *OCEANS*, pp. 1-6, 2008.

[127] A. Goalic, J. Trubuil, C. Laot, and N. Beuzelin, "Underwater acoustic communication using Reed Solomon Block Turbo Codes channel coding to transmit images and speech", in *OCEANS*, pp. 1-6, 2010.

[128] J. P. Odenwalder, "Error control coding handbook", DTIC Document, 1976.

[129] M. Chitre, "A high-frequency warm shallow water acoustic communications channel model and measurements", *The Journal of the Acoustical Society of America,* vol. 122, p. 2580, 2007.

[130] M. Stojanovic, J. Catipovic, and J. G. Proakis, "Adaptive multichannel combining and equalization for underwater acoustic communications", *The Journal of the Acoustical Society of America,* vol. 94, p. 1621, 1993.

[131] M. A. Chitre, J. R. Potter, and S.-H. Ong, "Optimal and near-optimal signal detection in snapping shrimp dominated ambient noise", *IEEE Journal of Oceanic Engineering,* vol. 31, pp. 497-503, 2006.

[132] S. M. S. Sadough and P. Duhamel, "On the interaction between channel coding and hierarchical modulation", in *IEEE International Conference on Communications*, pp. 1-5, 2009.

[133] C.-S. Lee, T. Keller, and L. Hanzo, "OFDM-Based turbo-coded hierarchical and non-hierarchical terrestrial mobile digital video broadcasting", *IEEE Transactions on Broadcasting,* vol. 46, pp. 1-22, 2000.

[134] S. Aijun, M. Badiey, A. E. Newhall, J. F. Lynch, H. A. DeFerrari, and B. G. Katsnelson, "Passive time reversal acoustic communications through shallow-water internal waves", *IEEE Journal of Oceanic Engineering,* vol. 35, pp. 756-765, 2010.

[135] R. F. Coates, *Underwater acoustic systems*: J. Wiley, 1989.

[136] A. Hutter, J. Hammerschmidt, E. de Carvalho, and J. Cioffi, "Receive diversity for mobile OFDM systems", in *IEEE Wireless Communications and Networking Confernce*, pp. 707-712, 2000.

[137] H. Esmaiel and D. Jiang, "SPIHT coded image transmission over underwater acoustic channel with unequal error protection using HQAM", in *IEEE International Conference on Information Science and Technology (ICIST)*, pp. 1365-1371, 2013.

[138] A. Katariya, A. Arya, and K. Minda, "Coded under water acoustic communication (UWA) with cryptography", in *International Conference on Computational Intelligence and Communication Networks*, pp. 493-497, 2010.

[139] S. Sandberg and N. Von Deetzen, "Design of bandwidth-efficient unequal error protection LDPC codes", *IEEE Transactions on Communications*, vol. 58, pp. 802-811, 2010.

[140] R. Puri and K. Ramchandran, "Multiple description source coding using forward error correction codes", in *Conference Record of the Thirty-Third Asilomar Conference on Signals, Systems, and Computers*, pp. 342-346, 1999.

[141] C. T. Kelley, *Iterative methods for optimization* vol. 18: Society for Industrial and Applied Mathematics, 1987.

[142] M. L. Fisher, "The Lagrangian relaxation method for solving integer programming problems", *Management science*, vol. 27, pp. 1-18, 1981.

[143] T. C. Yang, "Temporal resolutions of time-reversal and passive-phase conjugation for underwater acoustic communications", *IEEE Journal of Oceanic Engineering*, vol. 28, pp. 229-245, 2003.

[144] H. Esmaiel and D. Jiang, "Zero-pseudorandom noise training OFDM", *Electronics Letters*, vol. 50, pp. 650-652, 2014.

[145] J. A. Tropp, A. C. Gilbert, and M. J. Strauss, "Algorithms for simultaneous sparse approximation. Part I: Greedy pursuit", *Signal Processing*, vol. 86, pp. 572-588, 2006.

[146] L. Dai, J. Wang, Z. Wang, P. Tsiaflakis, and M. Moonen, "Spectrum- and energy-efficient OFDM based on simultaneous multi-channel reconstruction", *IEEE Transactions on Signal Processing*, vol. PP, pp. 1-13, 2013.

[147] Z. Wang, S. Zhou, G. B. Giannakis, C. R. Berger, and J. Huang, "Frequency-domain oversampling for zero-padded OFDM in underwater acoustic communications", in *IEEE Global Telecommunications Conference*, pp. 1-5, 2010.

[148] M. Palanivelan, S. Anand, and S. P. Venkatesan, "PAPR and ICI reduction in OFDM systems using modified raised cosine power pulse shape", *European Journal of Scientific Research*, vol. 72, pp. 618-627, 2012.

[149] J. Ahn and H. Lee, "Frequency domain equalisation of OFDM signals over frequency nonselective Rayleigh fading channels," *Electronics letters*, vol. 29, pp. 1476-1477, 1993.

[150] N. Al-Dhahir and J. M. Cioffi, "Optimum finite-length equalization for multicarrier transceivers", *IEEE Transactions on Communications* vol. 44, pp. 56-64, 1996.

[151] R. Li and G. Stette, "Time-limited orthogonal multicarrier modulation schemes", *IEEE Transactions on Communications*, vol. 43, pp. 1269-1272, 1995.

[152] C. Muschallik, "Improving an OFDM reception using an adaptive Nyquist windowing", *IEEE Transactions on Consumer Electronics*, vol. 42, pp. 259-269, 1996.

[153] Y. Zhao and S.-G. Haggman, "Sensitivity to Doppler shift and carrier frequency errors in OFDM systems-the consequences and solutions", in *IEEE 46th Vehicular Technology Conference*, pp. 1564-1568, 1996.

[154] Y. Zhao and S.-G. Haggman, "Intercarrier interference self-cancellation scheme for OFDM mobile communication systems", *IEEE Transactions on Communications*, vol. 49, pp. 1185-1191, 2001.

[155] P. Tan and N. C. Beaulieu, "Reduced ICI in OFDM systems using the better than raised cosine pulse", *IEEE Communications Letters,* vol. 8, pp. 135-137, 2004.

[156] H.-A. M. Mourad, "Reducing ICI in OFDM systems using a proposed pulse shape", *Wireless Personal Communications,* vol. 40, pp. 41-48, 2007.

[157] V. Kumbasar and O. Kucur, "ICI reduction in OFDM systems by using improved sinc power pulse", *Digital Signal Processing,* vol. 17, pp. 997-1006, 2007.

[158] S. Mohanty and S. Das, "A comparative study of pulse shaping functions for ICI power reduction in OFDM system", in *Annual IEEE India Conference*, pp. 312-316, 2008.

[159] S. Lmai, A. Bourre, C. Laot, and S. Houcke, "Advantages of pulse-shaping applied to OFDM systems over underwater acoustic channels", in *Oceans*, pp. 1-7, 2012.

[160] T. Pollet, M. Van Bladel, and M. Moeneclaey, "BER sensitivity of OFDM systems to carrier frequency offset and Wiener phase noise", *IEEE Transactions on Communications,* vol. 43, pp. 191-193, 1995.

[161] P. Tan and N. C. Beaulieu, "An improved DCT-based OFDM data transmission scheme", in *IEEE 16th International Symposium on Personal, Indoor and Mobile Radio Communications*, pp. 745-749, 2005.

[162] R. K. Martin *et al.*, "Unification and evaluation of equalization structures and design algorithms for discrete multitone modulation systems", *IEEE Transactions on Signal Processing,* vol. 53, pp. 3880-3894, 2005.

[163] T. van Waterschoot, V. Le Nir, J. Duplicy, and M. Moonen, "Analytical expressions for the power spectral density of CP-OFDM and ZP-OFDM signals", *IEEE Signal Processing Letters,* vol. 17, pp. 371-374, 2010.

[164] W. Jianming, Y. Chen, Z. Xiaoyang, and M. Hao, "Robust timing and frequency synchronization scheme for DTMB system", *IEEE Transactions on Consumer Electronics,* vol. 53, pp. 1348-1352, 2007.

[165] W. Jun, Y. Zhi-Xing, P. Chang-Yong, S. Jian, and Y. Lin, "Iterative padding subtraction of the PN sequence for the TDS-OFDM over broadcast channels", *IEEE Transactions on Consumer Electronics,* vol. 51, pp. 1148-1152, 2005.

[166] L. Ming, M. Crussiere, and J. Helard, "A novel data-aided channel estimation with reduced complexity for TDS-OFDM systems", *IEEE Transactions on Broadcasting,* vol. 58, pp. 247-260, 2012.

[167] M. Huemer, C. Hofbauer, and J. B. Huber, "Non-systematic complex number RS coded OFDM by unique word prefix", *IEEE Transactions on Signal Processing,* vol. 60, pp. 285-299, 2012.

[168] F. Jian, W. Jun, S. Jian, P. Chang-Yong, and Y. Zhi-Xing, "A simplified equalization method for dual PN-sequence padding TDS-OFDM systems", *IEEE Transactions on Broadcasting,* vol. 54, pp. 825-830, 2008.

[169] L. Dai, Z. Wang, and Z. Yang, "Next-generation digital television terrestrial broadcasting systems: Key technologies and research trends", *IEEE Communications Magazine* vol. 50, pp. 150-158, 2012.

[170] H. Esmaiel and D. Jiang, "Review article: multicarrier communication for underwater acoustic channel", *International Journal of Communications, Network and System Sciences,* vol. 6, pp. 361-376, 2013.

[171] H. Steendam, "On the pilot carrier placement in multicarrier-based systems", *IEEE Transactions on Signal Processing,* vol. 62, pp. 1812-1821, 2014.

[172] P. Changyong, D. Linglong, and Y. Zhixing, "TDS-OFDM based HDTV transmission over fast fading channels", *IEEE Transactions on Consumer Electronics,* vol. 59, pp. 16-23, 2013.

[173] D. Linglong, W. Zhaocheng, and C. Sheng, "A novel uplink multiple access scheme based on TDS-FDMA", *IEEE Transactions on Wireless Communications*, vol. 10, pp. 757-761, 2011.

[174] S. B. Wicker, *Error control systems for digital communication and storage* vol. 1: Prentice hall Englewood Cliffs, 1995.

[175] N. Hung Tuan, J. B. Andersen, and G. F. Pedersen, "The potential use of time reversal techniques in multiple element antenna systems", *IEEE Communications Letters*, vol. 9, pp. 40-42, 2005.

[176] D. Linglong, W. Zhaocheng, and Y. Zhixing, "Time-frequency training OFDM with high spectral efficiency and reliable performance in high speed environments", *IEEE Journal on Selected Areas in Communications*, vol. 30, pp. 695-707, 2012.

[177] M. Jingbo and K. Guihua, "A novel OFDM synchronization algorithm based on CAZAC sequence", in *International Conference on Computer Application and System Modeling*, pp. V14-634-V14-637, 2010.

[178] J. Gomes and V. Barroso, "Time-reversed OFDM communication in underwater channels", in *IEEE 5th Workshop on Signal Processing Advances in Wireless Communications*, pp. 626-630, 2004.

[179] H. C. Song, W. S. Hodgkiss, W. A. Kuperman, T. Akal, and M. Stevenson, "Multiuser communications using passive time reversal", *IEEE Journal of Oceanic Engineering*, vol. 32, pp. 915-926, 2007.

[180] S. S. Murugan and V. Natarajan, "Performance analysis of signal to noise ratio and bit error rate for multiuser using passive time reversal technique in underwater communication", in *International Conference on Wireless Communication and Sensor Computing*, pp. 1-4, 2010.

[181] T. Shimura, H. Ochi, Y. Watanabe, and T. Hattori, "Time-reversal communication in deep ocean Results of recent experiments", in *Workshop on Scientific Use of Submarine Cables and Related Technologies*, pp. 1-5, 2011.

[182] L. Zhiqiang and T. C. Yang, "Time reversal multicarrier communications over long multipath fading channels", in *Military Communications Conference*, pp. 1-6, 2012.

[183] D. Linglong, W. Zhaocheng, W. Jun, and Y. Zhixing, "Joint time-frequency channel estimation for time domain synchronous OFDM systems", *IEEE Transactions on Broadcasting*, vol. 59, pp. 168-173, 2013.

[184] K. Jae Won, W. Younghoon, K. Byung Hoon, and K. Kwang Soon, "Generalized Cross-Correlation Properties of Chu Sequences", *IEEE Transactions on Information Theory*, vol. 58, pp. 438-444, 2012.

[185] T. C. Yang, "Correlation-based decision-feedback equalizer for underwater acoustic communications", *IEEE Journal of Oceanic Engineering*, vol. 30, pp. 865-880, 2005.

[186] M. F. Duarte and Y. C. Eldar, "Structured Compressed Sensing: From Theory to Applications", *IEEE Transactions on Signal Processing*, vol. 59, pp. 4053-4085, 2011.

[187] D. L. Donoho, "Compressed sensing", *IEEE Transactions on Information Theory*, vol. 52, pp. 1289-1306, 2006.

[188] Y. Zhixing, W. Xiaoqing, W. Zhaocheng, W. Jintao, and W. Jun, "Improved channel estimation for TDS-OFDM based on flexible frequency-binary padding", *IEEE Transactions on Broadcasting*, vol. 56, pp. 418-424, 2010.

[189] H. Esmaiel and D. Jiang, "Time reversal time-domain synchronisation orthogonal frequency division multiplexing over multipath fading channels with significant tap delays", *The Journal of Engineering*, vol. 1, 2014.

[190] H. Esmaiel and D. Jiang, "OFDM Inter-Carrier Interference reduction using pulse shaping function for underwater acoustic communications systems", in *IEEE International Conference on Electronics, Communications and Computers (JEC-ECC)*, pp. 104-109, 2013.

[191] D. Van Welden, H. Steendam, and M. Moeneclaey, "Iterative decision-directed joint frequency offset and channel estimation for KSP-OFDM", *IEEE Transactions on Communications*, vol. 60, pp. 3103-3110, 2012.

[192] D. Van Welden and H. Steendam, "Near optimal iterative channel estimation for KSP-OFDM", *IEEE Transactions on Signal Processing*, vol. 58, pp. 4948-4954, 2010.

[193] B. Muquet, W. Zhengdao, G. B. Giannakis, M. de Courville, and P. Duhamel, "Cyclic prefixing or zero padding for wireless multicarrier transmissions?", *IEEE Transactions on Communications*, vol. 50, pp. 2136-2148, 2002.

[194] L. Deneire, B. Gyselinckx, and M. Engels, "Training sequence versus cyclic prefix-a new look on single carrier communication", *IEEE Communications Letters*, vol. 5, pp. 292-294, 2001.

[195] T. Xiaohu and G. Guang, "New constructions of binary sequences with optimal autocorrelation value/magnitude", *IEEE Transactions on Information Theory*, vol. 56, pp. 1278-1286, 2010.

[196] L. C. Quynh and S. Prasad, "Class of binary cipher sequences with best possible autocorrelation function", *Communications, Radar and Signal Processing, IEE Proceedings*, vol. 132, pp. 576-580, 1985.

[197] Z. W. Zheng, Y. Zhi-Xing, P. Chang-Yong, and Y.-S. Zhu, "Novel synchronization for TDS-OFDM-based digital television terrestrial broadcast systems", *IEEE Transactions on Broadcasting*, vol. 50, pp. 148-153, 2004.

[198] D. Wenbo, Y. Fang, P. Changyong, D. Linglong, and S. Jian, "Compressive sensing based channel estimation for OFDM systems under long delay channels", *IEEE Transactions on Broadcasting*, vol. 60, pp. 313-321, 2014.

[199] G. F. Edelmann, "An overview of time-reversal acoustic communications", *In Turkish International Conference in Acoustics*, 2005.

[200] D. Linglong, W. Zhaocheng, and Y. Zhixing, "Compressive sensing based time domain synchronous OFDM transmission for vehicular communications", *IEEE Journal on Selected Areas in Communications*, vol. 31, pp. 460-469, 2013.